THE

LONDON, EDINBURGH, AND DUBLIN

PHILOSOPHICAL MAGAZINE

AND

JOURNAL OF SCIENCE.

[SEVENTH SERIES.]

SUPPLEMENT, NOVEMBER 1936.

LXXII. *The Effect of One Salt on the Solubility of Another.* —Part VII. *Solubilities of Cobaltammines in Aqueous Sodium, Potassium, and Barium Thiocyanates.*

By Prof. J. R. PARTINGTON *and* Dr. H. J. STONEHILL †.

THE solubility determinations now described, together with those due to O'Neill and Partington (Trans. Far. Soc. xxx. p. 1134 (1934)), which they actually preceded, constitute a complete investigation of the effect of the thiocyanates of some uni- bi-, and ter-valent cations on the solubilities of two bi-univalent cobaltammine salts, viz., $\left[\mathrm{Co}\begin{matrix}(\mathrm{NH_3})_5\\ \mathrm{NCS}\end{matrix}\right](\mathrm{NO_3})_2$ (*iso*-thiocyanato-pentammine-cobaltic nitrate) and $\left[\mathrm{Co}\begin{matrix}(\mathrm{NH_3})_5\\ \mathrm{NCS}\end{matrix}\right]\mathrm{I_2}$ (*iso*-thiocyanato-pentammine-cobaltic iodide) in water at 25° C.

Experimental.

The solubility apparatus and the preparation of cobaltammine salts have been previously described (O'Neill and Partington, *loc. cit.*); in the analysis of the cobaltammines, ammonia was determined as before,

† Communicated by the Authors.

and cobalt by decomposing the complex with caustic soda, filtering off the cobalt oxide, redissolving in dilute sulphuric acid, neutralizing with ammonia and acetic acid, and finally precipitating at 80° with 8-hydroxyquinoline, drying the precipitate at 130° C., and weighing.

Results were as follows :—

Nitrate : % NH_3 found : 26·15, 26·05, 26·08 (theor. 26·11).
% Co found : 18·12, 18·18 (theor. 18·07).

Iodide : % NH_3 found : 18·71, 18·64 (theor. 18·68).
% Co found : 12·98, 13·03 (theor. 12·93).

B.D.H. potassium thiocyanate (A.R. grade), recrystallized three times from distilled water and then three times from redistilled 96 per cent. alcohol, was dried by heating at 105° C. for 24 hours *in vacuo* over P_2O_5, and stored *in vacuo* over P_2O_5 at room temperature for several weeks before use. Commercial sodium thiocyanate was recrystallized twice from distilled water, then six times from redistilled 96 per cent. alcohol to remove traces of sodium carbonate (the main impurity), and dried as for potassium thiocyanate. Barium thiocyanate was prepared by boiling B.D.H. ammonium thiocyanate (A.R. grade) in aqueous solution with excess of Merck's A.R. grade $Ba(OH)_2$, $8H_2O$ until all the ammonia was expelled ; on cooling, excess of baryta crystallized out and was filtered off, and the baryta still in solution was precipitated in the cold with carbon dioxide, the barium carbonate being filtered off. The liquid was evaporated to small bulk and the barium thiocyanate which crystallized out on cooling was recrystallized six times from conductivity water, then three times from redistilled 96 per cent. alcohol ; it was dried first in an oven at 130° C., and then over P_2O_5 *in vacuo*, as for potassium thiocyanate. All three thiocyanates were analysed by precipitation with silver nitrate in cold dilute nitric acid solution. The results agreed with theory.

Conductivity water (Sp. conductivity 0·5–0·7 $\times 10^{-6}$ mhos.) was used exclusively for all solubility determinations.

The ammonia determinations were carried out as previously described (O'Neill and Partington, *loc. cit.*),

except that the excess acid was titrated with approx. $\frac{N}{20}$ sodium carbonate to an end-point of pH 5·8, using methyl-red as indicator, the end-point being determined by comparison with a buffer-solution at pH 5·8, containing the same concentration of indicator as used in titration, and viewed under a " day-light " lamp in an otherwise darkened room, thus providing standardized conditions. The accuracy attained corresponds with a maximum error of 0·1 per cent. in the solubility result. All weights and apparatus were calibrated.

The thermostat containing the percolators was controlled to 24·98° ± ·01° C., as determined by a thermometer recently calibrated to within 0·02° C. by the N.P.L.

The cobaltammines were washed in the percolators with conductivity water until the solubilities had decreased to constant minimum values (5–6 days for the nitrate, *ca.* 14 days for the iodide), which were taken as the solubilities in pure water. Various specimens of the cobaltammines, prepared at different times, gave the same values of the solubilities in pure water, which have been confirmed by O'Neill and Partington (*loc. cit.*).

After the cobaltammines were thus washed, the thiocyanate solutions were passed through the percolators, starting with the most dilute solution in each series ; the percolators were thoroughly washed through with each successive solution before any liquid was collected for analysis.

No difference in the solubilities in pure water was observed when the interval between successive drops (*ca.* $\frac{1}{11}$ ml.) of liquid leaving the percolators was varied from 30 to 120 seconds, but below a 25-second interval appreciable unsaturation was observed. The rate generally adopted was about 100 seconds per drop (*ca.* 3 ml. per hour) ; a rate of 100 ml. per hour was used with a similar apparatus by Money and Davies (J. C. S. 1934, p. 400).

The experimental results are given in Table I. ; S is the solubility of the cobaltammine, S_0 being the value when pure water is the solvent, and m is the concentration of thiocyanate (" solvent salt ") in the solvent solution, all expressed in mol./litre at 25° C. The values of S are the mean of at least two determinations, and those of S_0

the mean of 13 and 4 determinations, for the nitrate and iodide respectively; for the iodide, S_0 was not so

TABLE I.

Experimental Solubility Results.

(i.) Solute, $\left[Co\begin{matrix}(NH_3)_5\\NCS\end{matrix}\right](NO_3)_2$; solvent, pure water.

$S_0 = 0{\cdot}003444$ $\log S_0 = -2{\cdot}4629$

$\mu = 0{\cdot}01033$ $\sqrt{\mu} = 0{\cdot}1017$

(ii.) Solute, $\left[Co\begin{matrix}(NH_3)_5\\NCS\end{matrix}\right]I_2$; solvent, pure water.

$S_0 = 0{\cdot}0008800$ $\mu = 0{\cdot}002640$

$\log S_0 = -3{\cdot}0555$ $\sqrt{\mu} = 0{\cdot}05138$

(iii.) Solute, $\left[Co\begin{matrix}(NH_3)_5\\NCS\end{matrix}\right](NO_3)_2$; solvent salt, KSCN.

No.	m.	S.	$-\log$ S.	μ.	$\sqrt{\mu}$.
1	0·0001004	0·003450	2·4622	0·01045	0·1022
2	·005018	·003476	2·4590	·01093	·1045
3	·001004	·003492	2·4570	·01148	·1071
4	·002007	·003507	2·4551	·01253	·1119
5	·0054805	·003616	2·4418	·01633	·1278
6	·01096	·003780	2·4226	·02230	·1493
7	·02016	·003973	2·4008	·03208	·1791
8	·02192	·004023	2·3955	·03399	·1844
9	·05040	·004519	2·3450	·06396	·2529
10	·1008	·005234	2·2812	·1165	·3413
11	·2016	·006345	2·1976	·2206	·4697

(iv.) Solute, $\left[Co\begin{matrix}(NH_3)_5\\NCS\end{matrix}\right](NO_3)_2$; solvent salt, NaSCN.

No.	m.	S.	$-\log$ S.	μ.	$\sqrt{\mu}$.
1	0·0001213	0·003451	2·4620	0·01048	0·1024
2	·0002426	·003461	2·4608	·01063	·1031
3	·0004851	·003478	2·4587	·01092	·1045
4	·001213	·003528	2·4525	·01180	·1086
5	·002426	·003559	2·4487	·01310	·1145
6	·005192	·003641	2·4388	·01611	·1269
7	·01038	·003787	2·4217	·02174	·1475
8	·02077	·004096	2·3876	·03306	·1818
9	·05192	·004637	2·3338	·06583	·2566
10	·1038	·005212	2·2830	·1195	·3457

TABLE I. (*cont.*).

Experimental Solubility Results.

(v.) Solute, $\left[\mathrm{Co}\begin{matrix}(\mathrm{NH_3})_5\\ \mathrm{NCS}\end{matrix}\right](\mathrm{NO_3})_2$; solvent salt, $\mathrm{Ba(SCN)_2}$.

No.	*m.*	S.	$-\log$ S.	μ.	$\sqrt{\mu}$.
1	0·0001079	0·003462	2·4607	0·01071	0·1035
2	·0002696	·003510	2·4546	·01134	·1065
3	·0005393	·003572	2·4472	·01233	·1111
4	·001079	·003593	2·4445	·01401	·1184
5	·002424	·003717	2·4298	·01842	·1357
6	·004849	·003905	2·4084	·02626	·1621
7	·009697	·004147	2·3823	·04153	·2038
8	·02424	·004799	2·3189	·08713	·2952
9	·04849	·005753	2·2401	·1627	·4034
10	·08339	·006596	2·1808	·2700	·5196

(vi.) Solute, $\left[\mathrm{Co}\begin{matrix}(\mathrm{NH_3})_5\\ \mathrm{NCS}\end{matrix}\right]\mathrm{I_2}$; solvent salt, KSCN.

No.	*m.*	S.	$-\log$ S.	μ.	$\sqrt{\mu}$.
1	0·0001004	0·0008860	3·0526	0·002758	0·05252
2	·0005018	·0008928	3·0493	·003180	·05639
3	·001004	·0008976	3·0469	·003697	·06080
4	·002007	·0009118	3·0401	·004743	·06887
5	·005481	·0009579	3·0187	·008354	·09140
6	·01096	·001004	2·9982	·01397	·1182
7	·02192	·001073	2·9693	·02514	·1586
8	·05481	·001217	2·9149	·05846	·2418
9	·1151	·001372	2·8628	·1192	·3453
10	·2016	·001553	2·8090	·2062	·4541

(vii.) Solute, $\left[\mathrm{Co}\begin{matrix}(\mathrm{NH_3})_5\\ \mathrm{NCS}\end{matrix}\right]\mathrm{I_2}$; solvent salt, NaSCN.

No.	*m.*	S.	$-\log$ S.	μ.	$\sqrt{\mu}$.
1	0·0001213	0·0008870	3·0521	0·002782	0·05275
2	·0002426	·0008937	3·0488	·002924	·05407
3	·001213	·0009059	3·0429	·003931	·06269
4	·002426	·0009179	3·0372	·005179	·07197
5	·005192	·0009429	3·0255	·008020	·08956
6	·01038	·0009910	3·0039	·01336	·1156
7	·02077	·001051	2·9785	·02392	·1547
8	·05192	·001176	2·9295	·05544	·2355
9	·1038	·001321	2·8791	·1078	·3283

TABLE I. (*cont.*).

Experimental Solubility Results.

(viii.) Solute, $\left[\mathrm{Co}\begin{matrix}(\mathrm{NH_3})_5\\ \mathrm{NCS}\end{matrix}\right]\mathrm{I_2}$; solvent salt, $\mathrm{Ba(SCN)_2}$.

No.	*m*.	S.	$-\log$ S.	μ.	$\sqrt{\mu}$.
1	0·0001079	0·0008859	3·0526	0·002981	0·05460
2	·0002696	·0008923	3·0495	·003486	·05904
3	·0005393	·0009000	3·0458	·004318	·06571
4	·001079	·0009096	3·0411	·005965	·07723
5	·002424	·0009525	3·0212	·01013	·1006
6	·004849	·001000	3·0000	·01755	·1325
7	·009697	·001078	2·9674	·03233	·1798
8	·02424	·001231	2·9097	·07643	·2765
9	·04849	·001407	2·8517	·1497	·3869
10	·08339	·001566	2·8053	·2549	·5049

Fig. 1.

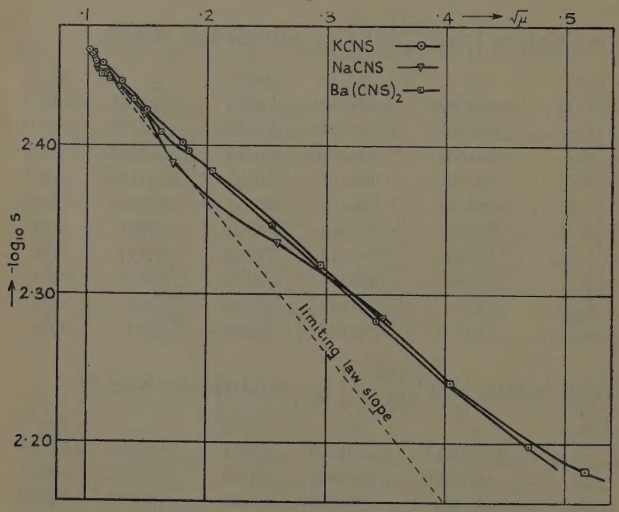

Solubilities of $\left[\mathrm{Co}\begin{matrix}\mathrm{NCS}\\ (\mathrm{NH_3})_5\end{matrix}\right](\mathrm{NO_3})_2$.

closely reproducible as for the nitrate. The ionic strength, μ, is defined as

$$\mu=\tfrac{1}{2}\sum_i (\text{conc. in m./l. of ion of species } i) \times(\text{valency of } i\text{-ion})^2. \quad . \quad . \quad (1)$$

The values of S_0 for the iodide and the nitrate are identical with those found by O'Neill and Partington (*loc. cit.*); the value for the nitrate has been again

Fig. 2.

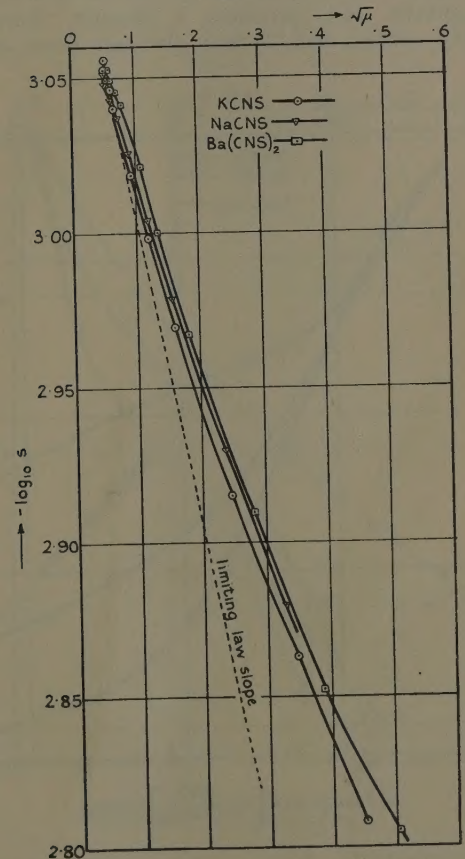

Solubilities of $\left[\mathrm{Co}\begin{matrix}\mathrm{NCS}\\(\mathrm{NH_3})_5\end{matrix}\right]\mathrm{I_2}$.

exactly confirmed by Mr. D. E. Coome (unpublished) in this Department since this work was completed. The latter obtained for the bromide, $S_0=0{\cdot}003336$.

These solubility results are plotted in the form of $-\log S$ against $\sqrt{\mu}$ in the accompanying graphs (figs. 1–4); in each case the earlier part of the curve ($\log \sqrt{\mu}$) is shown plotted on a large scale. From these large-scale curves it is seen (1) that, even at the lowest concentrations, each solvent salt produces a distinct, characteristic solubility curve; and (2) that, although these individual

Fig. 3.

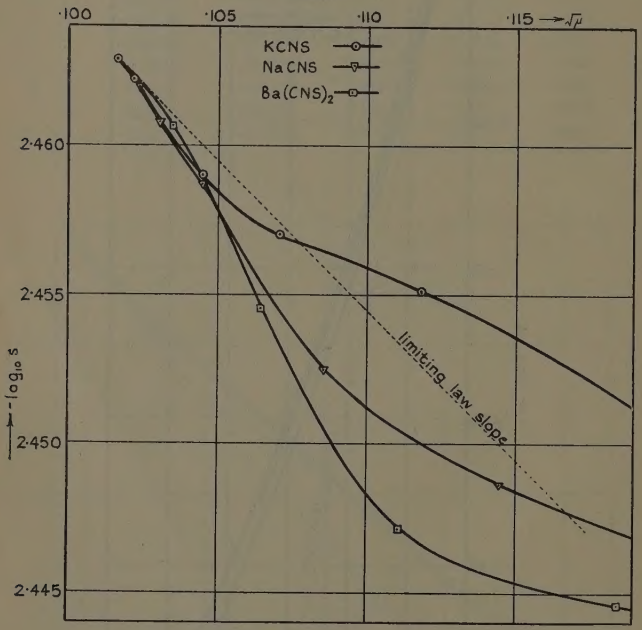

Solubilities of $\left[\mathrm{Co}\begin{matrix}\mathrm{NCS}\\(\mathrm{NH_3})_5\end{matrix}\right](\mathrm{NO_3})_2$.

curves naturally coalesce at the terminal point corresponding to S_0 for a given solute, it would be difficult to choose the best curve with which to extrapolate to zero ionic strength, in order to obtain absolute values of the logarithms of the activity coefficient by the usual method (Lewis and Randall, 'Thermodynamics,'

1923, p. 370). This method of extrapolation is therefore abandoned, and some other procedure is necessary if the experimental results are to be compared with theory.

The dotted straight lines drawn through the terminal points of the graphs have the theoretical slope of the

Fig. 4.

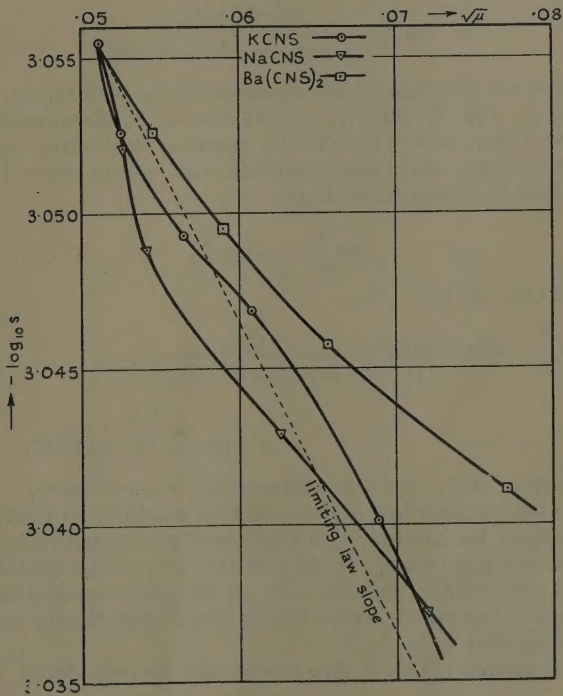

Solubilities of $\left[Co \begin{matrix} NCS \\ (NH_3)_5 \end{matrix} \right] I_2$.

Debye-Hückel limiting law; they indicate that the experimental curves do not always possess a limiting slope equal to this theoretical one, and that they do not always smoothly merge into the line representing the limiting law, but often meet it at a definite angle.

Discussion.

(i.) *The Debye-Hückel Theory.*

For a 2 : 1 type electrolyte in water at 25°, dielectric constant=78·54 (Wyman, Phys. Rev. xxxv. p. 623 (1930)) the Debye-Hückel theory (*Phys. Zeit.* xxiv. pp. 185, 334 (1923)) leads to the following equation for the logarithm of the mean ionic activity coefficient :—

$$-\log f = \frac{2\times 0{\cdot}5065\sqrt{\mu}}{1+(a.\sqrt{\mu}\,.\,10^8\times 0{\cdot}3287)}, \quad . \quad . \quad (2)$$

where a is the mean ionic diameter of the electrolyte.

If f_0 and S_0 refer to a solution of cobaltammine in pure water, and f and S to a solution containing added thiocyanate, then since solvent and solute salts have no ions in common, we have

$$\log \frac{S}{S_0} = -\log \frac{f}{f_0}, \quad . \quad . \quad . \quad . \quad . \quad (3)$$

and thus by (2) :

$$\log \frac{S}{S_0} = (2\times 0{\cdot}5065)\frac{\sqrt{\mu_0}}{1+(a_0\sqrt{\mu_0}.10^8\times 0{\cdot}3287)} - \frac{\sqrt{\mu}}{1+(a\sqrt{\mu}.10^8\times 0{\cdot}3287)}, \quad (4)$$

where a_0 and μ_0 refer to the solution in pure water.

A satisfactory test of this equation would be to ascertain whether, for any given solvent and solute salt-pair, the value of a given by (4) is positive, physically plausible, and reasonably constant over an adequate concentration range in the region where the Debye-Hückel theory might be expected to apply.

In solving (4) for a, two cases must be considered, viz.,

Case (A).... $a_0=a$.
Case (B).... a_0 not necessarily equal to a.

In case (A), equation (4) may be solved directly as a quadratic in a by using the experimental values of $\log \frac{S}{S_0}$. In case (B), it is necessary to assume arbitrary values for a_0 and then to calculate for each of these a_0-values a series of a-values corresponding with the

TABLE II.—Debye-Hückel a-values in Å. Case (A).

No.	1.	2.	3.	4.	5.	6.	7.	8	9.	10.	11.
(i.) $\left[\mathrm{Co}\begin{matrix}\mathrm{NCS}\\(\mathrm{NH_3})_5\end{matrix}\right]\mathrm{I_2}$ in NaSCN.											
a.....	*ca.*−42	*ca.*−39	−2·3	+3·30	+5·78	+4·50	+4·98	+4·75	+4 44		
(ii.) $\left[\mathrm{Co}\begin{matrix}\mathrm{NCS}\\(\mathrm{NH_3})_5\end{matrix}\right]\mathrm{I_2}$ in KSCN.											
a.....	*ca.*−36	*ca.*−6	+2·80	+3·60	+2·10	+3·16	+3·56	+3·20	+3·95	+3·73	
(iii.) $\left[\mathrm{Co}\begin{matrix}\mathrm{NCS}\\(\mathrm{NH_3})_5\end{matrix}\right]\mathrm{I_2}$ in $\mathrm{Ba(SCN)_2}$.											
a.....	+3·20	+7·10	*ca.*+11·0	*ca.*+13·5	*ca.*+7·7	+6·90	+5·75	+4·90	+4·36	+4·30	
(iv.) $\left[\mathrm{Co}\begin{matrix}\mathrm{NCS}\\(\mathrm{NH_3})_5\end{matrix}\right](\mathrm{NO_3})_2$ in NaSCN.											
a.....	*ca.*−5	*ca.*−8	*ca.*−7·7	*ca.*−7·4	*ca.*−1·5	+0·84	+1·50	+0·83	+1·77	+2·40	
(v.) $\left[\mathrm{Co}\begin{matrix}\mathrm{NCS}\\(\mathrm{NH_3})_5\end{matrix}\right](\mathrm{NO_3})_2$ in KSCN.											
a.....	*ca.*−4	*ca.*−4	−1·1	+4·34	+3·16	+2·30	+2·69	+2·44	+2·42	+2·18	+2·04
(vi.) $\left[\mathrm{Co}\begin{matrix}\mathrm{NCS}\\(\mathrm{NH_3})_5\end{matrix}\right](\mathrm{NO_3})_2$ in $\mathrm{Ba(SCN)_2}$.											
a	*ca.*−2·8	*ca.*−6·5	*ca.*−7·4	*ca.*−1·1	+0·53	+1·37	+2·67	+2·62	+2·12	+2·52	

TABLE III.—Debye-Hückel a-values in Å. Case (B).

a_0/No.	1.	2.	3.	4.	5.	6.	7.	8.	9.	10.	11.
(i.) $\left[\mathrm{Co}\begin{matrix}\mathrm{NCS}\\(\mathrm{NH_3})_5\end{matrix}\right]\mathrm{I_2}$ in NaSCN.											
1.....	−1·36	−3·05	−0·20	+2·02	+4·00	+3·66	+4·37	+4·47	+4·26		
2.....	−0·32	−2·02	+0·45	+2·60	+4·39	+3·88	+4·52	+4·51	+4·32		
3.....	+0·50	−1·45	+1·09	+3·12	+4·77	+4·11	+4·68	+4·61	+4·36		
4.....	+1·35	−0·55	+1·70	+3·66	+5·13	+4·38	+4·79	+4·70	+4·40		
5.....	+2·21	+0·11	+2·34	+4·18	+5·50	+4·60	+4·99	+4·77	+4·48		
(ii.) $\left[\mathrm{Co}\begin{matrix}\mathrm{NCS}\\(\mathrm{NH_3})_5\end{matrix}\right]\mathrm{I_2}$ in KSCN.											
2.....	−0·13	+0·50	+2·23	+2·68	+2·04	+2·89	+3·40	+3·54	+3·86	+3·68	
3.....	+0·75	+1·29	+2·94	+3·26	+2·39	+3·10	+3·53	+3·62	+3·91	+3·71	
4.....	+1·64	+2·06	+3·66	+3·85	+2·73	+3·33	+3·65	+3·68	+3·95	+3·74	
(iii.) $\left[\mathrm{Co}\begin{matrix}\mathrm{NCS}\\(\mathrm{NH_3})_5\end{matrix}\right]\mathrm{I_2}$ in $\mathrm{Ba(SCN)_2}$.											
3.....	+3·02	+3·94	+5·60	+8·35	+6·40	+6·25	+5·45	+4·77	+4·31	+4·25	
4.....	+3·91	+4·71	+6·26	+8·85	+6·70	+6·40	+5·57	+4·84	+4·36	+4·30	
5.....	+4·80	+5·50	+6·93	+9·35	+6·97	+6·67	+5·65	+4·89	+4·40	+4·33	
(iv.) $\left[\mathrm{Co}\begin{matrix}\mathrm{NCS}\\(\mathrm{NH_3})_5\end{matrix}\right](\mathrm{NO_3})_2$ in NaSCN.											
2.....	+1·89	+1·71	+1·47	+0·80	+1·20	+1·56	+1·72	+1·20	+1·80	+2·34	
3.....	+2·87	+2·66	+2·38	+1·62	+2·00	+2·19	+2·24	+1·51	+1·98	+2·48	
4.....	+3·86	+3·62	+3·30	+2·46	+2·74	+2·84	+2·71	+1·82	+2·16	+2·58	

(v.) $\left[Co\begin{matrix}NCS\\(NH_3)_5\end{matrix}\right](NO_3)_2$ in KSCN.

2.....	+1·93	+1·59	+1·68	+2·35	+2·38	+2·15	+2·42	+2·25	+2·33	+2·16	+2·04
3.....	+2·90	+2·52	+2·56	+3·20	+3·05	+2·64	+2·81	+2·63	+2·52	+2·27	+2·09
4.....	+3·89	+3·42	+3·44	+4·05	+3·70	+3·11	+3·16	+2·97	+2·70	+2·39	+2·17

(vi.) $\left[Co\begin{matrix}NCS\\(NH_3)_5\end{matrix}\right](NO_3)_2$ in $Ba(SCN)_2$.

2.....	+1·81	+0·83	+0·04	+1·11	+1·35	+1·63	+2·44	+2·49	+2·10	+2·27
3.....	+2·73	+1·69	+0·78	+1·82	+1·89	+2·03	+2·73	+2·65	+2·20	+2·34
4.....	+3·71	+2·53	+1·51	+2·52	+2·43	+2·42	+3·04	+2·81	+2·28	+2·39

(vii.) $\left[Co\begin{matrix}NCS\\(NH_3)_5\end{matrix}\right](NO_3)_2$ in *m* $La(SCN)_3$.

0.....	+0·38	+0·49	+0·89	+1·13	+1·56	+3·02	+3·48	+3·53	+3·59	+3·55
1.....	+1·35	+1·43	+1·72	+1·82	+2·11	+3·33	+3·71	+3·67	+3·68	+3·61
2.....	+2·34	+2·37	+2·58	+2·56	+2·70	+3·67	+3·93	+3·82	+3·78	+3·67
3.....	+3·31	+3·32	+3·47	+3·27	+3·26	+4·00	+4·14	+4·96	+3·87	+3·73
4.....	+4·30	+4·25	+4·34	+4·01	+3·83	+4·30	+4·34	+4·11	+3·96	+3·79
m.....	$\cdot0_4 77$	$\cdot0_3 154$	$\cdot0_3 385$	$\cdot0_3 77$	·00154	·005297	·01060	·02119	·0443	·0887

(viii.) $\left[Co\begin{matrix}NCS\\(NH_3)_5\end{matrix}\right]I_2$ in *m* $La(SCN)_3$.

0.....	+2·18	+2·43	+2·61	+3·39	+3·56	+5·10	+5·15	+5·01	+4·67	+4·41
1.....	+3·11	+3·30	+3·26	+3·81	+3·83	+5·23	+5·23	+5·07	+4·70	+4·43
2.....	+4·02	+4·16	+3·96	+4·21	+4·12	+5·35	+5·31	+5·13	+4·74	+4·45
3.....	+4·96	+5·00	+4·69	+4·64	+4·40	+5·46	+5·40	+5·21	+4·77	+4·48
4.....	+5·88	+5·84	+5·39	+5·07	+4·70	+5·55	+5·50	+5·31	+4·80	+4·51
m.....	$\cdot0_4 77$	$\cdot0_3 154$	$\cdot0_3 385$	$\cdot0_3 77$	·00154	·005297	·01060	·02119	·0443	·0887

experimental data. The results of the calculations under cases (A) and (B) are given in Tables II. and III. respectively; in these tables a_0 and a are in Å.U., and the results in each series are numbered in the same way as in Table I. For case B the results for $La(SCN)_3$ due to O'Neill and Partington (*loc. cit.*) are included.

It is clear from these tables that constant values of a over a range of concentration of solvent salt are not obtained by the application of the Debye-Hückel theory with either assumption (A) or (B). With assumption (A), in fact, the a-values are often negative and thus physically impossible, and although in (B) such negative values can be obviated by a suitable choice of a_0, the necessary a_0-value is in some cases improbably high.

Hückel (*Phys. Zeit.* xxvi. p. 93 (1925)) attempted to take into account the variation of the dielectric constant D of the solution with the concentration according to the linear formula

$$D = D_0 - \sum_i \alpha_i n_i \quad . \quad . \quad . \quad . \quad . \quad . \quad (5)$$

(n_i=number of ions of species i present, α_i are +ve constants, D_0=dielectric constant of pure solvent.) This leads to the equation

$$-\log f = \frac{2 \times 0{\cdot}5065\sqrt{\mu}}{1 + a\sqrt{\mu} \,.\, 10^8 \times 0{\cdot}3287} - C\mu, \quad . \quad . \quad (6)$$

instead of (2), where C is a constant. In order to see whether the equation would account for the variability of the Debye-Hückel a-values, the following graphical procedure was employed. The theoretical value of $\log \frac{S}{S_0}$, *i. e.*, $-\log \frac{f}{f_0}$, was calculated from (2), and the deviation between the experimental and theoretical values,

$$\triangle = \log \frac{S}{S_0} (\text{expt.}) + \log \frac{f}{f_0} (\text{theor.}), \quad . \quad . \quad . \quad (7)$$

was plotted against μ, using in turn the values a=0, 1, 2, 3, 4, and 5 Å. in the application of case (A); in applying case (B) the same procedure was adopted, using each of these values of a for each assumed value of a_0 (a_0=1, 2, 3, 4, and 5 Å.). If the second term on the right of (6) were correct, then for some value of a

in case (A), or, in case (B), for some chosen values of both a_0 and a, these plots should give a straight line, of slope $-C$, passing through the origin. The curves actually obtained were not linear for any positive value of a, but were irregular, the departure from linearity being most marked in the regions of low μ. A similar series of plots of Δ against $\sqrt{\mu}$, made with the object of testing the possibility of the correction-term being of the form $-C\sqrt{\mu}$, gave results of the same irregular kind.

(ii.) *The La Mer Extension of the Debye-Hückel Theory.*

The more complete mathematical solution of the Poisson-Boltzmann equation underlying the Debye-Hückel theory leads to the following equations for a 2 : 1 electrolyte in the presence of a second electrolyte in water at 25° (La Mer, Gronwall, and Greiff, *J. Phys. Chem.* xxxv. p. 2245 (1931)), when the dielectric constant for water at 25° is taken as 78·54 (Wymann, *loc. cit.*) :—

$$\begin{aligned}-\log f = 2\Big\{ & 1{\cdot}5407\frac{1}{10^8 a}\frac{x}{1+x} \\ & +0{\cdot}21862\,\frac{{q_2}^2}{(10^8a)^2}\,10^2[\mathrm{X}_2(x)-\mathrm{Y}_2(x)] \\ & +0{\cdot}43724\,\frac{q_2}{(10^8a)^2}(1-q_2)10^2\mathrm{Y}_2(x) \\ & -0{\cdot}15511\,\frac{{q_2}^2q_3}{(10^8a)^3}\,10^3[\tfrac{1}{2}\mathrm{X}_3{}^*(x)-2\mathrm{Y}_3{}^*(x)] \\ & -0{\cdot}15511\,\frac{{q_3}^2}{(10^8a)^3}\,10^3([\tfrac{1}{2}\mathrm{X}_3(x)-2\mathrm{Y}_3(x)] \\ & -0{\cdot}15511\,\frac{q_2}{(10^8a)^3}(2q_3+3q_2-3q_2q_3)10^3\mathrm{Y}_3{}^*(x) \\ & -0{\cdot}31022\,\frac{q_3}{(10^8a)^3}(3-q_3)10^3\mathrm{Y}_3(x)\Big\}, \quad . \quad . \quad . \quad (8)\end{aligned}$$

where

$$x = 0{\cdot}3287\times10^8 a\sqrt{\mu} \quad . \quad . \quad . \quad . \quad . \quad (9)$$

and q_2 and q_3 are obtained by putting $\nu=2$ and 3 in

$$q_\nu = \frac{n(\nu_1{z_1}^{\nu+1}+\nu_2{z_2}^{\nu+1})+n'(\nu_3{z_3}^{\nu+1}+\nu_4{z_4}^{\nu+1})}{n(\nu_1{z_1}^2+\nu_2{z_2}^2)+n'(\nu_3{z_3}^2+\nu_4{z_4}^2)}, \quad (10)$$

in which n denotes the concentration of electrolyte, the activity coefficient of which is f, and which gives rise to ν_1 cations (valency z_1) and ν_2 anions (valency z_2) per molecule, while n', ν_3, ν_4, z_3, z_4 are the corresponding quantities referring to the other electrolyte, all valencies having the correct algebraic signs. The X and Y functions of x are tabulated by the above authors (see also Gronwall, La Mer, and Sandved, *Phys. Zeit.* xxix. p. 358 (1928)) for values of x ranging from 0 to at least 0·40 (also higher values for some of the functions).

In the case where the solvent and solute salts are of the same valency type (*i. e.*, when $Ba(SCN)_2$ is the solvent salt in the present work) q_2 and q_3 take the constant values 1 and 3 respectively and are independent of S and m (i. e., n and n'), and (8) simplifies to the form of the equation given by La Mer, Gronwall, and Greiff for the case of a single electrolyte in solution, viz.,

$$-\log f = 2\left\{ 1{\cdot}5407 \cdot \frac{1}{10^8 a} \cdot \frac{x}{1+x} \right.$$

$$+0{\cdot}21862 \frac{1}{(10^8 a)^2} 10^2[\mathrm{X}_2(x) - \mathrm{Y}_2(x)]$$

$$-0{\cdot}15511 \frac{3}{(10^8 a)^3} 10^3[\tfrac{1}{2}\mathrm{X}_3{}^*(x) - 2\mathrm{Y}_3{}^*(x)]$$

$$\left. -0{\cdot}15511 \frac{9}{(10^8 a)^3} 10^3[\tfrac{1}{2}\mathrm{X}_3(x) - 2\mathrm{Y}_3(x)] \right\} . \quad . \quad (11)$$

In the general equation corresponding to (8) as originally published by La Mer, Gronwall, and Greiff, the powers of 10 are omitted in every term but the first, an error repeated by Chloupek, Daneš, and Danešova (*Coll. Czech. Chem. Comm.* v. p. 21 (1933)), who, however, pointed out another error in the original publication, namely, the incorrect use of q_2 instead of q_3 in the numerator of the fraction in the last term.

Equations (8) and (11) were applied in the calculation of a from experimental results in precisely the same way as for the Debye-Hückel equation, except that direct algebraic solution for a was impossible, as the equations corresponding to (4) were now of infinite degree in a, since the X and Y functions of x ($=0{\cdot}3287 \times 10^8 \sqrt{\mu} \cdot a$) are infinite series in x. A graphical method was there-

TABLE IV.—La Mer a-values in Å. Case (A).

No.	1.	2.	3.	4.	5.	6.	7.	8.	9.	10.	11.
(i.) $\left[\mathrm{Co}\begin{matrix}\mathrm{NCS}\\(\mathrm{NH_3})_5\end{matrix}\right]\mathrm{I_2}$ in NaSCN.											
m	$\cdot0_3$1213	$\cdot0_3$2426	·001213	·002426	·005192	·01038	·02077	·05192	·1038		
a.....	<1	<1	1·61	4·45	5·75	4·85	5·16	4·90	4·98		
(ii.) $\left[\mathrm{Co}\begin{matrix}\mathrm{NCS}\\(\mathrm{NH_3})_5\end{matrix}\right]\mathrm{I_2}$ in KSCN.											
m	$\cdot0_3$1004	$\cdot0_3$5018	·001004	·002007	·005481	·01096	·02192	·05481	·1151	·2016	
a.....	<1	0·73	4·05	4·51	3·50	4·07	4·28	4·18	4·28	4·02	
(iii.) $\left[\mathrm{Co}\begin{matrix}\mathrm{NCS}\\(\mathrm{NH_3})_5\end{matrix}\right]\mathrm{I_2}$ in $\mathrm{Ba(SCN)_2}$.											
m	$\cdot0_3$1079	$\cdot0_3$2696	$\cdot0_3$5393	·001079	·002424	·004849	·009697	·02424	·04849	·08339	
a.....	4·33	7·00	*ca.* 8·5	*ca.* 12·0	*ca.* 7·1	6·60	5·66	4·90	4·39	4·30	
(iv.) $\left[\mathrm{Co}\begin{matrix}\mathrm{NCS}\\(\mathrm{NH_3})_5\end{matrix}\right](\mathrm{NO_3})_2$ in NaSCN.											
m	$\cdot0_3$1213	$\cdot0_3$2426	$\cdot0_3$4851	·001213	·002426	·005192	·01038	·02077	·05192	·1038	
a.....	1·18	0·97	0·98	0·99	1·67	2·40	2·73	2·31	2·69	2·96	
(v.) $\left[\mathrm{Co}\begin{matrix}\mathrm{NCS}\\(\mathrm{NH_3})_5\end{matrix}\right](\mathrm{NO_3})_2$ in KSCN.											
m	$\cdot0_3$1004	$\cdot0_3$5018	·001004	·002007	·005481	·01096	·02016	·02192	·05040	·1008	·2016
a.....	1·03	1·14	1·68	4·69	3·72	3·19	3·40	3·21	3·07	2·77	2·68
(vi.) $\left[\mathrm{Co}\begin{matrix}\mathrm{NCS}\\(\mathrm{NH_3})_5\end{matrix}\right](\mathrm{NO_3})_2$ in $\mathrm{Ba(SCN)_2}$.											
m	$\cdot0_3$1079	$\cdot0_3$2696	$\cdot0_3$5393	·001079	·002424	·004849	·009697	·02424	·04849	·08339	
a.....	1·98	1·27	1·29	2·22	2·63	2·79	3·28	3·06	2·69	2·80	

TABLE V.—La Mer a-values in Å. Case (B).

a_0/No.	1.	2.	3.	4.	5.	6.	7.	8.	9.	10.	11.
(i.) $\left[\mathrm{Co}\begin{smallmatrix}\mathrm{NCS}\\(\mathrm{NH_3})_5\end{smallmatrix}\right]\mathrm{I_2}$ in NaSCN.											
3.....	2·45	2·17	2·70	3·42	4·40	4·20	4·65	4·69	4·78		
3·5.....	2·81	2·38	3·00	3·85	4·77	4·44	4·83	4·75	4·85		
4.....	3·11	2·55	3·25	4·20	5·04	4·62	4·96	4·80	4·90		
4·5.....	3·44	2·79	3·50	4·54	5·27	4·76	5·06	4·88	4·95		
5.....	3·70	2·98	3·75	4·78	5·40	4·85	5·13	4·92	4·98		
(ii.) $\left[\mathrm{Co}\begin{smallmatrix}\mathrm{NCS}\\(\mathrm{NH_3})_5\end{smallmatrix}\right]\mathrm{I_2}$ in KSCN.											
2.....	1·77	1·92	2·19	2·43	2·55	3·06	3·51	3·74	3·98	3·82	
3.....	2·48	2·65	3·16	3·41	3·23	3·69	3·96	4·02	4·15	3·95	
4.....	3·20	3·37	4·01	4·17	3·73	4·04	4·21	4·15	4·25	4·02	
4·5.....	3·52	3·72	4·43	4·52	3·92	4·19	4·35	4·21	4·31	4·05	
5.....	3·83	3·97	4·82	4·87	4·08	4·31	4·44	4·26	4·37	4·07	
(iii.) $\left[\mathrm{Co}\begin{smallmatrix}\mathrm{NCS}\\(\mathrm{NH_3})_5\end{smallmatrix}\right]\mathrm{I_2}$ in $\mathrm{Ba(SCN)_2}$.											
3.....	3·11	3·51	4·40	6·20	5·37	5·62	5·08	4·62	4·25	4·24	
4.....	4·03	4·50	5·42	7·00	5·95	5·91	5·34	4·81	4·35	4·30	
4·5.....	4·50	4·95	5·80	7·29	6·15	6·05	5·42	4·88	4·40	4·34	
5.....	4·93	5·35	6·10	7·50	6·26	6·18	5·48	4·91	4·45	4·38	
6.....	5·82	6·17	6·72	7·85	6·56	6·40	5·61	5·01	4·50	4·43	
(iv.) $\left[\mathrm{Co}\begin{smallmatrix}\mathrm{NCS}\\(\mathrm{NH_3})_5\end{smallmatrix}\right](\mathrm{NO_3})_2$ in NaSCN.											
2.....	1·99	1·97	1·93	1·86	1·95	2·07	2·18	2·14	2·36	2·67	
2·5.....	2·49	2·46	2·43	2·32	2·42	2·47	2·57	2·42	2·61	2·84	
3.....	2·97	2·92	2·87	2·70	2·81	2·85	2·91	2·66	2·80	2·96	
4.....	3·92	3·77	3·65	3·35	3·45	3·51	3·42	2·98	3·02	3·15	

(v.) $\left[\text{Co}\begin{matrix}\text{NCS}\\(\text{NH}_3)_5\end{matrix}\right](\text{NO}_3)_2$ in KSCN.									
2	1·99	1·98	2·10	2·18	2·20	2·42	2·38	2·59	2·44	2·52
2·5	2·49	2·46	2·47	2·60	2·66	2·85	2·78	2·83	2·70	2·64
3	2·98	2·89	2·91	3·10	3·13	3·05	3·21	3·05	2·85	2·73
4	3·96	3·77	3·78	4·08	3·93	3·68	3·70	3·59	3·31	3·06	2·81
(vi.) $\left[\text{Co}\begin{matrix}\text{NCS}\\(\text{NH}_3)_5\end{matrix}\right](\text{NO}_3)_2$ in $\text{Ba}(\text{SCN})_2$.									
2	1·86	1·84	2·04	2·18	2·28	2·63	2·71	2·54	2·65
2·5	2·48	2·20	2·43	2·55	2·62	2·93	2·90	2·68	2·80
3	2·66	2·48	2·75	2·83	2·88	3·18	3·06	2·77	2·88
4	3·36	3·04	3·40	3·37	3·32	3·56	3·26	2·87	3·00
2·88	2·80	2·57	2·37	2·65	2·73	2·82	3·10	3·02	2·76	2·81
(vii.) $\left[\text{Co}\begin{matrix}\text{NCS}\\(\text{NH}_3)_5\end{matrix}\right]\text{I}_2$ in $\text{La}(\text{SCN})_3$.									
3	4·74	4·71	4·62	4·60	4·44	5·15	5·11		
4	5·51	5·55	5·40	5·24	4·96	5·38	5·33		
4·5	5·86	5·93	5·78	5·53	5·21	5·48	5·43		
5	6·22	6·30	6·18	5·82	5·43	5·60	5·54		
(viii.) $\left[\text{Co}\begin{matrix}\text{NCS}\\(\text{NH}_3)_5\end{matrix}\right](\text{NO}_3)_2$ in $\text{La}(\text{SCN})_3$.									
2·5	3·02	3·01	3·23	3·33	3·32	3·79	3·85		
3	3·38	3·37	3·55	3·57	3·56	3·90	3·92		
3·5	3·81	3·80	3·91	3·85	3·80	4·02	4·00		
4	4·30	4·30	4·32	4·18	4·08	4·15	4·09		

fore used; in case (A) the theoretical value of $\log\frac{f_0}{f}$ was calculated for various integral values of a, and then by graphical interpolation the value of a, which made Δ vanish, was obtained; for case (B) the same procedure was adopted for each arbitrarily assumed a_0-value. This graphical method was tested by using it with the Debye-Hückel equation, when the resulting a-values could be compared with those calculated algebraically; it was found that the error in a never exceeded 0·03 Å., which is approximately the error due to the 0·1 per cent. experimental error in the solubility determinations.

These values of a graphically obtained are given in Table IV. for case (A) (i. e. $a_0=a$), and in Table V. for case (B) (a_0 not necessarily equal to a), the results for $La(SCN)_3$ due to O'Neill and Partington (*loc. cit.*) being included for the latter case.

The series in section (vi.) of Table V. for $a_0=2{\cdot}88$ Å. was included because this value of a_0 gives, with the La Mer equation, the same value of $-\log f_0$ for the nitrate (viz., 0·1030) as is obtained by putting $a_0=0$ in the Debye-Hückel equation (*i. e.*, the "limiting law"); La Mer Gronwall, and Greiff (*loc. cit.*) calculated $-\log f_0$ in this way for their solubility results, assuming that in the region where μ is lower than corresponds with S_0 the "limiting law" holds good. It seems that this procedure does not lead to the most constant series of a-values with the present results; a similar conclusion is reached on using the corresponding value $a_0=3{\cdot}15$ Å. for the iodide.

Both assumptions (A) and (B) lead to exclusively positive values of a on the La Mer theory, which is an improvement on the results obtained by the Debye-Hückel equation. The results from (A), however, vary considerably in any given series, and in view of the improbability of assumption (A) holding good if the solvent and solute salts are separately characterized by different a-values, these results will receive no further attention.

If we now consider the La Mer a-values derived on assumption (B), it is seen that, apart from some of the earlier results in each $\left[\mathrm{Co}\begin{matrix}\mathrm{NCS}\\(\mathrm{NH_3})_5\end{matrix}\right]\mathrm{I_2}$ series, where great

irregularities occur, a value of a_0 can be chosen for each series, which makes the resulting a-values reasonably constant. A little ambiguity certainly exists as to the precise a_0-value to be taken in any given series, since there is often little to decide between the superiority of two different a_0-values which differ at the most by 1/2 to 1 Å. This ambiguity can be removed in the following manner. For the solubilities of $\left[\mathrm{Co}\begin{matrix}\mathrm{NCS}\\(\mathrm{NH_3})_5\end{matrix}\right]\mathrm{I_2}$ we may choose the best a_0-values as below, the results for $\mathrm{La(SCN)_3}$ due to O'Neill and Partington (*loc. cit.*) being included :—

In NaSCN	a_0=4 or 3·5 Å (ambiguous)		
,, KSCN	a_0=4 or 4·5 Å.	,,	
,, $\mathrm{Ba(SCN)_2}$	a_0=4 or 4·5 Å.	,,	
,, $\mathrm{La(SCN)_3}$	a_0=4 or 4·5 Å.	,,	(O'Neill and Partington, a_0=5 Å.)

Since a_0=4 Å. is the only value common to all the four thiocyanates, this is the value chosen.

The method of choosing these most suitable a_0-values, from which a final selection is made, is to evaluate for each a_0-value the average a-value to which it gives rise, and thence the average absolute deviation of the individual a-value from the mean and also the range (difference between the largest and smallest) of the a-values. Those a_0-values which produce the smallest values of the range and of the mean absolute deviation from the mean a are chosen as the most suitable.

For the measurements with $\left[\mathrm{Co}\begin{matrix}\mathrm{NCS}\\(\mathrm{NH_3})_5\end{matrix}\right]\mathrm{I_2}$ only those results corresponding with a concentration greater than *ca.* 0·002 m./l. of $\mathrm{Ba(SCN)_2}$, or *ca.* 0·005 m./l. of NaSCN or KSCN, were used in evaluating these averages ; by this means all the large irregularities earlier in the series were avoided. This was done with the object of comparing the results with those of similar measurements and calculations of Chloupek, Daneš, and Danešova (*Coll. Czech. Chem. Comm.* v. p. 21 (1933) ; vi. p. 116 (1934)), in which no large irregularities were observed ; the minimum concentrations of solvent salt were, however, always 0·005 m./l. for a 1 : 1 salt (*e. g.*, $\mathrm{KNO_3}$) and 0·002 m./l. for a 2 : 1, 1 : 2 or higher valency type salt

($MgCl_2$, K_2SO_4, $MgSO_4$). Since the irregularities in the present results occur with concentrations of solvent salt below these limits, it was thought that there might be some connexion between the irregularities and the low concentration of solvent salt; this point is referred to later.

With $\left[Co\begin{matrix}NCS\\(NH_3)_5\end{matrix}\right](NO_3)_2$ no such irregularites occur; in fact, for any given value of a_0 the mean value of a is scarcely changed (*ca.* 0·05 Å.) by including the earlier results in the series. For this salt the best a_0-values are :—

In NaSCN a_0=2·5 or 3 Å.
,, KSCN a_0=3 Å.
,, $Ba(SCN)_2$ a_0=2·5 or 3 Å.
,, $La(SCN)_3$ a_0=3·5 Å. (O'Neill and Partington, a_0=3·72 Å.).

TABLE VI.

Mean Values of a in Å. (La Mer equation).

	$\left[Co\begin{matrix}NCS\\(NH_3)_5\end{matrix}\right](NO_3)_2$ (a_0=3·0.)	$\left[Co\begin{matrix}NCS\\(NH_3)_5\end{matrix}\right]$ (a_0=4·0.)
NaSCN	a=2·85	a=4·86
KSCN	a=3·03	a=4·07
$Ba(SCN)_2$	a=2·84	a=5·11
$La(SCN)_3$	a=3·88	a=5·34

Here, although 3·5 Å. is best for $La(SCN)_3$, the general value 3 Å. is chosen as being most suitable for the other three thiocyanates, and it differs by only 1/2 Å. from the present value for $La(SCN)_3$. The tables show that this difference in a_0 will not cause a very appreciable difference in the corresponding values of a.

The mean values of a obtained by using these finally selected a_0-values in the various series are given in Table VI.

The mean a-values of Table VI. might be expected to be approximately the sum of the cationic and anionic

radii for each thiocyanate. Since the anion is common, the order of increasing magnitude and the numerical differences of the a-values for the four thiocyanates should then be constant, independent of the solute salt, and also identical with the corresponding quantities derived from the crystallographic radii quoted in Table VII. (Pauling, J. A. C. S. xlix. p. 765 (1927); Goldschmidt, Trans Far. Soc. xxv. p. 253 (1929); Wasastjerna, *Soc. Sci. Fenn. Comm. Phys., Math.* xxxviii. p. 1 (1923)).

TABLE VII.

Crystallographic Cationic Radii.

	Pauling.	Goldschmidt.	Wasastjerna.
Na^+	0·95 Å.	0·98 Å.	1·01 Å.
K^+.....	1·33 „	1·33 „	1·30 „
Ba^{++} ...	1·35 „	1·43 „	1·40 „
La^{+++} ..	1·15 „	1·22 „	—

These indicate that

$$r_{Na^+} < r_{La^{+++}} < r_{K^+} < r_{Ba^{++}},$$

the average values of the differences of ionic radius being

$$r_{Na^+} - r_{La^{+++}} = 0{\cdot}22 \text{ Å.}, \qquad r_{La^{+++}} - r_{K^+} = 0{\cdot}12 \text{ Å.},$$

$$r_{K^+} - r_{Ba^{++}} = 0{\cdot}07 \text{ Å.}$$

The order of the experimental a-values in Table VI. and the numerical differences are not identical with the crystallographic data, and they alter when the solute salt is changed. We must, therefore, conclude that the mean a-value is not characteristic of the solvent salt; it is evidently affected by both salts present, and is characteristic of neither separately. This conclusion is unexpected, since in most of the cases investigated in which only one salt is present in solution the La Mer mean a-value, calculated from experimental results, agrees fairly well with the sum of the crystallographic radii of the anion and cation of the salt. Thus, La Mer and Cowperthwaite (J. A. C. S. liii. p. 4333 (1931)) found $a = 3{\cdot}64$ Å. for $ZnSO_4$, while crystallographic

data give 3·83 Å. for the mean distance between the centres of the Zn and S-atoms, and in those cases where a marked difference is found between the two sets of values there is always the possibility of some plausible explanation on the grounds of incomplete ionization or great deformation of an ion (La Mer, Cowperthwaite, and Barksdale, J. A. C. S., lvi. p. 544 (1934), find $a=0{\cdot}93$ Å. for TlCl; Goldschmidt's ionic distances indicate $a=3{\cdot}3$ Å.).

Chloupek, Daneš, and Danešova (*loc. cit.*) have investigated the solubilities of Ce $(IO_3)_3$ and of $Ca(IO_3)_2$ in a series of four solvent salts; they find, on applying the La Mer equations, a-values which are fairly constant in each series. The average values are given in Table VIII.

TABLE VIII.

Mean a-values in Å. (La Mer equation).

	$Ce(IO_3)_3$ ($a_0=3{\cdot}5$).	$Ca(IO_3)_2$ ($a_0=3{\cdot}45$).
KNO_3	$a=3{\cdot}6$	$a=3{\cdot}41$
K_2SO_4.....	$a=3{\cdot}35$ (omitting last result in average)	$a=3{\cdot}38$
$MgSO_4$	$a=3{\cdot}27$	$a=3{\cdot}46$
$MgCl_2$.....	$a=3{\cdot}57$	$a=3{\cdot}6$

For $Ce(IO_3)_3$ the order in increasing size of a is $MgSO_4<K_2SO_4<MgCl_2<KNO_3$, while for $Ca(IO_3)_2$ it is $K_2SO_4<KNO_3<MgSO_4<MgCl_2$. These results also show that the a-value is not characteristic of any single salt in the mixed solution, even if one is present in amounts negligibly small as compared with the other, but depends on all the ions present.

It is tacitly assumed in both the Debye-Hückel and the La Mer treatments that a represents some sort of mean value of the ionic diameter for all the ions present, the diameter being regarded as physically real for each ion and identical with the actual diameter of the ion, any rigidly bound solvent molecules being included. Whilst the agreement between the La Mer a-values

for several single electrolytes in solution and the crystallographic data indicates that in such cases a has a true physical significance, the results for mixed electrolytes do not seem to support this view. The precise sort of mean, weighted or otherwise, to be used in the latter case is a matter of doubt. For a solution containing two electrolytes with concentrations c_1, c_2, and mean ionic diameters a_1, a_2 respectively, the mean ionic diameter a for the whole solution is, according to Macdougall ('Thermodynamics and Chemistry,' 1926, p. 279):

$$a = \frac{c_1 a_1 + c_2 a_2}{c_1 + c_2}, \quad . \quad . \quad . \quad . \quad . \quad (12)$$

and according to Crockford and Thomas (J. A. C. S. lv. p. 568 (1933)) for two electrolytes of the same valency type:

$$a = \frac{c_1^2 a_1 + c_2^2 a_2}{c_1^2 + c_2^2} . \quad . \quad . \quad . \quad . \quad . \quad (13)$$

Neither formula applies to any of the present results or to those of Chloupek, Daneš and Danešova (*loc. cit.*), since according to (12) or (13) a cannot be constant unless $\frac{c_1}{c_2}$ is kept constant; and further, for a given set of solvent salts these equations would both lead to sets of a-values having the same order of increasing magnitude, independent of the solute salt. Both these deductions are contrary to the experimental results. It would seem, then, that for mixed electrolytes a does not necessarily represent a physical reality, but is rather to be considered as a purely mathematical parameter having some undefined connexion with ionic sizes, or, as Banks, Righellato and Davies (Trans. Far. Soc. xxvii. p. 621 (1931)) suggest, a property of the salts rather than of the ions, *i. e.*, a "chemical" rather than a "physical" attribute. Anomalous values of a derived from calorimetric measurements (Lange and Streeck, *Naturwissenschaften*, xxix. p. 259 (1931)) point in the same direction, although the experimental errors in this case are necessarily somewhat larger than those of other methods.

The irregularities in a found with small amounts of solvent salt (except $La(SCN)_3$), along with solute salt

$\left[\mathrm{Co}\begin{matrix}(\mathrm{NH_3})_5\\ \mathrm{NCS}\end{matrix}\right]\mathrm{I_2}$, cannot be due to a relatively large effect of atmospheric carbon dioxide on $\sqrt{\mu}$ when this is low, since the concentration of electrolyte ($H^+ + HCO_3'$), due to CO_2 in "equilibrium water" at 25° C., is $2{\cdot}05 \times 10^{-6}$ m./l. (Kendall, J. A. C. S. xxxix. p. 2465 (1917)), which is negligible as compared with at least 0·0009 m./l. of iodide present in all the solutions used. The irregularities may be due to incomplete washing of iodide, since it is freed from other electrolytes only with great difficulty, as is shown by the relatively poor reproducibility of S_0. Alternatively, as Neumann (J. A. C. S. lv. p. 879 (1933) suggests, the relatively great influence of small experimental errors in the solubility measurements upon the value of a when μ is very low may be the real cause.

One of the authors (H. I. S.) thanks the Department of Scientific and Industrial Research and the Chemical Society for grants which enabled this work to be carried out.

Summary.

The solubilities of *iso*-thiocyanato-pentammine-cobaltic nitrate and *iso*-thiocyanato-pentammine-cobaltic iodide have been determined in the presence of sodium, potassium, and barium thiocyanates.

Neither the simple limiting law of Debye and Hückel (point-ions) nor the first Debye-Hückel approximation (finite ion diameters) provide a satisfactory explanation of the experimental results. The modification due to Hückel, introducing the effect of concentration on dielectric constant, is also unsatisfactory.

The La Mer equation for unsymmetrical electrolytes gives a satisfactory explanation of the experimental data for ionic strengths up to at least 0·52, provided it is not assumed that $a = a_0$ in calculating mean ionic diameters, or that the mean ionic diameters calculated for mixed electrolytes in solution have any physical relation to crystallographic ionic diameters of individual ions.

Queen Mary College,
University of London.

LXXIII. *Vibrations of a Liquid Membrane exposed to High-Frequency Sound-Waves.* *By* JUL. HARTMANN *and* P. V. MATHES *.

[Plates VI. & VII.]

IN fig. 1 (Pl. VI.) is shown a photograph of a plane soap-film exposed to sound-waves of a frequency of 12,400 cycles per sec. and an intensity of ab. 3·4 erg/cm.^{3} measured at the surface of the film, which was hit perpendicularly by the waves. The diameter of the circular film was 7·2 mm. Its thickness was of the order of size of 1–3 hundredths of a millimetre. The photograph was produced by means of the optical arrangement indicated in fig. 2. G is the acoustic generator, a Hartmann air-jet

Fig. 2.

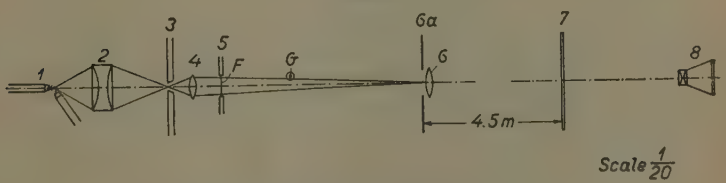

Arrangement for the observation of the effect of the sound-waves on the film.

generator †, F is the soap-film. Lens 4 forms an image of the illuminated slit in screen 3 on the iris diaphragm 6 *a*. Lens 6, again, produces an image of the surface of the film on the frosted glass screen 7. This image may be directly observed or a photograph of it may be taken by camera 8. Obviously the optical arrangement is that corresponding to the method of striæ. If the thickness of the film is not uniform but varying from point to point, say as indicated in fig. 3, then the bundle of light rays passing a certain zone of the film, for instance the zone *cd*, may by diffraction be bent off from the aperture of the iris diaphragm D, and so the corresponding zone will appear dark in the image on 7 or in the photograph. According as the image of the illuminated slit in 3 is, with no film, formed

* Communicated by the Authors.
† Phil. Mag. xi. p. 926 (1931).

at the centre of the diaphragm D or laterally with regard to the aperture, *i. e.*, outside the edge of the same, the aspect of the photograph varies. In the photograph (Pl. VI. fig. 1) the image of the slit was made to fall at the centre of the diaphragm. With other photographs the image was formed laterally to the aperture (Pl. VI. figs. 4 *a* & *b*) or below the same (Pl. VII. figs. 5 *a–f*).

The soap solution was made from "Lux" soap. About 10 g. of this material was dissolved in 80 cm.^{3} water, and 20 cm.^{3} glycerine was added, after which the solution was left to itself for 24 hours. From the product the appropriate solutions were made by adding 50–100 per cent. water.

We pass on to describe in detail a series of observations made with the arrangement indicated above. In the

Fig. 3.

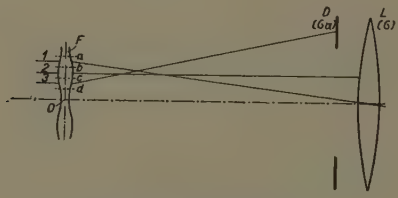

Explanation of the *modus operandi* of the optical arrangement.

latter the film was placed vertically. At the first moment after its production it was generally still too thick to be influenced visibly by the waves. Through the flow of liquid from its uppermost part this part would, however, in due time be reduced to a thickness at which it was able to respond to the action of the waves. Then the regularly arranged granules would appear covering smaller or larger zones of the film. The granulated zones would persist, though not in unaltered configuration, for some time without any appreciable change in the distance between the granules. When at last the thickness of the film had gone down under a certain limit the regularity of the granulation would cease shortly before the breakdown of the film. Figs. 4 *a* & *b* (Pl. VI.) are to illustrate the stage of regular "granulation" and the final stage with a film of 3·3 mm. diameter. Finally,

the changes in the aspect of a film of rectangular shape $4 \times 1{\cdot}2$ mm. are illustrated in figs. 5 *a–f* (Pl. VII.).

Already in fig. 1 (Pl. VI.) it will be seen that the granules are not everywhere arranged in the regular manner characteristic of fig. 4 *a* (Pl. VI.). At the bottom of the zone covered by granules it would even seem that there is no distinct granulation at all, but instead of this something like ripples on the surface of a water pool. Figs. 5 *a–f* (Pl. VII.) indeed show that such ripples form the first stage of the phenomenon. It is here seen, how, when the film has reached the proper thickness, a train of ripples appears at the top of the rectangular film where the thickness is less than lower down. Gradually these ripples develop and cover more and more of the film. At a certain stage something new happens in that the ripples begin to break up in equidistant granules, the distance between two adjacent granules being nearly equal to the distance between two consecutive ripples (Pl. VII. fig. 5 *c*). Then soon after again a new phenomenon is observed. The granules will within a smaller or larger region of the film, (Pl. VII. fig. 5 *d*) rearrange themselves in that regular way illustrated so strikingly in the picture of the circular film. With the small rectangular film the granules strive to arrange themselves in the same way as with the circular, but obviously the process of rearrangement is somehow hampered, so that the result is not always altogether perfect though distinct. Otherwise the stages of the process are the same as above. When the film has reached a certain thinness the granulation becomes more or less diffuse as seen, for instance, in fig. 5*f* (Pl. VII.) representing the film just before its breakdown.

Together with the observations now reviewed measurements of the distance $\frac{\lambda f}{2}$ between the granules or between consecutive ripples were undertaken. In fig. 6 the results of a great many measurements are represented in their dependency of the length of the sound-waves. It would seem that the distance $\frac{\lambda f}{2}$ does not vary linearly with the wave-length λ_a of the sound, but rather in a parabolic manner apart from the conditions at quite small wave-lengths (below 5 mm.). The effect of such short waves has not yet been examined.

Now, as to the explanation of the observations, there can be no doubt that the ripples and granules are the

Fig. 6.

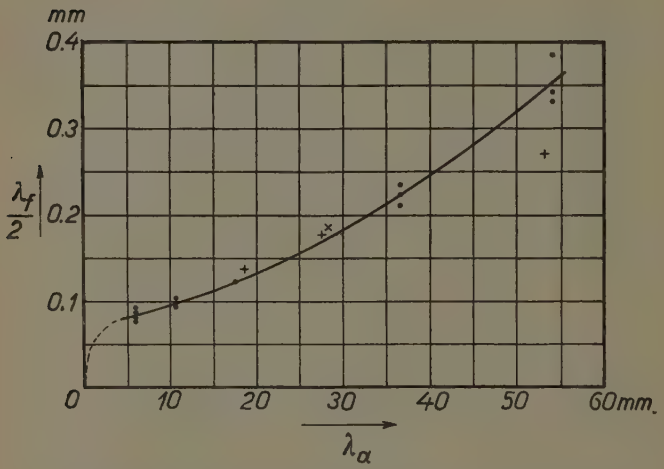

Variation of the distance between the granules or the ripples with the length of the sound-waves.
Points marked . from rectangular film with ripples.
Dimensions $4 \times 1{\cdot}2$ mm.^{2}.
Points marked + from circular film with granules.
Diameter 7·2 mm.
Points marked × from circular film with granules.
Diameter 3·34 mm.

Figs. 7, *a* & *b*.

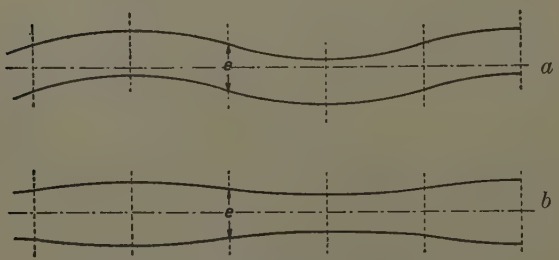

Transverse waves and capillary surface waves on a liquid film.

effect of stationary waves produced by the impact of the sound-waves. There are two types of waves to be considered. One is the transverse wave type indicated in fig. 7 *a* with which the film is bent as a whole into wave shape. The other type is that of capillary waves covering the two surfaces of the film as shown in fig. 7 *b*. In the former case the wave-length of the running or stationary waves is determined by

$$\lambda_f = \mathrm{T}\sqrt{\frac{2\mathrm{C}}{\rho e}}, \quad . \quad . \quad . \quad . \quad . \quad . \quad . \quad (1)$$

T being the period of the transverse vibrations, C the surface tension constant, ρ the density of the soap solution, and e the thickness of the film. An expression for the wave-length with the type in fig. 7 *b* may be derived from Lord Rayleigh's theory of capillary waves on the surface of a layer of liquid of the depth l in a tray with a horizontal bottom *. One only has to introduce half the thickness of the film, thus $\frac{e}{2}$, for l in Lord Rayleigh's formula :

$$\frac{\lambda^2}{\mathrm{T}^2} = \left(\frac{g}{2\pi}\lambda + \frac{\mathrm{C}}{\rho}\frac{2\pi}{\lambda}\tanh 2\pi\frac{l}{\lambda}\right) \quad . \quad . \quad . \quad (2)$$

As the action of gravitation will in our case be quite negligible and as $\frac{l}{\lambda} = \frac{e}{2\lambda}$ will be so small that $\tanh 2\pi\frac{l}{\lambda}$ may be replaced by $2\pi\frac{l}{\lambda}$, we derive from (2)

$$\lambda_f^2 = 2\pi\mathrm{T}\sqrt{\frac{\mathrm{C}e}{2\rho}} \quad . \quad . \quad . \quad . \quad . \quad . \quad (3)$$

Beforehand it would seem most likely that the impact of the sound-waves would give rise to waves of the transverse type in fig. 7 *a*. The question which of the two wave-types we are faced with may be settled by the introduction of numerical values for the constants in the formulæ (1) and (3) According to Lord Rayleigh the surface tension of a soap-film is at the first moment of its existence very closely equal to that of pure water, *i. e.*, 75 $\frac{\text{dyne}}{\text{cm.}}$ †. So we shall assume this value for C,

* 'Theory of Sound,' ii. second ed. p. 343 (1926).

† Royal Inst. Lecture, 28 March, 1890.

and for ρ we shall introduce the value 1. The thickness of the film is but roughly known. An idea of it was obtained in a curious way. Accidentally a film made of a rather strong solution solidified when covered partly by ripples. The film was mounted in a rectangular opening $4 \times 1{\cdot}2$ mm.^{2} cut in a mica sheet of 0·09 mm. thickness. Under a microscope it could be seen that the two surfaces with the ripples lay considerably under the corresponding surfaces of the mica sheet. From this observation it was estimated that the thickness of the film was 0·01 mm. or perhaps somewhat larger. If the value 0·001 cm. is introduced in (1) for e together with the values for C and ρ indicated above, we find, corresponding to $T = 10^{-4}$ sec., the wave-length $\lambda_f = 0{\cdot}39$ mm. Now from $T = 10^{-4}$ sec. a wave-length in air of $\lambda_a = 34$ mm. is calculated. From fig. 6 it is seen that sound-waves of this length produce ripples or granules a distance 0·21 apart. This is almost exactly equal to half the calculated value for λ_f, a strong evidence in favour of the conception that the ripples are the result of stationary transverse waves of the type indicated in fig. 7 *a*. If the same values as above are introduced in the formula (3) corresponding to the wave type of fig. 7 *b*, we find $\frac{\lambda_f}{2} = 0{\cdot}055$ mm., which is about four times smaller than the observed distance between the ripples. In order to raise the calculated $\frac{\lambda_f}{2}$ to the observed value, a thickness 2·56 mm. of the soap-film must be assumed. Such a thickness is, of course, quite out of the question.

The conception to which we are led by the above discussion is therefore as follows. The sound-waves impinging on the soap-film will, under certain conditions, set up trains of transverse waves on the film. These waves are reflected from the boundaries of the film and so stationary waves are produced. In the node lines of the latter liquid will accumulate, and so the ripples are formed which, again, under the influence of the sound-waves, will generally break up into granules. It should here be noted that it is, actually, not the solid boundaries of the film which act as reflectors but the liquid accumulations along the edges of the frame of the film (comp. Pl. VII. figs. 5 *a–f*). Again, it would seem that the

boundaries of the zones of granulation may also act as reflectors (Pl. VII. fig. 5 *d*).

Having established the origin of the ripples—and so of the granules too—we shall consider the question about their size. From a photograph like that of fig. 1 (Pl. VI.) one might get the impression that the height of the granules is almost of the same size as the distance between two adjacent granules. As the latter distance is, however, in the case considered 0·175 mm., and as the thickness of the film is a few hundredth of a millimetre at most, the conception suggested by the photograph is obviously false. In order to form an idea of how large must be at least the height of the granules in order to produce an optical effect of the kind in fig. 1, we may assume a small prism placed at the point O of the optical axis in fig. 3 with its plane of symmetry perpendicular to this axis. Such a prism of a small top angle α would refract an axial beam of light by an angle $\theta=(n-1)\alpha$, n being the coefficient of diffraction of the material of the prism. In the optical arrangement the distance from the film to the diaphragm D (fig. 3) was 60 cm., and the maximum diameter of the aperture of the diaphragm was 3 cm. So the axial beam of light would be deflected beyond the edge of the aperture if $\theta \geqq \frac{1\cdot5}{60}$, *i. e.*, if $\frac{\alpha}{2} \geqq \frac{1\cdot5}{60} \cdot \frac{1}{2(n-1)}$ or, with $n=1\cdot33$, if $\frac{\alpha}{2} \geqq \frac{1}{26\cdot4}$. If this condition is fulfilled the prism will appear dark on screen 7 (fig. 2). Thus, assuming the two surfaces of the film in fig. 1 to present sinusoidal undulations a minimum value of the amplitude y_0 in these undulations is determined by the formula $y_0 \cdot \frac{2\pi}{\lambda} = \frac{1}{26\cdot4}$. In fig. 1 λ was 0·175 mm., to which corresponds $y_0=0\cdot00105$ mm. In fig. 8 a film of 0·010 mm. thickness with such undulations is drawn in true proportions. Such, about, may be the real section of the film covered by the stationary waves apart from the feature that the thinner parts are performing transverse vibrations. The amplitude of these vibrations is undoubtedly very small, at any rate considerably less than the amplitude of the sound-waves, which at the surface of the film was about 0·01 mm. The vibrations

do not, of course, manifest themselves in the photographs. On the solidified film indicated above the ripples were plainly visible under suitable conditions of illumination. It could be established that the ripples were low compared to their mutual distance, but a direct measurement of their height proved unfeasible. In this connexion some observations with a curved soap-film and with a soap-bubble may be mentioned. When looked on radially the curved surface appeared dim, like a frosted lamp, while when regarded tangentially it was quite bright. Again, with the bubble an attempt was made at tracing a change of the excess-pressure in the interior of the bubble under the influence of sound-waves hitting the surface and producing the granulation described above. If there were any change it was below 1 per cent. of the excess-pressure.

Fig. 8.

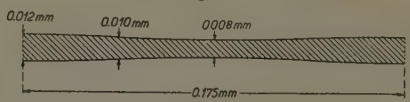

Probable shape of the section of the film with stationary transverse waves.

Possibly the most striking feature of the phenomenon in question is the breaking up into granules of the liquid accumulations or ridges along the node lines of the stationary waves, and the rearrangement of these granules in the regular triangular pattern. This breaking up is obviously the work of the surface tension, which makes the ridges unstable. The regularity of the division and the size of the distance between consecutive granules find, of course, their explanation in the fact that the film is continually battered by the sound-waves. It should be noted that, owing to the flatness of the ridges, waves along the latter must very closely have the same length as the stationary waves in which the ridges have their origin. The rearrangement of the granules further shows the great part the surface tension forces play in the phenomenon. The regular triangular pattern undoubtedly corresponds to a minimum of surface tension energy under the prevailing conditions, and this pattern does not interfere essentially with the

vibrations of the surface. *The natural state of vibration of a liquid film is thus obviously that to which three sets of stationary transverse waves under* 120° *with each other would give rise.* The setting up of this state does not meet with any greater difficulties with a film of an extension which is large compared to the distance between consecutive granules. Therefore, the triangular pattern is perfectly developed in Pl. VI. figs. 1 & 4 *a*. With the small rectangular films in Pl. VII. figs. 5 *a–f* the production of this pattern is hampered by boundary conditions. It would seem that one of the main directions of the triangular pattern must be parallel to the long sides of the rectangular film. On the other hand, the original stationary waves are formed by reflexion from the uppermost short side of the rectangle with which the ridges not yet broken up are therefore parallel. The two conditions lead to a controversy, in which the triangular pattern is apt to gain the upper hand (fig. 5 *d*), though the state of affairs will generally change from moment to moment.

A rather difficult point is the fact that the length of the stationary waves does not change appreciably during the time in which the waves can be observed. The phenomenon of granulation would seem bound to a rather definite value of the thickness of the film. When too thick, the amplitude of the transverse waves is too small to be observed. When the thickness of the film has become too small the film breaks down. In between there is no change in the length of the stationary waves, although it would seem most likely that the thickness of the film would undergo considerable changes. So far this point has not been cleared up. Again, there is the question why the liquid accumulates along the node lines with the stationary transverse waves. Although such an accumulation would not seem unlikely, as an effect of the vibrations of the film, the phenomenon calls for a theoretical discussion, which has, however, had to be postponed.

We take the opportunity of expressing our gratitude to the Trustees of the Carlsberg Foundation for financial support granted us in connexion with the above investigations.

Provisional Laboratory of Technical Physics,
Royal Technical High School, Copenhagen.

LXXIV. *The Frequency of Transverse Vibration of a Loaded Fixed-Free Bar.* *By* R. M. Davies, *M.Sc., F.Inst.P., Lecturer in Physics, University College of Wales, Aberystwyth* *.

Notation.

ρ = Density of the bar.
E = Young's Modulus of the material of the bar.
l = Length of the bar.
k = Radius of gyration of the cross-section of the bar about an axis through the centre of gravity, perpendicular to the plane of motion.
A = Area of cross-section.
$M' = \rho A l$ = Mass of the bar.
M = Mass of the load fixed to the free end of the bar.
$c = \frac{M}{M'}$ = Ratio of the mass of the load to the mass of the bar.
n = Natural frequency of vibration of the loaded bar when vibrating in the fundamental mode.
$\omega = 2\pi n$.
m = Frequency parameter (defined below).
$z = ml$; $\alpha = z^4$.

THE natural frequency of transverse vibration of a thin uniform bar of mass M′, fixed at one end, free at the other end, and loaded at the free end with a mass M devoid of rotatory inertia, is generally expressed in terms of the frequency parameter m, which is defined by the equation

$$m^4 = \frac{\rho\omega^2}{Ek^2} = \frac{4\pi^2\rho n^2}{Ek^2} \quad . \quad . \quad . \quad . \quad . \quad (1)$$

in the above notation. If z be substituted for ml, then equation (1) yields

$$n = \frac{k}{2\pi} \cdot \frac{z^2}{l^2} \sqrt{\frac{E}{\rho}} \quad . \quad . \quad . \quad . \quad . \quad . \quad (2)$$

The quantity z is a function of $M/M' = c$, and in order to express n in terms of the dimensions of the bar and the constants of the material of the bar it is necessary to

* Communicated by Vice-Principal Gwilym Owen, M.A., D.Sc.

find an expression for z in terms of c. This is the case in connexion with a method developed in this Laboratory [1] for the determination of Young's Modulus by a dynamical method using a loaded bar vibrating transversely; the accuracy of the experimental method is such that the error in the evaluation of z should not exceed 1 in 2000.

One method of deriving an expression for z in terms of c is an approximate method due to Rayleigh [2]; in this method a hypothetical type of displacement curve is assumed for the vibrating bar, and this displacement curve is used to calculate the kinetic and potential energies of the bar. The frequency can then be calculated in the usual way from the ratio of the kinetic and the potential energies.

The expression commonly used is a first approximation due to Rayleigh [2]; in the present notation this can be written

$$z_r^4 = \frac{3}{c+\frac{33}{140}} = \frac{3}{c+0{\cdot}23570}, \quad . \quad . \quad . \quad . \quad (3)$$

where z_r is the value of z given by this equation.

A more accurate expression of the same type is that due to Morrow [3], who uses a method of successive approximation for finding the displacement curve of the vibrating bar. In the present notation, z_m, the value of z given by Morrow, is

$$z_m^4 = \left\{ \frac{0{\cdot}00663084+0{\cdot}0261905\,c}{0{\cdot}08194+c/3} + \frac{c}{3} \right\}^{-1} . \quad . \quad (4)$$

An alternative method of deriving an expression for z in terms of c is to solve the differential equation of motion of the bar and to insert the boundary conditions appropriate to the free and fixed ends. This leads to the transcendental equation [4]

$$1+\cosh z \cos z = cz\,(\cosh z \sin z - \sinh z \cos z). \quad . \quad (5)$$

No explicit solution of this equation appears to have been given, and hitherto the equation has been solved for given values of c either by a graphical method or by a method of successive approximation. An approximate solution which is sufficiently accurate for the present purpose can be found by expansion in series of the terms

involving trigonometrical and hyperbolic functions in the equation.

Now [5],

$$1+\cosh z\cos z=2-\frac{2^2}{4!}z^4+\frac{2^4}{8!}z^8-\frac{2^6}{12!}z^{12}+\dots$$

$$=2-\frac{z^4}{6}+\frac{z^8}{2520}-\frac{z^{12}}{7{,}484{,}000}\dots, \quad . \quad . \quad (6)$$

and [5]

$$z(\cosh z\sin z-\sinh z\cos z)=2z\left(\frac{2z^3}{3!}-\frac{2^3z^7}{7!}+\frac{2^5z^{11}}{11!}-\dots\right)$$

$$=\frac{2z^4}{3}-\frac{z^8}{315}+\frac{z^{12}}{623{,}700}-\dots \quad (7)$$

These series are convergent for all values of z.

Using these expressions for the hyperbolic and trigonometrical functions, and putting $z^4=\alpha$, equation (5) becomes

$$2=\frac{(1+4c)}{6}.\alpha-\frac{(1+8c)}{2520}.\alpha^2+\frac{(1+12c)}{7{,}484{,}400}.\alpha^3-\dots \quad (8)$$

The relative magnitudes of the α, α^2, and α^3 terms in equation (8) will next be estimated. It is clear that the α, α^2, and α^3 terms are in descending order of magnitude, and retaining only the term in α it is seen that α is of the order of $12/(1+4c)$; α thus decreases as c increases. Using this estimate of the order of magnitude of α the ratio of the α^2 term to the α term is of the order of $\frac{1}{35}\cdot\frac{1+8c}{(1+4c)^2}$. This ratio is a maximum when $c=0$, and its value is then $1/35$; if $c>>1$, its value is $1/70\,c$. Similarly, the ratio of the α^3 term to the α term is of the order of $\frac{2}{17{,}325}\cdot\frac{1+12c}{(1+4c)^3}$; this ratio is a maximum when $c=0$, and the error committed in neglecting the α^3 term in comparison with the α term will thus never exceed 1 in 8000.

The α^3 term in equation (8) may thus be neglected, in which case the equation reduces to a quadratic equation in α whose roots are

$$\alpha=z^4=\frac{210}{8c+1}\left[(4c+1)\pm\sqrt{16c^2+\frac{31}{35}(8c+1)}\right]. \quad (9\,a)$$

As regards the significance of the signs preceding the square root term in this equation, the negative sign is that appropriate to vibration in the fundamental mode, whilst the positive sign is that appropriate to the first overtone. Since the value of z for the first overtone is large, equation (9 *a*) does not give a good approximation in this instance.

For the fundamental mode of vibration we thus obtain

$$\alpha = z^4 = \frac{210}{8c+1}\left[(4c+1) - \sqrt{16c^2 + \frac{31}{35}(8c+1)}\right]. \quad (9)$$

Some idea of the accuracy of this solution can be obtained by considering the case where $c=0$, *i. e.*, the case of the unloaded bar, for which the value of z^4 is known [6] to be 12·3624 and z is 1·87510. The value of z given by equation (9) is 1·87516 ; the error involved in the use of equation (9) in this case therefore amounts to less than 1 in 30,000. It is of interest to compare the values of z given by the approximations of Rayleigh and Morrow in this case ; the former yields the value $z_r = 1{\cdot}8888$, which is about 0·8 per cent. in error ; the latter yields $z_m = 1{\cdot}87492$, which is about 1 in 10,000 in error. To test the accuracy of equation (9) further, if a value of 1·5 is assumed for z substitution in the accurate equation (5) gives $c = 0{\cdot}35412$; using this value of c in equation (9), z is found to be 1·5000, using five-figure tables. Again, assuming z to be 1·0, equation (5) gives $c = 2{\cdot}7637$; substitution of this value of c in equation (9) gives $z = 1{\cdot}0000$. We therefore conclude that the values of z given by equation (9) are sufficiently accurate for the present purpose.

The variation of z with c is shown graphically in fig. 1, curve (A), and the variation of z^2 with c in fig. 1, curve (B) ; the values of z and of z^2 have been calculated using equation (9) In view of the widespread use of the Rayleigh formula, equation (3), the difference, Δz, between z_r and the values of z given by equation (9) has been calculated for various values of c ; the relation between $\triangle z$ and c is shown graphically in fig. 2.

Should greater accuracy than that given by equation (9) be required the α^3 term in equation (8) may be retained, in which case a cubic equation in α must be solved.

Fig. 1.

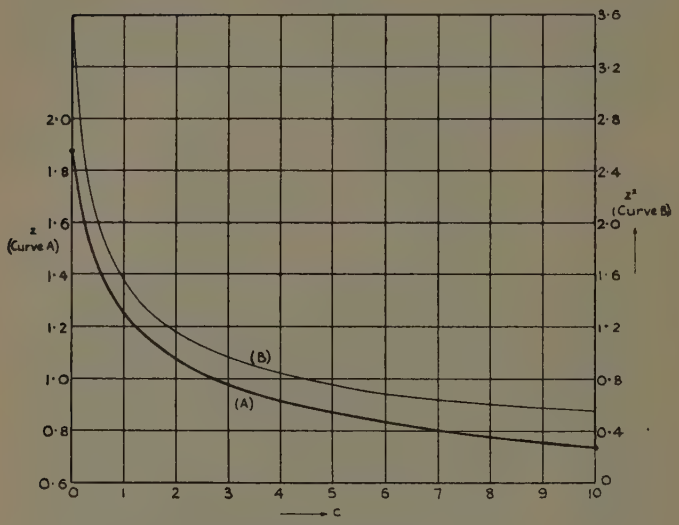

(A) Graph of z against c.
(B) Graph of z^2 against c.

Fig. 2.

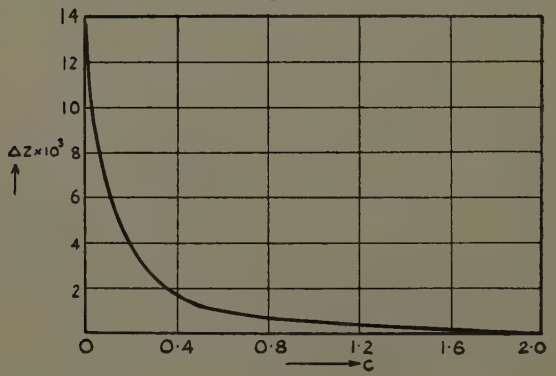

Graph of error, Δz, in the Rayleigh formula against c.

This may be done by reversing the series of equation (8); if this be done the solution obtained is

$$\alpha=z^4=\frac{12}{1+4c}\left\{1+\frac{1}{35}\cdot\frac{1+8c}{(1+4c)^2}-\frac{2}{35\times 495}\cdot\frac{1+12c}{(1+4c)^3}+\frac{2}{35^2}\cdot\frac{1+8c}{(1+4c)^2}\right\}, \quad \ldots \quad (10)$$

terminating the reversed series at the cubed term.

The accuracy of this solution may be tested by considering the case of $c = 0$; the value of z so obtained is 1·87506, which is of the same order of accuracy as that given by the simpler expression of equation (9). It thus appears that, owing to its comparatively slow convergence, the accuracy of the expression (10) is not very much greater than that of the simpler expression (9).

It may be noted that the method of expansion in series given above is, of course, applicable to the solution of the simpler equation

$$1+\cosh z.\cos z=0, \quad \ldots \quad (11)$$

which occurs in the theory of the transverse vibration of unloaded bars. In this case, neglecting the α^3 term, the roots are given by

$$\frac{\alpha^2}{2520}-\frac{\alpha}{6}+2=0$$

according to equation (6); whence, for the fundamental mode,

$$\alpha=z^4=210\left(1-\sqrt{\frac{31}{35}}\right)=12\cdot3638$$

and

$$z=1\cdot87516.$$

For purposes such as teaching this method forms a simple and direct alternative to the method of successive approximation generally used.

In conclusion, the author desires to express his sincere thanks to Vice-Principal Gwilym Owen for his help and encouragement, and to Mr. Thomas Lewis, Head of the Department of Applied Mathematics, for discussing and checking the results.

References.

(1) Davies and James, Phil. Mag. xviii. p. 1023 (1934); James and Davies, Phil. Mag. xviii. p. 1053 (1934).
(2) Lord Rayleigh, 'Theory of Sound,' p. 289 (London, 1894). G. Temple and W. G. Bickley, 'Rayleigh's Principle,' pp. 110 and 118 (Oxford, 1933).
(3) J. Morrow, Phil. Mag. xi. p. 354 (1906). G. Temple and W. G. Bickley, *op. cit.*
(4) J. Prescott, 'Applied Elasticity,' p. 213 (London, 1924).
(5) L. M. Milne-Thomson and L. J. Comrie, 'Standard Four-figure Mathematical Tables,' p. 228 (London, 1931).
(6) Lord Rayleigh, *op. cit.* p. 278.

March 1936.

LXXV. *A Probe Test for Positive Space-charge* *. *By* K. G. Emeléus, *M.A., Ph.D., and* W. L. Brown, *M.Sc., Queen's University, Belfast* †.

THE probe method which Langmuir devised for studying ionized gases (1) has been widely used, and much valuable information obtained by means of it. For many purposes it is not necessary to take into account refinements of the original theory; for example, the distortion of the discharge by rather large probes, although it can be partly allowed for and is not always inconsiderable (2), will not matter greatly if a rough survey of conditions in a tube or set of tubes is all that is required. However, even when such tolerance is permissible, current-voltage characteristic curves for the probe may be found which either obviously cannot be discussed even approximately in the conventional way, or, if they are at first sight amenable to the usual analysis, give absurd results which must be discarded. Examining numerous anomalous curves, we have found that one particular form is always obtained, in our experience, if the probe is put in a part of a discharge where there is considerable positive space-charge, and thus serves to indicate its presence.

1. *Experimental Details.*

The anomalous curve can be described at the same time as a test made to show its association with positive

* Reference was made to part of this work by the authors and Cowan, Phil. Mag. xvii. p. 146 (1934).

† Communicated by the Authors.

space-charge. For this purpose a double probe was made, consisting of two parallel wires of the same length and diameter insulated from one another. These were mounted in the negative glow or Faraday dark space of a cold cathode glow discharge between disk electrodes in a cylindrical tube. The wires were most conveniently mounted on a single pinch fused into a side-tube (fig. 1), but identical results were obtained if they were brought in separately from opposite sides of the main tube. The general nature of the results was also unaffected by change of position of the double probe in the plasma,

Fig. 1.

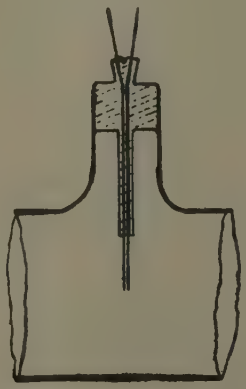

Double probe. The projecting wires are 5 mm. long pieces of 0·1 mm. diameter molybdenum, separated laterally by 0·06 mm.

by a slight inclination of the wires to one another or by small variations in their spacing [3].

A positive ion sheath was formed on one wire by holding it at a fixed negative potential relative to the anode. The potential of the second wire was then varied in the usual way to obtain its current-voltage characteristic curve. The greater the negative potential on the first wire the more deeply was the second likely to be embedded in the positive ion sheath on the first, although this certainly changed in shape and extent as the potential on the second wire was varied.

Part of a typical set of characteristic curves for the second wire is shown in fig. 2. The double probe was

0·65 cm. from the cathode in the Faraday dark space of a discharge in argon at 1·0 mm. pressure, with a cathode fall in potential of 298 volts and a current density of $3 \cdot 10^{-4}$ amp. cm.$^{-2}$. In the figure a positive current is one in which there is a net flow of negative electricity from the gas to the probe. The numbers

Fig. 2.

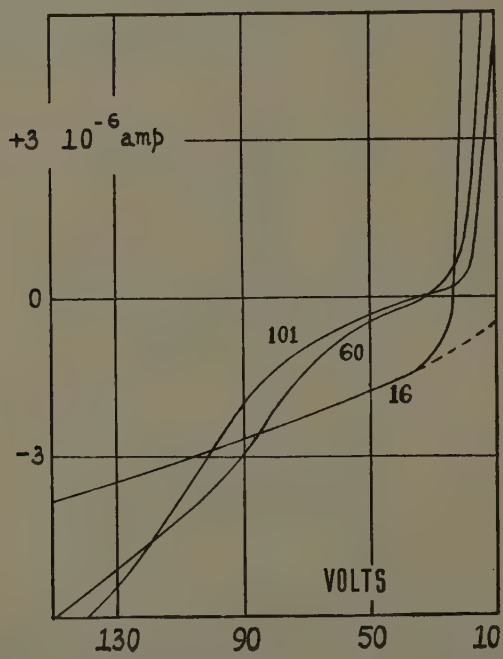

Current to one probe v its potential negative to the anode, the other probe being held meanwhile at fixed negative potentials relative to the anode given by the numbers against the curves.

against the curves give the fixed negative potential of the first wire relative to the anode.

With this potential −16 volts the curve is of regular form. The positive ion current to the probe extrapolates somewhat as is indicated by the broken line ; from the difference between this and the experimental

curve electron data and the space-potential (−16 volts relative to the anode) can be obtained by the semi-logarithmic method [1]. About the same value of space-potential was obtained by connecting the two probes and using them as a single probe. It follows that there can have been only a vanishingly small sheath of either sign on the first probe in the first part of the experiment. Notice that the positive ion line extrapolates to a positive ion current to the probe at the space-potential.

With a potential of −60 volts on the first probe this no longer occurs. The characteristic curve for the second has also a considerable region which is concave downwards, which is not the case for the parts of a regular curve corresponding to reception of positive ions. Both these effects persist, the second in more exaggerated form, with the fixed potential of the first probe −101 volts.

The sheaths on the first probe could not be seen very distinctly, but the second probe when insulated was definitely somewhere about the edge of the sheath on the first with the potential of the latter −60 volts, and definitely within it with the potential of the latter −101 volts. From these observations and the other circumstances of the experiment we conclude that the anomalous form of the curves for the second probe is closely connected with the presence of the positive space-charge on the other probe, and that whilst such curves may not be analyzed in the usual way, if they appear in any instance it is likely that considerable positive space-charge is present in the discharge, or part of a discharge, which is under investigation [4].

3. *Theory of the Anomalous Curves.*

This has not been worked out quantitatively. The space-charge effect is more pronounced than when a probe is partly shielded from a plasma by a lateral space-charge (disk probe) [1], or by a positive space-charge at its base (wire probe [5]), and a quantitative theory would have to proceed more on the lines of that of the flow of ions through an orifice in one probe to a second probe [6]. In hot cathode discharges at very low pressures curves somewhat like the anomalous ones of fig. 2 are obtained when a directed beam of high-energy electrons is present [7]. If such electrons were present here they

would have to originate in the sheaths or at the surfaces of the probes. Singularities might therefore be expected on the curves for the second probe at about the fixed negative potentials of the first probe. There is no definite evidence that they occur, and it seems more likely that the shape of the anomalous curves arises from an interaction of the two positive space-charges. The fact that for sufficiently small negative potentials large electron currents to the second probe are ultimately obtained must be due to imperfect shielding of it from the plasma by the positive sheath on the first probe with this particular geometrical arrangement ; this does not always happen (§ 4, 1).

4. *Applications.*

Anomalous curves of this type have been found in three discharges.

(i.) They are obtained invariably with a probe in the cathode dark space and at its junction with the negative glow. The boundary curves were at first misinterpreted, being analyzed as if of regular form [8], and it was not until their anomalous nature was recognized that the suspected existence of a large reversed electric field there was disproved [9]. Fig. 3 shows part of three characteristic curves obtained with a single probe 0·01 cm. diameter, 0·5 cm. long, parallel to the cathode in a discharge-tube similar to those previously referred to, in which a discharge was passing through argon at 0·3 mm. pressure. The cathode fall in potential was 290 volts and the tube current density 10^{-5} amp. cm.$^{-2}$. The curves labelled *a*, *b*, and *c* are for the probe 0·67, 0·52, and 0·40 cm. respectively from the cathode. The thickness of the cathode dark space was about 0·56 cm. Curve *a* is of regular form, curves *b* and *c* are generally similar to the anomalous curves of fig. 2. Such differences as exist between the curves of the two figures may be referred reasonably to differences in shape of the probes and space-charges. Curves similar to those of fig. 3 have been described recently by Ernst, and the space-potential located on them by a hot-wire method [10]. It is certain that there is a positive space-charge in the cathode dark space.

(ii.) The anomalous curves are obtained at the heads of striations in the positive column of a glow discharge

through iodine vapour [11], where it is also certain from other evidence that a positive space-charge is present.

(iii.) They are obtained throughout the greater part of a discharge-tube containing oxygen[2] or helium [11] at a pressure of the order of 0·1 mm., passing currents of the order of a microampere per cm.^{2} or less with a potential difference of a few hundred volts between anode and cathode. Existence of a positive space-

Fig. 3.

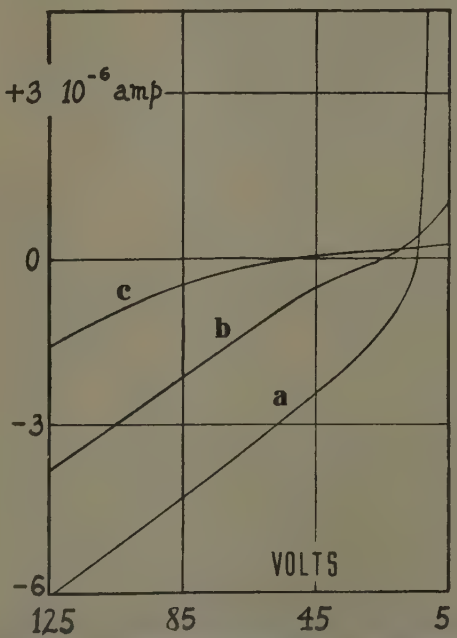

Current to a probe at various positions in the negative glow (*a*) and cathode dark space (*b* and *c*) *v* its potential negative to the anode. The currents of *a* are plotted to half scale.

charge in this case, although less certain than in the two preceding cases, is again likely.

Summary.

An anomalous form of current-voltage characteristic curve for probes in discharge-tubes has been shown to be

associated in a number of instances with the presence in the discharge of a pre-existing positive space-charge. When such curves are obtained in other instances, the existence of a positive space-charge may therefore be suspected.

References.

(1) Langmuir and Mott-Smith, General Elect. Rev. xxvii. pp. 449 ff., *cf* (1924).
(2) *Cf.* Greeves and Johnston, Phil. Mag. xxi. p. 659 (1936).
(3) It was also immaterial which probe was nearer the cathode.
(4) Normal curves were obtained for the second probe if the first had a small electron sheath round it.
(5) Sloane and Emeléus, Phys. Rev. xliv. p. 333 (1933).
(6) Langmuir, Tonks, and Mott-Smith, Phys. Rev. xxviii. p. 104 (1926).
(7) Langmuir and Jones, Phys. Rev. xxxi. p. 357 (1928).
(8) Emeléus and Harris, Phil. Mag. iv. p. 49 (1927).
(9) Emeléus and Sloane, Phil. Mag. xiv. p. 355 (1932).
(10) Ernst, *Helvetica Physica Acta*, viii. p. 381 (1935).
(11) Unpublished observations made in this laboratory.

LXXVI. *On the Fermi Theory of Beta Decay.* *By* W. G. Pollard, *Ph.D., The Rice Institute, Houston, Texas* †, *U.S.A.* ‡

Abstract.

The probability for beta disintegrations as given by the Fermi theory are derived for the forbidden as well as for the permissible transitions. Two of the approximations made by Fermi are improved, and the results are obtained for both types of transition from the more accurate expressions. A function of the maximum energy and the decay constant, which the theory shows should be constant, is found to have a different order of magnitude for the two types of transition. This difference can be eliminated by (1) using a larger value for the nuclear radius than the one obtained from alpha disintegrations, or (2) using the Fermi form of interaction energy for the permissible transitions and a special type of Uhlenbeck and Konopinski interaction for the forbidden transitions. Either assumption is capable

† Now Assistant Professor of Physics, The University of Tennessee, Knoxville, Tennessee.

‡ Communicated by Prof. H. A. Wilson, F.R.S.

of giving fair agreement over all nine bodies considered by Fermi.

The momentum distributions for simple type beta-ray spectra as calculated from the improved formulæ are compared with the experimental $H\rho$ curves. Good agreement is obtained with the Fermi type of interaction energy for ThC and ThC″ in the permissible transition group. It is especially good in the low velocity region. RaE is the only simple type spectrum in the forbidden group which has been measured. The agreement here is very poor, but is considerably improved by using the Uhlenbeck and Konopinski type of interaction.

Introduction.

IN the Fermi theory of beta radioactivity [1], comparison of the calculated and experimental frequencies of disintegrations suggests that there are two types of beta-ray disintegrations corresponding to "permissible" and "forbidden" transitions in the nucleus. Denote the nuclear angular momentum change in a beta disintegration by Δi. Then if $\Delta i=0$ is a permissible transition, the term corresponding to it in the expression for the disintegration probability is dominant and the others involving $\Delta i=1, 2, \ldots$ may be neglected. But if $\Delta i=0$ is a forbidden transition, then the term corresponding to it vanishes and the term corresponding to $\Delta i=1$ becomes dominant. Again the much smaller terms for $\Delta i=2, 3, \ldots$ may be neglected. Fermi calculated the decay constants of the beta-ray bodies by using only the $\Delta i=0$ term. He did not obtain the $\Delta i=1$ term explicitly, and so did not use it for those disintegrations in which $\Delta i=0$ is forbidden. A result obtained with the $\Delta i=0$ term was converted into the result for $\Delta i=1$ by multiplying by an average ratio of the two terms. Fermi estimated this ratio as $(\rho/\lambda)^2 \sim 1/100$, where ρ is the nuclear radius and λ the wave-length of the emitted beta-ray.

It is the purpose of this paper to derive an expression valid for any Δi and so obtain all the terms in the disintegration probability. The decay constants for the forbidden transitions can then be calculated directly. This is done on the assumption that the electron carries

off all, the neutrino none, of the angular momentum change Δi. It is desirable to calculate the term for $\Delta i=1$ because the ratio of the $\Delta i=0$ and $\Delta i=1$ terms is not a constant. It depends not only on the disintegration energy, but also on the partition of energy between the electron and neutrino, which is different for the two terms. Moreover, there has been some question as to the magnitude of this ratio as estimated by Fermi.

Another object incidental to this was to improve on two of the approximations made by Fermi with a view to improving the form of the calculated beta-ray spectra. It was found, however, that the more accurate expressions did not affect the final results very much. They are retained in the body of the paper because they do not add very much to the complexity of the results, and they eliminate any doubts that disagreements with experiment may be due to those approximations. Finally, the effect of the interaction "ansatz" proposed by Konopinski and Uhlenbeck [2] is considered in connexion with the forbidden transitions.

Derivation of the Formulæ.

The Fermi theory considers a beta disintegration as a process analogous to the emission of radiation from an excited electronic system. The heavy nuclear particles, neutrons and protons, play the part of the electronic system, while the electron-neutrino pairs constitute the radiation field. The energy of interaction between the two components, analogous to the interaction energy between electron and photon assemblies introduced by Dirac, is a more or less arbitrary element in the theory. It is required only to involve the Jordan and Klein operators a_s, a_s^* for the electron and b_σ, b_σ^* for the neutrino through products of the form $a_s b_\sigma$ and $a_\sigma^* b_\sigma^*$, and to be capable of representation in the form of a four vector.

In the application of the theory it is convenient to neglect the three-vector part of the interaction on the grounds that it is smaller than the scalar or time component by a factor v/c, where v is the velocity of the heavy particle in the nucleus. The form assumed by Fermi for the scalar part is

$$H_1=g(Q\tilde{\psi}\delta\phi+Q^*\tilde{\psi}^*\delta\phi^*), \quad \ldots \quad (1)$$

in which ψ and ϕ are the relativistic Jordan and Klein wave-functions for an assembly of electrons and neutrinos respectively, $\tilde{\psi}$ is the transposed matrix of ψ, Q and Q* are operators which pick out neutron to proton and proton to neutron transitions respectively, and g is an undetermined constant with dimensions energy $\times$ volume. δ is the Dirac matrix

$$\delta = \begin{pmatrix} 0 & -1 & 0 & 0 \\ 1 & 0 & 0 & 0 \\ 0 & 0 & 0 & 1 \\ 0 & 0 & -1 & 0 \end{pmatrix}.$$

We shall make use of a modification of this interaction "ansatz" introduced by Uhlenbeck and Konopinski (*loc. cit.*), in which H is proportional to $\frac{\partial \phi}{\partial t}$ and $\frac{\partial \phi^*}{\partial t}$ instead of to ϕ and ϕ^*. Denoting the proportionality constant by g', we may write this form of interaction

$$H_2 = g' \left(Q\psi\delta \frac{\partial \phi}{\partial t} + Q^*\tilde{\psi}^*\delta \frac{\partial \phi^*}{\partial t} \right). \quad . \quad . \quad (2)$$

Other forms of (2) are possible, but for zero neutrino rest mass they reduce to the same thing in the results.

The method employed by Fermi is to assume neutron and proton eigen solutions u_n and v_m of the wave equation for the nuclear assembly in the absence of the interaction energy (1). A wave function made up of a superposition of these eigenfunctions is then perturbed by the interaction in the ordinary way. The perturbation causes transitions between heavy particle states with the emission or absorption of electron-neutrino pairs. The probabilities for these transitions have resonance peaks at ΔE=electron energy+neutrino energy, where ΔE is the nuclear energy change in the transition. These probabilities may be summed in the usual way over all neutrino states in the neighbourhood of the resonance peak and over all electron states with momentum between p and $p+dp$. The result is the probability in time t for the simultaneous emission of a beta-ray in this momentum interval and a neutrino having the corresponding resonance energy.

This probability per unit time is

$$P(p)dp = \frac{m^2cg^2}{2\pi\hbar^4}(W_0 - W)^2 \sum_{dp} \left| \int v_m^* \tilde{\psi}\delta\phi u_n dV \right|^2, \quad . \quad (3)$$

where W_0 is the maximum total energy of the electrons in units of mc^2, and hence is equal to the disintegration energy ΔE for zero neutrino rest mass. $W_0 - W$ is thus the resonance value of the neutrino energy. The neutrino wave-function ϕ in (3) is to be understood as the one corresponding to this energy. The notation differs from Fermi's in that W_0 and W are measured in units of mc^2 and $\tilde{\psi}$ denotes only the transposed, not the transposed conjugate, matrix of ψ.

A difficulty arises in the calculation of the matrix element in (3). Although the interaction part $\tilde{\psi}\delta\phi$ is known from the hydrogen-like case, the nuclear wave-functions v_m and u_n are not known. For $\Delta i = 0$ this difficulty is unimportant because, although the coulomb field eigenfunctions for the electron with $j = \frac{1}{2}$ go to infinity at the origin, a suitable Gamow field could be found to make ψ constant inside the nucleus. Since zero angular momentum is assumed throughout for the neutrino, ϕ may be taken constant inside the nucleus for all Δi. Thus for zero angular momentum transfer the whole term $\tilde{\psi}\delta\phi$ may be removed from the integral. Following Fermi in the assumption of plane waves with arbitrary direction of propagation and spin orientation and zero rest mass for the neutrino, eq. 3 becomes in this case

$$P(p)dp = \frac{m^2cg^2}{2\pi\hbar^4}|M|^2(W_0 - W)^2 \sum_{dp} \tilde{\psi}^*(\rho)\psi(\rho), \quad . \quad (4)$$

where M is the matrix element $\int v_m^* u_n dV$. ρ again denotes the nuclear radius.

For values of $\Delta i = 0$, however, the coulomb field eigenfunctions go to zero as r^s at the origin. Here $s = \sqrt{(k+1)^2 - \gamma^2} - 1$ with $k = j - \frac{1}{2}$ and $\gamma \cong Z/137 \sim 0{\cdot}6$ for the natural beta radioactive bodies ($Z = 82{\cdot}2$). It is not then possible to treat ψ as constant inside the nucleus. Changing to a Gamow field would only make ψ drop off more rapidly in this region. In order to compute $P(p)dp$

for this case it is necessary to make some assumptions about the form of the nuclear wave-functions v_m and u_n.

There are two ways of picturing nuclear structure. First the nucleus may be regarded from the particle standpoint as analogous to a raindrop. That is, the assembly of neutrons and protons composing it may be pictured as packed together with uniform density inside a sphere by the mutual attractions between the separate particles. On this view, the probability of finding a particular neutron or proton in a nuclear element of volume would be pretty much the same for all points in the nucleus. This makes v_m and u_n constant inside a sphere of radius ρ and zero outside. The other point of view consists in regarding any one particle as executing motions in a radially symmetric self-consistent field of all the rest. This makes v_m and u_n solutions of a Schroedinger equation for some field $V(r)$. The simplest form to assume for $V(r)$ is the square hole potential. The proton and neutron eigenfunctions v_m and u_n then become Bessel functions whose order depends on the angular momentum of the corresponding particle, and which vanish at the boundary $r=\rho$. The number of loops inside the nucleus will depend on the energy.

For $k=1$, $\Delta i=1$ all four components of the electron wave-function are proportional to $r^{0\cdot908}$ to a first approximation. All other factors in ψ may be removed from the integral. The result obtained by taking v_m and u_n constant is

$$|\int v_m^* r^s u_n dV|^2 = 0\cdot59\rho^{2s}|M|^2, \quad . \quad . \quad . \quad . \quad (5)$$

and that obtained by taking v_m and u_n to be Bessel functions of the form $J_{\frac{1}{2}}(ar)/r$ and $J_{\frac{3}{2}}(br)/r$ is

$$|\int v_m^* r^s u_n dV|^2 = 0\cdot34\rho^{2s}|M|^2 \quad . \quad . \quad . \quad (6)$$

In both (5) and (6) s has the value 0·908 corresponding to $k=1$. Many other assumptions about the form of the nuclear wave-functions are of course possible, but these two at least indicate the results which might be expected from a more detailed description of the nucleus.

In general we may write

$$P(p)dp = D_k \frac{m^2cg^2}{2\pi\hbar^4}|M|^2(W_0-W)^2 \sum_{dp} \tilde{\psi}^*(\rho)\psi(\rho), \quad . \quad (7)$$

where from eqs. (4), (5), and (6), $D_0=1$ and $D_1=0{\cdot}59$ or $0{\cdot}34$, depending on the interpretation of the nuclear wave-functions.

If we use the Uhlenbeck and Konopinski interaction (2), then, since $\dfrac{\partial\phi}{\partial t}=-i(mc^2/\hbar)(W_0-W)\phi$, eq. (7) becomes

$$P(p)dp = D_k \frac{m^4c^5g'^2}{2\pi h^6}|M|^2(W_0-W)^4 \sum_{dp}\tilde{\psi}^*(\rho)\psi(\rho). \quad (8)$$

For the calculation of the term $\sum_{dp}\tilde{\psi}^*(\rho)\psi(\rho)$ Fermi employed Hulme's[3] integral representations of the radial part of Darwin's[4] relativistic eigenfunctions for the continuous energy spectrum in the hydrogen-like case. Hulme's integrals reduce to ordinary Euler integrals of the second kind when a term $\exp.(imcpru/\hbar)$ is set equal to 1. Since the value of the wave-functions at $r=\rho=9\times10^{-13}$ cm. (a mean value of the nuclear radius for the natural beta radioactive elements) is desired, and since $|u|\leqslant 1$, this is a fairly good approximation for small values of p. If we make, it and add the results for both types of solution (denoted by Darwin as $j=k+\frac{1}{2}$) for the same j, we obtain

$$\sum_{dp}\tilde{\psi}^*\psi = dp\,\frac{32\pi m^3c^3}{h^3}\,\frac{(k+1)^2(2k+1)}{[\Gamma(2s+3)]^2}\left(\frac{4\pi mc\rho}{h}\right)^{2s} \times p^{2s+2}e^{\pi\gamma W/p}|\Gamma(s+1+i\gamma W/p)|^2 . \quad (9)$$

The value of k to be understood here is $k=j-\frac{1}{2}$. The momentum p is measured in units of mc and $W=\sqrt{1+p^2}$. With $k=0$ this is exactly Fermi's result for $j=\frac{1}{2}$.

The errors introduced by the approximation

$$\exp.(imcpru/\hbar)=1$$

become appreciable for those beta-ray spectra involving values of p greater than 4 or 5. It seemed desirable, therefore, to improve it by setting $e^{i\frac{1}{2}\beta pu}\cong 1+i\frac{1}{2}\beta pu$ with $\beta=2mc\rho/\hbar$. In doing so, we neglect the variation of this factor with r. This is allowable, since we are dealing here only with a second approximation. The integrals representing ψ can still be evaluated with ease. It is found that the only effect of this improvement is to multiply (9) by the factor

$1-\frac{2\beta\gamma}{2s+3}\mathrm{W}$. The most important effect which it has on the final results is to make the calculated spectra slope off more slowly to their upper limit.

Fermi used the following approximation to the gamma function in (9)

$$p^{0\cdot6}e^{0\cdot6\mathrm{W}/p}\,|\Gamma(0\cdot8+i0\cdot6\mathrm{W}/p)|^2\cong 4\cdot5+1\cdot6p. \quad . \quad (10)$$

Values of the gamma function have been computed for small p by means of the usual asymptotic expansion [5] and for large p by means of a suitable expansion in an infinite product [6]. For $k=1$ it is best to write

$$p^{2s+2}\,|\Gamma(s+1+i\gamma\mathrm{W}/p)|^2 = p^3(s^2+\gamma^2\mathrm{W}^2/p^2)\,.\,p^{2s-1}|\Gamma(s+i\gamma\mathrm{W}/p)|^2.$$

TABLE I.

Approximations to the Gamma Function.

p.	$k=0$.			$k=1$.	
	Calc.	Fermi: Eq. (10).	Eq. (11).	Calc.	Eq. (12).
0	4·62	4·5	4·64	4·14	4·14
0·2	4·71	4·8	4·69	4·20	4·20
0·5	4·91	5·3	4·89	4·55	4·50
1·0	5·61	6·1	5·51	5·35	5·39
2	7·21	7·7	7·15	7·90	7·79
3	8·78	9·3	8·86	10·45	10·40
4	10·30	10·9	10·51	13·00	13·02
6	13·07	14·1	13·42	17·85	18·00
8	15·55	17·3	15·75	22·55	22·62
10	17·67	20·5	17·62	27·00	26·77

It was found that the most accurate simple approximations can best be obtained in terms of W instead of p.

The approximations used are

$$p^{0\cdot6}e^{0\cdot6\mathrm{W}/p}\,|\Gamma(0\cdot8+i0\cdot6\mathrm{W}/p)|^2 \cong 2\cdot45+2\cdot27\mathrm{W}-0\cdot077\mathrm{W}^2. \quad (11)$$

$$p^{0\cdot816}e^{0\cdot6\mathrm{W}/p}\,|\Gamma(0\cdot908+i0\cdot6\mathrm{W}/p)|^2 \cong 1\cdot07+3\cdot13\mathrm{W}-0\cdot057\mathrm{W}^2. \quad (12)$$

These approximations are compared with the calculated values in Table I. The approximation (10) used by Fermi is also shown.

Using the form (7) for $P(p)dp$ and eqs. (11) and (12), we obtain for $k=0$

$$P(p)\,dp = |M|^2 \frac{C\beta^{-0\cdot4}}{[\Gamma(2\cdot6)]^2}(1-\cdot022W)(2\cdot45+2\cdot27W -\cdot077W^2)(W_0-W)^2 p\,dp, \quad (13)$$

and for $k=1$

$$P(p)\,dp = D_1|M|^2 \frac{12C\beta^{1\cdot816}}{[\Gamma(4\cdot816)]^2}(1\cdot18W^2-\cdot82)\ (1-\cdot012W) \times(1\cdot07+3\cdot13W-\cdot057W^2)(W_0-W)^2 p\,dp, \quad (14)$$

with $$C = 256\pi^4 m^5 c^4 g^2/h^7.$$

The Decay Formula.

The decay constants can best be obtained by converting eqs. (13) and (14) into energy distributions in terms of the kinetic energy $E=W-1$. We have then

$$\lambda = 1/\tau = \int_0^{E_0} P(E)\,dE. \quad . \quad . \quad . \quad . \quad (15)$$

Substituting (13) in (15) and performing the integration gives

$$|M|^2 \frac{C\beta^{-0\cdot4}}{[\Gamma(2\cdot6)]^2}\ \frac{4\cdot54}{3}\ \tau E_0^3\ (1+0\cdot361E_0 +0\cdot0412E_0^2-0\cdot00133E_0^3) = 1.$$

In order to make our results correspond with Fermi's, we rewrite this relation as

$$\tfrac{1}{3}\tau E_0^3(1+0\cdot361E_0+0\cdot0412E_0^2-0\cdot00133E_0^3) = 1/4\cdot54\,|M|^{-2}C\beta^{-0\cdot4}[\Gamma(2\cdot6)]^{-2} = \alpha_1. \quad (16)$$

This result holds for those disintegrations in which $k=0$, $\Delta i=0$. The experimental values of E_0 and τ when placed in the left of eq. (16) determine the value of α_1. This value may be used to determine the undetermined constant g by the relation $\alpha_1=5\cdot68g^{-2}\,|\,M\,|^{-2}\times10^{-96}$ given by the middle term in (16). To get the corresponding result for $k=1$, $\Delta i=1$, eq. (14) is substituted in eq. (15), and both sides of the resulting equation multiplied by $5\cdot68g^{-2}\,|\,M\,|^{-2}\times10^{-96}=\alpha_1$, so that the theory predicts

the same constant for both $\Delta i=0$ and $\Delta i=1$ disintegrations. The result is

$$6{\cdot}16\times10^{-6}D_1{}_7E_0{}^3(1{\cdot}47+3{\cdot}05E_0+2{\cdot}25E_0{}^2$$
$$+0{\cdot}752E_0{}^3+0{\cdot}090E_0{}^4-0{\cdot}0019E_0{}^5)=\alpha_1. \quad (17)$$

α_1 is the same constant, $5{\cdot}68g^{-2}\mid M\mid^{-2}\times10^{-96}$, in both eqs. (16) and (17).

Values of this constant as given by eqs. (16) and (17) for the nine beta-ray bodies considered by Fermi are given under column A of Table II. The first set of

TABLE II.

Relation between Half-period and Maximum Energy.

	Element.	λ (hours).	E_0.	A.	B.	C.
				α_1: Eq. (16).	α_1: Eq. (16).	Fermi.
$\Delta i=0$.	UX_2	0·026	4·54	2·7	2·7	3·0
	ThC″ ...	0·076	3·56	3·1	3·1	3·3
	AcC″....	0·115	2·74	1·8	1·8	2·0
	RaB	0·645	1·27	0·7	0·7	0·9
	ThB_2....	15·3	0·705	2·3	2·3	2·7
				α_1: Eq. (17).	α_2: Eq. (18).	
$\Delta i=1$.	RaC	0·47	6·17	0·16	1·4	190
	ThC.....	2·4	4·44	0·12	0·6	230
	$MsTh_2$...	8·8	4·01	0·25	1·0	640
	RaE	173	2·39 3·00	0·29 0·97	0·5 2·4	1800

elements represent disintegrations in which $\Delta i=0$ is a permissible transition and the second set those in which $\Delta i=0$ is forbidden. Eq. (16) was used to get α_1 for the first set and eq. (17) for the second. The value 0·59 from eq. (5) corresponding to constant v_m and u_n was used for D_1 in eq. (17). To get the results corresponding to D_1 from eq. (6), the values of α_1 in the second group must be multiplied by $0{\cdot}34/0{\cdot}59=0{\cdot}58$. For comparison the values of the same constant computed by Fermi, using his expression for $k=0$ throughout, are shown under column C. Differences between Fermi's values and those obtained here for this constant in the first group

are the result of the different approximations used. The values used for E_0 are those of Sargent [7] for UX_2, AcC″, and $MsTh_2$; Gurney for RaB [8], RaC [9], and ThB [10]; Henderson [11] for ThC and ThC″; Champion [12] and Scott [13] for RaE. Two values were used for RaE because there is such a wide divergence of results on this element. These two values seem to be the most reliable.

It will be noted that α_1 has a different order of magnitude in the two groups. This means that the ratio of occurrences of $\Delta i=1$ transitions to $\Delta i=0$ transitions is too small. It is desirable, therefore, to consider the possibility of increasing this ratio without changing the theory radically. There are two possibilities: (*a*) the value of the nuclear radius for beta disintegrations might be different from its value for alpha disintegrations; (*b*) the law of interaction might differ for disintegrations in which $\Delta i=1$ from its form for those in which $\Delta i=0$. Assuming the first suggestion, it is found that the constant α_1 can be given the same order of magnitude in both groups by taking ρ about three times larger.

The other possibility is to introduce another form of interaction energy for the forbidden transitions. The simplest variation on the Fermi form is that proposed by Uhlenbeck and Konopinski. Using eqs. (8) and (15), we find

$$3{\cdot}70\times10^{-6}D_1{}^{7}E_0{}^{5}(1{\cdot}47+2{\cdot}03E_0+1{\cdot}07E_0{}^{2}$$
$$+0{\cdot}269E_0{}^{3}+0{\cdot}025E_0{}^{4}+0{\cdot}00042E_0{}^{5})$$
$$=5{\cdot}68g'^{-2}(\hbar^2/m^2c^4)\,|\mathrm{M}\,|^{-2}\times10^{-96}=\alpha_2. \quad (18)$$

We propose, therefore, to represent the relation defined by eq. (15) between the decay constant and the maximum energy by the constant α_1 for those transitions in which $\Delta i=0$ is permissible and by α_2 for those transitions in which it is forbidden. In column B of Table II. values of α_2 calculated by means of this relation with $D_1=0{\cdot}59$ are given for the second group, and the values of α_1 are repeated from column A for the first group. Obviously we can state no *a priori* relation between the values of α_1 and α_2 since they involve the different undetermined constants g and g'. But the experimental results show that they are of the same order of magnitude. Comparing

the definition of α_1 in terms of g with that of α_2 in eq. (18) in terms of g', it is seen that $g' \sim gmc^2/\hbar$. Another way of expressing this result is that the experimental values show that the constant g is, roughly, the same as g', provided time is measured in the rational relativistic unit $mc^2/\hbar$. For if we put $t=(mc^2/\hbar)\mathrm{T}$, eqs. (1) and (2) become, when we confine our attention to the part which gives rise to beta disintegrations,

$$\left.\begin{aligned} \mathrm{H} &= g\mathrm{Q}\tilde{\psi}\delta\phi \quad \text{for } \Delta i=0, \\ \mathrm{H} &= g\mathrm{Q}\tilde{\psi}\delta\frac{\partial\phi}{\partial \mathrm{T}} \quad \text{for } \Delta i=1. \end{aligned}\right\} \quad . \quad . \quad . \quad (19)$$

The variation in the quantities α_1 and α_2, which according to this theory should be constants, is too great to establish this result definitely; but it can at least be said that eqs. (19) hold in order of magnitude.

The Continuous Beta-ray Spectra.

The fraction $d\mathrm{F}$ of beta-rays emitted from a beta disintegrating body with momenta between p and $p+dp$ is proportional to the probability $\mathrm{P}(p)dp$ per unit time that a disintegration will occur in which the beta-ray is emitted in this momentum interval. Thus the momentum distribution in a beta-ray spectrum predicted by this theory can be obtained simply by adjusting the curve $\mathrm{P}(p)$ to have unit area. The calculated curves for $\Delta i=0$ transitions were obtained from eq. (13), and those for $\Delta i=1$ transitions from eq. (14) or from eq. (14) with $(\mathrm{W}_0-\mathrm{W})^4$ in place of $(\mathrm{W}_0-\mathrm{W})^2$.

In comparing experimental results on beta-ray spectra with the distributions predicted by this theory, two points should be kept in mind. First, the observed spectra are always momentum or $\mathrm{H}\rho$ rather than energy distributions. It would seem more logical, therefore, to use the momentum distributions directly for comparison instead of following the customary method of converting the experimental curves from $\mathrm{H}\rho$ to energy and then comparing. This is particularly important because the experimental energy distributions do not all pass through the origin. Those that do not are made to pass through the origin chiefly out of a conviction that they should do so.

The second point is that the Fermi theory in its present form applies only to simple type spectra. In a simple type disintegration there is only one possible final state for the neutron→proton transition. No provision is made in the theory for disintegrations in which there are two or more empty proton levels into any of which the neutron might go. For such disintegrations the beta-ray spectrum would be made up of a superposition of

Fig. 1.

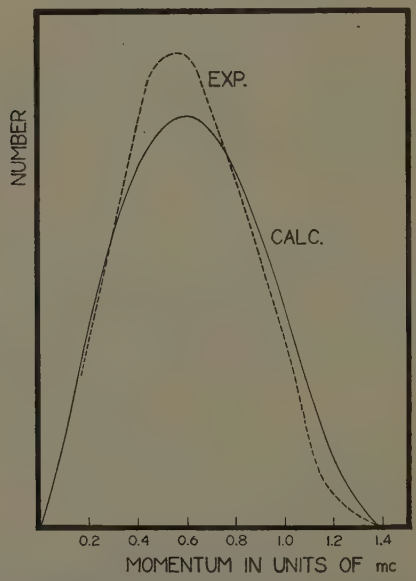

Comparison of calculated and experimental momentum distributions for the continuous beta-ray spectrum of thorium B. Simple type permissible transition.

several spectra of the simple type. Each component would correspond to a neutron transition into a particular one of the several possible final states.

In the first group of beta-ray bodies for which eq. (9) is applicable, thorium B and thorium C″ are very probably of the simple type [14]. The uranium X_2 and actinium C″ spectra have not been obtained experimentally. The

gamma-rays emitted in the RaB . C disintegration suggest that the RaB continuous beta-ray spectrum is complex, although this is not certain. We have, therefore, chosen thorium B and thorium C″ to compare with the calculated spectra in the $\Delta i=0$ group. The experimental curves are those of Gurney [10] for thorium B and Sargent [15] for thorium C″. Sargent's distribution was obtained from Gurney's combined thorium C+C″ spectrum through a consideration of the absorption data on both bodies. In each case the experimental and calculated curves have been adjusted to have the same area. The

Fig. 2.

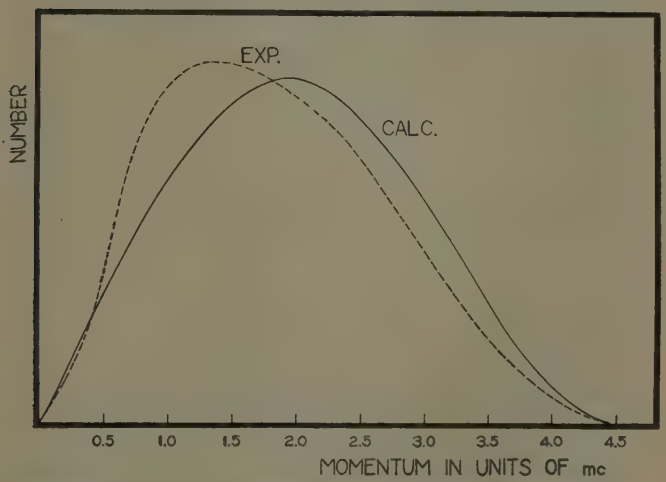

Comparison of the calculated and experimental momentum distributions for the continuous beta-ray spectrum of thorium C″. Simple type permissible transition.

thorium B curves are compared in fig. 1 and those for thorium C″ in fig. 2. The agreement is within the limits of experimental error, and is particularly good in the low energy region.

In the second $\Delta i=1$ group the spectra of radium C and thorium C are almost certainly complex [14], and that of mesothorium II has not been obtained experimentally. This leaves only radium E for comparison of the results for $\Delta i=1$. This spectrum has been obtained directly

by Kovarik and McKeehan [16], Madgwick (*loc. cit.*), and Scott (*loc. cit.*), and indirectly from absorption data by Sargent [15]. None of these experimental curves agree very well with each other. Those of Sargent and Scott were chosen here. They are the broken curves in fig. 3. The dotted curve was drawn from values calculated with eq. (10) using $W_0=3{\cdot}38$. The agreement is very poor and the curve has the opposite form of asymmetry from that required. Changing ρ to $2{\cdot}2\times10^{-12}$ does not affect the form of the distributions appreciably. So, although this corrects the discrepancy between the

Fig. 3.

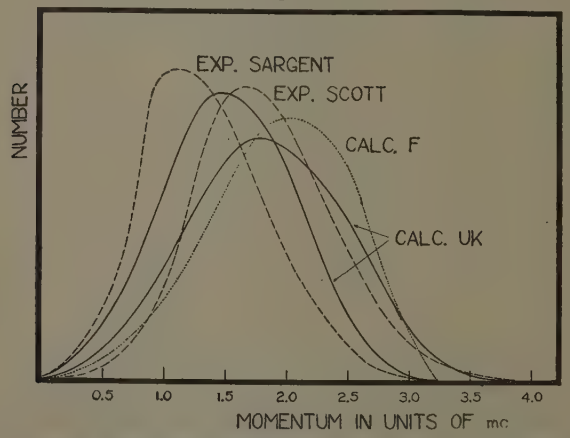

Momentum distributions for the continuous beta-ray spectrum of radium E. Simple type forbidden transition. Broken curves: experimental momentum distributions due to Scott and Sargent. Solid curves: calculated momentum distributions for $W_0=3{\cdot}38$ and $W_0=4{\cdot}00$ using the Konopinski and Uhlenbeck type of interaction energy. Dotted curve: calculated distribution for $W_0=3{\cdot}38$ using the Fermi type of interaction energy.

decay constants for $\Delta i=0$ and $\Delta i=1$, it does not improve the $\Delta i=1$ spectra. Assuming the other suggestion, that the Uhlenbeck and Konopinski form of interaction is operative for forbidden transitions, the solid curves in fig. 3 corresponding to $W_0=3{\cdot}38$ and $W_0=4{\cdot}0$ are obtained. The higher energy curve agrees roughly with Scott's curve, but gives too many low velocity electrons. However, O. W. Richardson has obtained

results on radium E beta-rays, which indicate that more low energy electrons are emitted than the magnetic analysis curves show [17]. The low energy curve agrees rather poorly with Sargent's spectrum, but shows the right number of low velocity electrons. The disagreement between calculated and experimental curves, although fairly large, is no worse than that between the experimental curves themselves. On the whole, we may say that the agreement may be within the limits of experimental error even though it is not within the limits set by the separate investigators on their own experiments.

The corresponding energy spectra still do not pass through the origin. One of the best arguments indicating that the energy distribution of radium E beta-rays should be zero at the origin is based on the agreement between the average energy calculated from Madgwick's energy distribution (which does pass through the origin) and the average energy calculated from the heating effect. But if Scott's curve is correct, the average energy is $4{\cdot}7\times10^5$ electron volts, which is far from the heating effect value of $3{\cdot}4\times10^5$ e.v. A large number of low energy electrons would have to be added to Scott's spectrum to bring his value down to this.

Concluding Remarks.

It seems, therefore, that the best all round agreement is obtained by assuming the Fermi form of interaction for the permissible transitions and the Uhlenbeck and Konopinski form for the forbidden transitions. This gives, roughly, the proper momentum distributions for both classes, and it makes the decay constants agree with the theory for all nine bodies. This latter result is, of course, trivial, since the constant g' is adjustable in terms of g. It is rather striking, however, that the experimental results should give such a simple and reasonable relation. As a matter of fact, it is the simplest that could be expected, since the introduction of a time derivative in the second form of interaction makes the ratio g/g' depend on the unit of time. Since relativistic wave-functions are used, the rational relativistic unit would be expected. It is rather satisfying that it turns out this way.

There are, however, theoretical difficulties in this assumption. It is difficult to see why the law of inter-

action between heavy and light particles should be different in some nuclei than in others. Certainly it would be preferable to use only one form throughout. A possible explanation is that the Fermi form is applicable when the empty proton level corresponds to the same spin as the neutron, while the Uhlenbeck and Konopinski form operates when the proton level corresponds to the opposite spin. In the first case the nucleus would not be required to change in angular momentum; in the second it has to transfer at least one unit to the emitted particles. It is reasonable that different laws of interaction might operate in the two cases.

In conclusion, I wish to express my appreciation for the many valuable discussions on this problem which I have had with Professor H. A. Wilson, and for the interest he has shown in it.

References.

(1) E. Fermi, *Zeits. f. Physik*, lxxxviii. p. 161 (1934).
(2) E. J. Konopinski and G. Uhlenbeck, Phys. Rev. xlviii. p. 7 (1935).
(3) H. R. Hulme, Proc. Roy. Soc. A, cxxxiii. p. 381 (1931).
(4) C. G. Darwin, Proc. Roy. Soc. A, cxviii. p. 654 (1928).
(5) The formula

$$|\Gamma(\alpha+i\beta)|^2 \sim 2\pi\beta^{2\alpha-1}e^{-\pi\beta}e^{-\frac{2}{12\beta^2}(1+0\cdot148/\beta^2)}$$

was used. See, for example, Whittaker and Watson, 'Modern Analysis,' second edition, p. 270.
(6) Mellin's formula,

$$\frac{[\Gamma(\alpha)]^2}{|\Gamma(\alpha+i\beta)|^2} = \prod_{s=0}^{\infty}(1+\beta^2/(\alpha+s)^2)$$

was used. See Nielsen, 'Handbuch der Theorie der Gammafunktion,' p. 63.
(7) B. W. Sargent, Proc. Roy. Soc. A, cxxxix. p. 659 (1933).
(8) R. W. Gurney, Proc. Roy. Soc. A, cix. p. 540 (1925). This value may be too low because it was estimated from the intersection of the RaC and RaB+C spectra after fitting the two at high energies.
(9) R. W. Gurney, Proc. Roy. Soc. A, cix. p. 540 (1925). This value is also checked by D'Espine, *Ann. Physique*, xvi. p. 32 (1931); Feather, Phys Rev. xxxv. p. 1559 (1930); and Madgwick, Proc. Camb. Phil. Soc. xxiii. p. 970 (1927).
(10) R. W. Gurney, Proc. Roy. Soc. A, cxii. p. 380 (1926). This value may be too low for the same reason as that given for RaB.
(11) W. J. Henderson, Proc. Roy. Soc. xxv. p. 331 (1929).
(12) F. C. Champion, Proc. Roy. Soc. A, cxxxiv. p. 672 (1932).
(13) F. A. Scott, Phys. Rev. xlviii. p. 391 (1935).
(14) C. D. Ellis and N. F. Mott, Proc. Roy. Soc. A, cxxxix. p. 369 (1933); and cxli. p. 502 (1933).
(15) B. W. Sargent, Proc. Camb. Phil. Soc. xxviii. p. 538 (1922).
(16) Kovarik and McKeehan, Phys. Rev. viii. p. 574 (1916).
(17) O. W. Richardson, Proc. Roy. Soc. A, cxlvii. p. 442 (1934).

LXXVII. *Electrostatic Energy as the Mutual Energy of Vibrating Particles.* *By* E. Taylor Jones, *D.Sc., Professor of Natural Philosophy in the University of Glasgow* *.

IN a recent paper † the hypothesis was examined that the electrostatic attraction or repulsion of two electrons is the result of the interaction of their natural vibrations, by which they are caused to vibrate with a common frequency, different from their undisturbed frequency, as a coupled system. It was shown that, in accordance with a certain assumed law of the interaction, two electrons repel each other if their vibrations are in the same phase and attract each other if their phases are opposite. According to this view of the nature of electrostatic action the question whether two electrons are of the same or of different kinds is therefore determined by the manner in which they vibrate with their common frequency when in presence of each other; they are of the same kind if they vibrate in the same phase, and of different kinds if their vibrations are opposite in phase. The vibrations being free from damping, the only phase differences that occur are 0 and π.

It was further shown that at all but extremely short distances the mutual energy and force of two stationary electrons indicated by the vibrational theory agree with the electrostatic energy and force if the magnitude of the "charge" e of an electron is given by

$$e^2 = \frac{hk}{2\pi\sqrt{a}}, \quad \ldots\ldots\ldots \quad (1)$$

or, which is equivalent, by

$$e = \frac{h}{2\pi c_0}\sqrt{k}\,\sqrt{m_0}. \quad \ldots\ldots\ldots \quad (2)$$

In these expressions h is Planck's constant, c_0 is the velocity of light *in vacuo*, k is the coupling of two stationary electrons at unit distance apart, a is $4\pi^2\nu_0^2$, and ν_0, m_0 are the frequency and mass of an electron at rest and far removed from other electrons.

* Communicated by the Author.
† Phil. Mag. xxi. p. 337 (1936).

In the paper referred to the vibrational theory was also applied to a number of other systems consisting of small numbers of electrons arranged in configurations of simple regular form, with the result that the mutual vibrational energy of such systems again agrees with the electrostatic energy if the charge of an electron is given by the expression (1) or (2). In other systems reasons were found for supposing that the vibration sometimes fluctuates between two modes, the average vibrational energy in such cases being suggested as the equivalent of the electrostatic energy.

In general it is not convenient to determine the common frequency of a system from the equations of motion of the individual electrons of which it is composed. In some cases, however, it is possible to divide the electrons into two groups, each group being of simple regular form, and to calculate the frequency of the whole system from the frequencies which the groups have when separate and the interaction between them when they are coupled together. If the square of the periodicity (*i. e.*, $4\pi^2\nu^2$) of the first group when separate be denoted by a_1, that of the second group by a_2, and if the coupling of each electron of the first group with all those of the second group is b_1 *, and similarly the coupling of each electron of the second group with all those of the first group is b_2, the equations for the vibratory motion of the coupled system are

$$\left.\begin{aligned} \ddot{x}+a_1x+b_1z=0, \ldots \\ \ddot{z}+a_2z+b_2x=0, \ldots \end{aligned}\right\} \quad . \quad . \quad . \quad . \quad (3)$$

where x and z represent the displacements in the vibratory motion of two typical electrons, one in each group. It is, of course, an essential condition that b_1 should be the same for all the members of the first group, which is the case if all the electrons of the first group are similarly situated, in regard to sign as well as position, with respect to those of the second group. Also b_2 must be the same for all the members of the second group.

Assuming $x = \mathrm{A}e^{int}$, $z = \mathrm{B}e^{int}$, $(n = 2\pi\nu)$, and substituting in (3), we find

$$\left.\begin{aligned} (-n^2+a_1)\mathrm{A}+b_1\mathrm{B}=0, \ldots \\ (-n^2+a_2)\mathrm{B}+b_2\mathrm{A}=0. \ldots \end{aligned}\right\} \quad . \quad . \quad . \quad (4)$$

* I. e., b_1 is the sum of the values of the coupling of all members of the second group with one member of the first group.

The common frequencies of the whole system are therefore given by the equation

$$(n^2-a_1)(n^2-a_2)=b_1b_2, \quad . \quad . \quad . \quad . \quad . \quad (5)$$

that is, by

$$n^2=\frac{a_1+a_2}{2}\pm\tfrac{1}{2}\sqrt{(a_1-a_2)^2+4b_1b_2}. \quad . \quad . \quad (6)$$

and the ratio of the amplitudes of vibration in the two groups is

$$\left.\begin{aligned}\frac{B}{A}&=\frac{n^2-a_1}{b_1}\\&=\frac{b_2}{n^2-a_2}\end{aligned}\right\} \quad . \quad . \quad . \quad . \quad . \quad . \quad (7)$$

As an illustration of the group formula (6) we will calculate two of the frequencies of a system of four electrons placed symmetrically in the same straight line (fig. 1).

Taking the two inner electrons x, y as the first group, the outer electrons z, u as the second, and denoting the coupling of x and y by c, that of z and u by c', that of

Fig. 1.

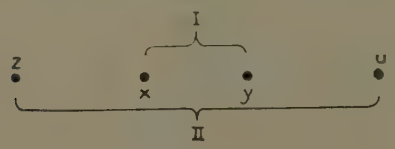

x and z (or y and u) by b, and that of x and u (or y and z) by d, we have, if the two electrons in each group are of the same kind,

$$\left.\begin{aligned}a_1&=a+c, \ldots\\a_2&=a+c', \ldots\\b_1=b_2&=b+d. \ldots\end{aligned}\right\} \quad . \quad . \quad . \quad . \quad . \quad (8)$$

If all four electrons are of the same kind the frequency of the system is given by

$$n_1^2=a+\frac{c+c'}{2}+\tfrac{1}{2}\sqrt{(c-c')^2+4(b+d)^2}. \quad . \quad . \quad (9)$$

Using the geometrical relations

$$\frac{1}{c}+\frac{2}{b}=\frac{1}{c'},$$

$$\frac{1}{c}+\frac{1}{b}=\frac{1}{d},$$

we can express b and d in terms of c and c', and denoting n_1^2-a by N_1, we have

$$\frac{N_1}{c}=\frac{1}{2}\left(1+\frac{c'}{c}\right)+\frac{1}{2}\sqrt{\left(1-\frac{c'}{c}\right)^2+\frac{4b_1^2}{c^2}}, \quad . \quad (10)$$

where

$$\frac{b_1}{c}=4\frac{c'}{c}\cdot\frac{1}{1-c'^2/c^2}. \quad . \quad . \quad . \quad . \quad (11)$$

Values of N_1/c calculated by (10) for various values of the ratio c'/c,, (*i. e.*, of the ratio of the distance between the inner to that between the outer particles) are shown in curve N_1 (fig. 2).

If c is constant the ordinate of curve N_1 in fig. 2 represents the manner in which the frequency of the system (or, rather, the quantity n_1^2-a) varies as the outer particles move from infinity towards the inner ones.

Since $$n_1^2=a+N_1,$$

and N_1 is small in comparison with a except when c'/c is very nearly equal to unity, we have

$$n_1=\sqrt{a}+\frac{N_1}{2\sqrt{a}}$$

$$=2\pi\nu_1.$$

The total mutual vibrational energy of the four particles is therefore

$$4h(\nu_1-\nu_0)=\frac{hN_1}{\pi\sqrt{a}}. \quad . \quad . \quad . \quad . \quad . \quad (12)$$

The ordinate of curve N_1 in fig. 2 is therefore proportional to the mutual vibrational energy of the system except at points for which the abscissa c'/c is very nearly equal to unity *.

* The outer particles must approach the inner ones to within about 10^{-11} cm. in order that this proportionality should fail to be appreciably exact (*l. c.* p. 341).

In order to exhibit the comparison between this energy and the electrostatic energy we will follow the plan adopted in the previous paper *. Assuming that the " charge " e of an electron has the normal value given by (1), we find that the mutual vibrational energy (12) is

$$4h(\nu_1-\nu_0)=2e^2N_1/k,$$

Fig. 2.

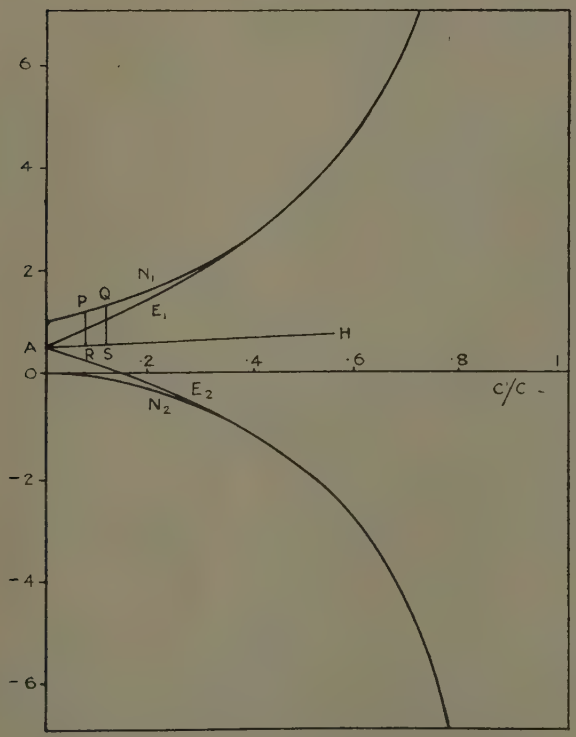

Frequency and energy curves for system of four particles.

and if this is equated to the electrostatic energy E_1 we have

$$N_1=\frac{kE_1}{2e^2}. \quad . \quad . \quad . \quad . \quad . \quad . \quad (13)$$

* *L. c.* p. 349.

Consequently the value of the electrostatic energy E_1, calculated in the usual way from the expression $\Sigma e^2/r$, and multiplied by the factor $k/2e^2c$, should be equal to N_1/c.

The value of E_1 for this system is

$$E_1 = \Sigma e^2/r$$

$$= \frac{e^2}{k}\{c+c'+2(b+d)\}$$

$$= \frac{e^2c}{k}\left(1+\frac{c'}{c}+8\frac{c'}{c}\cdot\frac{1}{1-c'^2/c^2}\right), \quad . \quad . \quad (14)$$

and $kE_1/2e^2c$ is therefore equal to one-half the quantity in brackets in (14). Values of this quantity for various values of c'/c are shown by the curve E_1 in fig. 2. If the mutual vibrational energy were equal to the electrostatic energy, and if the "charge" had the normal value (1), this curve would coincide with curve N_1 (fig. 2). It is found that the two curves have very large and equal ordinates at $c'/c=1$, and that they run closely together over the range $c'/c=1$ to about 0·5 *. Nearer the origin they separate, and when $c'/c=0$, *i. e.*, when the two outer particles are infinitely far away, the value of $kE_1/2e^2c$ is only one-half that of N_1/c. the latter quantity being unity, the former 0·5. In this configuration ($c'/c=0$) the common frequency of the whole system is equal to that of the first group alone, i. e., $n_1^2=a+c$.

By equation (7), however, we find that the ratio of the amplitude of vibration in the second group to that in the first group in this mode is

$$\frac{B}{A} = \frac{b_2}{n_1^2-a_2},$$

which is zero when $c'/c=0$, since $b_2(=b_1)=0$ by (11), and $n_1^2-a_2=c$. It follows that when $c'/c=0$ the outer particles have zero amplitude in the mode N_1, the energy of the vibration in this mode is that of two particles instead of four, and the ordinate of curve N_1 (fig. 2) at zero abscissa should therefore be halved, which makes it equal in value to $kE_1/2e^2c$ at this point. In this state of the system, in which the two outer particles are infinitely far removed from the inner ones, the outer

* At $c'/c=0{\cdot}5$ the value of N_1/c is 3·428, that of $kE_1/2e^2c$ is 3·417. At $c'/c=0{\cdot}6$, $N_1/c=4{\cdot}555$, and $kE_1/2e^2c=4{\cdot}550$.

particles are vibrating, not in the common mode $a+N_1$ (here $a+c$) of the whole system, but with their natural undisturbed frequency $\sqrt{a}/2\pi$, which is to be regarded as a " partial oscillation " of only a portion of it.

It appears, therefore, that, when allowance is made for the partial oscillation, the mutual vibrational energy agrees with the electrostatic energy in the extreme configurations $c'/c=0$ and 1, and very approximately also over the range from $c'/c=0{\cdot}5$ to 1. The question occurs here as to the manner in which the vibrations of the system changes from the modes $a+c$ (2 particles) and a (2 particles) to the mode $a+N_1$ (4 particles) as the outer particles are moved gradually inwards from an infinite distance. It is highly improbable that this change takes place in one step only, since this would involve a sudden and permanent increase in the energy of the system at a stage in which the outer particles are far removed from the inner ones. It is much more probable that (as suggested in the former paper in connection with a similar problem *) the partial oscillation tends to persist, and that the common mode $a+N_1$ appears at first intermittently, the energy fluctuating between the values appropriate to the two states of vibration until the common mode is finally established. The lower limit of the fluctuations is represented by the straight line AH (fig. 2), the ordinate of which, $\frac{1}{2}(1+c'/c)$, is proportional to the sum of the energies of the two groups vibrating in the modes $a+c$ and $a+c'$.

We suppose the outer particles z and u to move inwards with small uniform velocity, this motion being maintained, and the particles x and y being kept fixed, by suitable forces acting through the external connexions of the system. The initial energy of the system is represented by the point A (fig. 2), and at first the energy increases along the line AH. After a time a fluctuation occurs, in which the energy increases from the line AH to the curve N_1, the change being represented by the vertical line RP (fig. 2). This increment of energy must be supplied by external impulsive forces †, the magnitude of the increase being

* *Loc. cit.* p. 350.

† The impulsive forces must be supposed to act through the vibratory coordinates and to be due to other electrons which should, in strictness, be included in the system. For simplicity, however, we are regarding these forces as " external."

$$\frac{4h\sqrt{a+N_1}}{2\pi}-\frac{2h\sqrt{a+c}}{2\pi}-\frac{2h\sqrt{a+c'}}{2\pi}=\frac{h}{\pi\sqrt{a}}\left(N_1-\frac{c+c'}{2}\right), \quad . \quad . \quad . \quad (15)$$

since N_1, c, and c' are small in comparison with a. Later the second part of the fluctuation occurs, which may be represented by QS (fig. 2), the energy falling again to the lower level, and this change requires impulsive forces in the opposite direction. As the movement proceeds the average energy of the system increases gradually, and represents, according to the vibrational theory, the electrostatic energy of the system. The total work done by the external forces up to any stage of the motion is the sum of the work done by the impulsive forces and that done in the intervals between them. The intervals for which the system is in the higher energy mode increase in duration relatively to those in which it is at the lower level until c'/c passes the value 0·5, when the lower energy modes practically cease to appear and the common mode is established.

Another mode of vibration of the 4-particle system is that in which the frequency is given by

$$\frac{N_2}{c}=\frac{1}{2}\left(1+\frac{c'}{c}\right)-\frac{1}{2}\sqrt{\left(1-\frac{c'}{c}\right)^2+\frac{4b_1^2}{c^2}}, \quad . \quad (16)$$

b_1 having again the value given by (11). The amplitude equation for this mode is, by (7),

$$\frac{B}{A}=\frac{b_2}{n_2^2-a_2},$$

and since n_2^2 is less than a_2 * the phases in the two groups are opposite. This evidently represents the case in which the two particles of each group are of the same kind but different in kind from those of the other group.

The electrostatic energy of this system is

$$E_2=\frac{e^2c}{k}\left(1+\frac{c'}{c}-8\frac{c'}{c}\frac{1}{1-c'^2/c^2}\right), \quad . \quad . \quad (17)$$

and the values of N_2/c and $kE_2/2e^2c$ are shown in curves N_2 and E_2 (fig. 2). The ordinates of these two curves have very great and equal negative values when

* By the general equation (6) n_1^2 is greater than both a_1 and a_2, and n_2^2 is less than both.

$c'/c=1$, and, as in the first mode, the two curves almost coincide over the range down to $c'/c=0{\cdot}5$ *. At smaller values of c'/c, i. e., as the outer particles recede further from the inner ones, the curves diverge, the ordinate of curve N_2 becoming zero (i. e., $n_2{}^2=a$), that of curve E_2 $+0{\cdot}5$ when $c'/c=0$. It is to be remembered that, as in all similar problems, N_2 gives the frequency (more precisely, the value of $n_2{}^2-a$) of the whole system, and does not take account of partial oscillations. It is obvious, however, that when $c'/c=0$ the two groups are vibrating with different frequencies, the outer group alone having the common frequency $\sqrt{a}/2\pi$ of the whole system, the inner group having zero amplitude in this mode but making a partial oscillation of frequency $\sqrt{a+c}/2\pi$. The amplitude equation (7) also indicates that the inner group has zero amplitude when $N_2=0$, for

$$\frac{A}{B}=\frac{b_1}{n_2{}^2-a_1}=0,$$

since $b_1=0$, $n_2{}^2-a_1=-c$ when $c'/c=0$. In this configuration the mutual energy of the system is merely that of the inner group—that is, $hc/2\pi\sqrt{a}$, which is equal to the electrostatic energy E_2 if the charge has the value (1). The divergence between the N_2 and E_2 curves (fig. 2) is to be accounted for by the persistence of the partial oscillation and by energy fluctuations the upper limit of which is represented by the line AH, the lower limit by curve N_2.

Another system that can be treated by the group formula (6) is that of eight electrons placed at the corners of two concentric and similarly situated squares (fig. 3). The inner square forming group I, the outer group II, the coupling of two diagonally opposite electrons in group I being denoted by c, that in group II by c', the equations for this system are

$$\left.\begin{aligned} a_1&=a+(2\sqrt{2}+1)c,\\ a_2&=a+(2\sqrt{2}+1)c',\end{aligned}\right\} \quad . \quad . \quad . \quad . \quad . \quad (18)$$

$$\frac{b_1}{c}=\frac{b_2}{c}=4\frac{c'}{c}\left(\frac{1}{1-c'^2/c^2}+\frac{1}{\sqrt{1+c'^2/c^2}}\right). \quad . \quad (19)$$

* At $c'/c=0{\cdot}5$ N_2/c and $kE_2/2e^2c$ have the values $-1{\cdot}928$ and $-1{\cdot}917$. At $c'/c=0{\cdot}6$ the values are $-2{\cdot}955$ and $-2{\cdot}950$.

For the first mode, in which all eight electrons are of the same kind, and the second mode, in which the electrons of each group are of the same kind but are different from those of the other group, the frequency equations are

$$\left.\begin{matrix} N_1/c \\ N_2/c \end{matrix}\right\} = 1{\cdot}914\left(1+\frac{c'}{c}\right) \pm \sqrt{3{\cdot}662\left(1-\frac{c'}{c}\right)^2 + \frac{b_1^2}{c^2}}, \quad (20)$$

and the corresponding values of the electrostatic energy E_1, E_2, are given by

$$\left.\begin{matrix} kE_1/4e^2c \\ kE_2/4e^2c \end{matrix}\right\} = 1{\cdot}914\left(1+\frac{c'}{c}\right) \pm \frac{b_1}{c}. \quad (21)$$

Fig. 3.

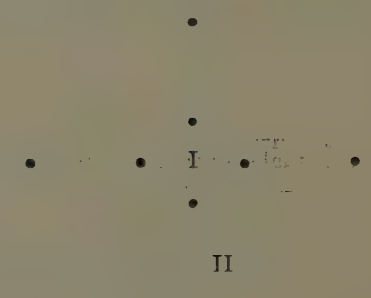

The four curves representing values of N_1/c, $kE_1/4e^2c$, N_2/c, $kE_2/4e^2c$ for various values of c'/c are indicated in fig. 4 by N_1, E_1, N_2, E_2. The form of the curves in this case is generally similar to that in the previous problem, the chief difference being that in fig. 4 the N_2 curve over a portion of its course near the origin lies above the horizontal axis. This indicates that when the outer particles are sufficiently far from the inner square the effect of the group I particles in lowering the frequency of group II is not as great as the frequency-raising effect of the group II particles upon each other. The N_2 curve, however, falls to zero when $c'/c=0$—that is, when the outer square is infinitely large—in which case a partial oscillation of frequency $\sqrt{a}+3{\cdot}828c/2\pi$ appears in the inner group. The difference between the N_1 and E_1

curves and that between the N_2 and E_2 curves may be accounted for, as in the previous problem, by the persistence of the partial oscillation and fluctuations of the vibrational energy which result from it. The lower limit of the fluctuations in the first mode and the upper

Fig. 4.

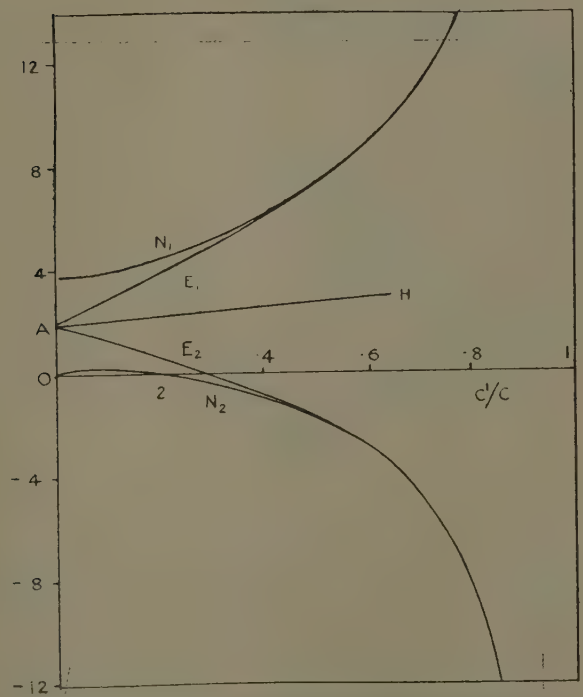

Frequency and energy curves for system of eight particles.

limit in the second mode are represented by the straight line AH (fig. 4), the ordinate of which is $1{\cdot}914\ (1+c'/c)$.

In fig. 5 are shown the curves for a system of sixteen particles placed at the corners of two concentric and similarly situated cubes, c being the coupling of two diagonally opposite particles in the inner cube (group I),

c' that in the outer cube (group II). The equations for this system are

$$\left.\begin{aligned} a_1 &= a+(3\sqrt{3}+3\sqrt{3}/\sqrt{2}+1)c \\ &= a+9{\cdot}871\,c, \ldots\ldots \\ a_2 &= a+9{\cdot}871c', \ldots\ldots \end{aligned}\right\} \ldots \quad (22)$$

Fig. 5.

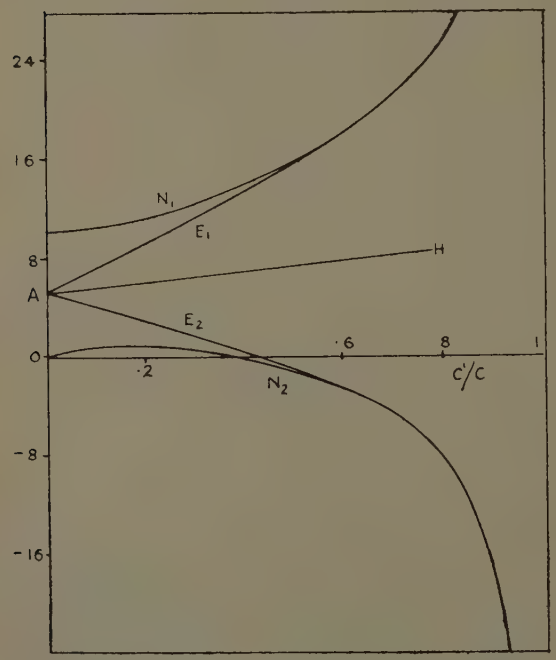

Frequency and energy curves for system of sixteen particles.

$$\frac{b'}{c}=\frac{b_2}{c}=4\frac{c'}{c}\left(\frac{1}{1-c'^2/c^2}+\frac{2{\cdot}598}{\sqrt{3(1+c'^2/c^2)+2c'/c}}+\frac{2{\cdot}598}{\sqrt{3(1+c'^2/c^2)-2c'/c}}\right), \quad (23)$$

$$\left.\begin{matrix} N_1/c \\ N_2/c \end{matrix}\right\} = 4{\cdot}935\left(1+\frac{c'}{c}\right) \pm \sqrt{24{\cdot}35\left(1-\frac{c'}{c}\right)^2 + \frac{b_1^2}{c^2}}, \quad (24)$$

$$\left.\begin{matrix} kE_1/8e^2c \\ kE_2/8e^2c \end{matrix}\right\} = 4{\cdot}935\left(1+\frac{c'}{c}\right) \pm \frac{b_1}{c}. \quad . \quad . \quad . \quad . \quad . \quad . \quad (25)$$

The positive portion of curve N_2 (fig. 5) covers a greater range of values of c'/c than that in the problem of two squares (fig. 4), as might be expected, but otherwise the curves for the two systems are generally similar. In the system of two cubes, if $c'=0$ the two groups are oscillating independently, the inner with frequency $\sqrt{a+9{\cdot}871\,c}/2\pi$, the outer with frequency $\sqrt{a}/2\pi$. Of these two values the former represents the "common frequency" in the first mode, the latter in the second mode. The line AH in fig. 5, of ordinate $4{\cdot}935(1+c'/c)$, represents the lower and upper limits of the energy fluctuations in the first and second modes respectively.

Of the same nature is the problem of two concentric spherical surfaces having equal numbers of electrons distributed over them. If N is the number on each sphere, and r_1, r_2 are the radii of the inner and outer spheres, we have

$$\left.\begin{aligned} a_1 &= a+\Sigma b \,* \\ &= a+kN/r_1 \\ &= a+Nc, \\ a_2 &= a+Nc', \end{aligned}\right\} \quad . \quad . \quad . \quad . \quad . \quad (26)$$

c being written for k/r_1 (*i. e.*, the coupling of two electrons at distance r_1 apart), and c' for k/r_2. Also

$$\begin{aligned} b_1 = b_2 &= kN/r_2 \\ &= kc'. \quad . \quad . \quad . \quad . \quad . \quad . \quad (27) \end{aligned}$$

Hence, by (6),

$$\left.\begin{matrix} N_1/cN \\ N_2/cN \end{matrix}\right\} = \frac{1}{2}\left(1+\frac{c'}{c}\right) \pm \frac{1}{2}\sqrt{\left(1-\frac{c'}{c}\right)^2 + \frac{4c'^2}{c^2}}, \quad (28)$$

N_1 being the value of n^2-a when the charges on the two spheres are of the same kind, N_2 when they are of different kinds.

* *L. c.* p. 347.

Assuming that N is not so large that N_1 fails to be small in comparison with a *, we have for the mutual vibrational energy in the first mode

$$2Nh(\nu_1-\nu_0)=hNN_1/2\pi\sqrt{a},$$

and this being equated to the electrostatic energy E_1, we find that N_1/cN should be equal to kE_1/N^2e^2c, and

Fig. 6.

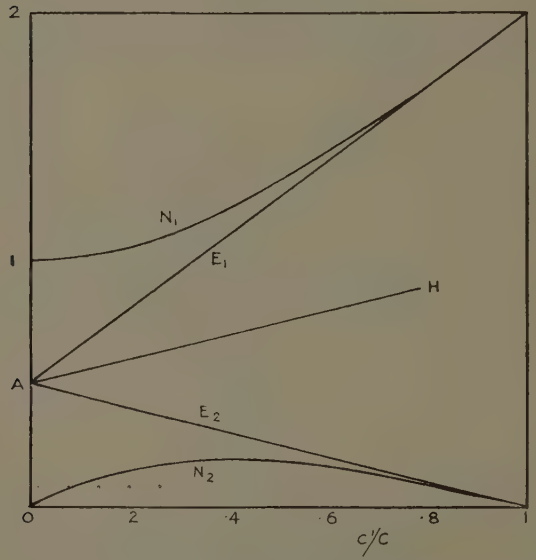

Frequency and energy curves for system of particles on two concentric spheres.

similarly N_2/cN equal to kE_2/N^2e^2c, if e has the usual value (1). The equations for E_1 and E_2 are

$$\left.\begin{matrix} kE_1/N^2e^2c \\ kE_2/N^2e^2c \end{matrix}\right\} = \frac{1}{2}\left(1+\frac{c'}{c}\right) \pm \frac{c'}{c}. \quad . \quad . \quad . \quad (29)$$

In fig. 6 the curves marked N_1, E_1, N_2, E_2 give values of N_1/cN, kE_1/N^2e^2c, N_2/cN, kE_2/N^2e^2c for various values

* In practice a sphere can be charged so strongly that cN, and therefore also N_1, is not small in comparison with a. In condensers, however, the mode is $a+N_2$, and c'/c being not far short of unity, N_2/a is always small in such systems.

of c'/c. The radius of the inner sphere being kept constant, the curves show how these quantities vary in value as the radius of the outer sphere diminishes from infinity to equality with that of the inner one. It is seen that the four quantities are positive over the whole range, and that the ordinates of curves N_1, E_1, and those of N_2, E_2, have equal and finite values (the latter both zero) if $c'/c=1$. At the other end, where $c'/c=0$, the divergence of the frequency and energy curves is greatest, this being due to the fact that N_1 and N_2 do not now represent the actual state of oscillation of the system. In this configuration the inner sphere is vibrating with its own frequency $\sqrt{a+c}\mathrm{N}/2\pi$, the outer sphere with the frequency $\sqrt{a}/2\pi$. The divergence between the frequency and energy curves at other values of c'/c is to be accounted for, as in the other problems, by fluctuations of the state of vibration between the common mode and the partial modes, one limit of the fluctuation (viz., that corresponding to the partial modes) being represented in fig. 6 by the line AH, the ordinate of which is $\frac{1}{2}(1+c'/c)$.

It may be noted that in each of the problems here discussed the divergence between the N_1 and E_1 and between the N_2 and E_2 curves arises entirely from the term $(a_1-a_2)^2$ under the square root in the frequency equation (6), and that the divergences would disappear, and no partial oscillations or fluctuations would make their appearance, if the two groups into which the system is divided had equal frequencies when not coupled to each other. It appears also that this relation, $a_1-a_2=0$, is also the condition that the amplitudes of vibration in the two groups oscillating with their common frequency, as given by the ordinary dynamical theory of the vibrations, should be equal. For by equation (7) the amplitude ratio in the first mode in any of these systems is

$$\frac{\mathrm{B}}{\mathrm{A}}=\frac{n_1^2-a_1}{b_1},$$

and by (6)

$$n_1^2-a_1=-\frac{a_1-a_2}{2}+\tfrac{1}{2}\sqrt{(a_1-a_2)^2+4b_1^2},$$

so that when $a_1=a_2$, $n_1^2-a_1=b_1$, B=A, and the vibrational energies of the two groups are also equal. The

same result holds for the second mode in each of the systems considered. It seems that though the amplitude relation indicated by the ordinary dynamical theory is, if taken strictly, in general inconsistent with the quantum condition which requires that all electrons vibrating with a given frequency should have the same energy, it can nevertheless be interpreted in a manner which is quite in accordance with this condition. If $B/A = \pm 1$ the energies of vibration of the electrons are all equal. If either B/A or A/B is zero a part of the system ceases to oscillate with the common frequency. In each of these cases the result given by the ordinary theory agrees with the quantum condition, and the system can oscillate steadily without fluctuations. But if B/A and A/B are neither zero nor ± 1 the ordinary theory indicates that the electrons in the two groups are vibrating with different energies in the same frequency, and this is contrary to the quantum condition. In these circumstances the system responds to the divergent conditions by fluctuating between two states of vibration, the time spent in one or the other depending in some way on the ratio B/A, such that if, for example, B/A changes from 0 to 1 the proportion of the time spent in the common mode also increases from zero to unity.

It may also be remarked that, quite apart from any vibrational theory of electrostatic action, there are many theorems in ordinary electrostatics which can in general only be interpreted as representing average effects of rapidly fluctuating conditions. This arises from the fact that an electric charge is always an integral multiple of a finite unit. For example, if a charge is placed at the centre of a hollow conducting sphere, an equal and opposite charge is, according to a well-known theorem, induced upon and is spread uniformly over the inner surface of the sphere. If the charge at the centre is that of one positive electron, or one proton, then one negative electron is required to be uniformly spread over the sphere, which can only mean that it appears at different places on the surface, with an equal probability of its being at any two points upon it. Even if the central charge were much greater, say that of 10^4 positive electrons, there would still be much fluctuation on the spherical surface if this is not very small. If its radius is 10 cm. it would have about eight electrons per sq. cm.,

the positions of which would require to vary considerably and rapidly in order to produce the effect of a uniform surface density. Another theorem in electrostatics states that if a point-charge e is placed outside and at distance f from the centre of an earthed conducting sphere of radius r, the induced charge on the sphere is $-er/f$. If the inducing charge is that of one proton, and $f=10$ cm., $r=1$ cm., then the induced charge is one-tenth of that of a negative electron. This can only be interpreted as meaning the time-average of the induced charge, and the induced charge at any given moment is quite indeterminate, being that of any number of electrons with a maximum probability of the number being zero. Many other examples might be given, and it can be said that in all electrostatic systems of charged conductors the electrons which by their excess or their deficiency are responsible for the surface charges are in general continually in motion in such a way that the average value of the charge on a given small area of a surface agrees with that indicated by the electrostatic laws.

Returning to the problem of the concentric spheres we note (fig. 6) that if c'/c is nearly equal to unity the mutual vibrational energy in the second mode agrees with the electrostatic energy if the charge of an electron has the normal value (1). This covers the case of a charged parallel-plate condenser regarded as a spherical condenser with its plates very near each other. The condenser system may also be treated independently by the group formula (6) if we consider portions of the plates removed from the edges or regard the disks as being surrounded by guard-rings. The external radius of each guard-ring being R, the distance between the plates d (supposed small in comparison with R), and the number of electrons per unit area on each plate being N′, we have, for the electrons on the disks,

$$a_1=a_2=2\pi k\mathrm{N}'\mathrm{R},$$

$$b_1=b_2=2\pi k\mathrm{N}'(\mathrm{R}-d),$$

if d^2/R^2 is so small as to be negligible. Hence by (6)

$$\mathrm{N}_2=2\pi k\mathrm{N}'d,$$

and the excess of the vibrational energy of the electrons

on the disks over their energy when far removed from one another and from all other electrons is

$$2N'Sh(\nu_2-\nu_0)=e^2N'SN_2/k$$
$$=2\pi e^2N'^2Sd,$$

if S is the area of each disk, and e, the charge of an electron, has the value given by (1). The energy excess is therefore $Q^2/2C$, if $Q(=N'eS)$ is the charge on each disk, and $C=S/4\pi d$.

We have supposed the charge on each plate to be that of a group of single electrons. It is clear, however, that in the condenser system, and in all the other systems considered in this and the former paper, each electron may be replaced by a subgroup of electrons, the linear dimensions of each of the subgroups being small in comparison with the distances between them. Provided the subgroups in each group are all similar and of simple regular form (*e. g.*, spheres or cubes), and the form and position of the groups are such that b_1 is the same for all the members of the first group, and b_2 for those of the second group, the frequency and the vibrational energy of any such system may be calculated by the method illustrated in the present paper.

Natural Philosophy Department,
The University, Glasgow.
July 1936.

LXXVIII. *The Structure of Aluminium, Chromium, and Copper Films Evaporated on Glass.* *By* R. Beeching, *A.R.C.S., B.Sc.* *

[Plates VIII. & IX.]

Introduction.

DURING the course of research, conducted with a view to establishing the best method of preparing evaporated metal films for mirrors, specimens of aluminium, chromium, and copper films on glass were examined by electron diffraction. Several interesting features in their structure were observed, although, owing to the necessity for keeping the immediate practical

* Communicated by Prof. A. O. Rankine, D.Sc., F.R.S.

object in view, it was not possible to examine some of the effects in detail.

Preparation of Specimens.

The evaporation, which was not performed by the author, was carried out in a metal chamber, the initial pressure in which was of the order of 10^{-4} mm. of mercury. When the evaporation was begun there was a momentary drop in pressure, followed by a rise to two or three times the initial value. After the evaporation was over the pressure was lower than at the beginning. which suggests that the evaporating process has a "gettering" effect.

In order that specimens of suitable dimensions for electron diffraction examination might be prepared with minimum handling, the metal was evaporated on to glass strips about 1 cm. wide and about 5 cm. long. These were divided into six parts by diamond scratches on the face upon which the metal was to be evaporated. A sharp tap with a file on the back face was sufficient to break the strips into pieces. The metal was evaporated from a filament placed slightly to one side of the glass strip, so that one edge of the strip was coated as well as the face to be examined. This was done in order to enable contact to be made with the metal film, to prevent charging up when the electron beam was incident upon the specimen surface.

A standard method of cleaning the glass was adopted. The strips were washed in aqua regia, then in distilled water, rubbed hard with clean cotton-wool soaked in hydrogen peroxide solution, and finally dried on dry cotton-wool. In order to prevent contamination from handling, rubber gloves washed with ammonia were worn. This method of cleaning is that recommended by Mr. E. W. Foster of the Imperial College of Science for the preparation of sputtered silver films, where conditions of cleanliness are of extreme importance. The cleaning procedure was probably more stringent than was necessary, but was adopted to eliminate uncertainty in the results as far as possible.

Aluminium Films: Scheme of Examination.

It was decided first of all to vary the thickness of the films, then the path from heater to mirror, also the

speed of evaporation, and finally the vacuum conditions. Under each set of evaporating conditions three strips of specimens were prepared. One of these was examined without further treatment, one was heated to 250° C. in an air-oven, and one was washed with methylated spirits before examination. One strip was washed with methylated spirits because it has been suggested that this treatment hardens the film. It is difficult to imagine a possible mechanism for such hardening, and, in fact, no such effect was observed. Electron diffraction examination showed no change in structure, and the washed specimens were found to scratch as easily as the unwashed ones.

Change of Thickness of the Film.

The structure of the evaporated films was found to vary in a very marked manner with increasing thickness. Very thin films, about 100–200 Å. thick (*i. e.*, films which were barely visible by transmitted light, but which appeared to reflect quite well and had a metallic lustre by reflected light), gave electron diffraction patterns which showed no trace of aluminium metal. A considerable number of plates of this pattern were taken, and the mean crystal spacings calculated from them are shown in Table I. The intensities of the rings are not given, as these were found to vary from specimen to specimen. A typical pattern is shown in fig. 1 (Pl. VIII.).

The compound producing these rings is almost certainly some form of aluminium oxide (Al_2O_3). There are several reasons for supposing this. Firstly, the residual gas in the apparatus was air, and since no known form of aluminium nitride exists the oxide seems the obvious choice. Added to this the diffraction pattern shows the compound to have a crystal structure with a face-centred cubic lattice of cube side $a=7{\cdot}82$ Å. In this respect the structure is similar to that of γAl_2O_3, which has a face-centred cubic lattice the cube side of which has been given as 7·77 Å. and 7·90 Å. by different workers. The ring intensities in the pattern from thin films were, however, quite different from those in the γAl_2O_3 pattern. According to Verwey * the structure of γAl_2O_3 is a face-centred cubic lattice of oxygen with aluminium atoms

* Verwey, *Zeit. f. Krist.* xci. p. 65 (1935).

distributed at random, in certain proportions, over a limited number of possible positions in the cell. In the case of another form of the oxide, $\gamma' Al_2O_3$, Verwey * suggests a similar structure with even less constraints upon the positions of the aluminium atoms. It would seem quite probable, therefore, that the compound giving rise to the patterns obtained from very thin films of aluminium is some form of Al_2O_3 related to the γ form. The supposition that the compound is Al_2O_3 is strengthened by the fact that films of evaporated chromium

TABLE I.

Plane.	Observed spacing.	Spacing of γAl_2O_3.
111	4·56 Å.	4·49 Å.
200	3·87	3·88
211	3·20	3·17
220	2·73	2·74
311	2·33	2·34
222	—	2·24
400	1·98	1·94
331	—	1·78
420	—	1·74
422	1·65, very faint.	1·58
511 } 333 }	—	1·49
440	1·39	1·37
531	—	1·31
442 } 600 }	—	1·29
620	1·22	1·23
533	—	1·18
622	—	1·17
444	1·12	1·12
	Cube side $a = 7·82$ Å.	$a = 7·77$ Å. Steinheil.

give a similar pattern when heated. The only oxide of chromium which would be expected to have a crystal structure similar to that of an aluminium oxide is Cr_2O_3.

Thicker films of aluminium, about 500–1000 Å. thick (*i. e.*, films which are quite blue by transmitted light, but which are too thick to allow print to be read through them), give patterns showing both oxide rings and the ordinary aluminium pattern. Usually only one or two

* Verwey, 'Laboritoria.' N. V. Phillips, Gloeilampenfabrieken, Eindhoven, Holland (1935).

oxide rings appear, and, as a rule, the aluminium rings tend to be rather diffuse, indicating small crystal size. In some cases the pattern consists of very diffuse aluminium rings with no oxide rings. A probable explanation of these patterns is that in some cases the upper surface of the film consists of aluminium and oxide mixed, while in others the oxygen prevents the formation of large crystals without actually going into combination. (Large crystals, as referred to here, mean crystals of over 100 Å. side, while crystals so small as to give really diffuse rings have dimensions of about 20 Å.)

Still thicker films of aluminium (*i. e.*, films which are almost or quite opaque) give sharp ring patterns due to crystals of aluminium more than about 100 Å. square. In nearly all cases these patterns show a tendency for the aluminium crystals to orientate with a cube face parallel to the glass surface. A further account of the orientation of these films will be included later.

Variation of the Distance from Heater to Mirror.

Variation of the distance from heating filament to the specimen surface appears not to affect the film, provided the thickness of the film is about the same in each case, except that films prepared at about 8 cm. from the heater, which was the shortest path used, tended to contain oxide rather more than the others.

The Speed of Evaporation.

The speed at which a certain thickness of film may be reached depends upon the distance from the heater to the specimen and upon the rate of evaporation. In the case of fast evaporation it took from 5–10 secs. to prepare a film, while a film prepared very slowly might take a minute or more to deposit. The slower the evaporation the poorer the electron diffraction pattern produced in so far as the intensity of the rings, compared with the diffusely scattered background, becomes less and the rings themselves tend to be diffuse. When the rate of evaporation is very slow even an opaque film, such as would normally give a sharp ring-pattern, gives only two diffuse rings. There are two possible explanations of this effect. Either the crystals in the surface are very small or the surface is so flat that there are no fine

projections through which the electron beam can penetrate. Since it seems unlikely that a very flat surface will result in this particular case only, the first explanation is the more probable. One would normally expect larger crystal size to result from the slower crystal growth consequent upon slower evaporation. This effect is probably offset by the fact that more gas is trapped in the metal during a slow evaporation.

Effect of Poorer Vacuum Conditions.

A number of specimens prepared under poorer vacuum conditions, the initial pressure being of the order of 10^{-3} mm., were examined The effect of the increased pressure appeared to be similar to that due to the slowing down of the evaporation. The diffraction rings were diffuse, and in one or two cases oxide rings were observed in the patterns from quite thick films. These films became cloudy when heated to 250° C., and this will be discussed further under the next heading.

The Effect of Heating the Films to 250° C.

The effect of heating all the types of specimen so far discussed was investigated. In the case of the very thin films, which already showed an oxide film, there was no change either in the appearance or the structure of the film when it was heated to 250° C. Those thicker films, which were partly oxide and partly aluminium, gave a pattern which showed no aluminium rings at all after heating. The pattern obtained was such as would be produced by a face-centred cubic lattice of side $a=5{\cdot}53$ Å. As this spacing is equal to half the face diagonal of the γAl_2O_3 cube, the ring spacings are common to the two patterns. This is shown in Table II., while the actual pattern is shown in fig. 2 (Pl. VIII.).

It is very probable that this oxide is another form of partially organized crystal related to γAl_2O_3.

Many of the crystals in the film were orientated with a cube face parallel to the plane of the specimen, this being indicated by sharp spots on the rings produced by the spacing between the cube faces (*i. e.*, the (200), (400), (600) rings).

In the case of films of similar thickness to those referred to above prepared under poorer vacuum conditions

the specimens became clouded with a white bloom when heated to 250° C. Electron diffraction examination of this surface film showed it to be composed of a mixture of the two oxides which have already been described. The oxide crystals were much bigger than in the case of films prepared under better vacuum conditions. This was indicated by the presence of marked spots in many parts of the rings. The crystals of the oxide of type I. showed a tendency to orientate on a (111) face, while those of type II. tended to orientate with a cube face parallel to the glass surface. The crystals were of the

TABLE II.

Plane.	Observed spacing.	Calc. spacing, $a=5{\cdot}53$ Å.	Intensity.
111	3·27 Å.	3·20	m
200	2·78	2·77	s
211	2·32	2·26	ff
220	1·96	1·95	ss
311	1·65	1·67	m
222	1·58	1·59	m
400	1·38	1·38	f
331, 420	1·23	1·25	ss
422	1·11	1·13	s
511, 333	—	1·06	—
440	—	·98	—
531	—	·94	—
442, 600	·92	·92	ff

ss, very strong; s, strong; m, medium; f, faint; ff, very faint.

order of 10^{-3} cm. square (estimated from the size of the spots on the rings), and were therefore of sufficient size to affect the reflecting power by virtue of their roughness alone.

The thick films, which were pure aluminium on the surface, showed no change when heated to 250° C. It is probable that, both before and after heating, they were covered with an exceedingly thin protective film of oxide, which might not show up under electron diffraction examination owing to the relative weakness of the pattern arising from such a thin layer, compared with the pattern from the aluminium itself. Aluminium forms a very good

protective layer, and we should expect this layer to be very thin, of the order of a few molecules thick, since it would kill its own growth.

Orientation of the Aluminium Crystals.

As has been mentioned earlier the aluminium crystals in the thick films showed a tendency to orientate with a cube face parallel to the surface. This tendency was, however, disturbed by the direction in which the aluminium was fired on. Although this effect had no direct bearing upon the main problem to be investigated, and could not therefore be studied in detail, it was thought worth while to examine the general nature of the phenomenon. Further work on this effect might provide a very valuable check on any proposed dynamic theory of crystal growth. As has already been explained aluminium was evaporated on to one face and one edge of the glass strips by firing the metal obliquely on to the face to be examined (at an angle from 20–40° with the surface) from a filament parallel to the strip, but to one side of it. When a small specimen, cut from the strip, was examined in the diffraction camera with the beam crossing the surface in a direction perpendicular to the length of the strip, the pattern was arced symmetrically about the centre line in such a way as to indicate that all the crystals tended to orientate on a cube face. When the electron beam was fired across the specimen face in a direction parallel to the length of the strip the pattern was arced symmetrically about a line making an angle of about 10° with the centre line of the pattern, on the side remote from the line of fire of the incident metal. The type of pattern is shown in fig. 5 (Pl. IX.). This means that the aluminium crystals were orientated with a cube face parallel to a plane whose normal lay in the plane of incidence of the evaporated metal, and was inclined at an angle of about 10° to the normal to the specimen surface. When the angle between the direction of incidence of the evaporated metal and the specimen surface was increased to 45° the electron diffraction pattern showed the crystals to be orientated with a cube face roughly parallel to a plane whose normal lay in the plane of incidence of the metal, and which made an angle of about 15° with the normal to the specimen

surface, on the side of it nearer the heating filament. The type of pattern is shown in fig. 6 (Pl. IX.).

Specimens were also prepared with the metal fired normally on to the glass surface. In this case the crystals were found to be orientated with a cube face parallel to the specimen surface (fig. 7, Pl. IX.). It is difficult to come to a very definite conclusion with so little detailed information, but it seems quite likely that the orientation observed might be due to the conflict of tendencies on the part of the crystal to grow with a cube face parallel to the surface and also with a cube face perpendicular to the direction of incidence of the metal.

Chromium Films.

In the case of chromium, films of varying thickness were examined. Exceedingly thin, almost invisible films gave a pattern consisting of a few rings due to oxide and a few diffuse rings probably due to chromium. When heated such films gave an oxide pattern with a ring arrangement identical with that from heated aluminium films.

Thicker films of chromium gave a diffuse ring pattern due to small crystals of the pure metal. Even films thick enough to be opaque showed this pattern, there being no increase in crystal size with increasing film thickness corresponding to that observed with aluminium. On heating, these films became coated with a purplish bloom and electron diffraction examination showed this to be the same form of oxide as that formed on thin films, the cube side being $a=5{\cdot}46$ Å., which was slightly smaller than the corresponding aluminium oxide spacing. The mean spacings from a number of plates are shown in Table III., while the actual pattern is shown in fig. 3 (Pl. VIII.).

In the case of one specimen of medium thickness the oxide layer formed on heating was a mixture of the oxide mentioned above and an oxide similar in structure to the type I. aluminium oxide referred to earlier. The pattern is shown in fig. 4 (Pl. VIII.).

Aluminium on Chromium Films.

Thick films of aluminium were evaporated on to chromium films on glass. Orientated aluminium patterns,

similar to those from thick aluminium films on glass, were obtained. Heating the films to 250° C. made no difference to the surface.

Copper Films, on Glass and on Aluminium on Glass.

Films of copper of varying thickness were examined, and in no case was a pattern of pure copper obtained. With some of the thicker specimens copper rings were observed in addition to the predominating pattern due to cuprite, Cu_2O. One set of copper specimens, ranging

TABLE III.

Plane.	Observed spacing.	Calc. spacing, $a=5{\cdot}46$ Å.	Intensity.
111	3·27	3·16	m
200	2·74	2·72	s
211	2·22	2·23	ff
220	1·94	1·93	ss
311, 222	1·60	1·64, 1·57	m
400	1·35	1·36	f
331, 420	1·22	1·25, 1·22	s
422	1·10	1·11	m
333, 511	—	1·05	—
440	—	·96	—
531	—	·92	—
442, 600	·90	·91	ff

from a film which was barely visible to one which was almost opaque, gave a peculiar pattern, which is shown in fig. 8 (Pl. IX.). The very strong ring and the sharper rings are probably due to Cu_2O, while the innermost ring and the third ring, which are diffuse, have not yet been accounted for. The very strong ring corresponds to the (110) ring from cuprite, but is far stronger than this ring should be. A similar set of specimens of copper, on aluminium on glass, gave a ring pattern with spacings corresponding to those of cuprite, but with different intensities, the (110) ring again being abnormally strong.

Although the actual crystal structure and nature of the compounds formed has not been determined in all

cases, it is most probable that oxygen is either trapped in or combined with the copper in all these films.

When the films are heated to 250° C. they tarnish very readily. This film of tarnish, which is thick enough to show interference colours, was shown by electron diffraction examination to consist of cuprite. The readiness with which the tarnishing occurs is probably due to the presence of oxygen trapped in the film.

Mechanical Properties of the Films.

In the case of aluminium the thinner films were found to adhere best. They were unaffected by the sticking on and pulling off of a piece of adhesive tape, while some of the thicker films would not stand this test. All the aluminium films could be scratched easily with the point of a knife, but were able to withstand fairly well vigorous rubbing with dry cotton-wool. They could be washed with wet cotton-wool without suffering any harm. The films were able to withstand the attack of both concentrated hydrochloric and nitric acids for some time (*i. e.*, about 30 sec. in the case of HCl and much longer in the case of HNO_3).

The chromium films were very hard, it being impossible to scratch them with the point of a knife. Aluminium on chromium films also appeared to withstand this test, but this may have been only apparent. The aluminium may have been scratched off, although the scratch was not visible on account of the opaque chromium backing.

Summary and Discussion.

It has been shown that thin evaporated films of aluminium, chromium, and copper consist mainly of the respective oxides of the metals, although these oxides have not their usual crystal forms. The actual structures of these oxides have not been fully determined, but it seems probable that in the case of aluminium the oxide is related to γAl_2O_3. The structure of the oxide present in a thin film of chromium is similar to that present in a thin film of aluminium.

The oxides formed on both metals after heating to 250° C. have the same structure and almost the same spacing. It is just possible that the form of oxide observed on heated aluminium films is the same as that

observed by Steinheil * on an aluminium foil which had been subjected to atmospheric oxidation. There is a difference in the cube side and in the relative intensities of the rings. The latter difference might easily be due to orientation, since Steinheil's pattern was obtained by transmission. The spacing found by Steinheil was 5·35 Å., which differs from the value found in this work by about 4 per cent., which is rather greater than would be expected after allowing for experimental errors.

In view of the non-tarnishing properties common to aluminium and chromium it is of interest to notice that they both form oxides of the same structure in addition to the common rhombohedral forms.

Thick films of aluminium and chromium were apparently pure metal on the surface. It is suggested that the protective oxide layer, which must have been present, was so thin as not to be observed.

Under normal evaporating conditions the initial pressure in the chamber was such that the mean free path for the metal atoms was greater than the distance from heater to mirror. It seems unlikely, therefore, that the oxygen in the films was picked up by the metal atoms in crossing between the filament and the mirror. It is possible that some gas was liberated from the filament itself, but as aluminium oxide is stable at high temperatures it seems probable that most of the oxygen would have remained trapped in this form in the case of aluminium. The most likely explanation of the presence of an oxide film on the glass would seem to be that the gas is liberated from the glass itself under the action of the bombardment by metal atoms. This is supported by the fact that the orientation of the oxide crystals is unaffected by the direction of incidence of the metal, which suggests that the combination with the oxygen probably occurs after the metal atoms have struck the glass.

The manner in which the orientation of the metal atoms in thick films is governed by the position of the filament with respect to the glass surface shows that there is a predominating direction of arrival of the metal atoms at the surface. This must not be taken, however, as an indication that the atoms travel straight from the filament to the glass. That this is not so may be shown by

* A. Steinheil, *Ann. Physik*, (5) p. 19 (1934).

attempting to form a shadow (*i. e.*, a patch free of metal) on a glass plate by interposing a stop between the plate and the filament. If the distance from heater to plate is about 10 cm., and the distance from stop to plate is 2 cm., only a very ill-defined shadow is obtained. The reason for this is that there is a high concentration of metal atoms in the neighbourhood of the filament (the number of atoms liberated is about 10^{20}/sec.), and this cloud acts as a source of atoms. Near the filament many collisions occur, and the farther out the atoms travel the fewer collisions there will be. Thus, although the majority of the atoms arriving at the specimen surface have a direction approximately parallel to the line joining filament and specimen, they do not arrive without first having made collisions with other metal atoms.

The readiness with which oxide layers form on the metal films when they are heated to 250° C. suggests that there is a good deal of oxygen trapped in the films themselves. Certainly far thicker oxide layers form than would be the case with the metal in its ordinary state. This is especially so in the case of chromium films and of aluminium films prepared under poor vacuum conditions.

The Imperial College of Science,
S. Kensington.
9th June, 1936.

LXXIX. *Identical Relations between the Field Equations in the General Field Theory of Schouten and van Dantzig.* *By* N. G. Shabde, *D.Sc.* (*Nag.*), *D.Sc.* (*Edin.*), *Mathematics Department, College of Science, Nagpur, India* *.

Introduction.

EMMY NÖETHER †, by generalizing certain results of Hilbert ‡, has proved a theorem to the effect that :

If F is a function of n quantities f, which are themselves

* Communicated by the Author.
† *Göttingen Nachrichten*, p. 236 (1918).
‡ *Göttingen Nachrichten*, p. 395 (1915).

functions of the m coordinates $(x^0, \ldots, x^{m-1})$ and their derivatives, and if the integral

$$\int \mathrm{F}\, dx^0 dx^1 \ldots . dx^{m-1}$$

is invariant with respect to arbitrary transformations of the coordinates $x^0, x^1, \ldots x^{m-1}$, then in the system of the n Lagrangian differential equations, which belong to the variational problem,

$$\delta \int \mathrm{F}\, dx^0 \ldots dx^{m-1} = 0,$$

there are always m, which are a consequence of the $n-m$ others, in the sense that between the n quantities f and their total differential coefficients with respect to $x^0, \ldots x^{m-1}$, m linearly independent relations are identically satisfied.

The object of the present note is to work out this theorem for the case of the variational integral, which occurs in the general field theory of Schouten and van Dantzig *, namely

$$\int \mathrm{N}\sqrt{\mathrm{G}}.d\tau,$$

where N is the projective scalar curvature and

$$d\tau = dx^0 dx^1 dx^2 dx^3 dx^4.$$

Now

$$\delta \int \mathrm{N}\sqrt{\mathrm{G}}.d\tau = \sum_{\lambda\mu} \int \sqrt{\mathrm{G}}.\mathrm{P}_{\lambda\mu}.\delta \mathrm{G}^{\lambda\mu} d\tau, \quad . \quad . \quad . \quad , \quad (1)$$

where

$$\mathrm{P}_{\lambda\mu} \equiv \Big[\mathrm{K}_{\lambda\mu} - \tfrac{1}{2}\mathrm{K} g_{\lambda\mu} + (q^2 - 2pq + 2p) \Big\{ \tfrac{1}{2} g_{\lambda\mu} \sum_{\rho\sigma} q_{\rho\sigma} q^{\rho\sigma} + 2q_\lambda . \sum_\rho \overset{\mathrm{R}}{\nabla}_\rho q^\rho_\mu - 2 \sum_\rho q^\rho_\lambda q_{\mu\rho} \Big\} \Big] = 0,$$

are the field equations, with the usual notations.

§ 1.

Let us first find the value of $\delta \mathrm{G}^{\lambda\mu}$. Comparing $\mathrm{G}^{\lambda\mu}$ and $\mathrm{G}^{\lambda\mu} + \delta \mathrm{G}^{\lambda\mu}$, as they correspond to a transformation of coordinates, we have

$$\mathrm{G}^{\lambda\mu} + \delta \mathrm{G}^{\lambda\mu} = \mathrm{G}^{\alpha\beta} \frac{\partial (x^\lambda + \delta x^\lambda)}{\partial x^\alpha} . \frac{\partial (x^\mu + \delta x^\mu)}{\partial x^\beta},$$

* *Zeitschrift für Physik*, lxxviii. pp. 639–667 (1932), "Generale Feldtheorie."

$$=G^{\alpha\beta}.\frac{\partial x^{\lambda}}{\partial x^{\alpha}}.\frac{\partial x^{\mu}}{\partial x^{\beta}}+G^{\alpha\beta}\frac{\partial x^{\lambda}}{\partial x^{\alpha}}.\frac{\partial(\delta x^{\mu})}{\partial x^{\beta}}+G^{\alpha\beta}\frac{\partial x^{\mu}}{\partial x^{\beta}}.\frac{\partial(\delta x^{\lambda})}{x^{\alpha}},$$

$$=G^{\lambda\mu}+G^{\lambda\beta}.\frac{\partial(p^{\mu})}{\partial x^{\beta}}+G^{\alpha\mu}.\frac{\partial(p^{\lambda})}{\partial x^{\alpha}},$$

where $p^{\lambda}=\delta x^{\lambda}$ and $p^{\mu}=\delta x^{\mu}$.

Hence $$\delta G^{\lambda\mu}=G^{\lambda\beta}\frac{\partial(p^{\mu})}{\partial x^{\beta}}+G^{\alpha\mu}\frac{\partial(p^{\lambda})}{\partial x^{\alpha}}.$$

This is a comparison of the projector $G^{\lambda\mu}$ at $x^{\alpha}+\delta x^{\alpha}$ in the new coordinate system with the value at x^{α} in the old coordinate system. There would be no objection to using this value of $\delta G^{\lambda\mu}$ provided we took account of the corresponding $\delta(d\tau)$. We prefer to keep $d\tau$ fixed in comparison, and must compare the values at x^{α} in both the systems. It is therefore necessary to subtract the change $\delta x^{\alpha}.\frac{\partial G^{\lambda\mu}}{\partial x^{\alpha}}$ of $G^{\lambda\mu}$ in the distance δx^{α}. Hence

$$\delta G^{\lambda\mu}=G^{\lambda\alpha}.\frac{\partial(p^{\mu})}{\partial x^{\alpha}}+G^{\alpha\mu}.\frac{\partial(p^{\lambda})}{\partial x^{\alpha}}-\frac{\partial G^{\lambda\mu}}{\partial x^{\alpha}}p^{\alpha}, \quad . \quad (2)$$

where $p^{\alpha}=\delta x^{\alpha}$.

§ 2.

Using (2), (1) becomes

$$\int\Sigma_{\lambda\mu}\sqrt{G}P_{\lambda\mu}.\delta G^{\lambda\mu}\,d\tau$$

$$=\Sigma_{\lambda\mu\alpha}\int\sqrt{G}.P_{\lambda\mu}\left(G^{\lambda\alpha}\frac{\partial p^{\mu}}{\partial x^{\alpha}}+G^{\mu\alpha}\frac{\partial p^{\lambda}}{\partial x^{\alpha}}-\frac{\partial G^{\lambda\mu}}{\partial x^{\alpha}}.p\right)d\tau=0.$$

Integrating this by parts, supposing the p's and their first and second derivatives to vanish at the boundary, we get

$$\Sigma_{\alpha\lambda\mu}\int\left[\frac{\partial}{\partial x^{\alpha}}\{P_{\lambda\mu}\sqrt{G}.G^{\lambda\alpha}\}p^{\mu}+\frac{\partial}{\partial x^{\alpha}}\{P_{\lambda\mu}\sqrt{G}.G^{\alpha\mu}\}p^{\lambda}\right.$$

$$\left.+\frac{\partial G^{\lambda\mu}}{\partial x^{\alpha}}p^{\alpha}.P_{\lambda\mu}.\sqrt{G}\right]d\tau=0.$$

Changing the dummy suffixes α and μ in the first term into μ and α respectively, and similarly interchanging the

dummy suffixes α and λ in the second term on the left, we get

$$\sum_{\lambda\mu\alpha}\int\Big[\frac{\partial}{\partial x^\mu}\{P_{\lambda\alpha}\sqrt{G}\,.\,G^{\lambda\mu}\}+\frac{\partial}{\partial x^\lambda}\{P_{\alpha\mu}\,.\,\sqrt{G}\,.\,G^{\lambda\mu}\}+\frac{\partial G^{\lambda\mu}}{\partial x^\alpha}\,.\,P_{\lambda\mu}\sqrt{G}\Big]\,p^\alpha\,d\tau=0.$$

Since p^α is arbitrary, its coefficients in this equation must vanish. Hence

$$\sum_{\lambda\mu}\Big[\frac{\partial}{\partial x^\mu}\{P_{\lambda\mu}G^{\lambda\mu}\sqrt{G}\}+\frac{\partial}{\partial x^\lambda}\{P_{\alpha\mu}\sqrt{G}\,.\,G^{\lambda\mu}\}+\frac{\partial G^{\lambda\mu}}{\partial x^\alpha}P_{\lambda\mu}\sqrt{G}\Big]=0.$$

$$(\alpha=0,\ 1,\ 2,\ 3,\ 4.)$$

Interchanging λ and μ in the second term, we get

$$\sum_{\lambda\mu}\Big[\frac{\partial}{\partial x^\mu}\{(P_{\lambda\alpha}+P_{\alpha\lambda})\sqrt{G}\,.\,G^{\lambda\mu}\}+\frac{\partial G^{\lambda\mu}}{\partial x^\alpha}\,P_{\lambda\mu}\sqrt{G}\Big]=0. \quad (3.1)$$

$$(\alpha=0,\ 1,\ 2,\ 3,\ 4.)$$

Substituting in (3.1)

$$\frac{\partial G^{\lambda\mu}}{\partial x^\alpha}=-\sum_\sigma\left\{\begin{matrix}\mu\\ \alpha\sigma\end{matrix}\right\}G^{\lambda\sigma}-\sum_\sigma\left\{\begin{matrix}\lambda\\ \alpha\sigma\end{matrix}\right\}G^{\mu\sigma}, \quad . \quad (3.2)$$

and putting

$$X^{\mu}_{.\alpha}=\tfrac{1}{2}(P^{\mu}_{.\alpha}+P^{\mu}_{\alpha}) \quad . \quad . \quad . \quad . \quad . \quad (3.3)$$

we have

$$\Big[\sum_\mu\Big[2\,\frac{\partial}{\partial x^\mu}\{X^{\mu}_{.\alpha}\}\sqrt{G}+2X^{\mu}_{.\alpha}\frac{\partial\sqrt{G}}{\partial x^\mu}\Big]-\sqrt{G}\Big[\sum_{\sigma\mu}\left\{\begin{matrix}\mu\\ \alpha\sigma\end{matrix}\right\}P^{\sigma}_{.\mu}+\sum_{\sigma\lambda}\left\{\begin{matrix}\lambda\\ \alpha\sigma\end{matrix}\right\}P^{\sigma}_{\lambda.}\Big]\Big]=0. \quad (3.4)$$

$$(\alpha=0,\ 1,\ 2,\ 3,\ 4.)$$

Or interchanging the dummy suffixes μ and σ in the first term of the second [ ]-bracket, and changing the dummy suffix λ into μ, and interchanging it with the dummy suffix σ in the second term of the second [ ]-bracket in (3.4), and remembering that

$$\frac{1}{\sqrt{G}}\,.\,\frac{\partial\sqrt{G}}{\partial x^\mu}=\sum_\sigma\left\{\begin{matrix}\sigma\\ \mu\sigma\end{matrix}\right\}, \quad . \quad . \quad . \quad (3.5)$$

we get

$$\left[2\sqrt{G} \sum_{\mu} \left[\frac{\partial}{\partial x^{\mu}} (X^{\mu}_{.\alpha}) + \sum_{\sigma} \left\{ \begin{matrix} \sigma \\ \mu\sigma \end{matrix} \right\} X^{\mu}_{.\alpha} \right] - 2\sqrt{G} \sum_{\sigma} \left\{ \begin{matrix} \sigma \\ \alpha\mu \end{matrix} \right\} X^{\mu}_{.\sigma} \right] = 0, \quad (3.6)$$

$$(\alpha = 0, 1, 2, 3, 4.)$$

or

$$\sum_{\mu} \left[\frac{\partial}{\partial x^{\mu}} (X^{\mu}_{.\alpha}) + \sum_{\sigma} \left\{ \begin{matrix} \sigma \\ \mu\sigma \end{matrix} \right\} X^{\mu}_{.\alpha} \right] - \sum_{\sigma\mu} \left\{ \begin{matrix} \sigma \\ \alpha\mu \end{matrix} \right\} X^{\mu}_{.\sigma} = 0. \quad (3.7)$$

Now

$$\left.\begin{aligned} &\text{(i.)} \quad \nabla_{\mu} X^{\mu}_{.\alpha} = \frac{\partial X^{\mu}_{.\alpha}}{\partial x^{\mu}} - \sum_{\sigma} \Pi^{\sigma}_{\alpha\mu} X^{\mu}_{.\sigma} + \sum_{\sigma} \Pi^{\mu}_{\sigma\mu} X^{\sigma}_{.\alpha}, \\ &\text{(ii.)} \quad \Pi^{\mu}_{\sigma\mu} = \left\{ \begin{matrix} \mu \\ \sigma\mu \end{matrix} \right\}, \\ &\text{(iii.)} \quad \Pi^{\sigma}_{\alpha\mu} = \left\{ \begin{matrix} \sigma \\ \alpha\mu \end{matrix} \right\} - (q-1) q^{\sigma} q_{\alpha\mu} + (q-1) q_{\alpha} q^{\sigma}_{.\mu} \\ &\qquad\qquad + (p-1) q_{\mu} q^{\sigma}_{.\alpha}. \end{aligned}\right\} \quad (3.8)$$

Making use of (3.8) (i.) in (3.7), we have

$$\sum_{\mu\sigma} \left[\nabla_{\mu} X^{\mu}_{.\alpha} + \Pi^{\sigma}_{\alpha\mu} X^{\mu}_{.\sigma} + \left\{ \begin{matrix} \sigma \\ \mu\sigma \end{matrix} \right\} X^{\mu}_{.\alpha} = \Pi^{\mu}_{\sigma\mu} X^{\sigma}_{.\alpha} - \left\{ \begin{matrix} \sigma \\ \alpha\mu \end{matrix} \right\} X^{\mu}_{.\sigma} \right] = 0. \quad (3.9)$$

$$(\alpha = 0, 1, 2, 3, 4.)$$

Since $$\Pi^{\mu}_{\alpha\mu} X^{\sigma}_{.\alpha} = \left\{ \begin{matrix} \mu \\ \sigma\mu \end{matrix} \right\} X^{\sigma}_{.\alpha} = \left\{ \begin{matrix} \sigma \\ \mu\sigma \end{matrix} \right\} X^{\mu}_{.\alpha},$$

we see that the third and the fourth terms in (3.9) cancel out. Then, making use of (3.8) (iii.) in (3.9), we finally arrive at the identities between the field equations in the form

$$\sum_{\mu\sigma} [\nabla_{\mu} X^{\mu}_{.\alpha} - \{(q-1) q^{\sigma} q_{\alpha\mu} - (q-1) q_{\alpha} q^{\sigma}_{.\mu} - (p-1) q_{\mu} q^{\sigma}_{.\alpha}\} X^{\mu}_{.\sigma}] = 0. \quad (3.10)$$

$$(\alpha = 0, 1, 2, 3, 4.)$$

Or, changing the dummy suffix σ into λ, we have the identities

$$\sum_{\lambda\mu} [\nabla_{\mu} X^{\mu}_{.\alpha} - \{(q-1) q^{\lambda} q_{\alpha\mu} - (q-1) q_{\alpha} q^{\lambda}_{.\mu} - (p-1) q_{\mu} q^{\lambda}_{.\alpha}\} X^{\mu}_{.\lambda}] = 0. \quad (3.11)$$

$$(\alpha = 0, 1, 2, 3, 4.)$$

LXXX. *On the Radiation Resistance of Tapered Wire Transmission Lines.* *By* S. S. Banerjee, *M.Sc.*, *and* B. N. Singh, *M.Sc.*, *Demonstrators in Physics, Hindu University, Benares* *.

Introduction.

THE radiation resistance of straight parallel-wire high-frequency transmission lines, and also the effect of bends of various types on the same, have already been studied by one of the authors both theoretically and experimentally, and published in this Journal [1]. Due to the increasing importance of the subject in connexion with the transmission and reception of ultra-short waves, which are extensively being employed during recent years in aircraft and modern television, the study of the radiation resistance has been extended to that of the tapered wire high-frequency transmission lines. It is a matter of frequent experience that the transmission lines, instead of remaining always parallel to each other throughout their run from the input end to the output end, they may happen to be substantially inclined to each other and also bent in different planes, owing to the unavoidable conditions in the layout of the design.

In the present communication we have described the results of study of the radiation resistance of tapered wire high-frequency transmission lines with and without bends both theoretically and experimentally. It has been observed that the radiation resistance of the tapered wire system without bends rapidly increases with angles between the wires beyond three degrees. The radiation resistances of straight tapered wires for half wave-length long and one wave-length long have been determined separately, for one is not exactly half of the other as in the case of the parallel wire system without bends. For the sake of convenience it may be remembered that in the case of the parallel wire system two types of bends were considered: first when the pair of wires is bent in its own plane, and second when it is bent such that the perpendicular to the plane containing the bent arms is parallel to the shortest length between the wires.

* Communicated by the Authors.

It has been found in the case of parallel wire system that there is a considerable increase in the radiation resistance in the first type of bend, but there is hardly any perceptible change of the radiation resistance in the second type of bend. But in the case of the tapered wire system there is the usual increase in the radiation resistance in the first type of bend, and in the second type of bend, however, there is found a measurable *decrease* of resistance for sharp bends. It may be pointed out at once that the second type of bend, which we are referring to in the case of the tapered wire system, cannot be defined exactly in the similar way as in the case of parallel wire system. This is due to the fact that the perpendicular to the plane containing either pair of adjacent bent arms is not exactly parallel to the shortest length between the wires. It has been further observed that even in the case of the parallel wire system the second type of bend has the effect of decreasing the radiation resistance, which can be observed when the wires are widely separated. The theoretical discussions on the observed decrease of the radiation resistance in both the systems of transmission lines, of parallel wires, and tapered wires have been given.

Theoretical Considerations.

For the calculation of the radiation resistance of the tapered wire system the method of "induced e.m.f." has been followed throughout the present investigation which was also employed previously in calculating the radiation resistance of the parallel wire transmission lines.

We have shown below, firstly the calculation of the radiation resistance of tapered wire system of only one-half wave-length long, and secondly the calculation for the system when it is one wave-length long. This is done because the radiation resistance in the latter case is not exactly twice that of the former as in the system of parallel wires with small separation, which will be explained subsequently.

The total radiation resistance (R_T) of the tapered wires 1 and 2 (fig. 1) when the currents in the two wires are in antiphase is given by

$$R_T = 2(R_{11} - R_{12}), \quad . \quad . \quad . \quad . \quad . \quad (1)$$

where R_{11} is the radiation resistance of the wire 1 or 2 and R_{12} is the value of the radiation resistance of one wire due to the other wire. R_{11} is calculated from Pistolkors' [2] formula given by

$$R_{11}=30[\epsilon+\log(2ml)-Ci(2ml)] \text{ ohms}, \quad . \quad . \quad (2)$$

where ϵ=Euler's constant (0·5772) and $m=2\pi/\lambda$. R_{12} is calculated as shown below.

In order to calculate R_{12} we have to find out the value of electric field E_r at any point 0 (fig. 1) along the wire 2 due to the current in the wire 1. For this we have to

Fig. 1.

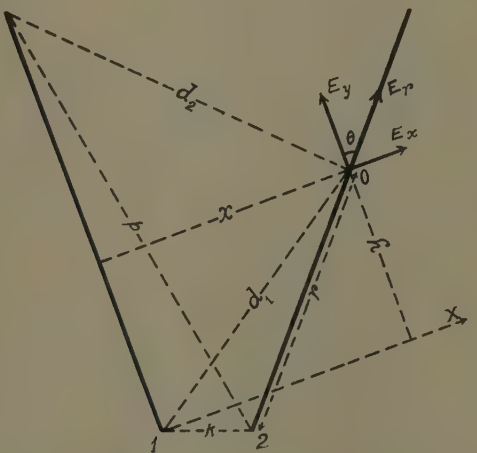

find out the value of the electric intensity E_y parallel to the wire 1 and E_x perpendicular to this direction.

$$\therefore \quad E_r=E_x \sin\theta+E_y \cos\theta, \quad . \quad . \quad . \quad . \quad (3)$$

where θ is the angle between the two wires.

Now the values of E_x and E_y are given below after Carter [3], when the wires are multiples of half wavelengths,

$$E_x=-j30I\left[\frac{e^{-jmd_2}}{d_2}\cdot\frac{y-l}{x}(-1)^n-\frac{e^{-jmd_1}}{d_1}\cdot\frac{y}{x}\right] \text{ volts/cm.}, \quad (4)$$

and

$$E_y=j30I\left[\frac{e^{-jmd_2}}{d_2}(-1)^n-\frac{e^{-jmd_1}}{d_1}\right] \text{ volts/cm.} \quad . \quad (5)$$

From fig. 1 it will be observed that

$$x = k \sin \theta/2 + r \sin \theta$$

and

$$y = k \cos \theta/2 + r \cos \theta,$$

where k is the distance between the two input ends of the wire and θ is the angle between the opposite arms of the tapered wires ;

$$d_1 = \sqrt{k^2 + r^2 + 2kr \sin \theta/2},$$

$$d_2 = \sqrt{p^2 + r^2 - 2pr \cos (\theta + \phi)},$$

where ϕ is the angle which p makes with y-axis,

$$p = \sqrt{l^2 + k^2 + 2kl \sin \theta/2},$$

and

$$\phi = \sin^{-1}\left(\frac{k \cos \theta/2}{\sqrt{l^2 + k^2 + 2lk \sin \theta/2}}\right).$$

Substituting these values of x, y, d_1 and d_2 in equations (4) and (5), the values of E_x and E_y are obtained.

Substituting subsequently these values in equation (3), we get

$$\begin{aligned} R_{12} = 30 \cos \theta \Big[& \int_0^l \frac{\sin md_2}{d_2} \cdot \sin mr\, dr \\ & + \int_0^l \frac{\sin md_1}{d_1} \cdot \sin mr\, dr \Big] \\ & - 30 \sin \theta \Big[\int_0^l \frac{\sin md_2}{d_2} \cdot \frac{y - l}{x} \sin mr\, dr \\ & + \int_0^l \frac{\sin md_1}{d_1} \cdot \frac{y}{x} \cdot \sin mr\, dr \Big]. \quad . \quad . \quad . \quad . \quad (6) \end{aligned}$$

The values of the integrals are computed graphically.

Now the total radiation resistance of the tapered wires for one wave-length will be calculated.

For the sake of convenience each wire is divided into two parts each of half wave-length long (fig. 2). Thus, considering the proper phases of the current in each portion,

$$R_T = 4R_{11} + 4R_{13} - 2R_{12} - 4R_{34} - 4R_{14}. \quad . \quad . \quad (7)$$

R_{12} and R_{34} can be calculated by the equation (6), and R_{11} by equation (1).

R_{13} is calculated in a similar way as R_{12}, and its value is obtained by equation (6) with the following values of d_1, d_2, x, and y.

From fig. 2 it will be observed that

$$x=q \sin (\theta+\phi)+r \sin \theta,$$

$$y=q \cos (\theta+\phi)+r \cos \theta,$$

$$d_1=\sqrt{q^2+r^2+2qr \cos \phi},$$

and $$d_2=\sqrt{p^2+r^2+2pr \sin \theta/2},$$

Fig. 2.

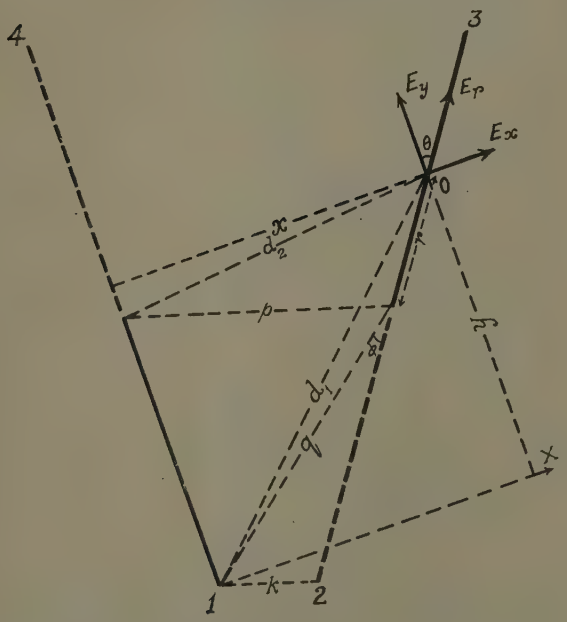

where $$p=k+2l \sin \theta/2,$$

$$q=\sqrt{k^2+l^2+2kl \sin \theta/2},$$

and $$\phi=\sin^{-1}\left(\frac{k \cos \theta/2}{\sqrt{l^2+k^2+2lk \sin \theta/2}}\right).$$

R_{14} can be calculated from the expression for R_{13} by putting $P=0$, $q=1$, and $\theta=0$.

It has been mentioned before that the radiation resistance of tapered wires half wave-length long is not exactly

half of the resistance of the wires one wave-length long. This will be now clear from the expression of the total resistance given in equation (7) for tapered wire system one wave-length long, which is not exactly double of that given by equation (1) for wires half wave-length long. But in the case of parallel wire system the radiation resistance of wire 1 due to the wire 2 (fig. 2) is the same as that of wire 3 due to the wire 4 ; and also the resistances of wire 1 due to wire 3 and due to wire 4 are very nearly equal when the separation between the wires is small. Thus for parallel wires with small

Fig. 3.

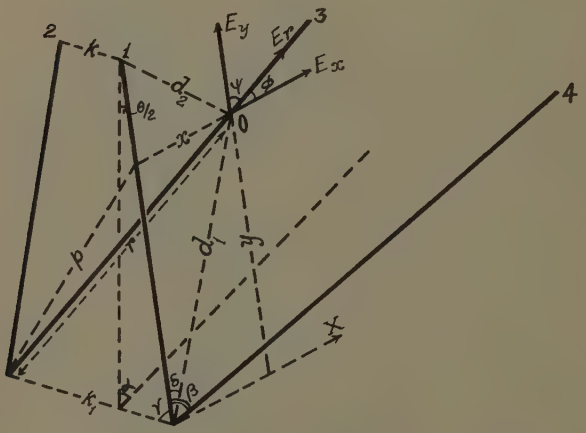

separation the value of R_T reduces to $4(R_{11} - R_{12})$, which is exactly double of the total resistance for the wires half wave-length long given in equation (1). The change of the radiation resistance for tapered wires as the angle between the opposite arms is increased is shown in fig. 4 for half wave-length, and that for full wave-length is shown in fig. 5.

In the following paragraphs we will consider how the radiation resistance can be calculated when the tapered wires are bent in the same sense as in the case of parallel wires when they are bent so that the perpendicular to the plane containing the bent arms is parallel to the shortest length between the wires.

From fig. 3 it will be seen that the total resistance of the system is given by equation (7).

The methods of calculation of all the terms of the right-hand expression of equation (7) except R_{14} and R_{13} have been indicated previously. R_{14} can be evaluated easily from the formula given by

$$R_{14}=30l\int_0^l \frac{\sin md}{d}\cdot\frac{\sin ms}{s}ds, \quad . \quad . \quad . \quad (8)$$

where d is the distance from the upper end of the wire 1 to any point on the wire 4 at a distance s from the lower end, and is equal to $\sqrt{l^2+s^2-2ls\cos\beta}$, where β is the angle between the wires 1 and 4, and is equal to

$$\cos^{-1}(\cos^2\theta/2\cos\alpha-\sin^2\theta/2),$$

and α is the angle between the plane containing the wires 1 and 2, and that containing wires 3 and 4.

For evaluating R_{13} it must be noted in fig. 3 that the wires 1 and 3 are two skew wires. E_x is in the plane containing the wire 1 and the lines d_1 and d_2, and it is perpendicular to the wire 1. E_y is perpendicular to E_x and parallel to the wire 1. Let the inclinations of E_x and E_y to the wire 3 be denoted by ϕ and ψ respectively;

$$\therefore \quad E_r=E_y\cos\psi+E_x\cos\phi,$$

where E_r is the total intensity due to E_x and E_y along the wire 3 and r is the distance along the wire.

Then by the usual mathematical deductions it can be shown that

$$\begin{aligned}R_{13}=30\cos\psi&\left[\int_0^l\frac{\sin md_2}{d_2}.\sin mr\,dr\right.\\&\left.+\int_0^l\frac{\sin md_1}{d_1}.\sin mr\,dr\right]\\&-30\left[\int_0^l\frac{\sin md_2}{d_2}\cdot\frac{y-l}{x}.\cos\phi\sin mr\,dr\right.\\&\left.+\int_0^l\frac{\sin md_1}{d_1}\cdot\frac{y}{x}.\cos\phi\sin mr\,dr\right], \quad . \quad . \quad . \quad (9)\end{aligned}$$

where $$\psi=\cos^{-1}(\sin^2\theta/2+\cos^2\theta/2\cos\alpha),$$

$$\phi=\cos^{-1}\left(\frac{r^2+x^2-p^2}{2rx}\right),$$

$$x=d_1 \sin \delta,$$

$$y=d_1 \cos \delta,$$

$$p^2=y^2+{k_1}^2-2yk_1 \sin \theta/2,$$

and $$k_1=k+2l \sin \theta/2$$

(k=distance between the wires at the input end),

$$d_1=\sqrt{r^2+{k_1}^2+2rk_1 \sin \theta/2},$$

$$d_2=\sqrt{l^2+{d_1}^2-2ld_1 \cos \delta},$$

$$\delta=\cos^{-1}(\sin \theta/2 \cos \gamma+\cos \theta/2 \sin \gamma \cos \alpha),$$

$$\gamma=\cos^{-1}\left\{\frac{{d_1}^2+{k_1}^2-r^2}{2k_1 d}\right\}.$$

It may be remarked that when the wires are parallel the value of R_{14} and R_{13} can be calculated from the equations (8) and (9) respectively by putting $\theta=0$. This verifies also the general formulæ derived above for R_{13} and R_{14}.

Now we will show below how the radiation resistance of the bent tapered wires will decrease for small angular bends. It will be observed that in the expression for the total resistance given by equation (7) resistances R_{11} and R_{12} of the wire 1 (fig. 3), due to itself and due to the wire 2 respectively, and the resistance R_{34} of the wire 3 due to wire 4, will not be affected by the bend of the type considered above. If there be any change brought forth in the total resistance of the system due to the bend it will be only for the resistances R_{13} and R_{14} of wire 1 due to wires 3 and 4, both of which will increase as the angle between the bent arms will decrease. It will be further observed that the resistance R_{14} of wire 1 due to wire 4 is always greater than the resistance R_{13} of wire 1 due to wire 3. The rate at which the resistance R_{14} changes with the bend is, however, greater than the rate at which the resistance R_{13} changes. Therefore the total radiation resistance of the system will have a tendency to decrease itself with the bending if there be any change at all. The change of the total radiation resistance due to the sharp angles between the bent arms is shown in fig. 6.

Experimental.

The experimental method of finding out the radiation resistance of tapered wires consists in measuring the attenuation constant of the system by a similar method as adopted in the case of parallel wire system. In the case of parallel wire system, when the leakance between the wires is negligible, the resistance per unit length is given by

$$R=2\alpha\sqrt{L/C},$$

where α is the attenuation constant, L and C are the inductance and capacity for unit length of the wires.

If, however, the wires are inclined to each other the values of L and C do not remain constant throughout the whole length of the wires. If the separation of the wires changes continuously from a to b it can be shown that the mean value of $\sqrt{L/C}$ will be equal to

$$\frac{120}{b-a}\int_a^b \log_e \frac{2x}{d}\,dx,$$

where d is the diameter of the wires.

$$\therefore \quad R=\frac{240\alpha}{b-a}\int_a^b \log_e \frac{2x}{d}\,dx.$$

The attenuation constant α is determined experimentally by the resonance curve method. For this the system of wires was excited by means of an ultra-short wave oscillator generating waves of about 60 megacycles per second. As a short-circuiting metal bridge is moved along the length of the wires the deflexions in a Duddell thermogalvanometer connected at the input end of the system are observed, and the resonance curves are plotted from them. From the "half-width" of the resonance curves, α can be readily calculated by the equation

$$\alpha=\frac{2\pi e}{n\lambda^2},$$

where e is the "half-width" of the resonance curve and n the number of resonance point from the input end.

The observational results are shown in Tables I., II., and III. below. In Tables I. and II. are shown the variation of the radiation resistance of tapered wires without bend with different angles between the two

opposite arms for half wave-length long and one wave-length long respectively. In Table III. is shown the variation of the radiation resistance of the tapered wires with bend.

TABLE I.

Angle between the opposite arms.	Total resistance in ohms (observed).	Total resistance in ohms (calculated).
0°	1·88	1·71
2°	4·27	3·96
4°	6·01	5·60
6°	7·62	7·41
8°	10·02	10·05
10°	14·46	15·95

TABLE II.

Angle between the opposite arms.	Total resistance in ohms (observed).	Total resistance in ohms (calculated).
0°	3·76	3·41
2°	9·02	9·29
4°	15·42	15·68
6°	23·74	22·91
8°	30·75	29·13
10°	40·60	38·60

TABLE III.

Angle between the opposite arms 4°.

Angle between the bent arms.	Total resistance in ohms (observed).	Total resistance in ohms (calculated).
60°	13·88	13·58
45°	13·10	12·71
35°	12·34	11·91
25°	10·79	11·20
10°	9·25	9·67

The third column in the above tables consists of the radiation resistance calculated along with the ohmic resistance of the wires. Figs. 4, 5, and 6 show variation

Fig. 4.

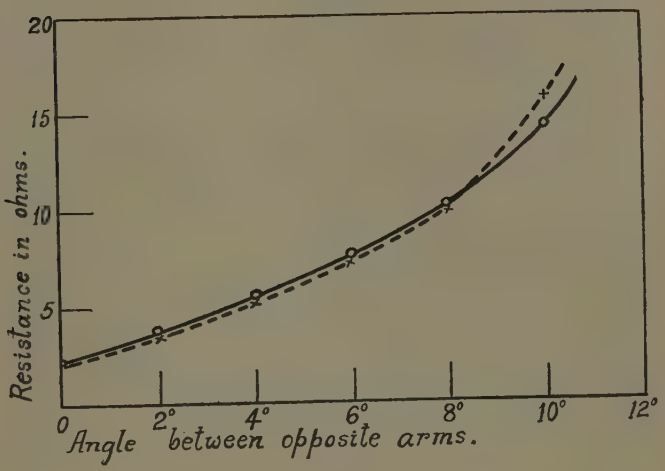
20
15
10
5
Resistance in ohms.
0
2°
4°
6°
8°
10°
12°
Angle between opposite arms.

Fig. 5.

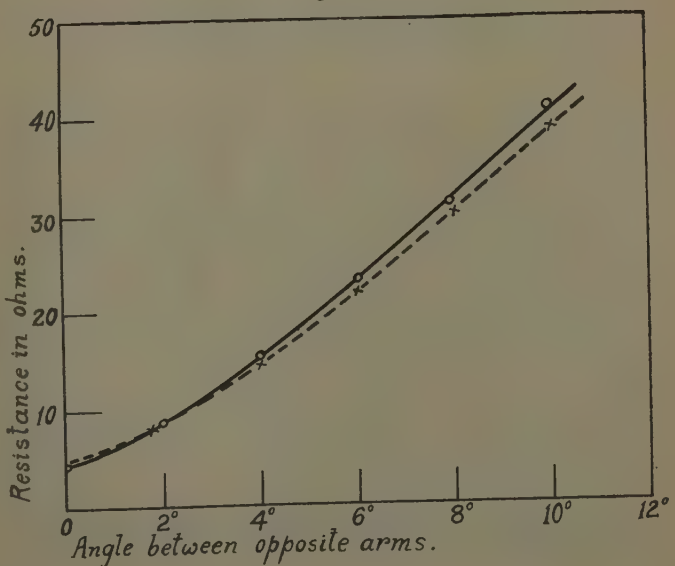
50
40
30
20
10
Resistance in ohms.
0
2°
4°
6°
8°
10°
12°
Angle between opposite arms.

of the radiation resistance in three different cases given in the tables. The dotted lines show the calculated values of the radiation resistance and the continuous lines those experimentally determined.

Fig. 6.

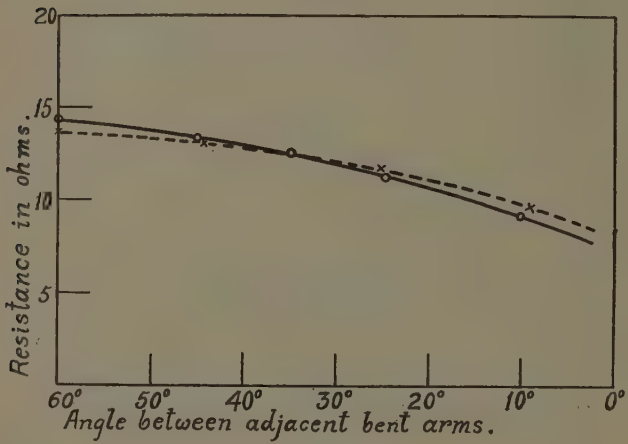

Summary and Conclusions.

The radiation resistance of high-frequency transmission lines when they are tapered has been studied theoretically and experimentally in the present investigation. It is found that the radiation resistance increases fairly rapidly as the angle between the two opposite arms of the tapered wires is increased. The loss due to radiation becomes appreciable for angles beyond three degrees. The radiation resistances for tapered wires of one wave-length long and half wave-length long have been determined separately, as the resistance of the former is not exactly twice that of the latter as in the case of the parallel wire system. The effect of tapering on the radiation resistance is more pronounced when the lengths of the wires are one wave-length long.

The change in the radiation resistance of the tapered wires caused by bends in the system has also been investigated. As in the case of the parallel wire system

the radiation resistance of the tapered wires increases when they are bent in their own plane; but the resistance is found to decrease if the tapered wires are bent in the same sense as in the case of parallel wires when they are bent so that the perpendicular to the plane containing the bent arms is parallel to the shortest length between the wires. In the case of the parallel wire system no appreciable change in the radiation resistance is recorded in this type of bend when the separation between the wires is small. The present investigation therefore further confirms that there is no additional loss due to radiation in this type of bend either when the wires are tapered or if they are widely separated when parallel.

In conclusion, the authors desire to express their grateful thanks to Prof. P. Dutt, M.A. (Cantab.), Head of the Physics Department, for his keen interest and constant help throughout the course of the investigation.

References.

(1) S. S. Banerjee, Phil. Mag. xix. p. 787 (1935).
(2) A. A. Pistolkors, Proc. I. R. E. xvii. p. 562 (1929).
(3) P. S. Carter, Proc. I. R. E. xx. p. 1004 (1932).

Physics Laboratory,
Benares Hindu University,
Benares (India).

LXXXI. *On the Laplacian of a Vector Point Function.* *By* Newman A. Hall *and* Francis Clauser *.

IN the text-books and journals there has existed a great deal of confusion regarding the validity and meaning of the well-known formula of vector analysis,

$$\nabla^2 u = \nabla\nabla . u - \nabla \times \nabla \times u, \quad . \quad . \quad . \quad . \quad (1)$$

where u is a vector point function, in a general system of curvilinear coordinates †.

* Communicated by Prof. H. Bateman, M.A., Ph.D.

† Compare R. Gans, 'Vector Analysis,' p. 46, and J. J. Slade, American Math. Monthly, xl. p. 483 (1933), with J. Spielrein, 'Vektorrechnung' (erste Aufl.), p. 179, and G. B. Jeffery, Phil. Mag. (6) xxix. pp. 445–455.

Inasmuch as it is becoming more and more necessary to use this formula, or a corrected one, in hydrodynamics, theory of vector potential, and other branches of applied mathematics, it is well to investigate the situation more thoroughly.

The difficulty in general seems to be this: just what meaning should be given to the left-hand side of (1) in an arbitrary curvilinear coordinate system? As has been very clearly shown previously *, if u_1, u_2, u_3 are the components of a vector u, the assumption that $\nabla^2 u$ is a vector with components $\nabla^2 u_1$, $\nabla^2 u_2$, $\nabla^2 u_3$ restricts the applicability of (1) to a rectangular coordinate system.

However, this is not a necessary assumption, nor is it found to be in accord with the physical application. If we rewrite (1) in the tensor notation, replacing the left side by its equivalent as it arises in the physical problems † and the quantities on the right side by their equivalents according to standard methods ‡, we obtain

$$g^{st}u_{r,\,st} = g^{st}u_{s,\,tr} - \frac{1}{g}\,e^{tpl}e^{mns}g_{pr}g_{lm}u_{n,\,st}, \quad . \quad . \quad (2)$$

where u has been replaced by its component, u_r.

To prove the tensor equation (2), it will be sufficient to show that it holds at the origin of an arbitrary geodesic coordinate system §. We can there replace the covariant derivatives by ordinary derivatives, so that (2) assumes the form of (1) in rectangular coordinates. Since this latter is an obvious identity, it is clear that (2), and hence (1), is valid in all three dimensional Riemannian geometries.

Reference to the position of the free index, r, in (2) indicates that the differential operator on the left is a scalar operator, whereas, as is well known, those on the right are vector operators. This suggests a method whereby the correct interpretation of (1) may be given in ordinary vector notation.

We may represent a vector in an arbitrary orthogonal curvilinear coordinate system by

$$\bar{u} = u_1\bar{e}_1 + u_2\bar{e}_2 + u_3\bar{e}_3, \quad . \quad . \quad . \quad . \quad . \quad (3)$$

* Slade, *loc. cit.*

† A. J. McConnell, 'Applications of the Absolute Differential Calculus,' p. 281 (1935).

‡ *Ibid.* p. 151.

§ O. Veblen, 'Invariants of Quadratic Differential Forms,' pp. 38–43.

where u_1, u_2, u_3 are the components of the vector $\bar{u}$ and e_1, e_2, e_3 are unit vectors along the coordinate curves. The left of (1) may then be written

$$\nabla^2\bar{u} = \nabla^2(u_1e_1)+\nabla^2(u_2\bar{e}_2)+\nabla^2(u_3\bar{e}_3). \quad . \quad . \quad (4)$$

Since, from the above discussion, we are to take ∇^2 as a scalar operator, the unit vectors, $\bar{e}_1$, can be removed from the parenthesis if, and only if, they are constant in direction, which they are not in general *.

On the other hand, for the right of (1), since the differential operators are vector operators, the differentiation of the unit vectors is not involved. For this reason it is usually more convenient to use (1) in evaluating the Laplacian of a vector point function rather than to proceed directly by (4). In the case of orthogonal curvilinear coordinates where

$$ds^2 = h_1^2\,dx_1^2+h_2^2\,dx_2^2+h_3^2\,dx_2^2, \quad . \quad . \quad . \quad (5)$$

we obtain in this manner the standard formula :

$$\begin{aligned}\nabla^2\bar{u} = {} & \left\{\frac{1}{h_1}\frac{\partial}{\partial x_1}(\nabla.\bar{u})+\frac{1}{h_2h_3}\left[\frac{\partial}{\partial x_3}\left\{\frac{h_2}{h_3h_1}\left(\frac{\partial h_1u_1}{\partial x_3}-\frac{\partial h_3u_3}{\partial x_1}\right)\right\}\right.\right. \\ & \left.\left.-\frac{\partial}{\partial x_2}\left\{\frac{h_3}{h_1h_2}\left(\frac{\partial h_2u_2}{\partial x_1}-\frac{\partial h_1u_1}{\partial x_2}\right)\right\}\right]\right\}e_1 \\ & +\left\{\frac{1}{h_2}\frac{\partial}{\partial x_2}(\nabla.\bar{u})+\frac{1}{h_3h_1}\left[\frac{\partial}{\partial x_1}\left\{\frac{h_3}{h_1h_2}\left(\frac{\partial h_2u_2}{\partial x_1}-\frac{\partial h_1u_1}{\partial x_2}\right)\right\}\right.\right. \\ & \left.\left.-\frac{\partial}{\partial x_3}\left\{\frac{h_1}{h_2h_3}\left(\frac{\partial h_3u_3}{\partial x_2}-\frac{\partial h_2u_2}{\partial x_3}\right)\right\}\right]\right\}\bar{e}_2 \\ & +\left\{\frac{1}{h_3}\frac{\partial}{\partial x_3}(\nabla.u)+\frac{1}{h_1h_2}\left[\frac{\partial}{\partial x_2}\left\{\frac{h_1}{h_2h_3}\left(\frac{\partial h_3u_3}{\partial x_2}-\frac{\partial h_2u_2}{\partial x_3}\right)\right\}\right.\right. \\ & \left.\left.-\frac{\partial}{\partial x_1}\left\{\frac{h_2}{h_1h_3}\left(\frac{\partial h_1u_1}{\partial x_3}-\frac{\partial h_3u_3}{\partial x_1}\right)\right\}\right]\right\}\bar{e}_3, \\ & \qquad . \quad . \quad . \quad (6)\end{aligned}$$

where

$$\nabla.\bar{u} = \frac{1}{h_1h_2h_3}\left[\frac{\partial}{\partial x_1}(h_2h_3u_1)+\frac{\partial}{\partial x_2}(h_3h_1u_2)+\frac{\partial}{\partial x_3}(h_1h_2u_3)\right].$$

A direct verification of the validity of (1) in a simple case may be illustrative.

* In this connexion see Spielrein, *loc. cit.* pp. 122–125.

Let us take the vector $u=a\bar{\theta}_1$ in cylindrical coordinates where a is a scalar constant and $\bar{\theta}_1$ is the unit vector along the curves $r=$const., $z=$const. Obviously if we consider $\bar{\theta}_1$ constant then $\nabla^2(a\bar{\theta}_1)=0$. However, to consider the actual variation of $\bar{\theta}_1$ resolve in rectangular coordinates so that

$$\bar{\theta}_1 = \bar{i}\cos\theta + \bar{j}\sin\theta.$$

Then

$$\begin{aligned}\nabla^2(a\bar{\theta}_1) &= a\nabla^2[\bar{i}\cos\theta+\bar{j}\sin\theta] \\ &= -\frac{a}{r^2}[\bar{i}\cos\theta+\bar{j}\sin\theta] \\ &= -\frac{a\bar{\theta}_1}{r^2},\end{aligned}$$

which agrees with the result obtained by using (6).

California Institute of Technology.

LXXXII. *The Surface Tension of a Moving Mercury Sheet.* *By* H. O. Puls, *B.Sc., Senior Wantage Scholar, University of Reading* *.

Abstract.

Bond's method of using the impact of two liquid jets for the determination of surface tensions is applied to mercury. The mercury is circulated, and a device for the continuous measurement of the rate of flow of the liquid is described. A method for determining the momentum of the jet is developed, from which the radius of the jet is deduced.

The value of the surface tension of mercury in contact with air at 20° C. is given as $475{\cdot}5\pm2$ dynes/cm.

A survey of the results of other workers is added.

---

1. *Introduction.*

THIS experiment was undertaken with two objects in view—firstly, it was to be ascertained whether the method of determination of surface tension as

* Communicated by W. N. Bond, D.Sc., F.Inst.P.

described by W. N. Bond[1] in his paper on "The Surface Tension of a Moving Water Sheet" was generally applicable; secondly, if it were applicable, then to determine the value of the surface tension of mercury, about which a good deal of doubt still existed. The advantage of this type of experiment, where the surface is renewed at the rate of about 100 times a second, becomes even more apparent with mercury than with water. Surface contamination of the mercury is prevented, as the mercury is withdrawn from beneath the surface of a reservoir, and is not exposed to the atmosphere until it forms the sheet; there is not then sufficient time for the surface to become contaminated. Similarly, surface absorption of gases is reduced to a minimum. Finally, the angle of contact need not be known.

The essential parts of the experiment are similar to those described by Bond. Two cylindrical jets of mercury meet with their axes coinciding in a vertical line. A circular horizontal sheet of mercury is formed where they meet. Modifications were made in the apparatus to increase the ease with which measurements and adjustments could be made; other variations had to be introduced, as only a limited supply of mercury was available.

The theory of the method is identical with that of Bond's experiments, so that I shall only recapitulate the formulæ used in the calculation of the results. They are as follows:—

If S is the surface tension, Q is the volume of liquid supplied in unit time, r is the radius of each jet, ρ is the density of the liquid, and R is the radius of the sheet, then the first approximation is

$$S_1 = \frac{Q^2\rho}{2R\pi^2(2r)^2}.$$

The second approximation is

$$S_2 = \frac{Q^2\rho}{(2R-r)\pi^2(2r)^2} - \frac{r^2g\rho}{2}\left(1 - \frac{\Delta}{2R} - \frac{h}{R}\right).$$

The final value is given by

$$S_3 = \frac{Q^2\rho}{(2R-r)\pi^2(2r)^2} - \frac{r^2g\rho}{2}\left\{\frac{S_1}{S_2} - \frac{\Delta}{2R} - \frac{h}{R}\right\},$$

where Δ=distance between nozzles, h=distance between horizontal top of sheet and point of contact of vertical tangent to the sheet.

2. *The Apparatus.*

I shall describe in detail only those parts of the apparatus which differ materially from Bond's. The limited supply of mercury necessitated a method for circulating it. A motor-car oil-circulating pump was found suitable. This consisted of two steel interlocking gear wheels fitting tightly into a steel case. By rotating one of them the liquid is dragged round with it. It was found to be impossible to stop leakage round the driving spindle, but this was overcome by building up a channel round the spindle and conducting the leakage back to the sump. The pump was driven by a 1/6th H.P. electric motor, whose speed could be regulated by a sliding rheostat. When running at full speed the pump was capable of pumping about 10 c.c. per sec. to a height of 90 cm. The pump was fed from a sump which could contain sufficient mercury to keep the pump always filled. The mercury was withdrawn from the bottom of the sump, so that only mercury free from surface dirt was pumped through the system. The mercury was pumped to a glass reservoir A (fig. 1), from which an overflow led back to the sump. The pump was always run at such a speed that the overflow was just covered, thus keeping a constant pressure in the supply pipe. This pipe led off from the base of the reservoir, thus again keeping surface dirt out of the system. The reservoir could be moved in a vertical direction to give different rates of flow. The nozzles were of similar construction to that described by Bond. It is essential that they should be sufficiently symmetrical to work either way up. The lower nozzle D_1 was firmly fixed through the bottom of a collecting bowl E, which was 17 cm. in diameter. The upper nozzle D_2 was held by two adjustable clamps F. Each clamp was at the end of a differential screw G, giving a fine adjustment in one horizontal direction. Each screw was fixed to the end of a long beam H, hinged about a fixed point near the screw, and adjustable at the other end by a screw I, giving a fine adjustment in another horizontal direction.

The other two degrees of freedom, a vertical motion, and a rotary motion do not need such fine adjustment, the necessary movements being easily done directly. It was not found necessary to include a metal cone for the liquid sheet to cling to, as it was sufficiently stable

Fig. 1.

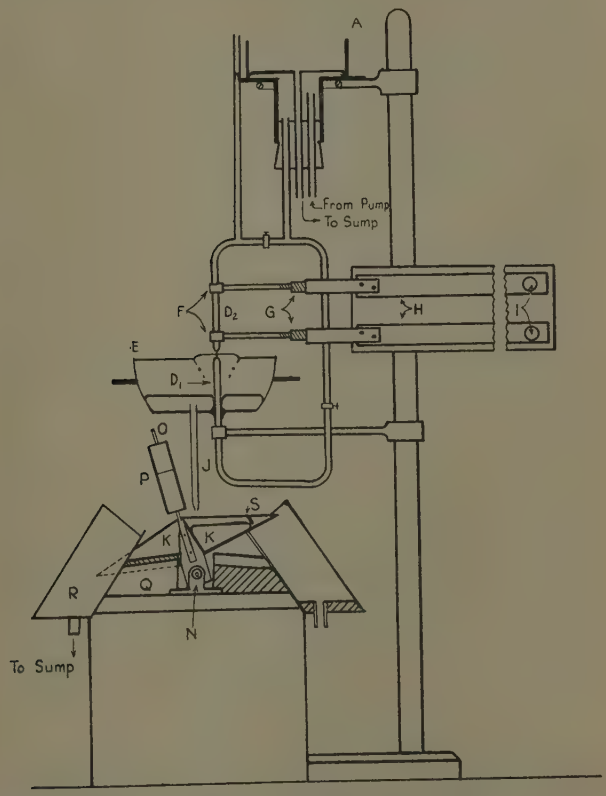

without. The collecting bowl had an outlet J which led to a device for measuring the rate of flow.

3. *The Measurement of the Rate of Flow.*

Two scoops K, made of synthetic resin, were firmly mounted on a wooden block, in such a way that when

the top of one scoop is horizontal the bottom of the other slopes downwards. The central block has a knife-edge protruding centrally from each side. Each knife-edge bears in a hole in a steel bracket N firmly mounted on a base-plate. To raise the centre of gravity of the system a long steel screw O is fixed to each side of the block, and heavy steel weights P can be adjusted on these screws. In the position of rest one of the scoops lays on felt padding mounted on a wooden block Q, shaped to fit the scoop. Mercury from the collecting bowl is conducted through the tube J to a point centrally above the knife-edge. This normally delivers the mercury into one of the scoops. When this becomes filled to a certain point the equilibrium of the system becomes unstable, and the scoop tips over, mercury then being delivered into the other scoop. The mercury flowing out of the scoop is collected in a wooden container R, so shaped as to prevent splashing, and thence returned to the sump. The scoops are covered with cellophane, leaving only a narrow slit for the mercury to enter and a space at the end for emptying. A vertical baffle S is fixed near the tip of each scoop to prevent too sudden emptying of the scoop.

The "Rocker" was so constructed that each scoop could contain more than 100 c.c. of mercury. Under normal working conditions the rocker tipped over about every 12 seconds. A calibration of the rocker was made before and after a series of experiments, and was found to be very nearly constant after the rocker had had a considerable amount of use. This type of metering device has the advantage that it measures the rate of flow over the whole experiment, and any slight irregularities in the flow are automatically compensated for.

4. *The Measurement of the Radius of the Jet.*

The radius of the jet which is required is that radius which it would have had if the velocity were constant across the transverse section (the mass and momentum per second being unchanged). This radius I shall call the effective radius. The nozzles were so constructed that the effective radius was nearly equal to the actual radius. Owing to slight irregularities, however, the jet does not move along with a constant radius. Attempts

were made to measure directly the diameter of the jets by letting them flow in a horizontal direction and measuring with a travelling microscope. The nozzle was so arranged that the point at which the diameter of the jet was being measured was at the same height as the nozzle, so that the liquid would have the same momentum as at the end of the nozzle. The diameter was measured at various places along the jet, from the edge of the nozzle to a point fifty jet diameters away. The series of results were, however, so conflicting that no great value was attached to them, especially as it was estimated that the radius of the jet would not have reached its effective value even at the place at which the jet breaks into drops.

The measurement of the internal diameter of the nozzles themselves gave the values $0{\cdot}0816 \pm 0{\cdot}0008$ and $0{\cdot}0812 \pm 0{\cdot}0006$ cm. These results are useless without some knowledge of the velocity distribution of the liquid in the jet after it has left the nozzle. To estimate the velocity distribution an experment was carried out in which the rate of flow from the nozzles was found for various heads of liquid. This showed that there was a slight deviation from the theoretical value. The value finally adopted for the ratio $\frac{\text{calc. rate of flow}}{\text{obs. rate of flow}}$ was $1{\cdot}020_7$.

We may proceed to deduce the effective radius of cross-section of the jet. Assuming that the velocity in the middle of the jet has the theoretical value $v = \sqrt{2gh}$, where h is the head of liquid, and assuming as an approximation that

$$\text{(velocity at a distance ``}a\text{'' from the axis)} = v\left\{1 - \left(\frac{a}{r_1}\right)^n\right\}$$

(where r_1 denotes the radius of the nozzle), then

$$\text{(observed volume per sec.)} = \int_0^{r} 2\pi a v \left\{1 - \left(\frac{a}{r_1}\right)^n\right\} da$$

$$= \frac{\pi r_1^2 v}{1 + \frac{2}{n}}.$$

Thus the observed rate of flow is obtained by dividing the rate of flow predicted by the simple theory, namely $\pi r_1^2 v$, by $\left(1+\frac{2}{n}\right)$.

Hence $1+\frac{2}{n}=1{\cdot}020_7$ and $n=96{\cdot}6$.

Further, we have

$$\begin{aligned}&\text{(actual momentum per sec.}\\ &=\int_0^r 2\pi a\,.\,\rho v^2\left\{1-\left(\frac{a}{r_1}\right)^n\right\}^2 da\\ &=\pi r_1^2\rho v^2\left(1-\frac{4}{n+2}+\frac{2}{2n+2}\right)\\ &=\pi r_1^2\rho v^2(1-0{\cdot}0304)\\ &=\rho\,\frac{(\text{observed volume per second})^2}{\pi r_1^2}\times 1{\cdot}011.\end{aligned}$$

Hence the actual momentum per second is 1·1 per cent. greater than that predicted by the simple theory.

Alternatively we may assume a formula given by Bond [2] for the velocity distribution in a case approximating to the one under consideration, giving

$$\begin{aligned}&\text{(velocity at a distance ``}a\text{'' from the axis)}\\ &=v\tanh\{B(r_1^2-a^2)\},\end{aligned}$$

where B is a constant.

Proceeding with the calculation as before, we find that the actual momentum per second is 1·15 per cent. greater than that predicted by the simple theory.

The "effective radius" of the jet will therefore be 0·55 per cent. less than that of the nozzles. Applying this correction to the measured radius of the nozzles, we have

$$\text{(effective radius of jet)}=0{\cdot}081{,}0\pm 0{\cdot}000{,}5\text{ cm.}$$

As it is really the momentum of the jets which enters into the calculation of the surface tension it was decided to attempt a direct measurement of this, and hence deduce the effective radius. A similar experiment was carried out by Buff [3]. If we allow the jet of mercury to impinge normally on a flat vertical plate which is suspended in such a way that it is free to move in the direction of

the jet we can find the force on the plate, and hence the momentum of the jet.

Let v be the velocity of the jet, m be the mass impinging on the plate in unit time, F be the force on the plate, r be the effective radius of the jet, and S the approximate surface tension of the liquid. Then besides the force due to the impact of the jet there are other small forces. (*a*) there is a back pull due to surface tension; this will be equal to $2\pi r\mathrm{S}$; (*b*) there is an extra force on the plate due to the excess of the pressure inside the jet over atmospheric pressure. This will be $\pi r^2 . \frac{\mathrm{S}}{r}$.

Hence
$$\mathrm{F}=mv+\pi r\mathrm{S}-2\pi r\mathrm{S}$$
$$=\frac{m^2}{g\rho\pi r^2}-\pi r\mathrm{S}.$$

Therefore
$$r^2=\frac{m^2}{(\mathrm{F}+\pi r\mathrm{S}).g\rho}.$$

For the correction term I have taken

$$\mathrm{S}=475 \text{ dynes/cm.},$$
$$r=0{\cdot}08 \text{ cm.},$$
and
$$\rho=13{\cdot}55 \text{ gm./c.c.}$$

The experimental details for this determination of the radius are as follows:—A flat steel plate A (fig. 2), about 10 cm. square, was mounted on the end of a brass rod B, 60 cm. long. To the upper end of the rod was attached a brass ring C carrying a steel knife-edge D, mounted in the same plane as the plate. The plate A had mounted on it another steel plate E, so that there was a distance of 0·1 cm. between the two plane surfaces. The plate E had a hole 0·4 cm. in diameter in it, through which the mercury was directed. The object of the second plate was to correct for the increased deflexion that would be caused by the back splashing of the mercury from the plate A. The mercury leaves the space between the plates with only a vertical velocity, all its horizontal momentum having been given up to the pendulum. The rate of flow is determined by the rocker as before. The deflexion of the pendulum (about 2 cm.) is measured at a marked point by a horizontally travelling microscope. The distance to the knife-edge from the

point of measurement, from the point of application of the mercury jet, and from the centre of gravity were measured with a cathetometer. The pendulum weighed about 1 kg. From a knowledge of these values the force F (which is about 12 gm. weight) can be calculated. The value obtained by this method is

$$(\text{effective radius of jet}) = 0{\cdot}080,6_7 \pm 0{\cdot}000,16 \text{ cm.}$$

Owing to the very much higher accuracy of this method than the others attempted, considerably more importance was attached to this value than to the others.

Fig. 2.

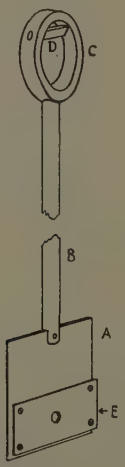

The value finally used for r was the weighted mean of the last two determinations, which gives

$$r = 0{\cdot}080,7_0 \pm 0{\cdot}000,15 \text{ cm.}$$

5. *The Experiment.*

The pump was set going at such a speed that enough mercury was being transferred to the reservoir to maintain the required rate of flow. When the reservoir was full the screw-clips leading to the nozzles were opened, the top one being kept more open than the lower one to prevent upward splashing. The upper nozzle

was then adjusted so that the mercury sheet floated in a horizontal plane anywhere between the nozzles, which were three to four jet-diameters apart. When it did so the jets were accurately aligned. Then the screw-clips were adjusted so that the sheet floated about half-way between the nozzles. For the measurement of the diameter of the sheet a scale engraved on the front of a thick glass mirror was used. This was placed behind and above the sheet, inclined at an angle of 45° to the vertical. On looking into the mirror in a horizontal direction the image of the sheet appears behind the image of the scale. By getting the scale-marking and its image in the same line parallax is avoided. The diameter was measured in ten directions during each experiment. At the same time the number of times that the rocker tipped over was counted, a stop-clock giving the whole time of the experiment, and hence the time taken for each emptying of the rocker. The temperature of the mercury in the upper reservoir was taken immediately before and after each experiment, the mean value being taken as the temperature of the mercury during the experiment. h and Δ were measured with a pair of vernier calipers. To obtain different rates of flow the position of the reservoir was altered.

6. *Experimental Results.*

All the experiments were conducted with one pair of nozzles. The effective radius of the jets was $r=0{\cdot}0807_0\pm0{\cdot}00015$ cm. The density of mercury at the temperature of working was taken from tables. The correction terms have the values :

(i.) $$\frac{h}{\mathrm{R}}\cdot\frac{r^2g\rho}{2}=7{\cdot}8 \text{ dynes/cm.}$$

This is the mean of the experimental value deduced from measurements of h, and the theoretical value, $\frac{r^2g\rho}{\mathrm{S}}\cdot\frac{r^2g\rho}{2}$, which agree to within 1 per cent.

(ii.) $$\frac{r^2g\rho}{2}=43{\cdot}3 \text{ dynes/cm.}$$

(iii.) $\frac{\Delta}{2\mathrm{R}}$ varies according to Δ and R.

(iv.) To reduce the values to 20° C., an approximate value of the temperature coefficient of surface tension of mercury was assumed (−0·38 dynes/cm. per degree Centigrade).

A table showing the results of nineteen separate experiments is appended.

The mercury used in experiments A to J had been in the apparatus for some months; after experiment J it was redistilled.

Expt.	Temp. °C.	gm./sec.	2R, cm.	Δ, cm.	S_{20}, dynes/cm.
A	18·6	7·308	5·219	0·66	516·6
B	17·3	8·472	7·037	0·64	509·1
C	18·45	7·004	5·353	0·58	457·0
D	18·2	6·928	5·163	0·55	464·1
E	20·15	7·384	5·743	0·50	473·8
F	19·8	8·345	7·418	0·52	465·1
G	22·25	7·955	6·733	0·55	467·5
H	23·05	7·045	5·202	0·56	478·7
I	21·15	4·190	1·959	0·36	464·7
J	17·2	4·904	2·595	0·39	472·8
K	17·0	7·435	5·918	0·47	463·3
L	19·75	8·024	6·725	0·49	476·0
M	20·75	7·450	5·827	0·41	474·3
N	21·45	6·849	4·935	0·41	475·4
O	15·4	7·393	5·678	0·46	479·5
P	19·75	7·099	5·252	0·48	479·9
Q	20·75	7·338	5·594	0·58	481·6
R	19·35	7·310	5·511	0·61	485·7
S	18·9	6·800	4·801	0·32	507·7

Experiments A, B, G to L, Q to S had nozzle *a* on top and *b* below.

Experiments C to F, M to P had nozzle *b* on top and *a* below.

The arithmetic mean of the above determinations of the surface tension at 20° C. is

$$S_{20}=477\pm2 \text{ dynes/cm.}$$

Three of the nineteen values appear to be rather high, and it is possible that the median gives a better estimate than the mean.

The median value is

$$S_{20}=475{\cdot}5\pm2 \text{ dynes/cm.}$$

7. *Discussion of Results.*

The value 475·5±2 dynes/cm. for the surface tension of mercury at 20° C. compares favourably with some of

Sur. tens., dynes/cm.	Worker, method, and reference.
340	Bashforth and Adams. 'An Attempt to Test the Theories of Capillary Action,' pp. 73–80 (Camb., 1883).
432	Kalähne. Capillary waves. *Ann. d. Phys.* vii. p. 440 (1902).
436·8	Th. Lohnstein. Shape of drops. Wied. *Ann.* liv. p. 722 (1895).
440·5	Laplace. Méc. cél. iv. p. 538 (Paris, 1845).
442·1	Poisson. Drops. Nouv. Théor. d. l'action capillaire, p. 319 (1831).
454·0	Siedentopf. Shape of drops. Wied. *Ann.* lxi. p. 252 (1897).
458·2	Magie. Curv. of surface in capillary. Wied. *Ann.* xxv. p. 428 (1885).
458·9	M. Cantor. Pressure in bubbles. Wied. *Ann.* xlvii. p. 415 (1892).
459·4	W. D. Harkins and E. H. Grafton. Drop weight: freshly distilled. J. Amer. Chem. Soc. xlii. (ii.) p. 2536 (1920).
464·9	Harkins and Grafton. Drop weight: 2 months old mercury. *Loc. cit.*
464·9	Sieg. Diss., Berlin, 1887.
471·0	P. Lenard. Vibrating drop. Wied. *Ann.* xxx. p. 238 (1887).
472	Hagemann. Vibrating jet. Disser., Freiburg, 1914.
473·2	F. Sauerwald and G. Drath. Max. press. in bubbles. *Z. anorg. Chem.* cliv. p. 79 (1926).
474	E. A. Owen and A. F. Dufton. Capil. rise between amal. Cu plates. Proc. Phys. Soc. xxxviii. p. 204 (1926).
485	E. A. Owen and A. F. Dufton. Capil. rise in amal. Cu tubes. *Loc. cit.*
487	International Critical Tables.
491·2	Grünmach. Capil. waves on new surface. *Ann. d. Phys.* (4) iii. p. 660 (1900).
405	Grünmach. Capil. waves on 30 min. old surface. *Loc. cit.*
494	J. Stöckle. Shape of drop. *Ann. d. Phys.* lxvi. p. 499 (1898).
500·0	J. Piccard. *Arch. sc. phys.* xxiv. p. 579 (1890).
505	G. Meyer. Vibrating jet. *Ann. d. Phys.* lxvi. p. 523 (1898).
532	J. G. Popesco. Surface 5 secs. old. *Ann. d. phys.* iii. p. 402 (1925).
547·2	Quincke. Capillary rise. Wied. *Ann.* lii. p. 19 (1894).
563	Satterly and Strachan. Stationary waves on vertical jet. Roy. Soc. Can. Trans. (iii.) xxix. p. 109 (1935).

the best generally accepted values. In particular it is in the neighbourhood of the values obtained by other dynamic methods, such as the vibrating jet and capillary

waves on a newly formed surface. For comparison I append a table of other workers' values for the surface tension of mercury in contact with air. The temperatures at which the measurements were made vary between 15° C. and 20° C., but the differences due to this are very small.

From this summary of results it will be seen that for experiments carried out under similar conditions to my own the surface tension should lie between 460 and 505 dynes per cm. The value of 487 dynes/cm. given by the International Critical Tables and 472 dynes/cm. quoted by the ' Handbuch der Physik ' are approximately confirmed by my own determination.

The distillation of the mercury halfway through the experiments produced no noticeable change in the value of the surface tension. This shows that the surface tension of a freshly formed surface is independent of the previous age of the mercury, so that any reduction in the value of the surface tension with time must be due only to contamination of the surface, either through dirt, oxidation, or surface absorption of gases. The extraordinary high values of some of the workers remain as yet unexplained.

8. *Acknowledgments.*

In conclusion, I would like to thank Prof. J. A. Crowther, in whose laboratories the work was carried out, and Dr. W. N. Bond, for their very helpful suggestions and kind interest throughout the work. My thanks are also due to Mr. J. Burgess, the laboratory steward, for help and advice in the making of the apparatus.

9. *References.*

(1) Bond, W. N., Proc. Phys. Soc. xlvii. p. 549 (1935).
(2) Bond, W. N., Proc. Phys. Soc. xl. p. 1 (1927).
(3) Buff, Pogg. *Ann.* cxxxvii. p. 497 (1896).

Department of Physics,
The University of Reading.
April 28th, 1936.

LXXXIII. *On the Meaning of Diffusion Potential.*

By E. A. Guggenheim, *M.A.**

ALTHOUGH the thermodynamics of cells with liquid-liquid junctions have been completely worked out [1], [2], [3], and there is nothing essentially new to add to the subject, they still appear to be incompletely understood by certain experimenters in this field. The confusion arises from the use of the expression "diffusion potential" in two different senses. The present note is an attempt to disperse this confusion.

In discussing cells with liquid-liquid junctions we may, without loss of generality, confine ourselves to cells containing only one type of electrode, say the hydrogen electrode, for instance

H_2	Electrode solution I	Intermediate solutions A, B, C, . .	Electrode solution II	H_2.

For any cell whatever may be obtained by compounding in series one cell of this type with two hydrogen electrodes, and at most two other cells without any liquid-liquid junctions. For example the cell

Ag	AgCl	Solution I	Intermediate solutions A, B, C, . . .	Solution II	Hg_2Cl_2	Hg

is equivalent to the three cells

Ag	AgCl	Solution I	H_2,

H_2	Solution I	Intermediate solutions A, B, C, . . .	Solution II	H_2,

H_2	Solution II	Hg_2Cl_2	Hg

in series. Of these three the first and last contain no liquid-liquid junctions; we shall therefore take the second as the most general type of cell requiring discussion.

We shall denote concentrations by C, activity coefficients by f, valencies (positive for cations, negative for anions) by z, transport numbers by t. Where necessary

* Communicated by Prof. F. G. Donnan, C.B.E., M.A., F.R.S.

we shall denote the various phases by superscripts and the various species by subscripts, the subscript i referring to any ionic species. We denote the Faraday by F, the gas constant by R, and the absolute temperature by T.

We commence by introducing quantities E^0_{El}, E^0_D, E^Δ_{El}, E^Δ_D, E_{El}, E_D, E^Δ, all having the dimensions of electromotive force and defined by the following formulæ:

$$E^0_{El} = \frac{RT}{F} \log \frac{C^{II}_{H+}}{C^{I}_{H+}}, \quad . \quad . \quad . \quad . \quad . \quad . \quad (1)$$

$$E^0_D = -\frac{RT}{F} \int_I^{II} \sum_i \frac{t_i}{z_i} d \log C_i, \quad . \quad . \quad . \quad (2)$$

$$E^\Delta_{El} = \frac{RT}{F} \log \frac{f^{II}_{H+}}{f^{I}_{H+}}, \quad . \quad . \quad . \quad . \quad . \quad . \quad (3)$$

$$E^\Delta_D = -\frac{RT}{F} \int_I^{II} \sum_i \frac{t_i}{z_i} d \log f_i, \quad . \quad . \quad . \quad . \quad (4)$$

$$E_{El} = \frac{RT}{F} \log \frac{C^{II}_{H+} f^{II}_{H+}}{C^{I}_{H+} f^{I}_{H+}}, \quad . \quad . \quad . \quad . \quad . \quad (5)$$

$$E_D = -\frac{RT}{F} \int_I^{II} \sum_i \frac{t_i}{z_i} d \log C_i f_i, \quad . \quad . \quad . \quad (6)$$

$$E^\Delta = \frac{RT}{F} \log \frac{f^{II}_{H+}}{f^{I}_{H+}} - \frac{RT}{F} \int_I^{II} \sum_i \frac{t_i}{z_i} d \log f_i, \quad . \quad . \quad (7)$$

the integrals to be evaluated across all the junctions between the two electrode solutions. It will be noticed that by definition

$$E_{El} = E^0_{El} + E^\Delta_{El}, \quad . \quad . \quad . \quad . \quad . \quad . \quad (8)$$

$$E_D = E^0_D + E^\Delta_D, \quad . \quad . \quad . \quad . \quad . \quad . \quad (9)$$

$$E^\Delta = E^\Delta_{El} + E^\Delta_D. \quad . \quad . \quad . \quad . \quad . \quad . \quad (10)$$

If the solutions were ideal E^Δ_{El} and E^Δ_D would, of course, be zero, and there would be no distinction between E_{El} and E^0_{El} nor between E_D and E^0_D. Since, however, solutions of electrolytes are not even approximately ideal the distinction between E_D and E^0_D is important.

Let us now consider the value of E, the electromotive force of the cell with two hydrogen electrodes. If the

solutions were all ideal the value of E would be simply the sum of E^0_{El}, the electrode potentials, and E^0_D, the diffusion potential. Since, however, the solutions are not ideal we have instead.

$$E = E^0_{El} + E^{\Delta}_{El} + E^0_D + E^{\Delta}_D. \quad . \quad . \quad . \quad . \quad (11)$$

By using (8), (9), and (10) we obtain the alternative formulæ

$$E = E_{El} + E_D, \quad . \quad . \quad . \quad . \quad . \quad . \quad . \quad (12)$$

$$E = E^0_{El} + E^0_D + E^{\Delta}, \quad . \quad . \quad . \quad . \quad (13)$$

but by contrast

$$E \neq E_{El} + E^0_D. \quad . \quad . \quad . \quad . \quad . \quad (14)$$

It is now easy to see how confusion arises when the same expression " diffusion potential " is used for the two quantities E^0_D and E_D. Consider, for example, a paper by Szabó [4]. His formula (2) is equivalent to our (12) provided his " diffusion potential " denoted by ϵ refers to our E_D. He states that if one could obtain a value for ϵ then this formula would enable one to compute E_{El} and so obtain values for the activity coefficient of a single ionic species ; this is true only if by ϵ he means our E_D. Since, however, E_D itself contains ionic activity coefficients this is not very helpful. However, on the previous page he refers to the computation of the " diffusion potential " ϵ by the use of Henderson's formula [5]. Now if the transition layers between the consecutive solutions are of the continuous mixture type [6], then Henderson's formula gives the correct evaluation of E^0_D. Szabó is now using the expression " diffusion potential " and the symbol ϵ to denote our E^0_D.

Suppose that the value of E has been measured, that the value of E^0_{El} is known from the composition of the electrode solutions, and that the value of E^0_D is calculated by use of Henderson's formula. Then by means of (13) we can compute E^{Δ}. This procedure was followed by Unmack and Guggenheim [7], who used the symbol E_s for the present E^{Δ}. But it is quite impossible to determine E^{Δ}_{El} and E^{Δ}_D separately. Now from the definition of E^{Δ} and by use of the identity

$$\sum_i t_i = 1 \quad . \quad . \quad . \quad . \quad . \quad . \quad . \quad (15)$$

it is always possible to transform E^{Δ} into an expression involving only mean activity coefficients and no ionic activity coefficients [1, 2]. Since, then, E^{Δ} is a function of mean activity coefficients of electrolytes and of transport numbers of ions, no information can be obtained concerning ionic activity coefficients; in fact it has been shown that these are physically undefined [8]. One is, of course, at liberty to assign in each solution any value one chooses to the activity coefficient of any one ionic species, say H^+, and then compute the corresponding conventional values for other ions.

Szabó has measured the electromotive force of the simple concentration cells

$$\mathrm{H_2} \;\Big|\; \begin{matrix}\mathrm{HCl}\\ \mathrm{C^I}\end{matrix} \;\Big|\; \begin{matrix}\mathrm{HCl}\\ \mathrm{C^{II}}\end{matrix} \;\Big|\; \mathrm{H_2}$$

For these cells we have the very simple formulæ

$$E_{El} = \frac{RT}{F} \log \frac{C^{II} f^{II}_{H+}}{C^{I} f^{I}_{H+}} = \frac{RT}{F} \int_{I}^{II} d \log C f_{H+}, \quad . \quad (16)$$

$$E_D = -\frac{RT}{F} \int_{I}^{II} t_{H+} d \log C f_{H+} + \frac{RT}{F} \int_{I}^{II} t_{Cl-} d \log C f_{Cl-}. \quad . \quad . \quad . \quad (17)$$

Suppose that specific values have been assigned to f_{H+} in each electrode solution and at each part of the transition layer between them. Let the quantity λ be defined for each solution by the ratio

$$\lambda = \frac{f_{H+}}{f_{H,\,Cl}} = \frac{f_{H,\,Cl}}{f_{Cl-}}. \quad . \quad . \quad . \quad . \quad . \quad . \quad (18)$$

Then, by substitution in (16) and (17), we obtain

$$E_{El} = \frac{RT}{F} \int_{I}^{II} d \log C f_{H,\,Cl} + \frac{RT}{F} \log \frac{\lambda^{II}}{\lambda^{I}}, \quad . \quad (19)$$

$$E_D = -\frac{RT}{F} \int_{I}^{II} t_{H+} d \log C f_{H,\,Cl} + \frac{RT}{F} \int_{I}^{II} t_{Cl-} d \log C f_{H,\,Cl} - \frac{RT}{F} \log \frac{\lambda^{II}}{\lambda^{I}}. \quad (20)$$

Thus, while E_{El} contains the term $\frac{RT}{F} \log \frac{\lambda^{II}}{\lambda^{I}}$, E_D contains the equal and opposite term $-\frac{RT}{F} \log \frac{\lambda^{II}}{\lambda^{I}}$. Hence E,

the sum of E_{El} and E_D, is independent of λ, and so no information can be obtained concerning λ by measurements of E. In fact by addition of (16) and (17) we obtain

$$E = \frac{RT}{F}\int_I^{II} t_{Cl^-}\{d \log C f_{H^+} + d \log C f_{Cl^-}\}$$

$$= \frac{RT}{F}\int_I^{II} 2t_{Cl^-} d \log C f_{H, Cl}. \quad . \quad . \quad . \quad . \quad . \quad (21)$$

According to the very accurate measurements of Schedlovsky and Longsworth [9] the value of t_{Cl^-} in HCl is ·175 for C=·01, and falls to ·169 at C=·1. Within the limits of accuracy of Szabó's measurements the value of t_{Cl^-} may be taken as constant, and so we have the simple formula

$$E = \frac{RT}{F} 2t_{Cl^-} \log \frac{C^{II} f^{II}_{H, Cl}}{C^{I} f^{I}_{H, Cl}} . \quad . \quad . \quad . \quad (22)$$

Szabó's data are in fact represented by this formula with the value $t_{Cl^-} = ·174 \pm ·007$. Szabó, however, interprets his data in a different manner, and uses them to assign values to the ionic activity coefficients. These values are in fact rather complicated functions of the $f_{H, Cl}$, and t_{Cl^-}. Of course no harm is done by assigning values to ionic activity coefficients in this curious manner provided the purely arbitrary nature of the values so assigned be realized, but it is difficult to see what uesful purpose is served thereby.

I am indebted to Dr. G. S. Hartley for his kind and constructive criticism.

References.

(1) Taylor, P. B., J. Phys. Chem. xxxi. p. 1478 (1927).
(2) Guggenheim, J. Phys. Chem. xxxvi. p. 1758 (1930).
(3) Guggenheim, 'Modern Thermodynamics' (Methuen, 1933).
(4) Szabó, *Z. Physik. Chem.* clxxiv. pp. 22 & 33 (1935).
(5) Henderson, *Z. Physik. Chem.* lix. p. 118 (1907).
(6) Guggenheim, J. Am. Chem. Soc. lii. p. 1315 (1930).
(7) Unmack and Guggenheim, *Kgl. Danske Vid. Selsk. Matt.-Fys. Medd.* x. nos. 8 & 14 (1930–31).
(8) Guggenheim, J. Phys. Chem. xxxiii. p. 842 (1929).
(9) MacInnes, Schedlovsky, and Longsworth, J. Am. Chem. Soc. liv. p. 2758 (1932).

The Sir William Ramsay Laboratories of
Inorganic and Physical Chemistry,
University College, London.

LXXXIV. *The Radial Distribution of Electrons in the Uniform Columns of Electrical Discharges.* *By* G. D. Yarnold, *M.A., D.Phil., and* S. Holmes, *B.Sc., University College, Nottingham* *.

THE uniform columns of electrical discharges in cylindrical tubes have been studied recently by Townsend †, and a theory has been put forward which gives a satisfactory explanation of the observed facts. The electric force Z in the column depends on the nature and pressure of the gas and upon the radius of the tube, but when these conditions are fixed the force is found to be independent of the current flowing in the tube, provided this is not so large as to cause appreciable heating of the gas. Moreover, the electric force in the uniform column of a high-frequency discharge excited by external sleeves is found to be the same as the electric force in the positive column of a direct current discharge under the same conditions. It therefore follows that the theory is equally applicable to the columns of direct current and electrodeless discharges.

The electric force in the uniform columns is not large, and the mean energy of the electrons seldom exceeds 3 or 4 volts. A small proportion of the electrons, however, have energies considerably in excess of the mean, and it is these electrons which generate fresh ions by collision and cause the emission of light. Since the electric force is independent of the current, it follows that the number of fresh ions generated per second in unit length of the tube is proportional to the current. In the steady state, therefore, the number of ions of each kind lost per second in unit length of the tube is proportional to the current. Thus the loss of ions must be attributed almost entirely to diffusion to the walls of the tube, since any loss due to the process of recombination would be proportional to the square of the current.

The rate of diffusion of the electrons to the walls of the tube is, however, much greater than the rate of diffusion of the positive ions. Thus a resultant positive charge accumulates in the gas which gives rise to an electric force R along the radius. The radial force R is

* Communicated by the Authors.

† J. S. Townsend, Phil. Mag. xi. p. 1112 (May, 1931).

small compared with the force Z. The rate at which the electrons move towards the walls is consequently decreased and the rate at which the positive ions move towards the walls is increased by the action of the radial force. The steady state is reached when equal numbers of electrons and positive ions reach the walls in the same time.

In order to determine the radial force R in terms of Z it is necessary to know how the number of electrons n per c.c. depends on the distance r from the axis of the tube. Townsend has shown theoretically that the number of electrons n is given by the relation

$$n = AJ_0(cr), \quad . \quad . \quad . \quad . \quad . \quad . \quad (1)$$

where J_0 represents a Bessel function of order zero and A is a constant depending on the current in the tube. The quantity c is given by the equation

$$c^2 = \frac{\alpha w(w+w')Z}{Kw'+K'w}, \quad . \quad . \quad . \quad . \quad . \quad (2)$$

in which α is the number of pairs of fresh ions produced by one electron in moving a distance of 1 cm. in the direction of the electric force and w and w' are the mobilities and K and K′ the coefficients of diffusion of the electrons and positive ions respectively.

The quantity c defined by equation (2) has dimensions minus one in length. It is therefore only a function of the radius of the tube, and is independent of the current and of the nature and pressure of the gas. It is not possible, however, to calculate c from the formula since the coefficient of ionization α cannot be measured by the usual methods when the electric force is as small as that obtaining in the uniform columns. In order to make an approximate calculation of the radial force, Townsend assumed that the number of electrons per c.c. at the surface of the tube ($r=a$) was one-half of the number per c.c. at the axis.

In the present work an attempt has been made to determine the radial distribution of the electrons, and two separate investigations have been carried out.

In the first investigation observations were made on direct current discharges in a tube in which the anode was divided into three concentric electrodes.

The internal diameter of the tube was 4 cm. and the length about 30 cm. The tube was connected to a Hyvac pump, a McLeod gauge, and a drying tube which contained phosphorus pentoxide, and could be filled with dry air at any desired pressure. The discharges were maintained by a high voltage generator and the current was controlled by a two-electrode valve.

The anode of the tube consisted of three concentric electrodes, A, B, and C, as shown in fig. 1. The gaps between adjacent electrodes were slightly less than 1 mm. wide.

Fig. 1.

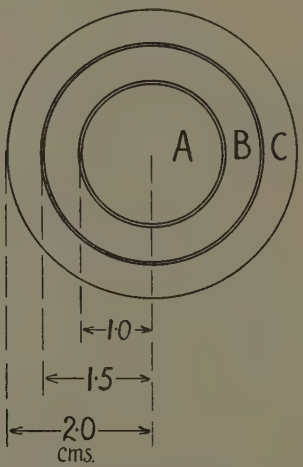

The radii of the electrodes measured to the centres of the gaps are shown in the figure. Thus, the central disk A receives those electrons in the positive column which lie within a distance of 1 cm. from the axis of the tube, the ring B receives those which lie between 1 cm. and 1·5 cm. from the axis, and the ring C receives those which lie between the walls of the tube and 1·5 cm. from the axis. The three electrodes, A, B, and C, were each connected to the source of high potential, and the currents received by them were measured separately with milliammeters.

The currents received by the three electrodes with different values of the total current and of the pressure

are given in Table I. The currents are expressed in arbitrary units, the total current being taken as 100 in each case. In every case the discharge completely covered the anode.

It will be observed that each electrode receives approximately the same fraction of the total current in every

TABLE I.

Pressure	0·52 mm.		1·2 mm.		2·7 mm.	
Current	13 ma.	22 ma.	12 ma.	28 ma.	15 ma.	30 ma.
A	45	49	49	48	46	45
B	35	32	34	33	38	38
C	20	19	17	19	16	17

case. Thus it follows that the radial distribution of the electrons is independent of both current and pressure.

If we assume that the radial distribution of the electrons is represented by equation (1), and assign various values to the quantity c, we may calculate the currents which would be received by the three electrodes. These currents may then be compared with the observed currents as shown in Table II.

TABLE II.

	Observed mean.	$c=0·76$.	$c=1·10$.	$c=1·20$.
A	47	32	43	48
B	35	33	35	35
C	18	35	22	17

Thus, if the number of electrons n_1 per c.c. near the surface of the tube ($r=a$) is one half of the number n_0 per c.c. at the axis, as was assumed by Townsend, we have $c=0·76$. The currents which would be received by the three electrodes in this case are given in the third column of Table II., and do not agree with the mean values of the observed currents given in the second column. If we

suppose that the ratio n_1/n_0 is equal to 0·1, then $c=1\cdot1$, while if $n_1=0$ we have $c=1\cdot2$. The calculated currents in these two cases are given in the fourth and fifth columns of the table respectively.

The best agreement is obtained by taking $c=1\cdot2$, which implies that the number of electrons per c.c. near the surface of the tube is zero. This is unsatisfactory on theoretical grounds, since the radial force R, which is shown by Townsend to be given by the equation

$$\frac{R}{Z}=\frac{\alpha w}{w'}\cdot\frac{1}{c^2n}\cdot\frac{dn}{dr},$$

then becomes infinite at the surface of the tube.

The experiments just described, however, show that the number of electrons n_1 per c.c. near the surface of the tube is, if not actually zero, at most a very small fraction of the number n_0 per c.c. at the axis. In fact, we may conclude from the measurements of the currents received by the three rings that the number of electrons per c.c. near the surface of the tube is certainly not greater than 10 per cent., and probably not greater than 5 per cent., of the number per c.c. at the axis of the tube.

In the second investigation observations were made of the light emitted by the uniform columns of discharges. Measurements were made of the quantity of light emitted by different sections of the columns at different distances from the axis of the tube.

If it could be supposed that the mean energy of the electrons in the uniform column was the same at all distances from the axis, then it would follow that the quantity of light i emitted per c.c. by the discharge at any point was proportional to the number of electrons n per c.c. at that point. In actual fact, however, the electrons lose energy as they move towards the sides of the tube. In the first place their motion outwards is opposed by the radial force R, and the proportion of their energy which the electrons lose on this account increases as the pressure is diminished. The electrons also lose energy in collisions during their motion outwards. The loss of energy arising from this cause increases as the pressure increases. Thus a certain number of electrons will emit a greater quantity of light when they are near the axis than when they are near the walls.

Hence, although the quantity of light emitted by any part of the column cannot be taken as a measure of the number of electrons in that part, the measurements are nevertheless of interest since they give information concerning the energy losses of the electrons.

It was found to be more convenient in these experiments to observe an electrodeless discharge in mercury vapour, since this gives very much more light than the discharges in air. Two pyrex tubes, 4·2 cm. and 2·6 cm. respectively in diameter and about 30 cm. in length, were evacuated and thoroughly degassed. About 1 cubic centimetre of pure mercury was distilled into each tube before sealing off. The tubes were supported in a specially constructed oven, heated electrically, which could be maintained at a uniform temperature throughout. The temperature of the oven was measured by several mercury-in-glass thermometers placed in suitable positions, and could be adjusted to any desired value up to about 170° C. Thus the pressure of the mercury vapour in the discharge-tubes could be adjusted to any desired value up to about 6 mm. by varying the temperature of the oven.

The discharges were excited by external sleeves connected to the ends of a coil in which oscillations were induced by a valve generator tuned to the same wavelength (approximately 50 metres) as the secondary circuit. The strength of the current in the discharge-tube was adjusted by means of the filament rheostat of the generator.

The light from the discharge was measured by means of a photoelectric cell A, as shown in fig. 2. This cell (Osram Type C.M.G. 8) was contained in a light-tight metal box B, to which was fixed a cylindrical tube C, 8 cm. in length, projecting into the oven. The tube C carried a series of three horizontal slits, each 1·5 cm. long and 2 mm. wide, which served to limit the light from the discharge-tube D. Thus the photoelectric cell only received light from the narrow strip of the discharge which is shaded in the figure. The box containing the cell could be moved vertically by a micrometer screw of 1 mm. pitch. The photoelectric cell was moved across the whole width of the tube in 2 mm. steps, so as to measure in turn the light emitted by each strip of the discharge. No light from the parts of the discharge near the sleeves was allowed to reach the cell, and the interior of the oven

was coated with dead black so as to minimize the necessary correction for stray light.

The photoelectric current was measured in the usual way by the steady deflexion of a quadrant electrometer used in conjunction with a xylol resistance of the order of 10^{12} ohms. The deflexions were measured on a scale at a distance of about 6 metres from the electrometer.

The measurements of the light from discharges in the tube of diameter 4·2 cm. with pressures of mercury vapour varying from 0·5 mm. to 5·0 mm. are exhibited graphically in fig. 3. The ordinates of the curves represent

Fig. 2.

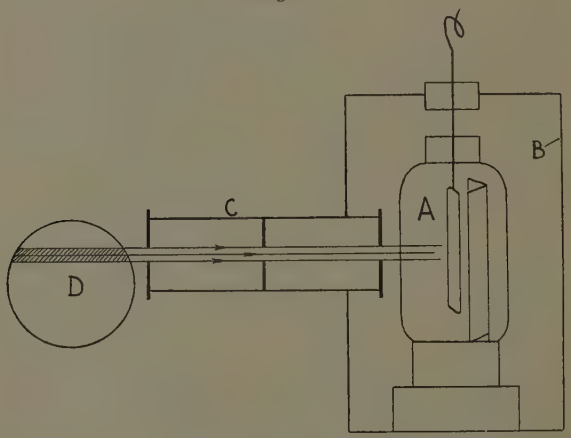

the quantities I of light emitted by strips of the discharge each 2 mm. wide whose mean distances r from the axis of the tube are represented by the abscissæ. The quantities I are measured in arbitrary units, the quantity of light from the central strip for which $r=0$ being taken as 100. Only one-half of each curve is shown in the figure. The half on the other side of the axis of I is, of course, exactly similar. At any given pressure it is found that an increase of the current in the tube by a factor of three or four does not produce any measureable change in the light distribution curve.

It will be noticed that in every case the light emitted by a strip of the discharge at the edge of the tube is only

3 or 4 per cent. of that emitted by the central strip. It will also be observed that the luminosity becomes concentrated in the central part of the tube as the pressure is increased. For example, the light emitted by a strip at a mean distance of 1·2 cm. from the axis is approximately 45 per cent. of the light emitted by the central strip when the pressure is 0·5 mm., but only 17 per cent.

Fig. 3.

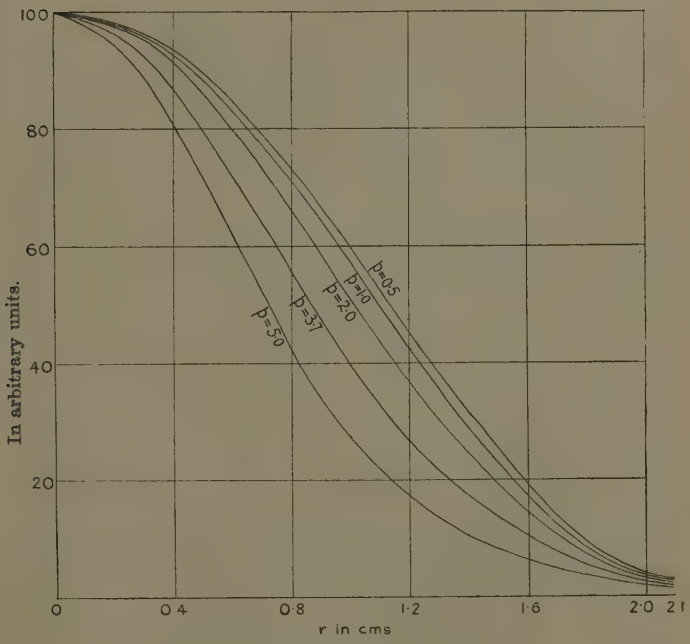

when the pressure is 5·0 mm. Similar results were obtained in the experiments with the narrow tube containing mercury vapour and with several tubes containing other gases.

From the curves given in fig 3 it is possible to calculate the quantity of light i emitted per c.c. by the discharge at different distances from the axis of the tube. The principle of the calculation is illustrated in fig. 4. The cross-section of the discharge is divided as shown into

strips (each 2 mm. wide in the actual calculations) by a series of horizontal lines, and into rings by a series of concentric circles. The areas intercepted on the figure are represented by a, b, c etc., as shown. Let the mean quantity of light emitted per c.c. by the sections of the discharge included between the successive circles be represented by $i_0, i_1, \ldots i_4$, and let the total quantity of light emitted by the successive strips be $I_0, I_1, \ldots I_4$, as

Fig. 4.

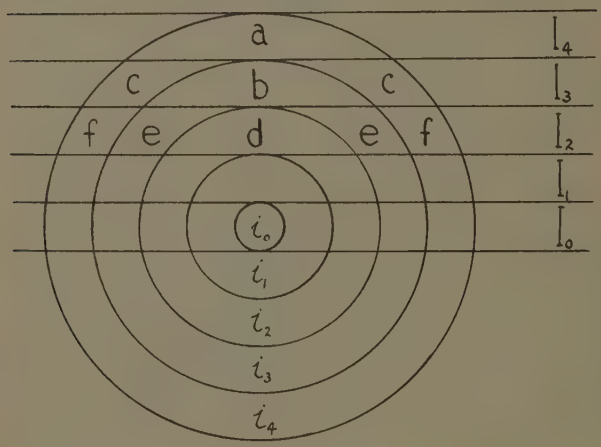

shown. Then we have the following equations from which $i_0, i_1, \ldots i_4$ may be determined :

$$I_4 = ai_4,$$
$$I_3 = bi_3 + 2ci_4,$$
$$I_2 = di_2 + 2ei_3 + 2fi_4, \text{ etc.}$$

The results of these calculations are given by the curves in fig. 5, where the ordinates i represent the quantity of light emitted per c.c. by the discharge at different distances r from the axis. The light is measured in arbitrary units such that the quantity of light emitted per c.c. at the axis is 100.

It may be supposed that the number of electrons n_1 per c.c. near the surface of the tube ($r = 2{\cdot}1$ cm.) is approxi-

mately 5 per cent. of the number n_0 per c.c. at the axis. The equation for n then becomes

$$n = AJ_0(1{\cdot}1r).$$

Thus if the quantity of light i emitted per c.c. by the discharge at any point were proportional to the number

Fig. 5.

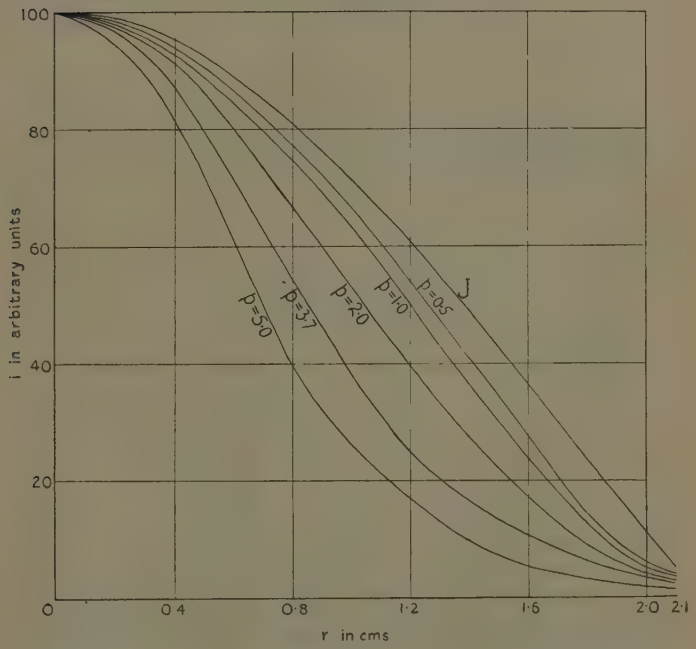

of electrons per c.c. at that point the light distribution would be given by the equation

$$i = 100J_0(1{\cdot}1r),$$

where i is measured in the same units as in the curves of fig. 5. The curve marked J in fig. 5 represents this hypothetical light distribution, and may be compared with the experimental curves obtained at the various pressures.

It will be seen that the curves obtained at the pressures 0·5 mm. and 1·0 mm. approximate fairly closely to the

hypothetical curve. This indicates that at these pressures the electrons only lose a small proportion of their energy in moving towards the walls of the tube. This loss must be attributed largely to the effect of the radial force which opposes their motion. At the higher pressures, however, the experimental curves diverge considerably from the hypothetical curve, and since the effect of the radial force is less at the higher pressures it must be concluded that the electrons lose a large proportion of their energy in collisions.

In conclusion, one of the authors wishes to express his thanks to the Miners' Welfare Committee for a grant which has enabled him to take part in this research.

LXXXV. *On Interactions of Electromagnetic Fields.* *By* Boris Podolsky, *B.S. in E.E., M.A., Ph.D., The Graduate School, University of Cincinnati, Cincinnati, Ohio, U.S.A.**

1. IN a recent paper by Japolsky † a model of elementary particles is proposed based upon Maxwell-Lorentz electromagnetic field equations without charges. Wave packets without singularities are constructed which are then assumed to represent elementary particles, the electromagnetic wave being assumed to be the de Broglie wave. The force of interaction between two such wave packets is then calculated, and is found to be inversely proportional to the square of the distance between the centres of the wave packets. Further, it is found that the sign of the force of interaction depends upon the relative sizes of the wave packets; for equal sizes there is a repulsion—to get an attraction equal to this repulsion it is necessary to have the ratio of the energies of the two packets equal to 1848, the ratio of the masses of a proton and an electron.

Unfortunately the method used by Japolsky for the calculation of the interaction between the wave packets, although at first sight plausible, is really untenable.

* Communicated by the Author.

† N. S. Japolsky, "A Theory of Elementary Particles," Phil. Mag. xx. pp. 417 & 641.

That two such wave packets or " whirls," as Japolsky prefers to call them, cannot possibly interact can be seen from the fact that Maxwell-Lorentz equations, namely *

$$\nabla \times \mathbf{E} + \frac{1}{c}\frac{\partial \mathbf{H}}{\partial t} = 0, \quad . \quad . \quad . \quad . \quad . \quad . \quad . \quad (1)$$

$$\nabla \times \mathbf{H} - \frac{1}{c}\frac{\partial \mathbf{E}}{\partial t} = 4\pi\rho\mathbf{v}/c, \quad . \quad . \quad . \quad . \quad . \quad (2)$$

$$\nabla . \mathbf{E} = 4\pi\rho, \quad . \quad . \quad . \quad . \quad . \quad . \quad (3)$$

$$\nabla . \mathbf{H} = 0, \quad . \quad . \quad . \quad . \quad . \quad . \quad . \quad (4)$$

are linear. This means that two solutions of these equations if superimposed again form a solution ; thus each wave packet is propagated independently of all other fields present. It is interesting, however, to see just where the method used by Japolsky for calculating the interaction between the " whirls " breaks down.

2. Japolsky's method is applicable in electrostatics. To show this let us consider, for example, the interaction between a field produced by a charge, say $\mathbf{E}_p$, and a given field $\mathbf{E}_0$. The energy of the field may be considered as consisting of three terms :

$$\mathrm{E} = \frac{1}{8\pi}\int (\mathbf{E}_0 + \mathbf{E}_p)^2 \, d\mathrm{V}$$

$$= \frac{1}{8\pi}\int \mathbf{E}_0^{\,2} \, d\mathrm{V} + \frac{1}{8\pi}\int \mathbf{E}_p^{\,2} \, d\mathrm{V} + \frac{1}{4\pi}\int \mathbf{E}_0 . \mathbf{E}_p \, d\mathrm{V}. \quad . \quad (5)$$

The last term may be called the energy of interaction between the field $\mathbf{E}_0$ and the field $\mathbf{E}_p$. Designating it by W we have

$$\mathrm{W} = \frac{1}{4\pi}\int \mathbf{E}_0 . \mathbf{E}_p \, d\mathrm{V}. \quad . \quad . \quad . \quad . \quad . \quad (6)$$

Japolsky's method of calculating the force acting upon the field $\mathbf{E}_p$ consists in differentiation of W. Thus

$$\mathbf{F} = \left(-\frac{\partial \mathrm{W}}{\partial x_p}, -\frac{\partial \mathrm{W}}{\partial y_p}, -\frac{\partial \mathrm{W}}{\partial z_p}\right) = -\frac{\partial \mathrm{W}}{\partial \mathrm{r}_p}, \quad . \quad (7)$$

* The dot (·) and the cross (×) represent respectively the scalar and the vector products of vectors.

where $\mathbf{r}_p$ is the vector of position of the packet, or the charge to which the field is supposed to be rigidly attached, $\mathbf{r}_p = (x_p, y_p, z_p)$.

To evaluate the right-hand member of eq. (7) we suppose that the packet is displaced through a short distance $\delta\mathbf{r}_p$. If now the coordinate system in which the integral of eq. (6) is evaluated is also supposed shifted in the same way, the only thing that will change in the integral of eq. (6) will be that $\mathbf{E}_0(\mathbf{r})$ will be replaced by $\mathbf{E}_0(\mathbf{r}+\delta\mathbf{r}_p)$. Thus, for example, we will have

$$\mathbf{F}_x = -\frac{\partial \mathrm{W}}{\partial x_p} = -\frac{1}{4\pi}\int \mathbf{E}_p \cdot \frac{\partial \mathbf{E}_0}{\partial x}\, d\mathrm{V} = -\frac{1}{4\pi}\int \frac{\partial}{\partial x}(\mathbf{E}_0 . \mathbf{E}_p)\, d\mathrm{V},$$

in which $\mathbf{E}_p$ is to be regarded as a constant with respect to the differentiation. Thus,

$$\begin{aligned}\mathbf{F} &= -\frac{1}{4\pi}\int \nabla_0 (\mathbf{E}_0 . \mathbf{E}_p)\, d\mathrm{V} \\ &= -\frac{1}{4\pi}\int [\mathbf{E}_p . \nabla \mathbf{E}_0 + \mathbf{E}_p \times (\nabla \times \mathbf{E}_0)]\, d\mathrm{V} \\ &= -\frac{1}{4\pi}\int \mathbf{E}_p . \nabla \mathbf{E}_0 d\,\mathrm{V}, \quad . \quad . \quad . \quad . \quad . \quad (8)\end{aligned}$$

since in electrostatics $\nabla \times \mathbf{E} = \mathbf{0}$. With the help of vector analysis this becomes

$$\mathbf{F} = -\frac{1}{4\pi}\int \mathbf{E}_0 \mathbf{E}_p . d\mathbf{S} + \frac{1}{4\pi}\int \mathbf{E}_0 \nabla . \mathbf{E}_p\, d\mathrm{V}, \quad . \quad . \quad (9)$$

where $d\mathbf{S}$ represents the element of the boundary surface of the space considered, taken in the direction of the outward normal to the surface.

In the absence of charges $\nabla . \mathbf{E}_p = 0$, and thus $\mathbf{F} = \mathbf{0}$, since the boundary surface can be taken so far that $\mathbf{E}_0$ and $\mathbf{E}_p$ vanish on S. In the presence of a charge there are two equivalent methods of procedure. We can regard the charge as a singularity of the field, or consider the charge to be continuous although concentrated within a very small region. In the first method $\nabla . \mathbf{E}_p = 0$ and $\mathbf{F}$ reduces to a surface integral taken over a small surface around the singularity; in the second, more convenient, method the surface integral disappears, and we have

$$\mathbf{F} = \frac{1}{4\pi}\int \mathbf{E}_0 \nabla . \mathbf{E}_p\, d\mathrm{V} = \int \rho \mathbf{E}_0\, d\mathrm{V} = \mathrm{Q}\mathbf{E}_0, \quad . \quad . \quad (10)$$

where we have made use of eq. (3) and the fact that the charge Q is concentrated within a very small volume. In what follows we shall use the second method exclusively.

3. When we come to electrodynamics, however, eq. (7) is no longer valid. This can be seen, for example, from the fact that the Lorentz expression for the force on a charged particle, viz.

$$= Q\left(\mathbf{E}+\frac{\mathbf{v}}{c}\times\mathbf{H}\right), \quad . \quad . \quad . \quad . \quad (11)$$

is not of this form.

The correct expression for the force acting upon a wave packet is the time rate of change of its momentum. As is well known the momentum of the field is given by

$$\mathbf{P} = \frac{1}{4\pi c}\int \mathbf{E}\times\mathbf{H}\, d\mathrm{V}. \quad . \quad . \quad . \quad . \quad (12)$$

If we again consider the interaction between the field ($\mathbf{E}_p$, $\mathbf{H}_p$) of a wave packet and the field ($\mathbf{E}_0$, $\mathbf{H}_0$) comprising all the other fields, then

$$\mathbf{P} = \frac{1}{4\pi c}\int \mathbf{E}_0\times\mathbf{H}_0\, d\mathrm{V} + \frac{1}{4\pi c}\int \mathbf{E}_p\times\mathbf{H}_p\, d\mathrm{V} + \frac{1}{4\pi c}\int (\mathbf{E}_0\times\mathbf{H}_p+\mathbf{E}_p\times\mathbf{H}_0)\, d\mathrm{V}.$$

The first two terms do not concern us at present. The last term may be called the momentum of interaction; let us designate it by $\mathbf{G}$. Thus

$$\mathbf{G} = \frac{1}{4\pi c}\int (\mathbf{E}_0\times\mathbf{H}_p+\mathbf{E}_p\times\mathbf{H}_0)\, d\mathrm{V}, \quad . \quad . \quad . \quad . \quad (13)$$

and

$$\mathbf{F} = \frac{d\mathbf{G}}{dt} = \frac{1}{4\pi c}\int \partial t(\mathbf{E}_0\times\mathbf{H}_p+\mathbf{E}_p\times\mathbf{H}_0)\, d\mathrm{V}. \quad . \quad (14)$$

In transforming this expression let us suppose that $\mathbf{E}_0$ and $\mathbf{H}_0$ are solutions of the Maxwell-Lorentz equations, eqs. (1)–(4), with $\rho=0$ at least at points at which $\mathbf{E}_p$ and $\mathbf{H}_p$ are not zeros. On the other hand, for $\mathbf{E}_p$ and $\mathbf{H}_p$ we shall at present make no special assumption except that they must of course satisfy the Maxwell-Lorentz equations.

Using then these equations in order to replace the time derivatives in eq. (14) by their equivalents, we obtain

$$\mathbf{F} = \frac{1}{4\pi}\int \Big[(\nabla \times \mathbf{H}_0)\times \mathbf{H}_p - \mathbf{E}_0 \times (\nabla \times \mathbf{E}_p) + \Big(\nabla \times \mathbf{H}_p - \frac{4\pi\rho\mathbf{v}}{c} \Big) \times \mathbf{H}_0 - \mathbf{E}_p \times (\nabla \times \mathbf{E}_0) \Big]\, d\mathrm{V}.$$

But

$$(\nabla \times \mathbf{H}_0)\times \mathbf{H}_p + (\nabla \times \mathbf{H}_p)\times \mathbf{H}_0 = \mathbf{H}_0 . \nabla \mathbf{H}_p + \mathbf{H}_p . \nabla \mathbf{H}_0 - \nabla (\mathbf{H}_0 . \mathbf{H}_p),$$

$$-\mathbf{E}_0 \times (\nabla \times \mathbf{E}_p) - \mathbf{E}_p \times (\nabla \times \mathbf{E}_0) = \mathbf{E}_0 . \nabla \mathbf{E}_p + \mathbf{E}_p . \nabla \mathbf{E}_0 - \nabla (\mathbf{E}_0 . \mathbf{E}_p),$$

$$\int \nabla (\mathbf{H}_0 . \mathbf{H}_p)\, d\mathrm{V} = \int \mathbf{H}_0 . \mathbf{H}_p\, d\mathbf{S} = 0,$$

and

$$\int \nabla (\mathbf{E}_0 . \mathbf{E}_p)\, d\mathrm{V} = \int \mathbf{E}_0 . \mathbf{E}_p\, d\mathbf{S} = 0.$$

Therefore

$$\mathbf{F} = \frac{1}{4\pi}\int (\mathbf{H}_0 . \nabla \mathbf{H}_p + \mathbf{H}_p . \nabla \mathbf{H}_0 + \mathbf{E}_0 . \nabla \mathbf{E}_p + \mathbf{E}_p . \nabla \mathbf{E}_0)\, d\mathrm{V} - \frac{1}{c}\int \rho\mathbf{v} \times \mathbf{H}_0\, d\mathrm{V}.$$

Further, since for any $\mathbf{A}$ and $\mathbf{B}$

$$\int \mathbf{A} . \nabla \mathbf{B}\, d\mathrm{V} = \int \mathbf{B}\mathbf{A} . d\mathbf{S} - \int \mathbf{B} \nabla . \mathbf{A}\, d\mathrm{V},$$

and $\nabla . \mathbf{H}_0 = \nabla . \mathbf{E}_0 = \nabla . \mathbf{H}_p = 0$, while $\nabla . \mathbf{E}_p = 4\pi\rho$, we obtain finally

$$\mathbf{F} = -\int \rho \mathbf{E}_0\, d\mathrm{V} - \frac{1}{c}\int \rho\mathbf{v} \times \mathbf{H}_0\, d\mathrm{V}. \quad . \quad . \quad (15)$$

In the absence of charges this expression vanishes, as was to be expected, showing that Japolsky's calculation of the force acting upon a "whirl" is invalid. For a concentrated charge this becomes

$$\mathbf{F} = -\mathrm{Q}\Big(\mathbf{E}_0 + \frac{\mathbf{v}}{c} \times \mathbf{H}_0 \Big), \quad . \quad . \quad . \quad . \quad . \quad (16)$$

which shows that only charged particles can produce forces acting on the field, and that then the action is equal and opposite to the reaction.

Cincinnati, Ohio.
March 27, 1936.

LXXXVI. *On Dr. Podolsky's Criticism.* *By* Dr. N. S. Japolsky, *formerly Lecturer, Technological Institute, Leningrad* *.

AN aspect of a new physical theory can be regarded as "untenable" on theoretical grounds if, and only if, it is proved to be in unavoidable contradiction with the fundamental principles on which this theory is, explicitly or implicitly, based.

Although the assumption that $\frac{1}{4\pi c}\mathrm{E}\times\mathrm{H}$ can be identified with the mechanical momentum density of e.m. waves is now very widely accepted, it should be borne in mind that this assumption results from an arbitrary extension to the e.m. waves of the relationship $\mathsf{E}=mc^2$ (where E is the energy, m the mass, and c the speed of light) postulated by the Theory of Relativity for the material particles, but *does not follow from the Maxwell Theory*, on which the criticized method of calculation of forces, as well as the theory of elementary particles of which this method is an organic part, are based.

In the criticized theory the concept of the inertial mass m originates from the consideration, on the basis of Maxwell Theory, of the motion of the *centre* of the Whirl, and, therefore, it relates *only to the Whirl as a whole*, and *not* to an element of its volume †, and, correspondingly, the relationship $\mathsf{E}=mc^2$ has been derived for a Whirl as a whole, and *not* for an element of its volume.

This makes Dr. Boris Podolsky's criticism, which is based on the identification of $\frac{1}{4\pi c}\mathrm{E}\times\mathrm{H}$ with the mechanical momentum density, invalid because of the unfounded criterion.

Moreover, the only thing which Dr. Podolsky has proved is the constancy of the *total* $\frac{1}{4\pi c}\int\mathrm{E}\times\mathrm{H}\,d\mathrm{V}$ (the total "momentum") for the whole system of two

* Communicated by the Author.

† Phil. Mag. ser. 7, xx. p. 456 and further.

wave packets, but *not* for each of these two wave packets separately.

In fact, he did not even attempt to show how in the total "momentum" density $\frac{1}{4\pi c}\,\mathrm{E}\times\mathrm{H}$ the components corresponding to each wave packet could be segregated.

It is well known that in a self-sufficient system the total mechanical momentum is constant; this, however, does not mean that the momentum of any member of the system is also constant and that hence the forces are absent.

Therefore Dr. Podolsky's criticism would be still invalid even if his criterion were correct.

Now let us consider the general statement which Dr. Podolsky made in the introductory part of his paper—that my method of determining forces must be "really untenable" in view of the additivity of solutions of the Maxwell equations.

It is quite correct that the Maxwell equations *by themselves* do not imply any interaction between the Whirls. This I never contested.

However, the Maxwell equations do not express the Maxwell Electrodynamics exhaustively.

The fundamental feature of Maxwell theory is that the "displacement currents" in any insulator, including the vacuum, have the same electrodynamic properties as the "conduction currents." The extension of this similarity to the forces of interaction between the currents is logically implied in Maxwell *theory* but *not* in the Maxwell *equations*. It only *limits the solutions* of these equations in the case of Whirls or other types of wave packets, if any, tending to conserve their configuration and containing finite energy.

Thus Dr. Podolsky's assertion that my method of determining the forces cannot be valid because of the additivity of solutions of the Maxwell equations is based on a misunderstanding.

Davy-Faraday Laboratory,
Royal Institution.
June 1936.

LXXXVII. *On the Wave-making Resistance of a Ship moving along in a Canal.* *By* L. N. SRETTENSKY, *D.Sc.*†

1. *Introductory Remarks.*

THE problem of the present work consists in establishing the formula for the calculation of the wave-making resistance of a ship moving along with steady motion in an infinitely deep canal of a given width.

As regards the ship we shall suppose that her outline will satisfy the restrictive assumptions of Michell's theory. We admit that the deviations of the points of the ship's surface from her vertical median plane are sufficiently small, and, moreover, that the tangent plane to the ship is but slightly inclined towards the vertical median plane.

The velocity potential of the relative fluid motion depending on the shifting of the ship with the velocity c in an unlimited fluid may be put down in the following way :

$$\Phi(x, y, z) = cx + \iint_{(S)} \left[\frac{1}{\sqrt{(x-\xi)^2+y^2+(z-\zeta)^2}} - \frac{1}{\sqrt{(x-\xi)^2+y^2+(z+\zeta)^2}} + \frac{g}{\pi c^2} \int_0^\infty dk \int_{-\pi}^{+\pi} \frac{e^{k(z+\zeta)+ik[(x-\xi)\cos\theta+y\sin\theta]}}{\frac{g}{c^2} - \mu i \cos\theta - k\cos^2\theta} d\theta \right] F(\xi, \zeta) . d\xi d\zeta. \quad . \quad . \quad . \quad (1)$$

In this formula the function $F(x, z)$ is determined by means of the equation of the ship's surface

$$y = +f(x, z) \text{ for } y > 0,$$
$$y = -f(x, z) \text{ for } y < 0,$$

by the following formula :

$$F(x, z) = -\frac{c}{2\pi} \cdot \frac{\partial f}{\partial x} . \quad . \quad . \quad . \quad . \quad . \quad . \quad (2)$$

The axes of coordinates are orientated in such a way that the axis OZ is set vertically upwards, the axis OX is directed against the velocity of the flow at infinity. The number μ in formula (1) is the coefficient of Rayleigh's

† Communicated by the Author.

dissipative forces †. (S) denotes the vertical median plane of the ship.

Formula (1) has been obtained from a Russian paper ‡. It affords no great difficulty to be convinced, *à posteriori*, that it gives, as a matter of fact, the velocity potential of the relative motion of the fluid, brought about by the shifting of our ship.

2. *The Calculation of the Limit* : $\lim_{\mu=0} \phi(x, y, z)$.

In order to obtain Michell's formula it will be sufficient to find the limit $\lim_{\mu=0} \phi\,(x, y, z)$ for $y=0$, but for the problem we are concerned with it is necessary to find this limit with any value of y. Let us examine the integral:

$$J = \frac{g}{\pi c^2} \int_0^{\infty} dk \int_{-\pi}^{+\pi} \frac{e^{k(z+\zeta)+ik[(x-\xi)\cos\theta + y\sin\theta]}}{\frac{g}{c^2} - \mu i \cos\theta - k\cos^2\theta}\, d\theta.$$

Let us introduce new variables of integration, α and γ. Assuming

$$\alpha = k\cos\theta, \quad \gamma = k; \qquad dk\,d\theta = + \frac{d\alpha\,d\gamma}{\sqrt{\gamma^2-\alpha^2}},$$

we obtain

$$J = \frac{2g}{\pi c^2} \int_0^{\infty} \gamma e^{\gamma(z+\zeta)}\, d\gamma \int_{-\gamma}^{+\gamma} \frac{e^{i(x-\xi)\alpha + iy\sqrt{\gamma^2-\alpha^2}}}{\frac{g}{c^2}\gamma - \mu i\alpha - \alpha^2} \cdot \frac{d\alpha}{\sqrt{\gamma^2-\alpha^2}}.$$

Let us carry out in this formula the passage to the limit when $\mu=0$. We have

$$J = \frac{2g}{\pi c^2} \int_0^{g/c^2} \gamma e^{\gamma(z+\zeta)}\, d\gamma \int_{-\gamma}^{+\gamma} \frac{e^{i(x-\xi)\alpha + iy\sqrt{\gamma^2-\alpha^2}}}{\frac{g}{c^2}\gamma - \mu i\alpha - \alpha^2} \cdot \sqrt{\gamma^2-\alpha^2}$$

$$+ \frac{2g}{\pi c^2} \int_{g/c^2}^{\infty} \gamma e^{\gamma(z+\zeta)}\, d\gamma \int_{-\gamma}^{+\gamma} \frac{e^{i(x-\xi)\alpha + iy\sqrt{\gamma^2-\alpha^2}}}{\frac{g}{c^2}\gamma - \mu i\alpha - \alpha^2} \cdot \frac{d\alpha}{\sqrt{\gamma^2-\alpha^2}}. \quad . \quad . \quad . \quad (3)$$

† H. Lamb, ' Hydrodynamics,' 5th ed. art. 242.

‡ L. N. Srettensky, " On Michell Theory " (' Applied Mathematics and Mechanics,' Leningrad, 1936).

With the alteration of γ between 0 and $\frac{g}{c^2}$ the roots α_1 and α_2 of the function $\frac{g}{c^2}\gamma - \mu i\alpha - \alpha^2$ tend to take the position on the axis α outside the segment $(-\gamma, +\gamma)$; in fact:

$$\lim_{\mu=0} \alpha_1 = -\sqrt{\frac{g}{c^2}\gamma}; \qquad \lim_{\mu=0} \alpha_2 = +\sqrt{\frac{g}{c^2}\gamma}. \quad . \quad (4)$$

Thus in the first line of formula (3) we can replace μ by zero. Hence

$$\lim_{\mu=0} \mathrm{J} = \frac{2g}{\pi c^2} \int_0^{g/c^2} \gamma e^{\gamma(z+\zeta)}\, d\gamma \int_{-\gamma}^{+\gamma} \frac{e^{i(x-\xi)\alpha + iy\sqrt{\gamma^2-\alpha^2}}}{\frac{g}{c^2}\gamma - \alpha^2} \cdot \frac{d\alpha}{\sqrt{\gamma^2-\alpha^2}}$$

$$+ \frac{2g}{\pi c^2} \int_{g/c^2}^{\infty} \gamma e^{\gamma(z+\zeta)}\, d\gamma \cdot \lim_{\mu=0} \int_{-\gamma}^{+\gamma} \frac{e^{i(x-\xi)\alpha + iy\sqrt{\gamma^2-\alpha^2}}}{\frac{g}{c^2}\gamma - \mu i\alpha - \alpha^2} \cdot \frac{d\alpha}{\sqrt{\gamma^2-\alpha^2}}.$$

. . . (5)

Let us attend to the calculation of the limit included in this formula.

The points α_1 and α_2 lie in the lower semi-plane not far from the real axis.

Let us denote by (Γ_1) any curve connecting the points $-\gamma$, $+\gamma$ and lying in the upper semi-plane; let (Γ_2) be any curve lying in the lower semi-plane and connecting the points $-\gamma$, $+\gamma$. In virtue thereof we shall have for the limit under investigation the two following expressions:

$$\lim_{\mu=0} \int_{-\gamma}^{+\gamma} = \int_{(\Gamma_1)} \frac{e^{i(x-\xi)\alpha + iy\sqrt{\gamma^2-\alpha^2}}}{\frac{g}{c^2}\gamma - \alpha^2} \cdot \frac{d\alpha}{\sqrt{\gamma^2-\alpha^2}};$$

$$\lim_{\mu=0} \int_{-\gamma}^{+\gamma} = \int_{(\Gamma_2)} \frac{e^{i(x-\xi)\alpha + iy\sqrt{\gamma^2-\alpha^2}}}{\frac{g}{c^2}\gamma - \alpha^2} \cdot \frac{d\alpha}{\sqrt{\gamma^2-\alpha^2}}$$

$$+ 2\pi \sqrt{\frac{c^2}{g\gamma}} \cdot \frac{\sin\left[(x-\xi)\sqrt{\frac{g\gamma}{c^2}}\right] e^{iy\sqrt{\gamma^2 - \frac{g\gamma}{c^2}}}}{\sqrt{\gamma^2 - \frac{g\gamma}{c^2}}}.$$

Hence

$$\lim_{\mu=0}\int_{-\gamma}^{+\gamma} = \int_{(K_1)} \frac{\cos(x-\xi)\alpha \cdot e^{iy\sqrt{\gamma^2-\alpha^2}}}{\frac{g}{c^2}\gamma-\alpha^2}\cdot\frac{d\alpha}{\sqrt{\gamma^2-\alpha^2}}$$

$$+\pi\sqrt{\frac{c^2}{g\gamma}}\cdot\frac{\sin\left[(x-\xi)\sqrt{\frac{g\gamma}{c^2}}\right]e^{iy\sqrt{\gamma^2-\frac{g\gamma}{c^2}}}}{\sqrt{\gamma^2-\frac{g\gamma}{c^2}}}$$

The first item of the right-hand side is an even function of the difference $x-\xi$. As an even function of $x-\xi$ we have also the first item of the right-hand side of formula (5). Having regard to all this we can give to the expression of the velocity potential (1) the following form :

$$\Phi(x, y, z) = cx + \iint_{(S)} \mathrm{P}(x-\xi\,;\ z+\zeta)\mathrm{F}(\xi, \zeta)\, d\xi\, d\zeta$$

$$+2\sqrt{\frac{g}{c^2}}\iint_{(S)} \mathrm{F}(\xi, \zeta)\, d\xi\, d\zeta \int_{g/c^2}^{\infty} e^{\gamma(z+\zeta)+iy\sqrt{\gamma^2-\frac{g\gamma}{c^2}}}$$

$$\times\sin\left[(x-\xi)\sqrt{\frac{g\gamma}{c^2}}\right]\cdot\frac{\sqrt{\gamma}\, d\gamma}{\sqrt{\gamma^2-\frac{g\gamma}{c^2}}}\,.$$

The function P is some even function of its first argument ; the exact expression of this function is for us a matter of small account.

3. *Determination of the Velocity Potential in the Case of the Motion of a Ship in a Canal of Constant Width.*

Let us assume that a ship of Michell's type is moving along at a constant velocity c in a canal of infinite depth and of a given width b. The motion occurs in the middle plane ZOX of the canal. Let us construct the values of the velocity potential at the points of the plane ZOX. Applying the method of images we find

$$\phi(x, o, z) = cx + 2\iint_{(S)} \mathrm{F}(\xi, \zeta)\, d\xi\, d\zeta \int_{g/c^2}^{\infty} e^{\gamma(z+\zeta)}$$

$$\times\sin\left[(x-\xi)\sqrt{\frac{g\gamma}{c^2}}\right]\cdot\frac{d\gamma}{\sqrt{\frac{c^2\gamma}{g}-1}}$$

$$+4\iint_{(S)} F(\xi, \zeta)\, d\xi\, d\zeta \sum_{n=1}^{\infty} e^{\gamma(z+\zeta)} \cos\left(nb\sqrt{\gamma^2 - \frac{g\gamma}{c^2}}\right) \times \sin\left[(x-\xi)\sqrt{\frac{g\gamma}{c^2}}\right] \cdot \frac{d\gamma}{\sqrt{\frac{c^2\gamma}{g} - 1}}$$

$$+\iint_{(S)} P_1(x-\xi, z+\zeta) F(\xi, \zeta)\, d\xi\, d\zeta, \quad . \quad . \quad . \quad . \quad . \quad (6)$$

where $P_1(x-\xi, z+\zeta)$ is the even function of the difference $x-\xi$. It may readily be shown that in applying the method of images the condition at the surface of our ship will be satisfied.

In point of fact from formula (1) it is easily seen that the condition at the surface of the ship in unlimited flow is satisfied, owing to the presence in that formula of the potential of a sheet of simple sources :

$$\iint_{(S)} \frac{F(\xi, \zeta)\, d\xi\, d\zeta}{\sqrt{(x-\xi)^2 + y^2 + (z-\zeta)^2}}.$$

The satisfactoriness of this condition is not affected by the presence of other terms in the right-hand side of formula (1). These terms represent an even function of y. From this remark it may be inferred that the conditions at the surface are also observed by function (6).

4. *Calculation of the Wave-making Resistance.*

The formula for the calculation of the wave-making resistance of a ship of Michell's type may be stated as

$$R = -4\pi\rho \iint_{(S)} F(x, z) \frac{\partial D}{\partial x}\, dx\, dz,$$

where D denotes the difference $\phi(x, y, z) - cx$. Let us substitute in this formula for D its value obtained from formula (6). It is perfectly clear that the even terms with respect to $x-\xi$ of the general expression D give a zero result.

Hence

$$R = R^* + 16\pi\rho \iint_{(S)} F(x, z)\, dx\, dz \iint_{(S)} F(\xi, \zeta)\, d\xi\, d\zeta \times \sum_{n=1}^{\infty} \int_{g/c^2}^{\infty} e^{\gamma(z+\zeta)} \cos\left(nb\sqrt{\gamma^2 - \frac{g\gamma}{c^2}}\right)$$

$$\times \cos\left[(x-\xi)\sqrt{\frac{g\gamma}{c^2}}\right] \frac{\sqrt{\frac{g\gamma}{c^2}}\,d\gamma}{\sqrt{\frac{c^2\gamma}{g}-1}}. \quad . \quad (7)$$

Here R* is the wave-making resistance of the ship moving along in unlimited mass of water :

$$R^* = \frac{16\pi\rho g^2}{c^4}\iint_{(S)} d\xi\,d\zeta \iint_{(S)} F(x,z)F(\xi,\zeta)\,dx\,dz$$
$$\times \int_1^\infty e^{\frac{g\lambda^2}{c^2}(z+\zeta)} \cos\left[\frac{g(x-\xi)\lambda}{c^2}\right] \frac{\lambda^2 d\lambda}{\sqrt{\lambda^2-1}}. \quad . \quad (8)$$

Let us introduce in the preceding formula a new variable λ according to the equation $\gamma = \frac{g\lambda}{c^2}$; we get

$$R = R^* + \frac{32\pi\rho g^2}{c^4}\iint_{(S)} F(x,z)\,dx\,dz \iint_{(S)} F(\xi,\zeta)\,d\xi\,d\zeta$$
$$\times \sum_{n=1}^{\infty} \int_1^\infty e^{\frac{g}{c^2}(z+\zeta)\lambda^2} \cos\left(\frac{bg}{c^2} n\lambda\sqrt{\lambda^2-1}\right)$$
$$. \cos\left[\frac{g\lambda}{c^2}(x-\xi)\right] . \frac{\lambda^2 d\lambda}{\sqrt{\lambda^2-1}}. \quad . \quad . \quad . \quad (9)$$

For the summation of the series of the right-hand side let us examine the series

$$\sigma = \tfrac{1}{2}\int_1^\infty e^{-\omega\lambda^2} \cos a\lambda . \frac{\lambda^2 d\lambda}{\sqrt{\lambda^2-1}}$$
$$+ \sum_{n=1}^{\infty} \int_1^\infty e^{-\omega\lambda^2} \cos(np\lambda\sqrt{\lambda^2-1}) \cos a\lambda . \frac{\lambda^2 d\lambda}{\sqrt{\lambda^2-1}},$$

having regard to the notation

$$0 < \omega < -\frac{g}{c^2}(z+\zeta); \quad a = \frac{g}{c^2}(x-\xi); \quad p = \frac{gb}{c^2}.$$

For the summation of the series σ let us consider its first m terms. We have

$$\tfrac{1}{2} + \cos\alpha + \cos 2\alpha + \ldots + \cos m\alpha = \frac{\sin\frac{2m+1}{2}\alpha}{2\sin\frac{\alpha}{2}}.$$

We obtain

$$2\sigma_m = \int_1^\infty e^{-\omega\lambda^2} \cos a\lambda \cdot \frac{\sin\left\{\frac{2m+1}{2} p\lambda\sqrt{\lambda^2-1}\right\}}{\sin\left\{\frac{p\lambda}{2}\sqrt{\lambda^2-1}\right\}} \cdot \frac{\lambda^2 d\lambda}{\sqrt{\lambda^2-1}}.$$

For the investigation of this integral let us introduce a new variable τ, regarding λ as equal to $ch\tau$. We find

$$2\sigma_m = \int_0^\infty e^{-\omega ch^2\tau} \cos(ach\tau) \cdot \frac{\sin\left\{\frac{2m+1}{4} psh2\tau\right\}}{\sin\left\{\frac{p}{4} sh2\tau\right\}} \cdot ch^2\tau \cdot d\tau.$$

In order to determine $\lim_{m=\infty} \sigma_m$ let us examine the roots of the equation

$$\frac{p}{4} sh2\tau = \pi k, \quad (k=0, 1, 2, 3, \ldots).$$

Let us denote them like this :

$$\tau_0=0, \ \tau_1, \ \tau_2, \ \tau_3, \ \ldots$$

Now we can put down $2\sigma_m$ in the following manner :

$$2\sigma_m = \sum_{k=0}^{\infty} \int_{\tau k}^{\tau k+1} e^{-\omega ch^2\tau} \cos(ach\tau) \cdot \frac{\sin\left(\frac{2m+1}{4} psh2\tau\right)}{\sin\left(\frac{p}{4} sh2\tau\right)} ch^2\tau \, d\tau.$$

Let us consider the general term of this series ; denoting by τ' a certain number between τ_k and τ_{k+1}, we find

$$\lim_{m=\infty} \int_{\tau k}^{\tau k+1} = \lim_{m=\infty} \int_{\tau_k}^{\tau'} + \lim_{m=\infty} \int_{\tau'}^{\tau_{k+1}};$$

but †

$$\lim_{m=\infty} \int_{\tau_k}^{\tau'} = \frac{\pi}{p} e^{-\omega ch^2\tau_k} \cos(ach\tau_k) \cdot \frac{ch^2\tau_k}{ch2\tau_k},$$

$$\lim_{m=\infty} \int_{\tau'}^{\tau_{k+1}} = \frac{\pi}{p} e^{-\omega ch^2\tau_{k+1}} \cos(ach\tau_{k+1}) \frac{ch^2\tau_{k+1}}{ch2\tau_{k+1}}.$$

† E. Goursat, 'Cours d'Analyse Mathématique,' IVme ed. t. i. p. 487.

Consequently

$$\lim_{m=\infty}\int_{\tau_k}^{\tau_{k+1}} e^{-\omega ch^2\tau}\cos(ach\tau)\cdot\frac{\sin\left(\frac{2m+1}{4}p\,sh\,2\tau\right)}{\sin\left(\frac{p}{4}sh\,2\tau\right)}\cdot ch^2\tau\cdot d\tau$$

$$=\frac{\pi}{p}\left\{e^{-\omega ch^2\tau_{k+1}}\cos(ach\tau_{k+1})\frac{ch^2\tau_{k+1}}{ch2\tau_{k+1}}\right.$$

$$\left.+e^{-\omega ch^2\tau_k}\cos(ach\tau_k)\frac{ch^2\tau_k}{ch2\tau_k}\right\};$$

therefore

$$\frac{2p}{\pi}\sigma=e^{-\omega}\cos a+2\sum_{k=1}^{\infty}e^{-\omega ch^2\tau_k}\cos(ach\tau_k)\cdot\frac{ch^2\tau_k}{ch2\tau_k}. \qquad (10)$$

Let us return now to the infinite series of formula (8); making use of the result (10), we may write this series in the following way :—

$$\sum_{n=1}^{\infty}\int_1^{\infty}e^{-\omega\lambda^2}\cos(np\lambda\sqrt{\lambda^2-1})\cos a\lambda\cdot\frac{\lambda^2\,d\lambda}{\sqrt{\lambda^2-1}}$$

$$=\frac{\pi}{2p}\left\{e^{-\omega}\cos a+2\sum_{k=1}^{\infty}e^{-\omega ch^2\tau_k}\cos(ach\tau_k)\frac{ch^2\tau_k}{ch2\tau_k}\right\}$$

$$-\tfrac{1}{2}\int_1^{\infty}e^{-\omega\lambda^2}\cos a\lambda\,\frac{\lambda^2\,d\lambda}{\sqrt{\lambda^2-1}}$$

Substituting this value in formula (9), and availing ourselves of formula (8), we find

$$\mathrm{R}=\frac{16\pi^2\rho g}{bc^2}\iint_{(S)}\mathrm{F}(x,z)\,dx\,dz\iint_{(S)}\mathrm{F}(\xi,\zeta)\,d\xi\,d\zeta$$

$$\times\left\{e^{\frac{g\lambda^2}{c^2}(z+\zeta)}\cos\frac{g}{c^2}(x-\xi)\right.$$

$$\left.+2\sum_{k=1}^{\infty}e^{\frac{g}{c^2}(z+\zeta)ch2\tau}\cos\left[\frac{g}{c^2}(x-\xi)ch\tau_k\right]\frac{ch^2\tau_k}{ch2\tau_k}\right\}.$$

Let us now introduce the infinite system of constants I_k and J_k, assuming

$$\mathrm{I}_k=\iint_{(S)}\mathrm{F}(x,z)e^{\frac{g}{c^2}ch2\tau_k\cdot z}\cos\left(\frac{gx}{c^2}ch\tau_k\right)dx\,dz,$$

$$\mathrm{J}_k=\iint_{(S)}\mathrm{F}(x,z)e^{\frac{g}{c^2}ch2\tau_k\cdot z}\sin\left(\frac{gx}{c^2}ch\tau_k\right)dx\,dz.$$

$$(k=0,\ 1,\ 2,\ 3,\ \ldots)$$

Now the formula for the wave-making resistance will be written in the following manner :—

$$R = \frac{16\pi^2\rho g}{bc^2}\left\{ I_0^2+J_0^2+2\sum_{k=1}^{\infty}(I_k^2+J_k^2)\frac{ch^2\tau_k}{ch2\tau_k}\right\}.$$

When $b\to+\infty$ the formula so obtained for the wave-making resistance of a ship moving along in a canal gives us the well-known formula of Michell for the calculation of the wave-making resistance of a ship moving in unlimited mass of water.

LXXXVIII. *On the Theory of Equilibrium in Alloys.*—I.

By William Hume-Rothery, *M.A.*, *D.Sc.**

1. *Introduction.*

In a previous paper [1] we have shown that in certain alloys of silver and copper with the elements of the B sub-groups, the maximum solid solubilities of the different solutes occur at approximately the same electron concentration, whilst in some ternary alloys the solid solubility isothermals are to a first approximation lines of constant electron concentration. These simple relations hold only when the atomic diameters of solvent and solute are not too different, a condition which may be expressed by saying that the "size factors" are favourable. In the present paper we discuss first the effect of lattice distortion upon the solid solubility limits in binary alloys of the above type. We then describe some characteristics of solid solubility isothermals in ternary alloys, and show that a characteristic type of solubility curve occurs when the two solute elements tend to unite to form a compound. The same type of curve is formed by the freezing-point isothermals of intermetallic compounds in some ternary systems, and we develop a preliminary theory of the crystallization of an intermetallic compound from liquid and solid solutions of ternary alloys.

* Communicated by Professor W. L. Bragg, F.R.S.

2. *The Relation between Electron Concentration and Lattice Distortion at the α-solid Solubility Limit of Binary Copper and Silver Alloys.*

The solid solubility limit represents the composition at which the solid solution is in equilibrium with a second phase. It seems desirable therefore at first to limit the discussion to cases where the α-solid solution is in equilibrium with phases of one type, and not to compare, for example, an alloy where the second phase has a body-centred cubic structure with one where the second phase has a γ structure. In attempting to correlate the different solubility curves with the lattice distortions we have at present to use X-ray data obtained at room-temperatures. Data for different copper alloys show that the coefficients of expansion seldom differ by more than 4×10^{-6}. Taking the lattice spacing of pure copper as 3·6 Å., the errors introduced by ignoring the differences between the coefficients of expansion are therefore of the order $1{\cdot}5 \times 10^{-5}$ Å. per °C., so that a comparison to within 0·01 Å. appears justified except at the highest temperatures, where the expansion sometimes becomes irregular.

In some silver and copper alloys the α-solid solubility curves are of a characteristic type, in which, above a certain temperature, the solid solubility diminishes with rise of temperature. Solid solubility curves of this type are known in most cases to correspond with an equilibrium between the α-solid solution and a body-centred cubic β phase. In the systems copper-gallium and copper-indium the crystal structures of the β phases have not yet been completely determined, although the incomplete work of Weibke [3] shows that the copper-gallium β phase resembles the copper-aluminium β phase, whilst the copper-indium β phase is described as of the body-centred cubic type with a superlattice structure. We have therefore included these systems in our discussion, since the α-solid solubility curves show the characteristic diminution in solubility with increasing temperature.

Fig. 1 shows some α-solid solubility curves of this type plotted in terms of electron concentration *, and it will be seen that, whilst some of these are roughly superposed,

* By electron concentration is meant the ratio of valency-electrons to atoms.

characteristic differences exist. In the system copper-silicon the solubility curve is clearly in an unstable region where the solubility varies rapidly with temperature, and we have therefore omitted this curve from discussion.

In fig. 2 the electron concentrations of alloys on the α-solid solubility curves of the copper alloys at 600°,

Fig. 1.

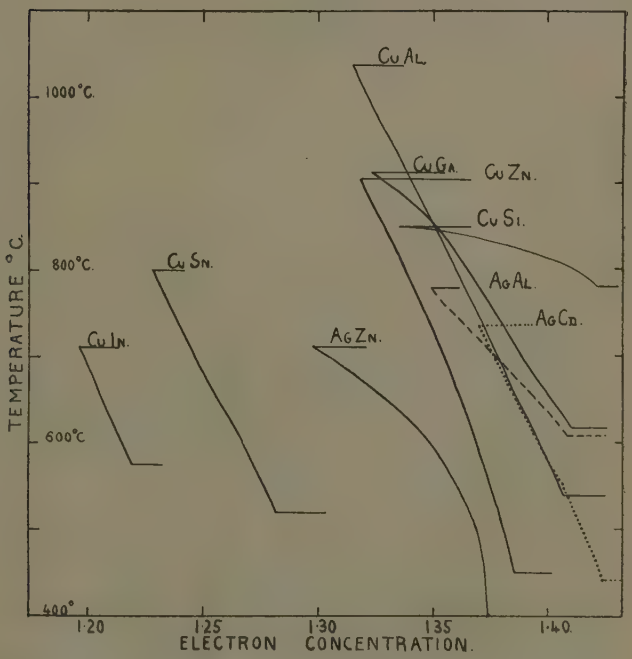

This figure shows the solid solubility curves of the α-solid solution of silver and copper alloys, where the α-solid solution is in equilibrium with a body-centred cubic β phase. The horizontal line at the top of each curve shows the eutectic or peritectic temperature above which the α-solid solution is in equilibrium with the liquid phase. The horizontal line at the foot of each curve shows the temperature at which the β phase decomposes or undergoes a transformation; in general the α-solid solubility curves change direction at these lower temperatures.

700°, and 798° C. are plotted against the mean lattice spacings of the same compositions measured at room-

temperature; the lattice spacings are from the sources indicated in reference [3]. These curves are of the general form shown in fig. 3, and clearly suggest that,

Fig. 2.

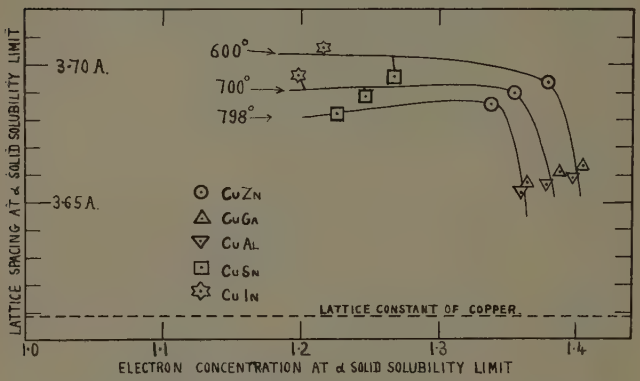

In this figure the electron concentrations of alloys on the α-solid solubility curves of copper alloys at 798°, 700°, and 600° C. are plotted against the lattice spacings of alloys of the same composition measured at room-temperature. The dotted line represents the lattice constant of the solvent metal (copper). The temperature of 798° C. is that of the α+Liquid $\rightleftharpoons$ β, peritectic reaction in the copper-tin system, and is thus the maximum temperature at which the α-solid solution exists in equilibrium with the body-centred cubic β phase in this system.

Fig. 3.

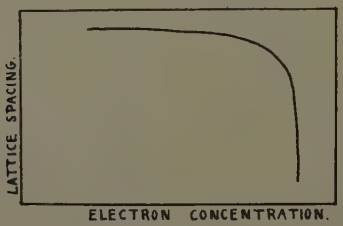

up to a certain point, lattice distortion affects the electron concentration at the solid solubility limit comparatively slightly, but that beyond this point a rapid change takes place, and the electron concentration at the solubility

limit falls sharply. The curves also suggest that in this type of equilibrium the mean lattice distortion * cannot exceed a certain value.

Fig. 4 shows similar curves for some of the silver alloys, and these are of interest as including examples of both lattice expansion and contraction [4]. These curves are of the same type as those in fig. 3, but the curves are not symmetrical about the line of zero lattice distortion. Comparison of the points for silver-zinc and silver-cadmium

Fig. 4.

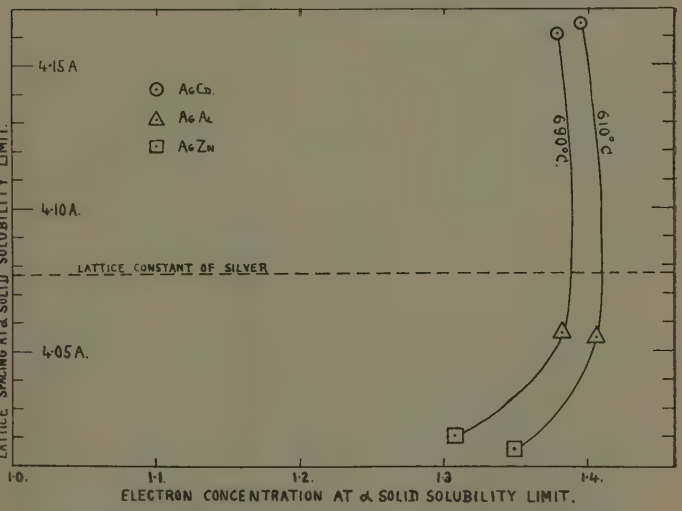

In this figure the electron concentrations of alloys on the α-solid solubility curves of silver alloys at 610° and 690° C. are plotted against the lattice spacings of alloys of the same composition measured at room-temperature. The dotted line represents the lattice constant of the solvent metal (silver).

suggests that a contraction of the mean lattice parameter has a greater effect than an expansion of the same amount. Comparison cannot be made at lower temperatures

* The expression "mean lattice distortion" is used to denote the change in lattice spacing of the solvent as measured by the ordinary methods of X-ray crystal analysis. It is well known that these give the mean lattice spacing of a solid solution, and that the production of sharp diffraction lines is not incompatible with the existence of regions of intense local distortion.

because in the system silver-aluminium the body-centred cubic form of the β phase is only stable above 608° C.

From the shape of the curve in fig. 3 it might at first be thought that in cases where the solute atoms produced a very marked distortion of the lattice, the solid solubility limits would occur at the compositions corresponding to the limiting lattice distortion in fig. 3. This, however, is definitely not the case. In the system copper-cadmium, for example, the maximum solid solubility of cadmium in copper is 1·7 atomic per cent.; the corresponding mean lattice spacing is 3·626 Å [5], whereas in the copper-zinc and copper-tin alloys referred to previously the mean lattice spacing reaches values as high as 3·69–3·70 Å. The system copper-cadmium is not one in which the α-solid solution is in equilibrium with a body-centred cubic β phase, so that it is not strictly comparable with the examples dealt with above; but examination of other systems, together with the ternary systems described below, shows clearly that in some cases there is no tendency for the solid solubility limits to occur at a constant lattice spacing when the solute atom is of unfavourable size factor. This suggests clearly that we have to consider the way in which the strain is spread through the lattice, and that whilst the mean lattice distortion is one factor affecting the solubility limits, we have also to take into account an intensely localized effect round the solute atoms, which, if too pronounced, causes a breakdown of the structure, and so limits the solid solution. If this hypothesis is accepted, and we attempt to estimate the magnitude of the intensely localized distortions round the different solute atoms, the first suggestion is naturally that this is indicated by the mean lattice distortion produced by one atomic per cent. of the different solutes in a given solvent, a procedure which is essentially equivalent to using the atomic diameters of Goldschmidt [6]. This method, however, appears unsatisfactory on account of the values for the maximum solid solubilities of the elements cadmium, indium, tin, and antimony in copper. The Goldschmidt atomic diameters and the mean lattice distortions produced by one atomic per cent. of solute increase with the valency in the above series of elements, but in spite of this the solubilities of indium (11·6 atomic per cent.) and tin (9·26 atomic per cent.) in solid copper

are much greater than that of cadmium (1·7 atomic per cent.). We have suggested elsewhere [7], from a consideration of the lattice distortions produced by different elements in solid solution in silver and copper, that the lattice distortion is a dual effect composed of two factors : (1) a valency effect such that increasing valency of the solute produces an increased expansion of the lattice, and (2) an atomic effect which may produce either an expansion or contraction. If there is appreciable overlapping of the atomic cores or ions, as, for example in crystals of copper where the closed *d* shells of electrons overlap considerably, we may perhaps regard the " atomic effect " as depending on the non-Coulomb repulsive forces between the overlapping electron shells of the atomic cores or ions, and the " valency effect " as either electronic, or due to the electrostatic repulsion between the ions which tends to push them apart. In a series of consecutive elements of regularly increasing valency, such as zinc, gallium, and germanium, the valency effect increases with increasing valency, but the atomic factor becomes smaller owing to a gradual closing up of the electron shells with increasing atomic number. From this point of view we can understand the relative solubilities of the elements cadmium to antimony in copper, since with increasing atomic number the atoms become smaller, and the atomic factor less pronounced, so that the solubility limits begin to approach the values to be expected from the normal valencies in Groups III. and IV. We can further understand why, in fig. 4, a given mean lattice contraction is more serious than the same amount of *mean* lattice expansion; for in all the alloys considered the valency of the solute is greater than that of the solvent, so that we expect the valency effect to produce an expansion, and the atomic effect will have to neutralize this expansion before a contraction in the mean lattice spacing can occur. A given mean lattice contraction will therefore imply a much more intense local distortion than the same mean lattice expansion where the two factors reinforce one another.

3. *The Three Types of Ternary Solid Solubility Isothermal.*

We may now consider the problem of ternary solid solutions, and may suppose that we have a given solvent

alloyed with two solutes, the limits of the solid solutions in the binary systems being given by the points A and B as shown in fig. 5 (*a*). The points A and B in the ternary diagram are joined by a straight line in fig. 5 (*a*), and for simplicity we propose to call the ternary solid solution represented by the area S A B the *ideal ternary solid solution*. In actual practice the ternary solid solubility

Fig. 5.

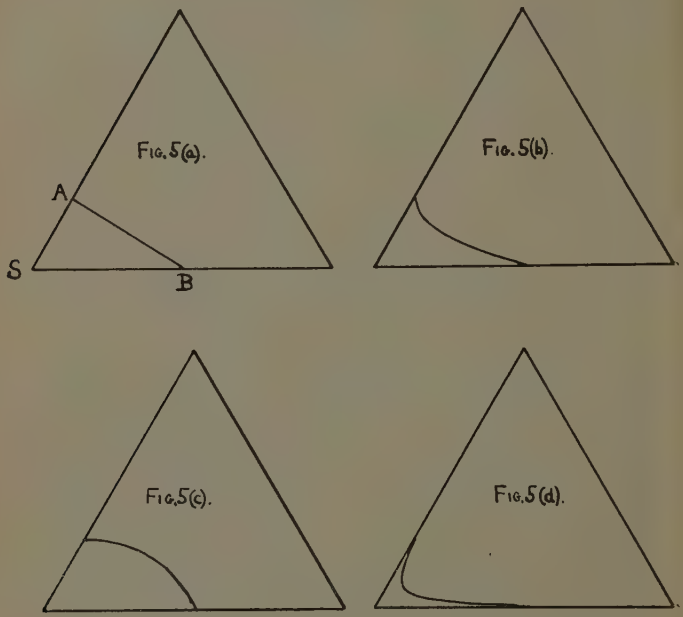

isothermals often differ from this ideal type, and figs. 5 (*b*), (*c*), and (*d*) show some of the more simple variations. We suggest that if the solid solution is comparatively dilute, the isothermal of type *b* may be expected in cases where one solute accentuates the lattice distortion produced by the other, particularly if one solute produces a relatively large distortion of the lattice, whilst type *c* may be expected where one solute relieves the distortion produced by the other. In both these cases, however, the behaviour

of concentrated solid solutions is more complex. Finally, we suggest that type *d* is found in cases where the two solute atoms tend to unite to form a compound with one another. We do not mean to imply that these types of solid solubility isothermals are to be expected only in the above circumstances, but rather that these circumstances are favourable to the production of the type concerned. The whole problem of solid solutions in ternary alloys is so complex that it may simplify the description if we summarize the main assumptions before describing the individual systems.

(1) In equilibria of the $\alpha\beta$ brass type the electron concentration is regarded as the predominant factor in determining the α-solid solubility isothermals when the size factors are definitely favourable.

(2) We assume that when the size factors are definitely favourable the relation between the mean lattice distortion and electron concentration at the solubility limit is of the kind shown in fig. 3. When, however, the size factors are no longer definitely favourable we assume that we have to consider an intensely localized distortion round the solute atoms.

(3) Both the mean lattice distortion and the localized distortion are regarded as complex effects involving an atomic factor which may either expand or contract the lattice, and a valency factor which acts so that increase of valency of the solute tends to expand the lattice.

(4) In accordance with our previous theory [8] we assume that at low temperatures there is always a tendency for solid solutions to take up more or less ordered structures in which the solute atoms keep far away from one another, so that the strain is distributed as uniformly as possible through the lattice. This tendency increases as the difference between the atomic diameters of solvent and solute becomes greater. In opposition to this, rise of temperature tends to produce a random structure.

(5) Where the two solute elements A and B can unite to form a compound $A_n B_m$, it is considered that the compound crystallizes from the solid solution when the tendency to form the solid compound is sufficiently great. The question as to whether the compound exists as such in the solid solution is not discussed, since we show that this does not affect the form of the equations in the elementary theory.

(6) When the two solutes form a compound which is stable in the liquid alloy, we imagine an equilibrium with the constituent elements of the type

$$n\mathrm{A}+m\mathrm{B} \rightleftharpoons \mathrm{A}_n\mathrm{B}_m$$

and regard the compound as crystallizing from the liquid when the activity product of the constituent elements exceeds a limiting value.

An example of an almost ideal ternary solid solution is that of copper-aluminium-zinc, which has been examined by Hansen and Bauer [9]. We have found that the lattice spacings of some ternary alloys are approximately additive functions of those to be expected from the binary systems, and if the lattice spacings of ternary copper-aluminium-zinc alloys are calculated in this way the points on the α-solid solubility isothermal lie on the curve connecting the points for copper-zinc and copper-aluminium in fig. 2.

As an example of a ternary solid solution of the type shown in fig. 5 (*b*) we may consider first the α-solid solubility isothermals in the $\alpha\beta$ equilibrium of the system copper-aluminium-tin, which has been examined in detail by Stockdale [10]. The α-solid solution area at low temperatures is less than that in an ideal ternary solid solution, and is less than that obtained by assuming that the solid solubility isothermals of the ternary alloys occur at compositions such that the electron concentrations and lattice spacings are related by curves of the type shown in fig. 3. The deviation from the ideal case is more marked at low than at high temperatures.

In these alloys the tin atom produces a relatively large expansion of the copper lattice, and in the binary copper-tin alloys the α-solid solubility limits vary from 7·5 atomic per cent. of tin at 798° C. to 9·26 atomic per cent. of tin at 500° C. These solid solutions are therefore comparatively dilute, and even with a purely random arrangement of atoms there will be relatively few places where two tin atoms are closest neighbours at a distance $a\sqrt{2}$, where a is the side of the unit cube. Using previous notation [8] this may be expressed by saying that there are comparatively few first-zone distances between solute atoms. Many alternative partly ordered structures can prevent the introduction of second-zone distances

($=a$) between solute atoms, whilst, when there are fewer than 12·5 atomic per cent. of solute atoms a more or less ordered structure can prevent the introduction of third-zone distances ($=\sqrt{\frac{3}{2}}a$) between two solute atoms. The atom of tin is much larger than that of copper, the atomic diameter of tin being almost on the border-line of what we have called the zone of favourable size factor (1). It seems reasonable to suppose therefore that at low temperatures the most stable structure in a binary copper-tin α-solid solution will be one in which the relatively large tin atoms are kept far away from one another, so that the intense local expansion of the lattice round each tin atom can be taken up by the surrounding copper atoms without a complete breakdown of the structure. In opposition to this tendency, rise of temperature favours the production of a random structure, as explained by Bragg and Williams [11].

In the binary copper-aluminium alloys the α-solid solubility limits are of the order 20 atomic per cent., so that whilst there are at least four solvent atoms to one of the solute the proportion of the latter is two to three times as great as in the copper-tin alloys. In spite of this greater proportion of solute atoms the mean lattice distortion at the α-solid solubility limit is less in the system copper-aluminium than in that of copper-tin. Both elements expand the lattice of copper, but the distortion in the copper-aluminium alloys is clearly of a much more gradual and uniform nature, and any tendency to form an ordered structure at a given composition will be much less marked in the copper-aluminium alloys than in the copper-tin series.

From the above considerations we may expect the replacement of aluminium atoms by tin atoms to affect the solid solubility limit in the following way :—

(*a*) When the aluminium is replaced by tin the electron concentration at the solubility limit will fall, because a constant electron concentration requires three atoms of aluminium to be replaced by two atoms of tin and one atom of copper, whereas the mean lattice distortion produced by one atom of tin equals approximately that produced by four atoms of aluminium. Unless therefore it is suggested that increased lattice distortion tends to increase the electron concentration at the solubility limit the conclusion is that the electron concentra-

tion will diminish in order to counterbalance the increased lattice distortion.

(*b*) When the aluminium is replaced by tin the total number of solute atoms per cent. will diminish on account of the relative valencies of the two elements and the relative lattice distortions which they produce in copper. For convenience we shall call the total number of solute atoms per 100 the *total solute percentage*.

(*c*) The initial replacement of aluminium by tin will produce a greater decrease in solubility than in the ideal case, because the number of solute atoms at the solubility limit is greater in the binary copper-aluminium alloys than in the binary copper-tin alloys, and this greater number of aluminium atoms will prevent the intensely localized expansion round the larger tin atoms from being taken up by the surrounding lattice, since this has already been strained in the direction of expansion from more numerous centres than in the binary copper-tin alloys.

(*d*) After a sufficient number of aluminium atoms has been removed, the total solute percentage will become sufficiently small for the intensely localized distortion round the tin atoms to be taken up more easily by the lattice, particularly if some kind of an ordered structure exists. A stage will therefore be reached at which the electron concentration and solubility limit diminish less rapidly than when the first tin atoms were added, and this effect will become more and more marked as the temperature becomes lower, since the tendency to relieve the strain by the formation of a partially ordered structure increases as the temperature falls.

It is clear that these considerations lead us to expect a solid solubility isothermal of the type shown in fig. 5 (*b*), but before describing actual examples we may consider what may be expected in very concentrated solid solutions. In the above argument we have assumed throughout that the solid solution is sufficiently dilute for it to be considered as a distorted lattice of the solvent, but when the proportion of the solvent and solute atoms are more nearly equal, different considerations may apply. If, for example, the size factors are sufficiently favourable for the primary solid solution to reach the equiatomic composition, the resulting alloy can no longer be regarded as a lattice of the solvent atoms with occasional regions

of distortion. It is much more a framework of solvent and solute atoms, and if the lattice spacing of this framework is greater than that of the pure solvent it is possible that a larger atom may fit more easily into the equiatomic solid solution than into the solvent, and in this case the resulting ternary solid solution may be greater than in the ideal case. This distinction between dilute and concentrated solid solutions appears even more important when the one solute relieves the lattice distortion produced by the other, and this case is considered later.

Fig. 6.

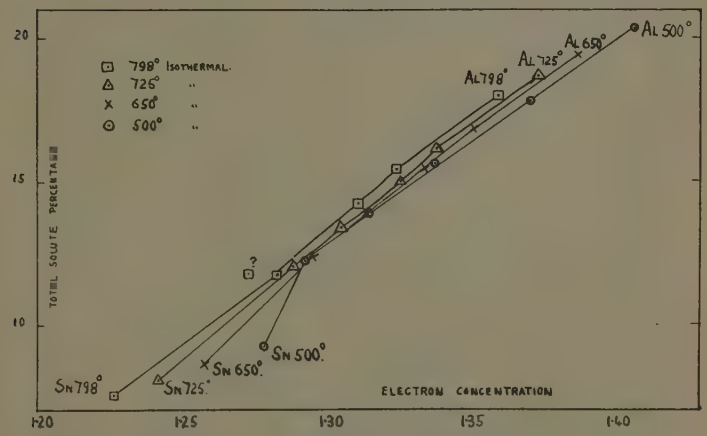

In this figure the electron concentrations of alloys on the α-solid solubility isothermals of copper-aluminium-tin alloys are plotted against the total solute percentages (*i. e.*, the atomic per cent. of aluminium plus that of tin). The points marked Al_{798}, Al_{725}, Al_{650}, and Al_{500}, and Sn_{798}, Sn_{725}, Sn_{650}, and Sn_{500}, refer to binary copper-aluminium, and copper-tin alloys at the temperatures 798°, 725°, 650°, and 500° respectively. The intermediate points refer to ternary alloys, and are calculated from Stockdale's diagram [10] showing the solubility limits in alloys containing 3, 5, 7, and 9 per cent. of tin by weight with varying proportions of aluminium. The anomalous point at 800° is from the 7 per cent. tin (by weight) series.

In the copper-aluminium-tin system the ternary isothermals of Stockdale at 725°, 650°, and 500° have the general form of fig. 5 (*b*), but in order to show the effect of the total solute percentage more clearly we have in

fig. 6 plotted the electron concentrations of different points on Stockdale's solubility isothermals at 798°, 725°, 650°, and 500° against the *total solute percentages*. The isothermals at 798°, 725°, and 650° refer to the $\alpha/\alpha+\beta$ solubility limit, and that at 500° to equilibrium between the α-solid solution and the phase with the "γ" structure, since the body-centred cubic "β" phases are only stable at the higher temperatures in these alloys. One of the 798° points lies entirely off the curve, but it is not possible to say whether this is due to experimental error or is a genuine phenomenon, since although the work was carried out in great detail the alloys were not all analysed, and some error may have occurred. The remaining points at 798° C. for the ternary alloys lie approximately on the straight line joining those for the two binary systems. The temperature of 798° C. is the maximum possible in the binary system copper-tin, since above this temperature the α-solid solution at its limit is in equilibrium with the liquid phase. At this temperature therefore the tendency to form an ordered structure will be the least. At the lower temperatures the points for the ternary alloys lie on approximate straight lines until the total number of solute atoms is small, when a bend occurs in the direction of higher solubility, the deviation becoming much more pronounced at the lower temperatures in accordance with expectation. It may be noted that the upper parts of the isothermals in fig. 6 are approximately on straight lines converging to the point Sn_{798}, so that a general relation exists between them.

A further example of this kind is the copper-zinc-tin α-solid solubility curve investigated by Tammann and Hansen, and Bauer and Hansen [12]. Fig. 7 shows the α-solid solubility curve determined from specimens annealed for six hours at 760° and slowly cooled in the furnace. The bend in the curve towards the region of higher solubility when the total solute percentage becomes small is quite definite. These results may be criticized as not referring to complete equilibrium, but the low temperature isothermals of Bauer and Hansen [13] confirm that the addition of small percentages of tin to the brasses reduces the α-solid solution area more than in the ideal case of fig. 5 (*a*).

Fig. 8 shows the 500° isotherm of the system copper-cadmium-zinc as determined by Jenkins [14], and here

again the bend in the solubility curve towards the region of higher solubility is apparent when the total solute percentage becomes small. According to Jenkins this

Fig. 7.

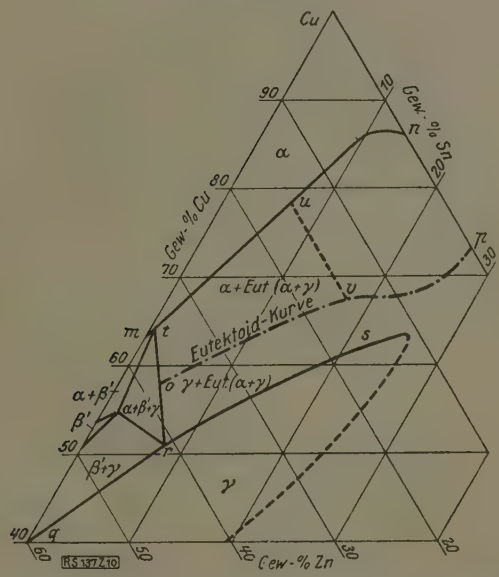

α-solid solubility curve of ternary copper-zinc-tin alloys at room-temperatures. Reproduced by permission from Bauer and Hansen (*Zeit. Metallkunde*, xxii. pp. 387, 405, 1930).

Fig. 8.

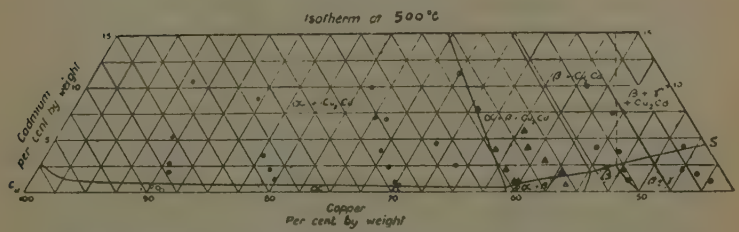

α-solid solubility curve of ternary copper-cadmium-zinc alloys at 500° C. (Reproduced by permission from Jenkins, J. Inst. Metals, xxxviii. p. 271, 1927.)

phenomenon is much more pronounced at room-temperature, as we should expect, but there is some doubt about the facts, since the work of Owen and Pickup [5] suggests that at low temperatures the solubility of cadmium in copper is much less than that given by Jenkins, although at 500° the two investigations are in agreement. The cadmium atom is considerably larger than that of copper, but although both atoms expand the lattice of copper the system copper-cadmium-zinc is not strictly analogous to the systems previously described since at the solubility curve the α-solution is in equilibrium with the Cu_2Cd phase, and not with a β or γ phase. It will be noted that at the zinc end of the α-solid solubility isothermal the short portion representing the boundary between the α and $\alpha+\beta$ areas is drawn so as to indicate a greater solid solubility than in the ideal case. The experimental evidence for this is inconclusive, but we have already shown (p. 1025) that in very concentrated solutions this may be expected. Curves showing this effect are given by Keinert [15] for the effect of small amounts of silver on the copper-zinc α-solid solution limits, where both solutes expand the lattice of copper, and of small amounts of copper on the silver-zinc α-solid solubility curve, where both solutes contract the lattice of silver. In these cases the total solute percentage is high, but the experimental data are unfortunately very incomplete.

Ternary Isothermals of the Type shown in Fig. 5 (*c*).

We may now investigate the case where one solute relieves the lattice distortion produced by the other, and may imagine a given solvent metal A, in which a solute L of larger atomic diameter forms a solid solution into which atoms of a second solute element S of smaller atomic diameter are introduced ; the argument can also be used for the opposite case. If the atomic diameter of the element L is so much greater than that of the solvent A that the solubility limit is small, the saturated solid solution of L in A is essentially a framework of A atoms. This contains occasional regions of marked expansion produced by the relatively large L atoms, which may be regarded as pushing the A atoms outwards. The accommodation of these regions of localized expansion is clearly facilitated if there are regions of contraction,

and no very definitely ordered structure is required in order to relieve the strain in this way. The position is very different if the saturated solution of L in A contains a large proportion of L atoms. In this case the saturated solid solution is a framework of L and A atoms, the framework being larger than that of A atoms alone. If, therefore, the atoms of S are considerably smaller than those of A, so that, to use a crude expression, they tend to be loose and unstable when in solid solution in A, it is clear that only a very definitely ordered arrangement of A, L, and S atoms can prevent the small S atoms from being even more loose and unstable when introduced into the larger framework of L and A atoms. In this case the strain may only be relieved by the formation of a definite superlattice structure, or in extreme cases perhaps only at definite ratios of the three kinds of atoms. Since the tendency to form ordered structures decreases with rise of temperature these effects may be complex, and the solubility isothermals may have different forms at high and low temperatures.

If the hypothesis on p. 1018 is accepted it may be necessary also to distinguish between alloys where the atomic and valency effects reinforce or oppose one another. In the silver-zinc alloys, for example, we expect the valency effect to expand the lattice of silver and the atomic effect to contract it, since the atom of zinc is undoubtedly smaller than that of silver. Here the two factors are in opposition, but in the copper-tin alloys the factors reinforce one another, since the atom of tin is undoubtedly larger than that of copper, and the valency effect reinforces this difference.

We may now consider the primary solid solution areas in certain ternary systems in order to see how the above deductions are confirmed.

Aluminium-rich Alloys with Magnesium and Silicon.

This system is of particular interest, since, whether we consider the Goldschmidt atomic diameters, the interatomic distances in the crystals of the elements, or the effect of atomic number on the "atomic factor," we expect the silicon atom to be smaller, and the magnesium atom to be larger than that of aluminium. The position is here complicated by the fact that the two solute elements tend to combine to form a stable compound

Mg_2Si, but, as can be seen from fig. 9 *, the work of Hanson and Gayler [16] shows the solubility of silicon in aluminium to be definitely increased by the addition of magnesium. This increase continues up to the point at which the solid solution is in equilibrium with the compound Mg_2Si, when the curve assumes quite a different form, which is described later.

Zinc-rich Alloys with Aluminium and Copper.

Both the Goldschmidt atomic diameters and the interatomic distances in the crystals of the elements indicate that the atom of aluminium is larger, and the copper atom smaller than that of zinc. On the other hand, from what was said before (p. 1019) we expect the difference

Fig. 9.

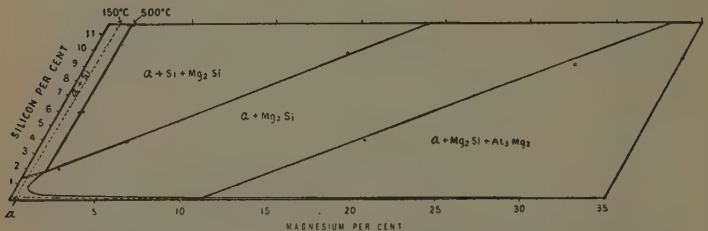

Showing the α-solid solution area in aluminium-rich alloys with magnesium and silicon. The full curve represents the solubility isothermal at 500° and the dotted curve that at 150°. (Reproduced by permission from Hanson and Gayler, J. Inst. Metals, xxvi. p. 321, 1921.)

between the zinc and copper atoms to be the result of the preponderance of the valency factor, since from the point of view of the atomic factor we should expect the copper atom to be larger than the zinc atom of higher atomic number. The zinc-rich alloys of this system have been investigated by Haughton and Bingham [17], and, as seen from fig. 10, the addition of aluminium increases the solid solubility of copper in zinc. The addition of copper has little effect on the solubility of aluminium in

* This diagram is in weight percentages, but the atomic weights of the three elements are nearly the same, so that the form is not altered by transferring to atomic percentages.

solid zinc, but the solubility isothermal clearly shows a much higher solid solubility than in the ideal case.

Fig. 10.

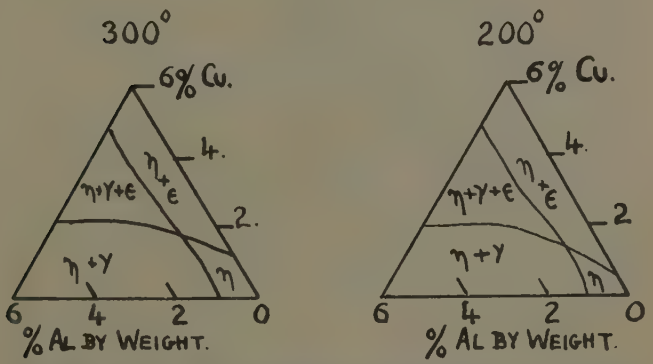

Showing the zinc-rich solid solution (η) in ternary zinc-aluminium-copper alloys. (From Haughton and Bingham, Proc. Roy. Soc. xcix. A, p. 47, 1921.)

Silver-rich Alloys with Antimony and Zinc.

Here the Goldschmidt atomic diameters and the lattice distortions in the binary solid solutions show the zinc

Fig. 11.

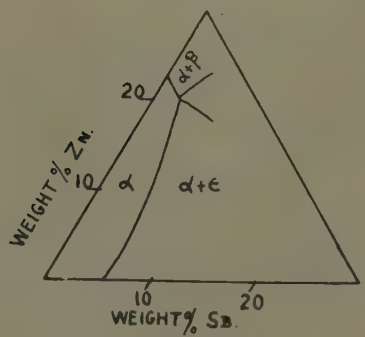

Showing the silver-rich solid solution in ternary silver-antimony-zinc alloys. (From Guertler and Rosenthal, *Z. Metallkunde*, xxiv. pp. 7, 30, 1932.)

atom to be smaller and the antimony atom to be larger than the atom of silver. From the point of view adopted above this implies that in the case of zinc the atomic factor has outweighed the valency effect; the closest distances of approach in the crystals of the elements also show the zinc atom to be smaller than the silver atom. With antimony the position is reversed, and the expansion of the mean lattice constant of silver by antimony must be the result of the valency effect; the interatomic distances in the crystals of silver and antimony are almost the same (2·88 Å. and 2·87 Å). The equilibrium diagram of this ternary system has been investigated by Guertler and Rosenthal [18], whose results are shown in fig. 11. Although not very detailed this work shows clearly that the area of the α-solid solution in the ternary system is greater than in the ideal case.

Copper-rich Alloys with Tin and Beryllium.

Here the tin atom is larger than that of copper from all points of view, whilst the beryllium atom is smaller if we consider either the Goldschmidt atomic diameters or the distances of approach in the crystals of the elements. The solubility isothermals of Rowland and Upthegrove [19] are very complex and confusing. At low temperatures part of the ternary α-solid solution area extends beyond the limits of the ideal case, but at higher temperatures this characteristic is lost.

Silver-rich Alloys with Cadmium and Copper.

Here the lattice of silver is expanded by cadmium and contracted by copper. According to Keinert [20] the solubility of copper in silver is little affected by the addition of cadmium, and a diagram is given in which the solubility of copper is unaffected by the addition of 10 per cent. (by weight) of cadmium, and then diminishes very slightly, so that the ternary solid solution area in the silver corner of the diagram is wider than in the ideal case. Unfortunately full details are not given, and the temperature to which the curve refers is not stated. The solubility of copper in solid silver is given as 9·4 per cent. by weight, which is greater than the value of 8·8 per cent. found in the very careful work of Stockdale [21] as the limiting value at the eutectic temperature. The work of Keinert cannot therefore be considered as conclusive.

The above examples suggest that where one solute atom is larger and the other smaller than that of the solvent there is a tendency for the ternary solid solution to exceed the limits of the ideal case, particularly where the total solute percentage is small.

The Solubility Limits of Intermetallic Compounds in Ternary Alloys.

On page 1030 we have noted that the form of the ternary solid solubility isothermal in the aluminium-rich alloys with magnesium and silicon changes its shape on reaching the composition at which the saturated solid solution is in equilibrium with the compound Mg_2Si. This is an example of the general case where two solute elements unite to form a compound which may decompose on heating. When the two solute elements form a compound, the picture presented is one in which there is a tendency for the solute atoms in the primary solid solution to unite to form the compound, and that when this tendency is sufficiently pronounced the compound precipitates from the solid solution. In the same way in molten aluminium-rich alloys with magnesium and silicon we regard the two solute elements as tending to form the compound Mg_2Si which crystallizes from the solution if its solubility is exceeded. The position visualized is thus very like that of the precipitation of a salt from a solution containing a common ion, the difference being that in the latter case the excess of one ion can only be added in the form of a salt with an ion of the opposite sign, whereas in the alloys the excess of either constituent can be added directly.

If the compound Mg_2Si exists as a definite molecular species in the liquid alloy, we have an equilibrium of the type

$$2Mg + Si \rightleftharpoons Mg_2Si.$$

If fMg, fSi, and $f$$Mg_2Si$ are the activity coefficients, and [Mg], [Si], and [Mg_2Si] the volume concentrations of the three species, then at equilibrium at a given temperature we may write as in the theory of electrolytes

$$f^2_{Mg}[Mg]^2 f_{Si}[Si] = K f_{Mg_2Si}[Mg_2Si]. \quad . \quad . \quad . \quad (1)$$

At the solubility isothermal where the liquid alloy is in equilibrium with the solid compound Mg_2Si, the

activity of the latter, $f_{Mg_2Si}[Mg_2Si]$, will be constant, and we shall have the solubility product relation

$$[Mg]^2[Si] = \frac{C}{f^2_{Mg} f_{Si}}, \quad . \quad . \quad . \quad . \quad . \quad . \quad (2)$$

where $$C = K[Mg_2Si] f_{Mg_2Si}.$$

In practice we do not measure [Mg], [Si], and $[Mg_2Si]$, but the total content of magnesium and silicon, which we may write $[Mg_{Total}]$ and $[Si_{Total}]$ respectively. Then, since each molecule of Mg_2Si contains two atoms of magnesium and one of silicon, if x is the concentration of Mg_2Si in any solution

$$[Mg] = [Mg_{Total}] - 2x,$$
$$[Si] = [Si_{Total}] - x,$$

and equation (2) may be written in the form

$$([Mg_{Total}] - 2x)^2([Si_{Total}] - x) = \frac{C}{f^2_{Mg} f_{Si}}. \quad . \quad . \quad (3)$$

If, as in the original theory of the solubility products of salts, we assume that all the activity coefficients are equal to unity, equation (3) assumes the form

$$([Mg_{Total}] - 2x)^2([Si_{Total}] - x) = C_1 = Kx. \quad . \quad . \quad (4)$$

Curves of this type are shown in fig. 12, and are of the double asymptotic type. The value of x chosen affects the positions of the asymptotes to which the curves approach at high concentrations of either constituent, whilst the values of C_1 affect the sharpness with which the asymptotes are approached. Where only a limited part of the curves can be seen it is often difficult to realize that they are approaching the same asymptote.

If the activity coefficient of the undecomposed compound Mg_2Si is unity and independent of concentration, but the coefficients for magnesium and silicon are variables, equation (3) assumes the form

$$([Mg_{Total}] - 2x)^2([Si_{Total}] - x) = \frac{C_1}{f^2_{Mg} f_{Si}}, \quad . \quad . \quad (5)$$

where f_{Mg} and f_{Si} are variables. If f_{Mg} and f_{Si} increase with the total solute concentration, the curves of fig. 13 approach the asymptotes more rapidly, although the asymptotes themselves remain unchanged. If, however,

f_{Mg} and f_{Si} diminish with increasing concentration the position is more complex, and an increase in solubility may result. In the theory of electrolytes this phenomenon is met with in cases where the activity coefficients of the ions diminish rapidly with increase in the total ionic strength of the solution.

In the more general case where the activity coefficient of the undecomposed compound Mg_2Si also varies with the composition, the term x in the above equations becomes a variable. We can then say little more than that the general form of the curve will remain the same

Fig. 12.

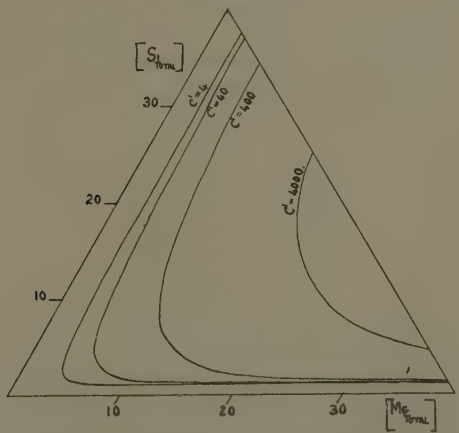

Curves of the type $([Mg_{Total}]-2x)^2([Si_{Total}]-x)=C^1$.
The curves are calculated for $x=1$ and $C^1=4$, 40, 400, and 4000 respectively.

in dilute solutions, whilst in the more concentrated solutions both the positions of the asymptotes and the sharpness with which they are approached will affect the form of the curve, and that a bending away from the asymptote may occur if the activity coefficients vary in a suitable way.

We may next consider the complications to be expected if the solute atoms of any one kind tend to unite together to form complex molecules. In the above system we shall expect this tendency to be more pronounced for

silicon than for magnesium, since silicon crystallizes in the diamond structure which is an example of the (8—N) rule, co-valent, or "riesenmolekul" type of crystal. Even in the case of bismuth, where the co-valent bonds are much less stable, it is known that, on melting the crystal, complexes or seed crystals remain in the liquid, and are gradually broken up on heating. With silicon, where the co-valent tendency is much more pronounced, we may therefore quite expect such complexes to be present in the molten alloys at the lower temperatures, particularly when the silicon content approaches the concentration at which silicon crystallizes from the melt, either instead of magnesium silicide, or together with the latter as a eutectic. In this case if, as a first approximation, we imagine the silicon complex molecules to be of the type Si_n, we shall have, in addition to the equilibria considered above, an equilibrium of the type

$$n\mathrm{Si} \rightleftharpoons \mathrm{Si}_n, \quad . \quad . \quad . \quad . \quad . \quad . \quad (6)$$

and at equilibrium

$$f_{\mathrm{Si}}^{n}[\mathrm{Si}]^{n} = \mathrm{K}' f_{\mathrm{Si}_n}[\mathrm{Si}_n], \quad . \quad . \quad . \quad . \quad . \quad (7)$$

which may be written in the form

$$[\mathrm{Si}_n] = \frac{1}{\mathrm{K}'} \frac{f_{\mathrm{Si}}^{n}}{f_{\mathrm{Si}_n}} [\mathrm{Si}]^{n}, \quad . \quad . \quad . \quad . \quad . \quad (8)$$

where f_{Si_n} is the activity coefficient of the complex molecule Si_n. The effect of this kind of complex formation is to reduce the activity of the free silicon atoms for a given total silicon content, since some of the silicon is now present as complex molecules. In this case we can no longer write the relation

$$[\mathrm{Si}] = [\mathrm{Si}_{\mathrm{Total}}] - x,$$

but instead we have

$$[\mathrm{Si}] = [\mathrm{Si}_{\mathrm{Total}}] - x - n[\mathrm{Si}_n], \quad . \quad . \quad . \quad . \quad (9)$$

since each Si_n molecule contains n atoms of silicon.

From (8) this may be written in the form

$$[\mathrm{Si}] = [\mathrm{Si}_{\mathrm{Total}}] - x - \frac{1}{\mathrm{K}'} \frac{f_{\mathrm{Si}}^{n}}{f_{\mathrm{Si}_n}} [\mathrm{Si}]^{n}. \quad . \quad . \quad (10)$$

The greater the value of n the more sudden will be the increase in the third term on the right-hand of equation (10) with increasing silicon content. The values of

[Si] will therefore become less than in the absence of complex formation, and hence the values of [Mg], and therefore of $[Mg_{Total}]$, will be greater than those required by the previous theory of equations (1) to (6), since the value of [Mg] must increase in order to compensate for the decrease in [Si]. Similar considerations apply if the magnesium forms complexes, and if the solvent aluminium forms complexes with either solute. The general effect of complex formation by the solutes is therefore to increase the concentration limits within which the compound is retained in solution.

In the above theory we have dealt with volume concentrations, but data for the densities of molten alloys are lacking. Liquid aluminium has a much higher density than liquid magnesium at the same temperature, so that with alloys containing a considerable percentage of magnesium the atomic concentrations of the solutes will be less than they would be if no change in volume took place, since the volume of the alloy will increase when one atom of aluminium is replaced by one of magnesium. The same relation is shown between the atomic volumes and atomic diameters in solid aluminium and magnesium. With silicon the position is less certain. The density of solid silicon is less than that of aluminium, but this is largely due to a difference in the type of crystal structure, since the aluminium and magnesium lattices are of the close-packed types, whilst that of silicon is not. From the position of the elements in the periodic table we should expect the atomic volume of aluminium to be intermediate between those of magnesium and silicon, in which case if both solutes were present the changes in density would to some extent be neutralized. As a first approximation we shall therefore examine the atomic percentage diagram, a procedure which is equivalent to taking the volume occupied by 100 atoms as the unit. It must be emphasized that this may only be justified as a first approximation, since the validity of the activity concept when applied to atomic percentage compositions is sometimes disputed.

Fig. 13 shows the freezing-point data for the system aluminium-magnesium-silicon as determined by Hanson and Gayler [16], the area A, B, C, D being that in which the compound Mg_2Si crystallizes from the melt. Owing

to the approximate equality of the atomic weights of the three elements this diagram is substantially unaltered on being transferred to atomic percentages, and the general resemblance of the Mg_2Si isothermals to those of fig. 12 is apparent. In fig. 14 we have transferred the 600°, 630°, 660°, 690°, and 720° isothermals to atomic percentage compositions, and have plotted $\lceil[Mg_{Total}]\rceil$ against $\lceil[Si_{Total}]\rceil$ on a logarithmic scale, where the symbol $\lceil[Mg_{Total}]\rceil$ in double brackets implies atomic percentage composition instead of volume concentration. When plotted in this way the middle parts of the isothermals form a series of parallel straight lines of gradient approximately $-2/1$. These parts of the isothermals are therefore of the general type required by equation (4) with small values of x.

Fig. 13.

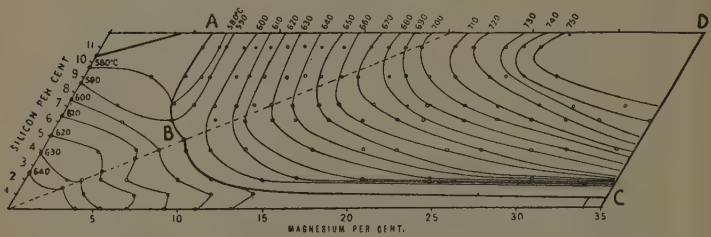

Liquidus isothermals for the aluminium-rich alloys with magnesium and silicon. The area A, B, C, D is that in which the compound Mg_2Si crystallizes from the melt. (Reproduced by permission from Hanson and Gayler, J. Inst. Metals, xxvi. p. 337, 1921.)

At the extremities the isothermals bend so as to give greater solubility than those to be expected from a linear logarithmic relation, this effect being apparent at much lower percentages of silicon than of magnesium, in agreement with what might be expected from the tendency to complex formation (see p. 1037). Until the theory is further developed, and the volume concentrations are known, it appears undesirable to examine the curves in greater detail, or to attempt to estimate the values of the constant x which give the best straight lines in fig. 14. We may, however, reasonably claim that the form of the curves is very suggestive.

When we apply the above ideas to equilibrium between

the *solid* solution and the compound Mg_2Si we have to consider the following points :—

(1) It seems possible that in the solid state there is more justification for considering atomic percentage

Fig. 14.

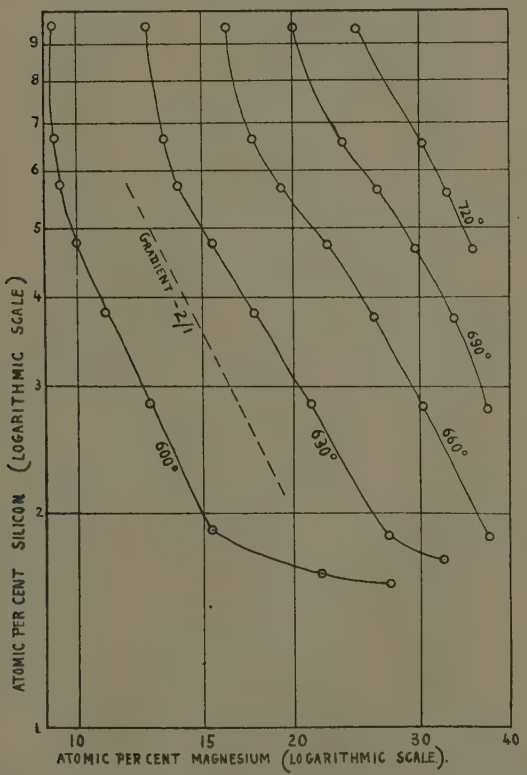

In this figure points on the Mg_2Si isothermals of fig. 13 have been transferred to atomic percentages, and are plotted on a logarithmic scale. The dotted line has a gradient of −2/1.

compositions than in the liquid state, for in solid crystals the atoms occupy points on a space lattice, and even if we assume a dynamic equilibrium the actual volume concentration may not be so fundamental as the number

of steps in the lattice which separate two atoms tending to unite together, and this is indicated by the relative numbers of the two atoms.

(2) We have also to consider whether a compound Mg_2Si can be considered as existing in the solid solution. The X-ray crystal analysis makes it certain that one atom of aluminium is not replaced by a molecule of Mg_2Si, but there is still the possibility that three adjacent atoms of aluminium are replaced by two of magnesium and one of silicon which are held more firmly to one another than to the other neighbouring atoms. If this view is accepted and the compound Mg_2Si is regarded as existing in the solid solution, the preceding theory can be applied almost unchanged, except for the possible substitution of atomic percentage compositions in place of volume concentrations, and the further modifications noted in (3) below. If, on the other hand, we do not regard the compound Mg_2Si as existing in the solid solution we have a position somewhat analogous to that in the electrochemical theories of complete dissociation of salts in solution. In this case we may regard the solubility equilibrium as determined by the balancing of the tendency of the compound to dissolve or decompose, and the tendency of the constituent atoms or ions to crystallize out. Alternatively we may regard the equilibrium as established through the medium of the vapour phase which contains Mg_2Si molecules in equilibrium with magnesium and silicon atoms or ions. In either case we obtain a solubility equation of the solubility product type with the appropriate activity coefficients.

(3) It may be necessary to modify the above equations in cases where the solid solubility is also affected by lattice distortion or electron concentration, since these factors were not considered in deducing the above simple equations.

Fig. 9 shows the results of Hanson and Gayler for the solubility limit of the α-solid solution of magnesium and silicon in aluminium when in equilibrium with the compound Mg_2Si. The dotted curve, representing the solubility isothermal at 150°, has clearly the characteristic double asymptotic form. The full curve, representing the results at 500°, has the same characteristics except for the bending away from the axis between 1 and 2 per cent. of silicon; but as this has been disputed by some

investigators we shall not discuss the matter further. These curves are not sufficiently detailed to justify comparison with theory, but part of the diagram concerned has recently been investigated in great detail by Keller and Craighead [24], whose solubility isothermals are shown in fig. 15. This refers to very small percentages

Fig. 15.

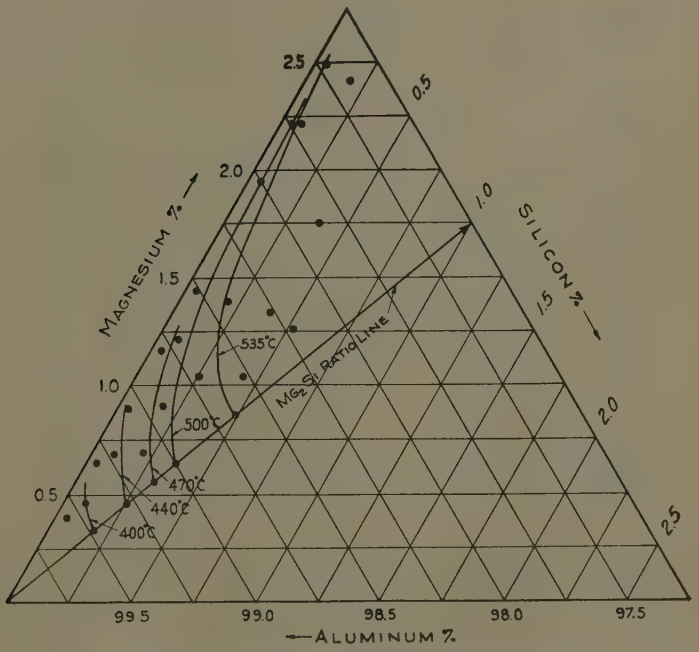

(Reproduced by permission from Keller and Craighead, A. I. M. E. Tech. Pub. 707 (Met. Tech. June 1936).)

of the solute elements, so that the error caused by ignoring volume changes is comparatively slight. In fig. 16 we have transferred the isothermals of fig. 15 to atomic percentages, and plotted these on a logarithmic scale. The isothermals form a series of approximately straight lines of gradient $-2/1$, which is the same gradient as that of the middle portions of the liquidus isothermals of fig. 14.

In the case of the 535° and 470° isothermals of fig. 15 the maximum deviation from a straight line is of the order 0·01 per cent. in the silicon content, and in the 440°

Fig. 16.

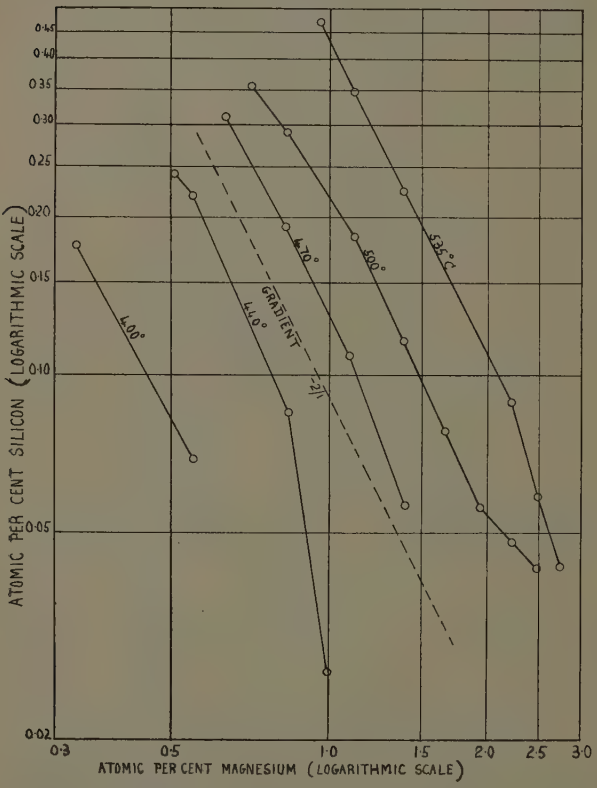

In this figure points on the solid solubility isothermals of fig. 15 have been transferred to atomic percentages and plotted on a logarithmic scale. The dotted line has a gradient of −2/1.

and 500° isothermals the deviation is of the order 0·02 per cent. silicon. In view of the fact that the isothermals are obtained by bracketing methods, and that slight

errors inevitably occur in measuring the exact centres of the lines in fig. 15 the agreement between experiment and theory is very satisfactory. It is particularly interesting to note how the liquidus isothermals of Hanson and Gayler when plotted logarithmically give lines of the same gradient as the solid solubility isothermals of Keller and Craighead.

From these figures we may tentatively estimate the heat of formation of the compound Mg_2Si, since if H is the heat of formation, and K the equilibrium constant the two are related by the equation

$$\frac{d \ln K}{dT} = -\frac{H}{RT^2}.$$

Inserting the values of K obtained from the 600° and 660° isothermals of fig. 14, and integrating by the usual methods, we find that the value of H is 196 kilojoules. This, however, is not necessarily the true heat of formation of the compound from its constituent elements in solution in aluminium, since equation (3) shows that the apparent constants of the isothermals involve both the true equilibrium constants and the activity coefficients, so that any variation of the latter is included in the variation of the constants of the isothermals. This will probably not alter the magnitude of the result which is quite reasonable. The heat of formation of the compound Mg_2Sn is 205 kilojoules, whilst the heats of formation * of MgS and MgO are 344 and 610 kilojoules respectively.

Application of the same method to the solid solubility isothermals of fig. 16 leads to a value about one-half as great as that obtained from the liquidus isothermals, but it is difficult to estimate the exact significance of this. If the compound Mg_2Si is regarded as existing in solid solution in aluminium, the above method leads to the heat of formation of the compound from its constituent elements in solid solution. If, however, the compound Mg_2Si does not exist as such in the solid solution, and we

* These figures are from the I. C. T. vol. v., and refer to the heats of formation of the solid compounds. A correction for the heat of fusion or solution is therefore required before they can be compared directly with the calculated values for Mg_2Si. The latent heats of fusion of metals (I. C. T. vol. ii.) are, however, small (5–25 kilojoules per gram atom) compared with the above.

regard the equilibrium as established through the vapour phase (see p. 1040), the value obtained by the above method involves both the heat of formation in the vapour and the heats of vaporization, which are much greater than those of fusion. Apart from this difficulty the problem of activity coefficients in solid solutions is so little understood that it is satisfactory to obtain a result of the right order of magnitude.

A further example of the above principle is given by the copper-rich alloys with tin and nickel. Fig. 17 (*a*) shows the results of Eash and Upthegrove [22] for the α-solid solubility isothermal at 780° C. The first addition of nickel to the copper-tin alloys produces a wider solid solution than that expected from a linear relation for the binary systems. In this part of the diagram the α phase is in equilibrium with the β body-centred cubic phase, and the form of the curve is readily understood. In the first place nickel contracts the lattice of copper, and so relieves the expansion produced by the tin atoms. Apart from this it is well known that nickel acts as an element of zero valency in electron compounds, and so for reasons of electron concentration we expect the solid solution area to be greater than that required by a linear relation. With further additions of nickel the α phase is in equilibrium with the θ phase, which Eash and Upthegrove identify as a compound of nickel and tin, possibly Ni_3Sn or Ni_4Sn, which may also take copper into solid solution. The form of the curve is shown in fig. 17 (*a*). Fig. 17 (*b*) shows the same system at 700°, and here the $\alpha/\alpha+\theta$ solubility curve is clearly beginning to assume the double asymptotic form, whilst at 575° (fig. 17 (*c*)) and 500° (fig. 17 (*d*)) this is more and more pronounced, and the curves have the general characteristics predicted above for cases where a relatively unstable compound decomposes on heating. When plotted logarithmically these curves do not, however, give a series of parallel lines, but curves of the type shown in fig. 18. The curvature at the ends corresponds with a smaller solubility of tin and a greater solubility of nickel than required by a simple straight line. The smaller solubility of tin may be ascribed to increased lattice distortion, and although the middle part of the logarithmic curve for the 500° isothermal has the gradient of 3/1 required for the compound Ni_3Sn, this does not apply to the remaining

isothermals. A more complete theory is thus needed, and for the present it can only be said that the curves of fig. 17 have the general qualitative characteristics to be expected when two solutes unite to form a compound.

The above examples confirm the view that the type of solid solubility isothermal shown in fig. 5 (*d*) occurs if the

Fig. 17.

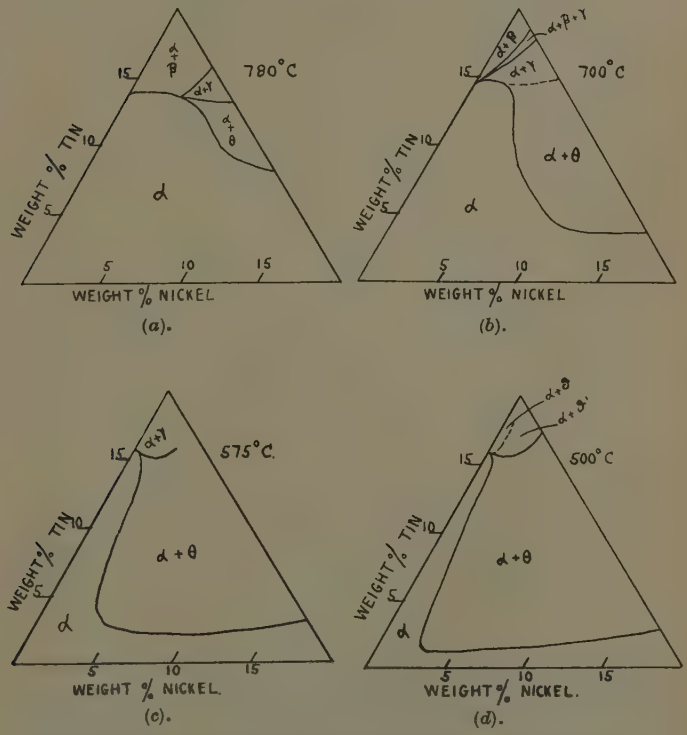

Showing the copper-rich α-solid solution in the system copper-nickel-tin. (After Eash and Upthegrove.)

two solute elements unite together to form a compound. If the above views are accepted we can also understand why the thermodynamic methods used by Jeffery and others [23] sometimes lead to confusing results when

applied to alloy systems. These methods assume that the solute atoms are either all in the form of a compound molecule of definite formula, or all in the form of free atoms; but in view of the relative instability of some intermetallic compounds at high temperatures it is more probable that compound molecules are in reversible equilibrium with their component elements, and this will affect the results unless one constituent of the compound is present in such excess that the mass action

Fig. 18.

effect represses the decomposition of the compound almost entirely.

Acknowledgments.

The author must express his gratitude to Professor F. Soddy, F.R.S., for laboratory accommodation and many other facilities for research work, and must thank Professor W. L. Bragg, F.R.S., Mr. J. H. Wolfenden, and Mr. R. P. Bell for much stimulating discussion. He must also acknowledge his indebtedness to the Council of the Royal Society for election to a research fellowship and for research grants. Thanks are also due to the Department of Scientific and Industrial Research, and the Aeronautical Research Committee for generous financial assistance.

References.

(1) W. Hume-Rothery, G. W. Mabbott, and K. M. Channel-Evans, Phil. Trans. Roy. Soc. A, ccxxxiii. p. 1 (1934).
(2) W. Hume-Rothery and G. V. Raynor. Unpublished work.
(3) The lattice spacings of the copper alloys are from the following sources :—
CuZn. E. A. Owen and L. Pickup, Proc. Roy. Soc. A, cxxxvii. p. 409 (1932).
CuAl. Obinata and Wasserman, *Naturwissenschaften*, xxi. p. 382 (1933).
CuGa. W. Hume-Rothery, G. V. Lewin, and P. W. Reynolds, paper to appear in the Proc. Roy. Soc. ; also F. Weibke, *Zeit. anorg. Chem.* ccxx. p. 293 (1934).
CuIn. F. Weibke and H. Eggers, *Zeit. anorg. Chem.* ccxx. p. 273 (1934).
CuSn. E. A. Owen and J. Iball, J. Inst. Metals, lvii. p. 267 (1935).
(4) The solubility data for the silver alloys are from the tables of Hume-Rothery, Mabbott, and Channel Evans (see ref. (1)). The lattice spacings are from the following sources :—
AgCd. H. Astrand and A. Westgren, *Zeit. anorg. Chem.* clxxv. p. 90 (1928).
AgZn. E. A. Owen and L. Pickup, Proc. Roy. Soc. cxl. p. 344 (1933).
AgAl. N. Ageew and D. Shoyket, J. Inst. Metals, lii. p. 119 (1933).
(5) E. A. Owen and L. Pickup, Proc. Roy. Soc. A, cxxxix. p. 526 (1933).
(6) V. M. Goldschmidt, *Z. physikal Chem.* cxxxiii. p. 397 (1928).
(7) W. Hume-Rothery, G. V. Lewin, and P. W. Reynolds (see (3)).
(8) W. Hume-Rothery and H. M. Powell, *Zeit. Krist.* xci. p. 23 (1935).
(9) M. Hansen and O. Bauer, *Zeit. Metallkunde*, xxiv. p. 73 (1932).
(10) D. Stockdale, J. Inst. Metals, xxxv. p. 187 (1926).
(11) W. L. Bragg and E. J. Williams, Proc. Roy. Soc. A, cxlv. p. 699 (1934).
(12) G. Tammann and M. Hansen, *Zeit. anorg. Chem.* cxxxviii. p. 137 (1924); O. Bauer and M. Hansen, *Zeit. Metallkunde*, xxii. pp. 387, 405 (1930).
(13) O. Bauer and M. Hansen, figs. 34–36 (ref. (12)).
(14) C. H. M. Jenkins, J. Inst. Metals, xxxviii. p. 271 (1927).
(15) M. Keinert, *Zeit. physikal Chem.* A, clx. p. 15 (1932).
(16) D. Hanson and M. L. V. Gayler, J. Inst. Metals, xxvi. p. 321 (1921).
(17) J. L. Haughton and K. Bingham, Proc. Roy. Soc. A, xcix. p. 47 (1921).
(18) W. Guertler and W. Rosenthal, *Z. Metallkunde*, xxiv. pp. 7, 30 (1932).
(19) E. S. Rowland and C. Upthegrove, 'Metals Technology,' Feb. 1935, A. I. M. M. E. Tech. Publ. no. 613.
(20) M. Keinert, *Zeit. physikal Chem.* A, clxii. p. 289 (1932).
(21) D. Stockdale, J. Inst. Metals. xlv. p. 127 (1931).
(22) J. T. Eash and C. Upthegrove, Trans. Amer. Inst. Mining Met. Eng. 1933, civ. p. 221.
(23) F. H. Jeffery, Trans. Faraday Soc. xxvi. p. 86 (1930).
(24) F. Keller and C. M. Craighead, 'Metals Technology,' June 1936, A. I. M. M. E. Tech. Publ. no. 706.

The Old Chemistry Department,
The University Museum, Oxford.

LXXXIX. *Characteristics of Transmission Lines at High Frequencies.* *By* T. WALMSLEY, *Ph.D., M.Inst.C.E.**

THIS article is divided into two parts; the first relates to the differential time delay and attenuation in air-insulated cables on frequencies up to 2000 kc./s.; the second deals with the effects on transmission lines of terminating with impedances having values differing from the line surge impedance.

I.

Characteristics of Concentric and Single-pair Cables at High Frequencies.

List of Symbols :

p=Resistivity.
u=Magnetic permeability of metal.
u^1=Magnetic permeability of dielectric.
K=Dielectric constant.
C=Capacitance.
R=Resistance.
L=Inductance.
G=Leakance.
d, l, x=Lengths.
f=Frequency.

$$m=2\pi\sqrt{\frac{2uf}{p}}.$$

β=Attenuation constant.
α=Wave constant.
z=Line impedance at any point.
z_0=Surge impedance of line.
Z_L=Terminal impedance.

$$k=\frac{z}{z_0}.$$

v_1, v_2=Velocity of wave propagation at frequencies f_1 and f_2.
t_1, t_2=Times of propagation at frequencies f_1 and f_2.
a, b, & c=Dimensions as shown in fig. 1.

The recent prominence given to concentric cables as applied to telephony and television justifies a theoretical

* Communicated by the Author.

estimate of some of their properties. In particular the attenuation and time delay at various frequencies are quantities whose values are important. An approximate estimate has therefore been made of these values for two particular air-insulated cables, and for comparison purposes similar values have been computed in the case of two single-pair air-insulated cables surrounded by a circular metallic sheath.

The formulæ used in the computation are as follows :—

Resistance.

(1) Concentric cable *.

$$\mathrm{R} = \frac{pm}{2\pi a}\left\{\frac{1}{\sqrt{2}} + \frac{1}{2ma} + \frac{3}{8\sqrt{2}m^2a^2}\right\} + \frac{2u}{mb\sqrt{2}} \cdot \frac{\sinh m(c-b)\sqrt{2} - \sin m(c-b)\sqrt{2}}{\cosh m(c-b)\sqrt{2} + \cos m(c-b)\sqrt{2}}.$$

(2) Single-pair cable.

Resistances have been computed by methods suggested in the Circular of the Bureau of Standards, No. 74. Due to the fact that the current density is more concentrated on the sides of the conductors adjacent to each other the values of resistance obtained by the above methods have been multiplied by 1·1 to correct for this "proximity" effect †.

Inductance.

(1) Concentric cable.

$$\ddagger \mathrm{L} = 2u' \log \frac{b}{a} + \frac{2u}{ma}\left(\frac{1}{\sqrt{2}} - \frac{3}{8\sqrt{2}m^2a^2} - \frac{3}{8m^3a^3}\right) + \frac{2u}{mb\sqrt{2}} \cdot \frac{\sinh m(c-b)\sqrt{2} - \sin m(c-b)\sqrt{2}}{\cosh m(c-b)\sqrt{2} + \cos m(c-b)\sqrt{2}}.$$

(2) Two-pair cable.

$$\dagger \mathrm{L} = 4u' \log \frac{c}{a} + \frac{4u}{ma}\,\frac{z(ma)}{u(ma)}.$$

* See 'Alternating Currents,' vol. i. by A. Russell.
† *Archiv für Electrotechnik*, xxviii. no. 12, by H. Kaden (1934).
‡ See 'Alternating Currents,' vol. i. by A. Russell.

Capacitance.

(1) Concentric cable.

$$C = \frac{1}{2 \log_e \frac{b}{a}}.$$

Fig. 1.

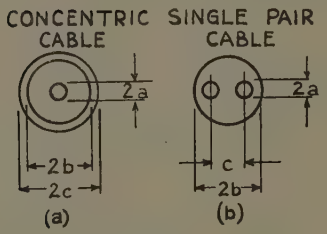

(2) Single-pair cable.

The capacitance is the resultant of the capacities between (A) the wires, (B) between the wires and sheath (fig. 1 (*b*)).

(A) $$* C_0 = \frac{kl}{2W}; \qquad \cosh \frac{W}{2} = S - a; \qquad S = a + \frac{c}{2}.$$

(B) $$* C_1 = \frac{kl}{2W_1}; \qquad \cosh \frac{W_1}{2} = \left\{ \frac{S\left(S - \frac{c}{2}\right)^{\frac{1}{2}}}{ab} \right\};$$

$$S = \frac{1}{2}\left(a + b + \frac{c}{2}\right).$$

The effective capacity between the conductors is $c_0 + \frac{1}{2}c_1$.

Attenuation.

$$\beta = \frac{R}{2}\sqrt{\frac{C}{L}} + \frac{G}{2}\sqrt{\frac{L}{C}} \quad \text{(at high frequencies).}$$

Note.—The second factor is usually negligible.

* See 'Alternating Currents,' vol. i. by A. Russell.

Wave Constant.

$$\alpha = \sqrt{\tfrac{1}{2}\{\sqrt{(R^2+\omega^2L^2)(G_1^2+\omega^2C^2)}-(G_1R-\omega^2LC)}.$$

Velocity of propagation $v=\omega/\alpha$.

More important than the actual velocities of propagation at various frequencies is the differential time delay. If, for example, over a band width of 1 megacycle the difference in time of travel over a cable were ·1 micro second the extreme of these differences would be 36°. In making computations of the differential time delay it is therefore necessary to remember that small differences are important, and to use approximations with discretion. Now the difference in time of propagation over a length (d) of cable

$$= t_1 - t_2 = \frac{d(v_2 - v_1)}{v_1 v_2}$$

$$= \frac{d\left\{\frac{\omega_2}{\alpha_2} - \frac{\omega_1}{\alpha_1}\right\}}{\frac{\omega_1\omega_2}{\alpha_1\alpha_2}}$$

$$= \frac{d\,(f_2\alpha_1 - f_1\alpha_2)}{2\pi . f_1 f_2}.$$

The evaluation of the differential times from this expression is extremely tedious, since α is dependent on L, R, and G, all of which vary with frequency. Fortunately, however, the variations in α due to the variations in L with frequency are much greater than the variations due to changes in R and G. Thus the error in the differential time delay due to ignoring R and G is not great, being less than 2 per cent. in the example about to be considered over a frequency range of 200 kc. to 2000 kc.

The approximate expression $\alpha = \omega\sqrt{LC}$ can therefore be used.

Now

$$t = \frac{d}{v} = \frac{d}{\omega/\alpha} = d\sqrt{LC},$$

and

$$\frac{\delta t}{\delta f} = \frac{d\sqrt{C}}{2\sqrt{L}} \cdot \frac{\delta L}{\delta f}.$$

Thus from the inductance-frequency curve the $\frac{\delta L}{\delta f}$-frequency curve can be obtained, from which by graphic methods the differential time-delay-frequency curve can be computed.

The actual dimensions assumed in making the computations were :—

	(1)	(2)
Concentric cable.		
	$2a = \cdot 1''$	$= \cdot 1$ cm.
	$2b = \cdot 4''$	$= \cdot 4$ cm.
(Fig. 1 (*a*)).	$2c = \cdot 5''$	$= \cdot 5$ cm.
Single-pair cable.		
	$2a = \cdot 1''$	$= \cdot 1$ cm.
	$2b = \cdot 4''$	$= \cdot 4$ cm.
(Fig. 1 (*b*)).	$2c = \cdot 5''$	$= \cdot 5$ cm.

Other values for C were taken in the case of the single-

Fig. 2.

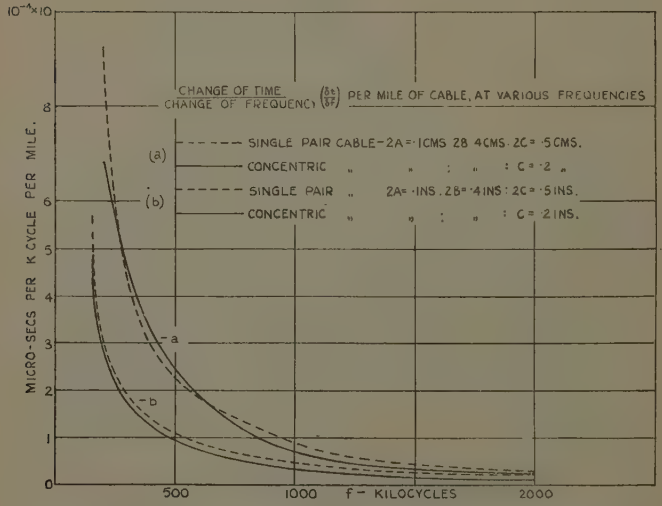

pair cable, but were found to produce very little difference in the attenuation and the differential time delay. The results are shown in figs. 2, 3, and 4.

Fig. 3.

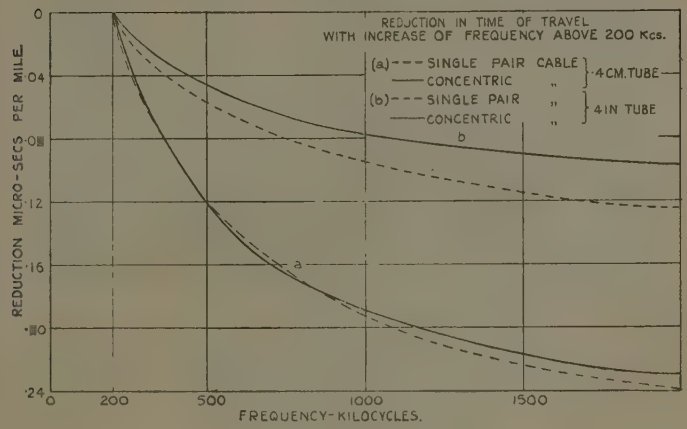

Fig. 4.

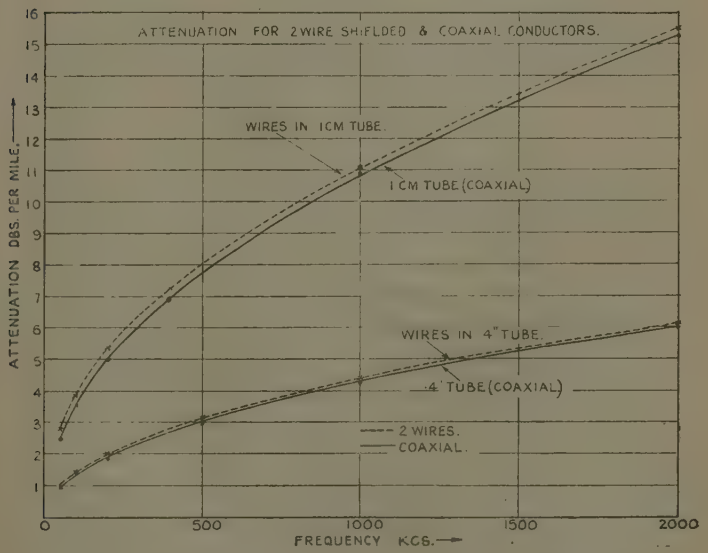

It is necessary to emphasize that the results being based on theoretical formulæ are merely pointers to what might be expected in practice. They must, in the

absence of practical confirmatory tests, be accepted with discretion.

II.

The Effect of Terminating Impedances on Transmission Lines carrying High-frequency Currents.

A problem of great interest and, in the case of radio aerial transmission lines of considerable practical importance, relates to the behaviour of the lines under various terminal conditions. The attenuation of the line is assumed to be negligible. Under these circumstances the following relationship obtains :

$$Z = Z_0 \frac{(Z_L+Z_0)e^{j\alpha x}+(Z_L-Z_0)e^{-j\alpha x}}{(Z_L+Z_0)e^{j\alpha x}-(Z_L-Z_0)e^{-j\alpha x}}$$

$$= Z_0 \frac{Z_L \cos \alpha x + Z_0 j \sin \alpha x}{Z_0 \cos \alpha x + Z_L j \sin \alpha x},$$

which, by multiplying numerator and denominator by $Z_0 \cos \alpha x - Z_L j \sin \alpha x$, and substituting the term KZ_0 for Z_L, becomes

$$Z = Z_0 \frac{K+0{\cdot}5\, j(1-K^2) \sin 2\alpha x}{\cos^2 \alpha x + K^2 \sin^2 \alpha x}.$$

The expression in this form readily lends itself to the illustration of several facts, some of which are well known whilst others are less known or have not hitherto been disclosed. In fig. 5 the ratio $\frac{Z}{Z_0}$ has been plotted for various values of K. For the particular purpose of this article the phase constant α has been taken as equal to $\frac{2\pi}{\lambda}$. The phase-angle

$$\phi = \arctan \frac{0\,5\,(1-K^2) \sin \frac{4\pi x}{\lambda}}{K}$$

has also been plotted in fig. 5.

The curves illustrate the well-known fact that an incorrectly matched transmission line has a varying impedance along its length. The various maxima and minima values of impedance occur at the same points

for different values of K ; the sequence of impedance and phase-angle values is repeated each half wave-length, and the separation between adjacent maximum and minimum values is quarter of a wave-length. In all cases the phase-angle becomes zero at quarter wave-length intervals. Thus the quadrature component of the impedance at these points becomes zero and the impedance is purely resistive. This fact may be utilized in matching aerials to transmission lines and in calculating the power fed into the aerials.

Fig. 5.

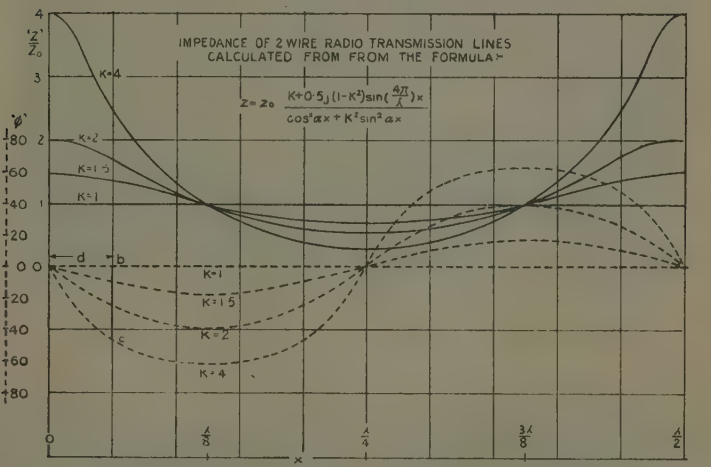

Another little-known fact deducible from the expression for Z and illustrated by the curves is that the scalar value of the line impedance for all values of K is equal to the surge impedance when $x = \frac{\lambda}{8}$, whilst the phase-angle ϕ is a maximum.

The curves have been plotted for the condition that the phase-angle of the load is zero, but by moving the scale of the horizontal ordinates either to the right or the left according to whether the phase-angle of the load is negative or positive the curves can be applied when the load is reactive. For example, if the phase-angle of the load were

given by the ordinate *bc* (fig. 5) then the antinode of current which coincides with the minimum value of line impedance, would be $\frac{\lambda}{4}-d$ from the load.

To take account of the phase-angle ϕ_2 of the load the expression for the impedance at any point x_L from the load should therefore be

$$Z = Z_0 \cdot \frac{K_1 + 0{\cdot}5j(1-K_1^2)\sin\frac{4\pi}{\lambda}(x_L+d)}{K_1^2\sin^2\frac{2\pi}{\lambda}(x_L+d)+\cos^2\frac{2\pi}{\lambda}(x_L+d)},$$

where K_1 is now the ratio of maximum to minimum current in the line. The value of ϕ_2 is obtained from the relationship

$$\text{arc tan}\frac{1-K_1^2}{2K}\sin\frac{4\pi d}{\lambda}=\phi_2.$$

The curves and formula suggest a ready means of ascertaining the values of the modulus and phase-angles of an aerial or other load terminating a transmission line. Thus the value of K_1 being known from the ratio of the measured values of the maximum to minimum current, and the distance $\frac{\lambda}{4}-d$ from the load to the minimum line voltage point being measured, then either by utilizing these values in the curves or by substituting in the expression for Z, the values of both the modulus and phase-angle of the impedance can be obtained. For example, if $K_1=2$ and $d=\frac{\lambda}{24}$,

$$\phi_2 = \text{arc tan}-\tfrac{3}{4}\sin\frac{\pi}{6} = -20{\cdot}5^\circ \text{ approx.};$$

also, since $x_L=0$, $Z=Z_L$,

$$\frac{Z_L}{Z_0}=\frac{\sqrt{K_1^2+\frac{(1-K_1^2)^2}{4}\sin^2\frac{4\pi d}{\lambda}}}{K_1^2\sin^2\frac{2\pi d}{\lambda}+\cos^2\frac{2\pi d}{\lambda}}=1{\cdot}78.$$

[*The Editors do not hold themselves responsible for the views expressed by their correspondents.*]

G. 1.

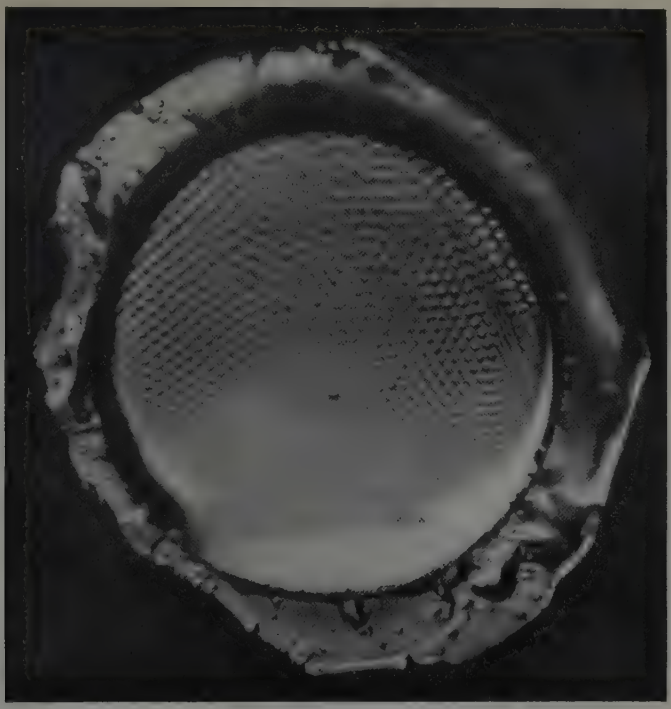

Regular "granulation" of surface of a plane soap-film under the influence of sound waves. $\lambda=27{\cdot}5$ mm. Intensity about $3{\cdot}4\ \frac{\text{erg}}{\text{cm.}^3}$. Diameter of film 7·2 mm.

FIG. 4*a*

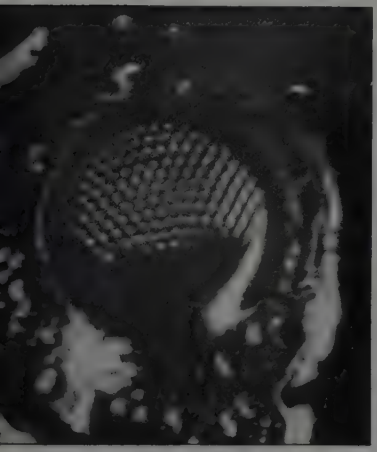

FIG. 4*b*.

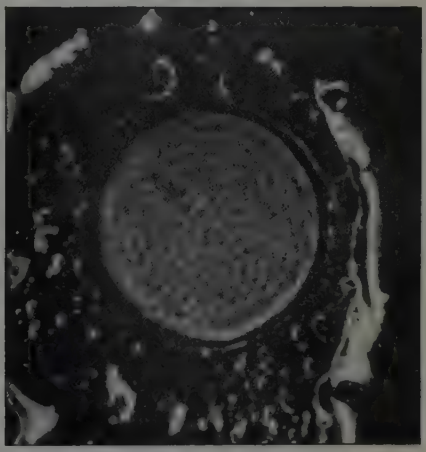

stages of the granulation phenomenon: (*a*) film at optimum thickness, (*b*) film too thin. $\lambda=28$ mm. Intensity about $3{\cdot}4\ \frac{\text{erg}}{\text{cm.}^3}$. Diameter of the film 3·3 mm.

FIGS. 5 *a–f*.

a. *b*. *c*. *d*. *e*. *f*.

Changes in the aspect of a rectangular film. $\lambda = 27{\cdot}5$ mm. Intensity about $3{\cdot}4\,\frac{\text{erg}}{\text{cm.}^3}$. Dimension of the film $4 \times 1{\cdot}2$ mm.^{2}.

Fig. 1.

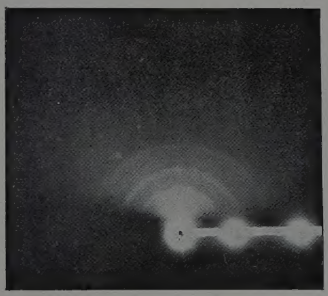

Aluminium oxide, type 1.

Fig. 2.

Aluminium oxide, type 2.

Fig. 3.

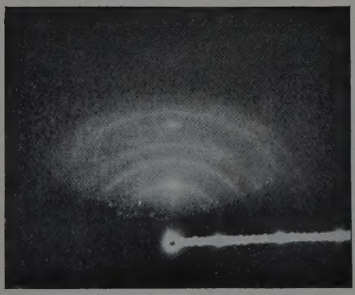

Chromium oxide.

Fig. 4.

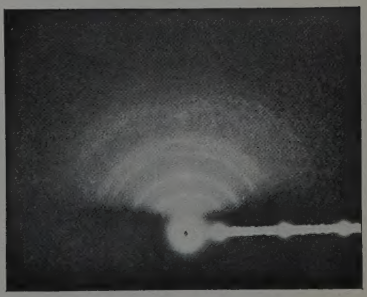

Chromium oxide.

FIG. 5.

Specimen as viewed approximately along electron beam.

FIG. 6.

Specimen as viewed approximately along electron beam.

FIG. 7.

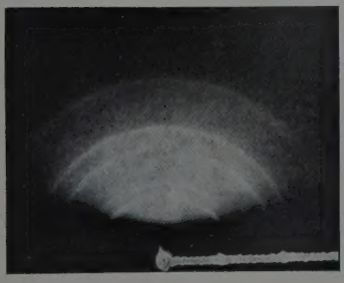

Aluminium normal incidence.

FIG. 8.

Copper film.